frontiers | Research Topics

Complement in nervous system disease

Edited by
Nikolaos Grigoriadis, Marina Boziki, Iliana Michailidou,
Frank Baas and Kees Fluiter

Published in
Frontiers in Cellular Neuroscience
Frontiers in Immunology

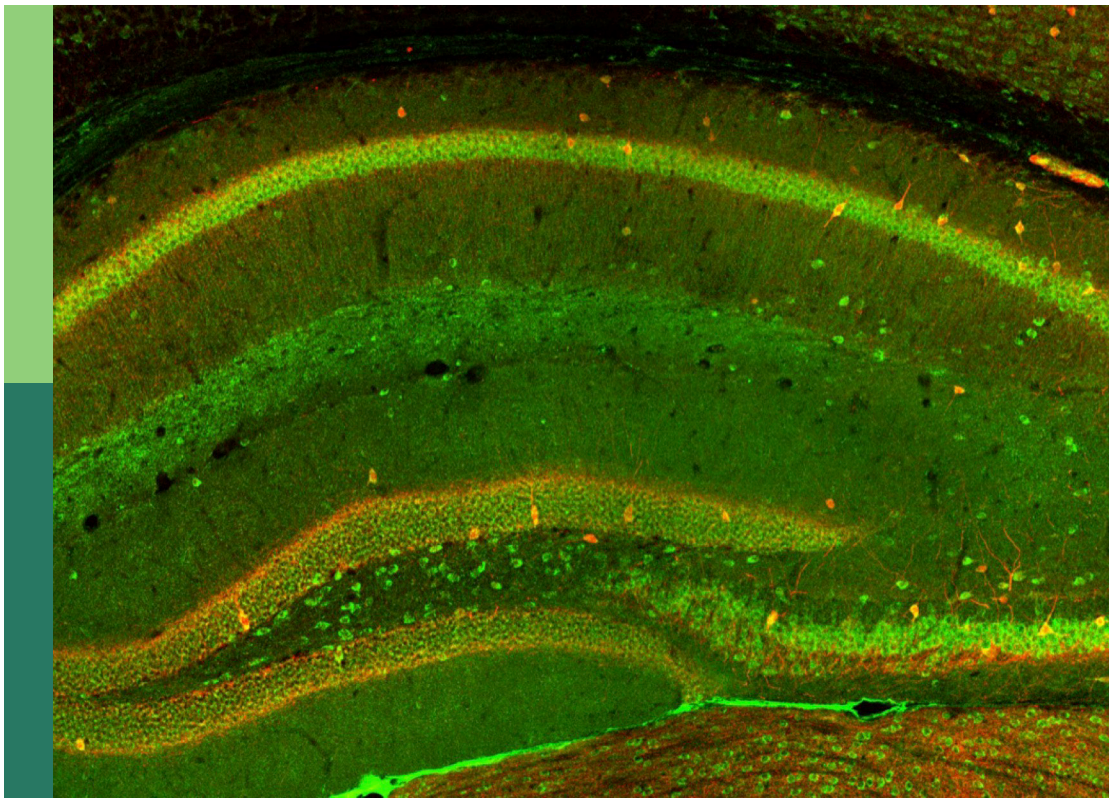

ISSN 1664-8714
ISBN 978-2-8325-3286-7
DOI 10.3389/978-2-8325-3286-7

About Frontiers

Frontiers is more than just an open access publisher of scholarly articles: it is a pioneering approach to the world of academia, radically improving the way scholarly research is managed. The grand vision of Frontiers is a world where all people have an equal opportunity to seek, share and generate knowledge. Frontiers provides immediate and permanent online open access to all its publications, but this alone is not enough to realize our grand goals.

Frontiers journal series

The Frontiers journal series is a multi-tier and interdisciplinary set of open-access, online journals, promising a paradigm shift from the current review, selection and dissemination processes in academic publishing. All Frontiers journals are driven by researchers for researchers; therefore, they constitute a service to the scholarly community. At the same time, the *Frontiers journal series* operates on a revolutionary invention, the tiered publishing system, initially addressing specific communities of scholars, and gradually climbing up to broader public understanding, thus serving the interests of the lay society, too.

Dedication to quality

Each Frontiers article is a landmark of the highest quality, thanks to genuinely collaborative interactions between authors and review editors, who include some of the world's best academicians. Research must be certified by peers before entering a stream of knowledge that may eventually reach the public - and shape society; therefore, Frontiers only applies the most rigorous and unbiased reviews. Frontiers revolutionizes research publishing by freely delivering the most outstanding research, evaluated with no bias from both the academic and social point of view. By applying the most advanced information technologies, Frontiers is catapulting scholarly publishing into a new generation.

What are Frontiers Research Topics?

Frontiers Research Topics are very popular trademarks of the *Frontiers journals series*: they are collections of at least ten articles, all centered on a particular subject. With their unique mix of varied contributions from Original Research to Review Articles, Frontiers Research Topics unify the most influential researchers, the latest key findings and historical advances in a hot research area.

Find out more on how to host your own Frontiers Research Topic or contribute to one as an author by contacting the Frontiers editorial office: frontiersin.org/about/contact

Complement in nervous system disease

Topic editors

Nikolaos Grigoriadis — Aristotle University of Thessaloniki, Greece
Marina Boziki — Aristotle University of Thessaloniki, Greece
Iliana Michailidou — Aristotle University of Thessaloniki, Greece
Frank Baas — Leiden University Medical Center (LUMC), Netherlands
Kees Fluiter — Leiden University Medical Center (LUMC), Netherlands

Citation

Grigoriadis, N., Boziki, M., Michailidou, I., Baas, F., Fluiter, K., eds. (2023). *Complement in nervous system disease*. Lausanne: Frontiers Media SA. doi: 10.3389/978-2-8325-3286-7

Table of contents

frontiers | Frontiers in Cellular Neuroscience

TYPE Editorial
PUBLISHED 07 August 2023
DOI 10.3389/fncel.2023.1268023

OPEN ACCESS

EDITED AND REVIEWED BY
Dirk M. Hermann,
University of Duisburg-Essen, Germany

*CORRESPONDENCE
Iliana Michailidou
✉ i.michailidou@lumc.nl

RECEIVED 27 July 2023
ACCEPTED 28 July 2023
PUBLISHED 07 August 2023

CITATION
Michailidou I, Fluiter K, Boziki M, Grigoriadis N and Baas F (2023) Editorial: Complement in nervous system disease.
Front. Cell. Neurosci. 17:1268023.
doi: 10.3389/fncel.2023.1268023

Editorial: Complement in nervous system disease

Iliana Michailidou[1]*, Kees Fluiter[2], Marina Boziki[1], Nikolaos Grigoriadis[1] and Frank Baas[2]

[1]Laboratory of Experimental Neurology and Neuroimmunology and the Multiple Sclerosis Center, 2nd Department of Neurology, AHEPA University Hospital, Aristotle University of Thessaloniki, Thessaloniki, Greece, [2]Department of Clinical Genetics, Leiden University Medical Center, Leiden, Netherlands

KEYWORDS

complement, immunity, neuroinflammation, neurodegeneration, therapy

Editorial on the Research Topic
Complement in nervous system disease

Complement is an ancient system for host anti-microbial aid with a major role in the remodeling of the developing nervous system. It serves the innate immunity, interfaces with the adaptive immunity (Ricklin et al., 2016; Reis et al., 2019), and mediates the elimination and refinement of synapses (Stevens et al., 2007; Schafer et al., 2012). It consists of more than 30 proteins which circulate in the serum and have an effector or regulatory role. Complement proteins are mainly produced by the hepatocytes (Zhou et al., 2016) and cannot enter the nervous system in the presence of an intact blood-brain/spinal cord barrier. However, some components are produced within the nervous system (Morgan and Gasque, 1997) to mediate developmental processes (Magdalon et al., 2020) or neuroimmune responses (Veerhuis et al., 2011; Michailidou et al., 2015, 2017).

Complement recognizes non-cognate antigens and devours "unwanted" cells or cell compartments (Ricklin et al., 2010; Nonaka and Nakanishi, 2019). Activation of complement occurs via three pathways, the classical, lectin, and alternative pathway (Figure 1). C1q is the initiator of the classical pathway. It binds to immune complexes or to "eat me" signals exposed by apoptotic cells and it has an important role in the pathogenesis of both neurological (Dalakas et al., 2020) and non-neurological (Coss et al., 2023) diseases. A systematic review by Schulz and Trendelenburg provides a comprehensive overview of all the studies published between 1998 and April 2022 which utilized the C1qKO mouse to induce experimental models, providing information on the molecular contribution of C1q to human diseases.

In neurological diseases, C1q was extensively studied for its role in synaptic pruning a process in which the degenerating synapse is stripped by microglia through a mechanism dependent on the complement C1q-C3 axis (Hong et al., 2016; Thion and Garel, 2018). The contribution of complement-mediated synapse pruning to neurodegeneration was first identified in a model of glaucoma in DBA/2J mice showing degeneration of retinal ganglion cells (Stevens et al., 2007). Later on other studies on human post mortem nervous tissues (Michailidou et al., 2015; Ramaglia et al., 2021) and experimental models of neurodegenerative diseases (Hong et al., 2016; Paolicelli et al., 2017; Michailidou et al., 2018) supported this finding and showed an effect of complement-mediated synaptic pruning on behavior (Lui et al., 2016), memory, and learning (Hong et al., 2016; Ramaglia et al., 2021). Now, a study by Zeng et al. suggested an involvement of the C1q-C3 axis in the degeneration of the human eye retina in high or pathological myopia. The authors

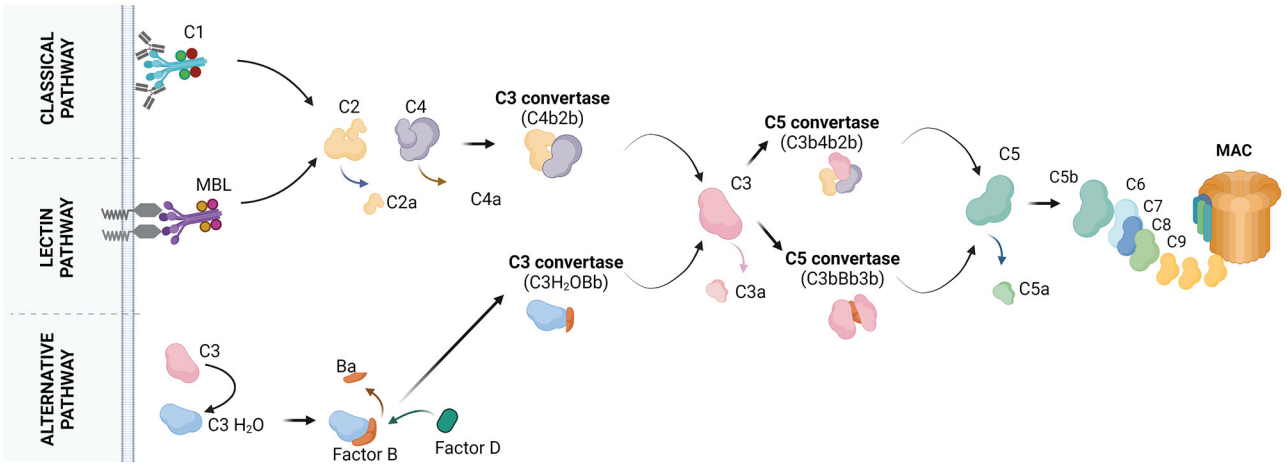

FIGURE 1
The molecular pathways of complement activation. Classical pathway: it starts with the binding of C1q to the target cell. C1q recognizes the target by the presence of bound antibodies. C1q can also bind to distinct molecules, patterns or structures. C1q is a subunit of the C1 complex which is further composed of the C1r and C1s proteases. Upon binding of C1q to the target, C1r and C1s get activated. C1s cleaves the C4 protein into C4a and C4b. C4a is released whereas, C4b is covalently bound to the target. C4b attracts C2 which is cleaved by C1s into C2a and C2b. C2a is released whereas, C2b binds C4b forming the C4b2b complex, also known as C3 convertase. C3 convertase cleaves C3 into C3a and C3b. C3b may bind the C3 convertase forming the C4b2b3b complex, also known as C5 convertase. C5 convertase cleaves C5 into C5a and C5b. C5b may associate with C6, C7, C8, and C9 to form the final product of complement activation, the membrane attach complex (MAC). Lectin pathway: it starts with the binding of mannose-binding lectin (MBL) or ficolins on the target cell. Circulating MBL or ficolins recognize the target by the presence of carbohydrate patterns. MBL is complexed with two components, the MBL-associated serine protease (MASP) 1 and MASP2. MASPs get activated upon binding of MBL to the target and cleave C4 and C2 to form the C3 convertase. The pathway continues with the formation of the C5 convertase and MAC. Alternative pathway: it starts with the spontaneous hydrolysis of C3 into C3(H_2O) and continues with the binding of factor B to C3(H_2O) for cleavage of factor B into Ba and Bb by factor D. This results in the formation of the fluid phase C3 convertase, C3(H_2O)Bb. C3(H_2O)Bb converts C3 into C3a and C3b. Some C3b molecules attach to the target and associate with factor B, which will be cleaved by factor D. This results in the formation of the C3 convertase C3bBb. The pathway continues with formation of the C5 convertase (C3bBb3b), cleavage of C5 and formation of MAC. Created with BioRender.com.

reported significantly higher intraocular levels of the C1q-C3 axis proteins compared to control eyes, and a negative correlation between the amounts of C1q-C3 axis proteins and deep layer retinal thickness. Because complement is a major component of both the systemic and the neuro-inflammation, it can mediate neuroimmune actions in response to infections (Vasek et al., 2016). Hao et al. showed that complement-mediated synaptic pruning and neuroinflammation were boosted in Alzheimer's disease upon entrance of the periodontitis-causing pathogen *Porphyromonas gingivalis* (*Pg*) in the brain.

Next to its role in synaptic pruning, complement has additional roles in the pathology of the nervous system some of which are (partially) defined whereas, others not. In this Research Topic, Veremeyko et al. present data supporting a novel role for the C4B-encoded C4 protein in epilepsy. This role of C4 is associated with the expression of immediate early genes during an epileptic seizure and affects the cognition of mice receiving convulsant and subconvulsant doses of pentylenetetrazole.

In multiple sclerosis (MS), complement has an established role in demyelination (Prineas et al., 2001; Barnett et al., 2009). In particular, C1q has an antigen recognition-associated effector function that allows the efficient destruction of antibody-targeted myelin (Morgan et al., 2021). Notably, T cells and astrocytes located within a MS lesion respond to activated complement by increasing the expression levels of RGC32, a gene driving neuroimmune responses. A mini review by Tatomir et al. explains how RGC32 regulates astroglial cell reactivity to promote glial scar formation in a MS lesion.

In the gray matter, Evans et al. show that complement deposition and/or activation is associated with compartmentalized inflammation which is a driver of subpial cortical demyelination (Howell et al., 2011; Ahmed et al., 2022) and MS progression (van Olst et al., 2021). By examining human post-mortem MS brains the authors identified an association between the amounts of meningeal/subpial complement proteins and the extent of cortical demyelination. In addition, they reported an increased density of phagocytic C3a receptor (R) 1+ and C5aR1+ microglial cells/macrophages at the expanding edge of subpial and leukocortical lesions, suggesting a role for complement in the expansion of MS lesions.

Therapeutic agents developed to target the complement system carry a clear potential to alleviate diverse diseases including neurological diseases. A study by Seidel et al. demonstrated an immunomodulatory effect of the terminal complement pathway inhibitor BB5.1 in the brain of obese $Ldlr^{-/-}$.Leiden mice. By means of immunohistochemistry and next generation sequencing, Seidel et al. showed that systemic administration of the BB5.1, a monoclonal antibody that blocks C5 cleavage, affected the microglial cell immunophenotype and modulated brain neuroinflammation in the obese mice. BB5.1 blocks the terminal complement pathway and is used in multiple animal studies as the equivalent of the anti-human C5 monoclonal

antibody Eculizumab (Zelek et al., 2020). Lekova et al. from Cardiff University published an article characterizing a novel anti-complement inhibitor blocking the C7 protein of the terminal complement system. In this article they assessed the *in vitro* function, binding epitopes, and mode of action of three monoclonal antibodies targeting the C7 protein. The authors concluded that one of them, the TPP1820 mAb was effective in preventing experimental myasthenia gravis (MG) and provided a stratification assay for the detection of MG patients which are predicted to respond to an anti-C7 therapy. Last but not least in the group of therapy-related articles of this Research Topic, Li et al. moved their focus upstream in the complement cascade to study the response of human and murine macrophages bearing the C3a receptor, the cognate receptor for the complement peptide C3a, to the C3a antagonist TLQP-21. TLQP-21 is a neuropeptide derived from the VGF precursor protein. The authors confirmed the binding of TLQP-21 to C3aR but reported a low potency of the human peptide to activate the human primary macrophages concluding that a C3aR-dependent action of TLQP-21 on macrophages may not be physiologically relevant in humans.

This Research Topic show that the complement system is involved in more pathways than only combatting microbes. It has many more important functions in development and maintenance of a healthy nervous system.

Author contributions

IM: Writing—original draft, Writing—review and editing. KF: Writing—review and editing. MB: Writing—review and editing. NG: Writing—review and editing. FB: Writing—review and editing.

Conflict of interest

The authors declare that the research was conducted in the absence of any commercial or financial relationships that could be construed as a potential conflict of interest.

Publisher's note

References

Ahmed, S. M., Fransen, N. L., Touil, H., Michailidou, I., Huitinga, I., Gommerman, J. L., et al. (2022). Accumulation of meningeal lymphocytes correlates with white matter lesion activity in progressive multiple sclerosis. *JCI Insight* 7. doi: 10.1172/jci.insight.151683

Barnett, M. H., Parratt, J. D. E., Cho, E.-S., and Prineas, J. W. (2009). Immunoglobulins and complement in postmortem multiple sclerosis tissue. *Ann. Neurol.* 65, 32–46. doi: 10.1002/ana.21524

Coss, S. L., Zhou, D., Chua, G. T., Aziz, R. A., Hoffman, R. P., Wu, Y. L., et al. (2023). The complement system and human autoimmune diseases. *J. Autoimmun.* 137, 102979. doi: 10.1016/j.jaut.2022.102979

Dalakas, M. C., Alexopoulos, H., and Spaeth, P. J. (2020). Complement in neurological disorders and emerging complement-targeted therapeutics. *Nat. Rev. Neurol.* 16, 601–617. doi: 10.1038/s41582-020-0400-0

Hong, S., Beja-Glasser, V. F., Nfonoyim, B. M., Frouin, A., Li, S., Ramakrishnan, S., et al. (2016). Complement and microglia mediate early synapse loss in Alzheimer mouse models. *Science* 352, 712–716. doi: 10.1126/science.aad8373

Howell, O. W., Reeves, C. A., Nicholas, R., Carassiti, D., Radotra, B., Gentleman, S. M., et al. (2011). Meningeal inflammation is widespread and linked to cortical pathology in multiple sclerosis. *Brain* 134(Pt 9), 2755–2771. doi: 10.1093/brain/awr182

Lui, H., Zhang, J., Makinson, S. R., Cahill, M. K., Kelley, K. W., Huang, H.-Y., et al. (2016). Progranulin deficiency promotes circuit-specific synaptic pruning by microglia via complement activation. *Cell* 165, 921–935. doi: 10.1016/j.cell.2016.04.001

Magdalon, J., Mansur, F., Silva, A. L. T. E., de Goes, V. A., Reiner, O., and Sertié A. L. (2020). Complement system in brain architecture and neurodevelopmental disorders. *Front. Neurosci.* 14, 23. doi: 10.3389/fnins.2020.00023

Michailidou, I., Jongejan, A., Vreijling, J. P., Georgakopoulou, T., de Wissel, M. B., Wolterman, R. A., et al. (2018). Systemic inhibition of the membrane attack complex impedes neuroinflammation in chronic relapsing experimental autoimmune encephalomyelitis. *Acta Neuropathol. Commun.* 6, 36. doi: 10.1186/s40478-018-0536-y

Michailidou, I., Naessens, D. M. P., Hametner, S., Guldenaar, W., Kooi, E.-J., Geurts, J. J. G., et al. (2017). Complement C3 on microglial clusters in multiple sclerosis occur in chronic but not acute disease: implication for disease pathogenesis. *Glia* 65, 264–277. doi: 10.1002/glia.23090

Michailidou, I., Willems, J. G. P., Kooi, E.-J., van Eden, C., Gold, S. M., Geurts, J. J. G., et al. (2015). Complement C1q-C3-associated synaptic changes in multiple sclerosis hippocampus. *Ann. Neurol.* 77, 1007–1026. doi: 10.1002/ana.24398

Morgan, B. P., and Gasque, P. (1997). Extrahepatic complement biosynthesis: where, when and why? *Clin. Exp. Immunol.* 107, 1–7. doi: 10.1046/j.1365-2249.1997.d01-890.x

Morgan, B. P., Gommerman, J. L., and Ramaglia, V. (2021). An "outside-in" and "inside-out" consideration of complement in the multiple sclerosis brain: lessons from development and neurodegenerative diseases. *Front. Cell. Neurosci.* 14, 600656. doi: 10.3389/fncel.2020.600656

Nonaka, S., and Nakanishi, H. (2019). Microglial clearance of focal apoptotic synapses. *Neurosci. Lett.* 707, 134317. doi: 10.1016/j.neulet.2019.134317

Paolicelli, R. C., Jawaid, A., Henstridge, C. M., Valeri, A., Merlini, M., Robinson, J. L., et al. (2017). TDP-43 depletion in microglia promotes amyloid clearance but also induces synapse loss. *Neuron* 95, 297.e6–308.e6. doi: 10.1016/j.neuron.2017.05.037

Prineas, J. W., Kwon, E. E., Cho, E. S., Sharer, L. R., Barnett, M. H., Oleszak, E. L., et al. (2001). Immunopathology of secondary-progressive multiple sclerosis. *Ann. Neurol.* 50, 646–657. doi: 10.1002/ana.1255

Ramaglia, V., Dubey, M., Malpede, M. A., Petersen, N., de Vries, S. I., Ahmed, S. M., et al. (2021). Complement-associated loss of CA2 inhibitory synapses in the demyelinated hippocampus impairs memory. *Acta Neuropathol.* 142, 643–667. doi: 10.1007/s00401-021-02338-8

Reis, E. S., Mastellos, D. C., Hajishengallis, G., and Lambris, J. D. (2019). New insights into the immune functions of complement. *Nat. Rev. Immunol.* 19, 503–516. doi: 10.1038/s41577-019-0168-x

Ricklin, D., Hajishengallis, G., Yang, K., and Lambris, J. D. (2010). Complement: a key system for immune surveillance and homeostasis. *Nat. Immunol.* 11, 785–797. doi: 10.1038/ni.1923

Ricklin, D., Reis, E. S., Mastellos, D. C., Gros, P., and Lambris, J. D. (2016). Complement component C3 - the "Swiss Army Knife" of innate immunity and host defense. *Immunol. Rev.* 274, 33–58. doi: 10.1111/imr.12500

Schafer, D. P., Lehrman, E. K., Kautzman, A. G., Koyama, R., Mardinly, A. R., Yamasaki, R., et al. (2012). Microglia sculpt postnatal neural circuits in an activity and complement-dependent manner. *Neuron* 74, 691–705. doi: 10.1016/j.neuron.2012.03.026

Stevens, B., Allen, N. J., Vazquez, L. E., Howell, G. R., Christopherson, K. S., Nouri, N., et al. (2007). The classical complement cascade mediates CNS synapse elimination. *Cell* 131, 1164–1178. doi: 10.1016/j.cell.2007.10.036

Thion, M. S., and Garel, S. (2018). Microglia under the spotlight: activity and complement-dependent engulfment of synapses. *Trends Neurosci*. 41, 332–334. doi: 10.1016/j.tins.2018.03.017

van Olst, L., Rodriguez-Mogeda, C., Picon, C., Kiljan, S., James, R. E., Kamermans, A., et al. (2021). Meningeal inflammation in multiple sclerosis induces phenotypic changes in cortical microglia that differentially associate with neurodegeneration. *Acta Neuropathol*. 141, 881–899. doi: 10.1007/s00401-021-02293-4

Vasek, M. J., Garber, C., Dorsey, D., Durrant, D. M., Bollman, B., Soung, A., et al. (2016). A complement-microglial axis drives synapse loss during virus-induced memory impairment. *Nature* 534, 538–543. doi: 10.1038/nature18283

Veerhuis, R., Nielsen, H. M., and Tenner, A. J. (2011). Complement in the brain. *Mol. Immunol*. 48, 1592–1603. doi: 10.1016/j.molimm.2011.04.003

Zelek, W. M., Menzies, G. E., Brancale, A., Stockinger, B., and Morgan, B. P. (2020). Characterizing the original anti-C5 function-blocking antibody, BB5.1, for species specificity, mode of action and interactions with C5. *Immunology* 161, 103–113. doi: 10.1111/imm.13228

Zhou, Z., Xu, M.-J., and Gao, B. (2016). Hepatocytes: a key cell type for innate immunity. *Cell. Mol. Immunol.* 13, 301–315. doi: 10.1038/cmi.2015.97

frontiers in Immunology

ORIGINAL RESEARCH
published: 01 February 2022
doi: 10.3389/fimmu.2022.816640

Periodontal Infection Aggravates C1q-Mediated Microglial Activation and Synapse Pruning in Alzheimer's Mice

*Xiaoxiao Hao[1], Zhaofei Li[1], Wei Li[2], Jannet Katz[1], Suzanne M. Michalek[3], Scott R. Barnum[4], Lucas Pozzo-Miller[2], Takashi Saito[5,6], Takaomi C. Saido[5], Qin Wang[7], Erik D. Roberson[8] and Ping Zhang[1]**

[1] Department of Pediatric Dentistry, School of Dentistry, University of Alabama at Birmingham, Birmingham, AL, United States, [2] Department of Neurobiology, School of Medicine, University of Alabama at Birmingham, Birmingham, AL, United States, [3] Department of Microbiology, School of Medicine, University of Alabama at Birmingham, Birmingham, AL, United States, [4] CNine Biosolutions, LLC, Birmingham, AL, United States, [5] Laboratory for Proteolytic Neuroscience, RIKEN Center for Brain Science, Wako, Japan, [6] Department of Neurocognitive Science, Institute of Brain Science, Nagoya City University Graduate School of Medical Sciences, Nagoya, Japan, [7] Department of Cell, Developmental and Integrative Biology, School of Medicine, University of Alabama at Birmingham, Birmingham, AL, United States, [8] Center for Neurodegeneration and Experimental Therapeutics, Alzheimer's Disease Center, Department of Neurology, School of Medicine, University of Alabama at Birmingham, Birmingham, AL, United States

OPEN ACCESS

Edited by:
Moncef Zouali, Institut National de la Santé et de la Recherche Médicale (INSERM), France

Reviewed by:
Ben J. Gu, University of Melbourne, Australia
Marta Olah, Columbia University Irving Medical Center, United States

***Correspondence:**
Ping Zhang
pingz@uab.edu

Specialty section:
This article was submitted to Molecular Innate Immunity, a section of the journal Frontiers in Immunology

Received: *16 November 2021*
Accepted: *11 January 2022*
Published: *01 February 2022*

Citation:
Hao X, Li Z, Li W, Katz J, Michalek SM, Barnum SR, Pozzo-Miller L, Saito T, Saido TC, Wang Q, Roberson ED and Zhang P (2022) Periodontal Infection Aggravates C1q-Mediated Microglial Activation and Synapse Pruning in Alzheimer's Mice. Front. Immunol. 13:816640. doi: 10.3389/fimmu.2022.816640

Periodontitis is a dysbiotic infectious disease that leads to the destruction of tooth supporting tissues. There is increasing evidence that periodontitis may affect the development and severity of Alzheimer's disease (AD). However, the mechanism(s) by which periodontal infection impacts the neurodegenerative process in AD remains unclear. In the present study, using an amyloid precursor protein (APP) knock-in (*App* KI) AD mouse model, we showed that oral infection with *Porphyromonas gingivalis* (Pg), a keystone pathogen of periodontitis, worsened behavioral and cognitive impairment and accelerated amyloid beta (Aβ) accumulation in AD mice, thus unquestionably and significantly aggravating AD. We also provide new evidence that the neuroinflammatory status established by AD, is greatly complicated by periodontal infection and the consequential entry of Pg into the brain *via* Aβ-primed microglial activation, and that Pg-induced brain overactivation of complement C1q is critical for periodontitis-associated acceleration of AD progression by amplifying microglial activation, neuroinflammation, and tagging synapses for microglial engulfment. Our study renders support for the importance of periodontal infection in the innate immune regulation of AD and the possibility of targeting microbial etiology and periodontal treatment to ameliorate the clinical manifestation of AD and lower AD prevalence.

Keywords: Periodontitis, *Porphyromonas gingivalis*, Alzheimer's disease, microglia, complement C1q, synapse loss

INTRODUCTION

Alzheimer's disease (AD), an age-related neurodegenerative disease of the central nervous system (CNS), is the most common cause of dementia and is characterized by progressive and irreversible decline in behavioral and cognitive function (1). AD affects more than 50 million people globally and is the sixth leading cause of death in the US (2). Despite great efforts, the cellular and molecular mechanisms underlying AD pathogenesis are not fully understood, and there is no effective therapy to cure or ameliorate this devastating disease (3, 4). Therefore, there is an urgent need to identify modifiable risk factors that impact AD, so that strategies that mitigate AD severity are implemented.

Periodontitis is a chronic infectious disease characterized by periodontal inflammation and alveolar bone loss, and is the primary cause of tooth loss in adults (5). Increasing evidence suggests that periodontitis is associated with a diversity of systemic disorders, including AD (6). In this regard, epidemiological studies indicate that there is a positive correlation between cognitive decline in AD patients and periodontitis (7, 8). In addition, periodontitis has been shown to positively associate with brain amyloid plaque development, a pathological hallmark of AD, in elderly and AD patients (9). Furthermore, *Porphyromonas gingivalis* (Pg), a keystone pathogen of periodontitis, as well as its virulence factors lipopolysaccharide (LPS) and gingipains, have been detected in the post-mortem brains from AD patients (10, 11). However, mechanisms underlying the association between periodontitis and the development of AD is lacking.

Microglia cells are the most common innate immune cells in the CNS and play a central role in maintaining the immune homeostasis in the brain (12). However, microglia overactivation can lead to sustained neuroinflammation and contribute to the pathogenesis of neurodegenerative diseases (13). The complement system, also known as the complement cascade, represents a major part of innate immunity and comprises an interactive network of soluble and membrane-associated proteins that activate, amplify, and regulate immunity and inflammation (14, 15). Although the complement system provides rapid recognition and response to dangers that threaten the host, a dysregulated complement system can also mediate destructive inflammation (15). Clinical and experimental studies have suggested the involvement of periodontal complement activation in the pathogenesis of periodontitis (6, 16, 17). There is also emerging evidence suggesting that aberrant complement activation is involved in AD development (18–20). However, the role complement and microglial activation in the association of periodontitis and AD is not clear.

In this study, using the amyloid precursor protein (APP) knock-in (*App* KI) mouse model, we sought to determine the effect of Pg infection on the progressive neurodegeneration of AD and the involvement of complement C1q in the process. We demonstrated the importance of micorglia and complement component C1q in the aggravation of AD neuropathologies in the presence of periodontal infection. Our study suggests a "two-hit" model of Pg-mediated aggravation of AD, with amyloid β (Aβ) accumulation as the first hit, and Pg brain invasion as the second hit to faciliate synaspse loss.

MATERIALS AND METHODS

Mice

C57BL/6 wild-type (WT) mice were obtained from Jackson Laboratories (Ellsworth, ME, USA). $App^{NL\text{-}G\text{-}F/NL\text{-}G\text{-}F}$ knock-in (*App* KI) mice (21) that carry the APP Swedish (KM670/671NL), Iberian (I716F), and Arctic (E693G) mutations were originally obtained under a material transfer agreement from Dr. Takaomi Saido (RIKEN Brain Science Institute, Japan), and had been backcrossed for more than 12 generations to obtain the C57BL/6 background. Animals were housed in an environmentally controlled facility at the University of Alabama at Birmingham (UAB), protocols for all animal studies were approved by the UAB Institutional Animal Care and Use Committee.

Bacterial Culture and Infection Model

Pg ATCC 33277 was cultured in trypticase soy broth (BD Biosciences) containing 1% yeast extract, 5 μg/mL hemin, and 1 μg/mL menadione and grown at 37°C in an anaerobic atmosphere of 10% H2, 5% CO2, and 85% N2 (22). Pg infection was carried out as previously described (23) with some modifications (**Figure 1A**). Briefly, age- and sex-matched WT and *App* KI mice (6 weeks of age) were randomly assigned to control or Pg-infected groups. Mice were provided drinking water containing kanamycin (1 mg/ml) for 7 days to reduce the indigenous oral microflora. After removing antibiotics for 3 days, experimental mice were given 100 μl of freshly harvested Pg (10^{10} CFU/ml) in 2% carboxymethylcellulose (CMC) and control groups received 100 μl of 2% CMC by oral gavage 3 times per week for 6 weeks. Mice were refrained from food and water intake for 1 hour (h) after infection.

Evaluation of Alveolar Bone Loss and Periodontal Inflammation

Groups of mice were sacrificed 2 weeks post the last dose of Pg to assess the establishment of periodontitis. Specifically, the right maxilla from each mouse was fixed and then stained with 1% methylene blue (24). The distance between the cementum-enamel junction (CEJ) and the alveolar bone crest (ABC) was measured at a total of seven buccal sites with the assistance of an Image J analysis system (NCBI). To assess periodontal inflammation, gingival tissues around the left maxillary molars were collected, homogenized, and analyzed for inflammatory gene expression as described below.

Behavioral Tests

Three behavioral tests were carried out at 4, 6 and 10 months of age (**Figure 1A**). On each testing day, groups of mice were transferred to the testing room 1 h before testing for acclimatization. On day 1 of indicated age, mice were tested for general locomotor activity and exploration habits in the open field (OF) test (25). On day 2, elevated zero maze (EZM) was conducted to evaluate anxiety-related behavior (26). After resting

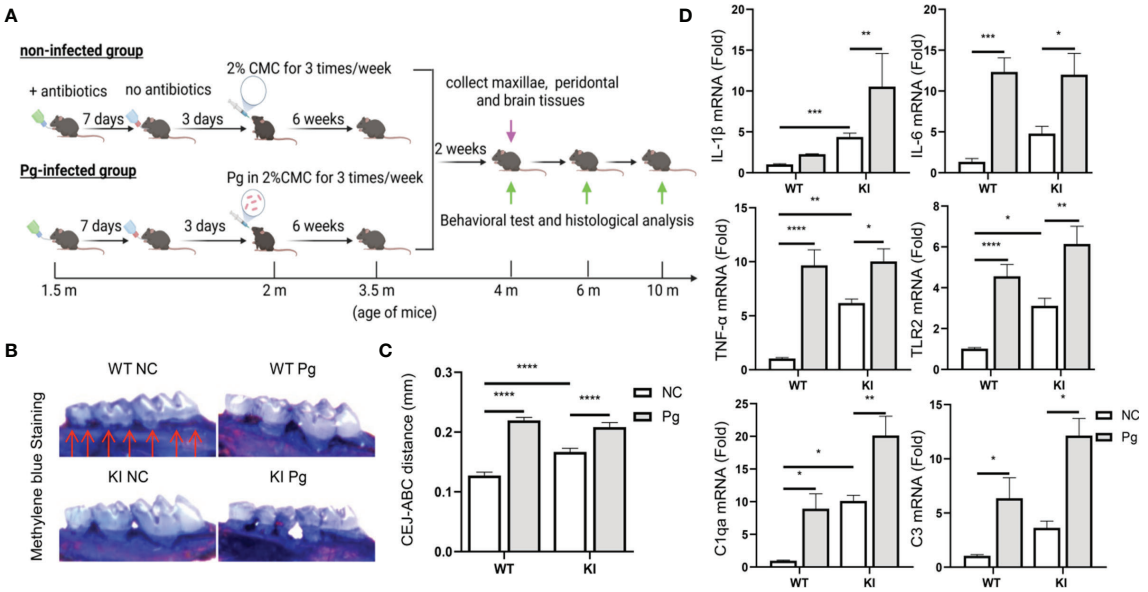

FIGURE 1 | Pg-induced alveolar bone loss and periodontal inflammation in *App* KI and WT mice following oral infection. **(A)** Schematic of the experimental design used in this study. m, month. **(B)** Representative methylene blue-stained maxillae from non-infected (NC) and Pg-infected WT and *App* KI mice (n=9 mice/group). Bone loss was assessed in a total of 7 buccal sites (red arrows) per mouse. **(C)** Alveolar bone loss in Pg-infected and non-infected WT and *App* KI mice; mm, millimeter; CEJ-ABC, cemento-enamel junction-alveolar bone crest. **(D)** Inflammatory cytokine and complement gene expression in gingival tissues from non-infected and Pg-infected WT and *App* KI mice. Gene expression was normalized to GAPDH and expressed as fold changes. Samples were done in duplicate (n=7 mice/group). Data are expressed as mean ± SEM. $^{*}P < 0.05$, $^{**}P < 0.01$, $^{***}P < 0.001$, $^{****}P < 0.0001$, by two-way ANOVA followed with Tukey correction.

for a day, mice were subjected to Morris water maze (MWM) for 5 days followed by probe trial to assess learning performance and reference memory, respectively (27). All behavioral tests were conducted during the light phase of the diurnal cycle and data were collected using an EthoVision video tracking system (Noduls).

Evaluation of Aβ Peptide Accumulation in the Brain

To evaluate brain Aβ peptide accumulation, groups of mice were anesthetized and perfused with PBS (28). Brains were collected after perfusion and one side hemispheres were dissected, and cortices and hippocampi were isolated and homogenized in carbonate buffer supplemented with proteinase inhibitor cocktail (29). The supernatants were collected as the carbonate-soluble parts. The pellets were subjected to further homogenization in guanidine solution, and the supernatants were collected as the carbonate-insoluble fractions. The levels of hAβ42 in the soluble and insoluble fractions were measured using a hAβ42-specific ELISA kit (Invitrogen, #KHB3442), following the manufacturer's instructions. The other side hemispheres were fixed in 4% paraformaldehyde (PFA) and used for immunohistochemistry staining as described below.

Immunohistochemistry and Immunofluorescence Staining

Formalin-fixed, paraffin-embedded hemispheres were sectioned in the coronal plane at 7 μm. For analysis of Aβ plaque depositions, sections were treated with 70% formic acid after de-paraffinization and rehydration (30). Following antigen retrieval, sections were probed with an anti-Aβ antibody (6E10) (Biolegend, #803004) followed by HRP-labeled secondary antibody (JacksonImmuno, #711-035-150). A Thyramide signal amplification kit (Perkin Elmer) was used to enhance the sensitivity of detection. Nuclei were stained with DAPI. For detection of microglial and C1q activation and colocalization, sections were stained with antibodies against IBA1 (Cell signaling, #17198), and/or C1qa (Abcam, #ab182451). Data were acquired with a KEYENCE BZ-800 microscope and images were processed using an ImageJ analysis system. To examine synapse loss, mice were perfused with PBS as described above, and then further perfused with 50-60 ml 4% PFA/PBS to facilitate rapid and even fixation (31). Brain sectioned at 35 μm thickness were prepared and free-floating sections were stained for PSD95 (Cell signaling, #3450S), SNAP25 (Abcam, #ab109105), or co-stained for IBA1 or C1q. For quantitative analysis of synapses and the presence of C1q at the synapses, regions of interest (ROI) were acquired with a Zeiss LSM-800 Airyscan confocal microscope and analyzed using Puncta analyzer (Duke University) run in the ImageJ analysis system (32). About 50-100 synapses ($SNAP25^{+}$ or $PSD95^{+}$puncta) were recorded per mouse per ROI and the number of $C1qa^{+}$ particles present per synapse was scored. For microglia engulfment, brain sections were imaged up to 25 Z-stacks at 0.33 μm steps (32). Ten to fifteen microglia within the hippocampus CA1 region and cortex, per mouse, were randomly selected and analyzed.

Genomic DNA Extraction of Brain Tissue and PCR Analysis of Pg

Genomic DNA (gDNA) was extracted from mice brain tissues using a Blood and Tissue Kit (Qiagen), followed by standard PCR and qPCR to assess for Pg specific *hum*Y gene and 16S ribosomal RNA (16S rRNA), respectively (33, 34). Primer sequences are listed in **Table S1**.

Fluorescence *In Situ* Hybridization (FISH) for Detection of Pg in Mouse Brain

FISH was conducted using probes specific to Pg 16S rRNA gene sequence on rehydrated brain sections, as previously described (35). Briefly, after deparaffinization and antigen retrieval, brain sections were probed with 5 pmol of Pg 16S rRNA-specific oligonucleotide POG (SILVA, ribosomal RNA database) 5'-CAA TAC TCG TAT CGC CCG TTA TTC-3' labeled with fluorescein isothiocyanate (synthesized at Integrated DNA Technologies). Data were acquired with a KEYENCE BZ-800 microscope and images were processed using ImageJ.

Quantitative Reverse Transcription PCR (RT-qPCR)

To analyze the gene expression of inflammatory cytokines and complement components in gingival tissues, brain tissues, or cultured microglia cells, tissues or cells were homogenized and total RNA were extracted using Direct-zol RNA Miniprep kit (ZYMO Research, #R2052). cDNA was synthesized using a PrimeScript RT Reagent kit (Takara, #RR037) using equal amount of RNA. RT-qPCR was performed using an ABI Prism 7500 fast system (Applied Biosystems) with the 2x qPCR Master Mix (NEB, #M3003). All primers information is listed in **Table S1**.

Complement Component ELISA

Brain tissues were collected from groups of mice, weighed and homogenized in PBS with protease inhibitors cocktail. Homogenized brain tissues then underwent 3 freeze-thaw cycles and supernantants were collected after centrifugation. The levels of C1qa and C3 in the supernatants were assessed by ELISA according to the manufacturer's instructions (Mybiosource, #MBS921993 and #MBS763294).

Preparation of Oligomeric Aβ (Aβo)

Aβo was prepared as previously described (36). Briefly, the $A\beta_{1-42}$ synthetic peptide (Bachem, #4045866) was suspended in 100% 1,1,1,3,3,3 hexafluoro-2-propanol (HFIP) and then incubated for complete solubilization under shaking at 37°C for 2 h. HFIP/peptide was dried in a flammable hood for 6-8 h, and re-suspended in DMSO. An oligomeric form of the peptide was further generated by pre-incubation for 24-72 h at 37°C before adding to the cultures.

Primary Microglia Culture

Primary microglia were generated from cerebral cortices of WT newborn pups (postnatal day 0), as previously described (37). Briefly, brains were harvested, and the meninges were removed. Cortices and hippocampi were then dissected into small pieces and triturated in Hanks' balanced salt solution (HBSS) and cultured in Dulbecco's modified eagle medium (DMEM) containing 16 mM HEPES, 1x non-essential amino acids, 1x L-glutamine, 10% fetal bovine serum (FBS) and 50 μg/ml gentamicin for 10 days until confluent. Microglia were collected and then re-suspended in fresh media and cultured for 18-24 h prior to stimulation. Microglia ($1x10^6$) were treated with Aβo (0.1 μM, 1 μM and 10 μM), Pg (MOI =50), Pg plus Aβo, or pre-treated with Aβo for 6 h followed by 24 h Pg stimulation. To test the role of complement activation in Pg-induced inflammatory responses in microglia, microglia were pre-incubated with 100 ng/ml C1 esterase inhibitor (C1-INH, Sigma, #E0518) for 4 h, followed by Aβo treatment for 6 h, and then by Pg stimulation for 24 h. To specially test the effect of C1q on Pg-induced inflammatory responses, microglia cells were transfected with lentivirus pLKO.1 puro containing C1qa shRNA (target sequence CCGGCTTCTATTACTTCAAC TCGAG) or scramble RNA. Successful transfection was verified by analyzing C1qa mRNA and protein expression in microglia. The stably transfected microglia were then stimulated with Pg (MOI=50) for 24 h. The cells were then collected, and RNA was extracted for analyzing the gene expression of inflammatory cytokines and complement components by RT-qPCR.

Microglia-Neuron Co-Culture

Primary neuronal cultures were prepared from the cortices of WT newborn mice using a Pierce™ primary neuron isolation kit (ThermoFisher, #88280). Neurons were used after 13-14 days of *in vitro* culturing (38). Primary microglia expressing C1qa shRNA or scramble vector were pretreated with Pg (MOI=50) for 4 h or left untreated, and then added to the neuron cultures (neuron: microglia ratio 3:1) (37). After 24 h, microglia cells were sorted from the co-cultures by FACS. The presence of synapses in microglia was analyzed by western blotting. To visualize microglia elimination of synapses, co-cultured cells were stained for IBA1 and PSD95, and then imaged on a Zeiss LSM-800 Airyscan confocal microscope as described above. Eight to ten microglia were analyzed per well, and the number of PSD95 puncta, as well as the puncta within microglia were quantified.

Western Blotting

Equal amount of proteins (30 μg/sample) from sorted microglial lysates were run on 4%-15% mini-protean TGX stain-free precast gels (Bio-Rad) and electrotransferred to PVDF membranes (Bio-Rad). Membranes were probed with specifc antibodies against C1qa (Santa Cruz, #sc-58920), PSD95 (Santa Cruz, #sc-32290), NeuN (Abcam, #ab104224), and Tubulin (Cell signaling, #2148). Membranes were visualized using an Odyssey infrared Imaging system (LI-COR) and processed on Image J software.

Statistical Analysis

All data are expressed as mean ± SEM and statistical significance was analyzed using GraphPad Prism (version 8.0.2, GraphPad Software Inc., San Diego, CA). One-tailed, unpaired Student *t*-

tests were used for comparison between two groups. One-way ANOVA or two-way ANOVA followed by Tukey's correction were used for analysis of more than two groups. A *P* value less than 0.05 was considered as significant.

RESULTS

Pg Infection Induces Alveolar Bone Loss and Increases Complement Activation in Periodontal Tissues

Following Pg infection, significantly increased alveolar bone loss were seen at 4 months of age in WT and *App* KI mice, when compared with their respective non-infected controls (**Figures 1B, C**). In addition, increased levels of Toll-like receptor 2 (TLR2) and inflammatory cytokine (IL-1β, IL-6 and TNF-α) gene expression were detected in the gingival tissues of WT and *App* KI mice following Pg infection (**Figure 1D**). Furthermore, Pg infection significantly increased the gene expression of C1qa, the subunit A of the initiating protein C1q of the classical complement pathway, and C3, the central component of the complement system (15), in the gingival tissues of *App* KI and WT mice (**Figure 1D**). Noteworthy, without Pg infection, higher levels of inflammatory cytokine and complement gene expression, as well as alveolar bone loss, were seen in *App* KI mice than in WT mice, indicating that AD mice have a higher baseline of periodontal inflammation.

Pg Infection Accelerates the Progression of Cognitive and Behavioral Impairment in *App* KI Mice

The main clinical symptom of AD is a decline in memory and cognitive function (39). Although associations between periodontitis and AD have been made, conclusive evidence of the influence of periodontitis on AD has not been clearly established. To assess the impact of periodontitis on the development of cognitive and behavioral impairment, behavioral tests were carried out at three time points (**Figure 1A**). We did not observe any significant behavior changes between any of the groups at 4 months of age (data not shown). However, at 6 months of age, compared to non-infected *App* KI mice, Pg-infected *App* KI mice showed significantly increased locomotor activity by OF test (**Figure 2A**), increased anxiety-related behavior by EZM test (**Figure 2B**), and impaired spatial learning and memory by MWW test and probe trial (**Figures 2C, D**). No significant difference was observed in WT mice with or without Pg infection, or between non-infected WT and *App* KI mice. At 10 months of age, non-infected *App* KI mice developed clear deficits in the MWM test when compared with non-infected WT mice (**Figures 2E, F**). In addition, Pg infection significantly increased the cognitive deficits in *App* KI mice. These results demonstrate that periodontal infection accelerates the progression of cognition and behavioral impairment in AD mice.

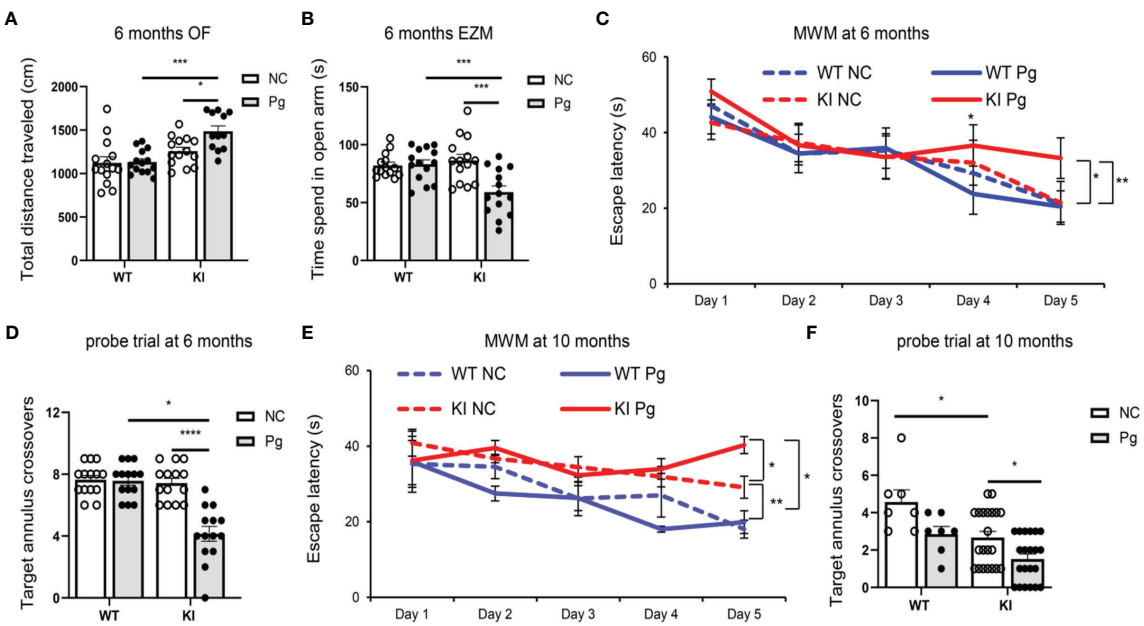

FIGURE 2 | Pg infection worsens cognitive and behavior impairment in *App* KI mice. **(A)** Total distance traveled in open field (OF) tests at 6 months of age. cm, centimeter. **(B)** Time spent in open arm in elevated zero maze (EZM) tests at 6 months of age. s, second. **(C, E)** Escape latency in Morris water maze (MWM) tests at 6 **(C)** and 10 **(E)** months of age. **(D, F)** Target annulus crossovers in probe trial tests at 6 **(D)** and 10 **(F)** months of age. A-D, n=14/group; E-F, n=21/group (*App* KI mice), n=7/group (WT mice). Data are expressed as mean ± SEM. **P* < 0.05, ***P* < 0.01, ****P* < 0.001, *****P* < 0.0001 by two-way ANOVA followed with Tukey correction.

Pg Infection Exacerbates Brain Aβ Production and Amyloid Plaque Deposition in AD Mice

The development of amyloid plaque, composed mainly of the peptide Aβ, is a pathological hallmark of AD (40). We next questioned how Pg infection influences brain Aβ accumulation and amyloid plaque deposition in *App* KI mice. At 4 months of age, accumulation of soluble and insoluble hAβ42 peptide was noted in the brains of *App* KI mice, and Pg infection significantly increased the accumulation of soluble hAβ42 in the hippocampus of *App* KI mice (**Figure 3A**). Time-dependent accumulation of hAβ42 in the brains of non-infected *App* KI mice was seen at 6 and 10 months of age (**Figures 3B–E**), compared to the level at 4 months. In addition, Pg infection further enhanced hAβ accumulation in *App* KI mice at 6 and 10 months of age. Consistently, immunohistochemical analysis of brain sections demonstrated significantly increased amyloid plaque deposition in non-infected *App* KI mice at 10 months of age compared to 6 months of age, as measured by the number of plaques, the average size of plaques, and the total area occupied by the plaques in hippocampus and cortex (**Figures 3F–H**). Furthermore, Pg infection significantly increased amyloid plaque deposition in *App* KI mice at 6 and 10 months of age.

Pg Invades the Brain and Potentiates Neuroinflammation and Complement Activation in AD Mice

Recent studies have shown that the number of Pg, and its LPS and gingipains, were significantly higher in the autopsied brain tissues of AD patients than in non-demented controls (10, 11), suggesting that Pg can pass the blood-brain barrier (BBB). To verify Pg brain invasion following oral gavage infection, we first assessed the presence of the *hmuY* gene, a highly specific gene essential for Pg survival and virulence (33), in the brains of WT and *App* KI mice. While non-infected WT and *App* KI controls were negative for the *hmuY* gene, both Pg-infected WT and *App* KI brains were positive for this gene (**Figure 4A**). We next analyzed the presence of Pg 16S rRNA. Both WT and *App* KI brains showed significantly increased expression of Pg 16S rRNA following Pg infection (**Figure 4B**). Noteworthy, a significantly higher level of Pg 16S rRNA was detected in the brain tissues from *App* KI mice as compared to those from WT mice following Pg infection. The presence of Pg in the brain tissues

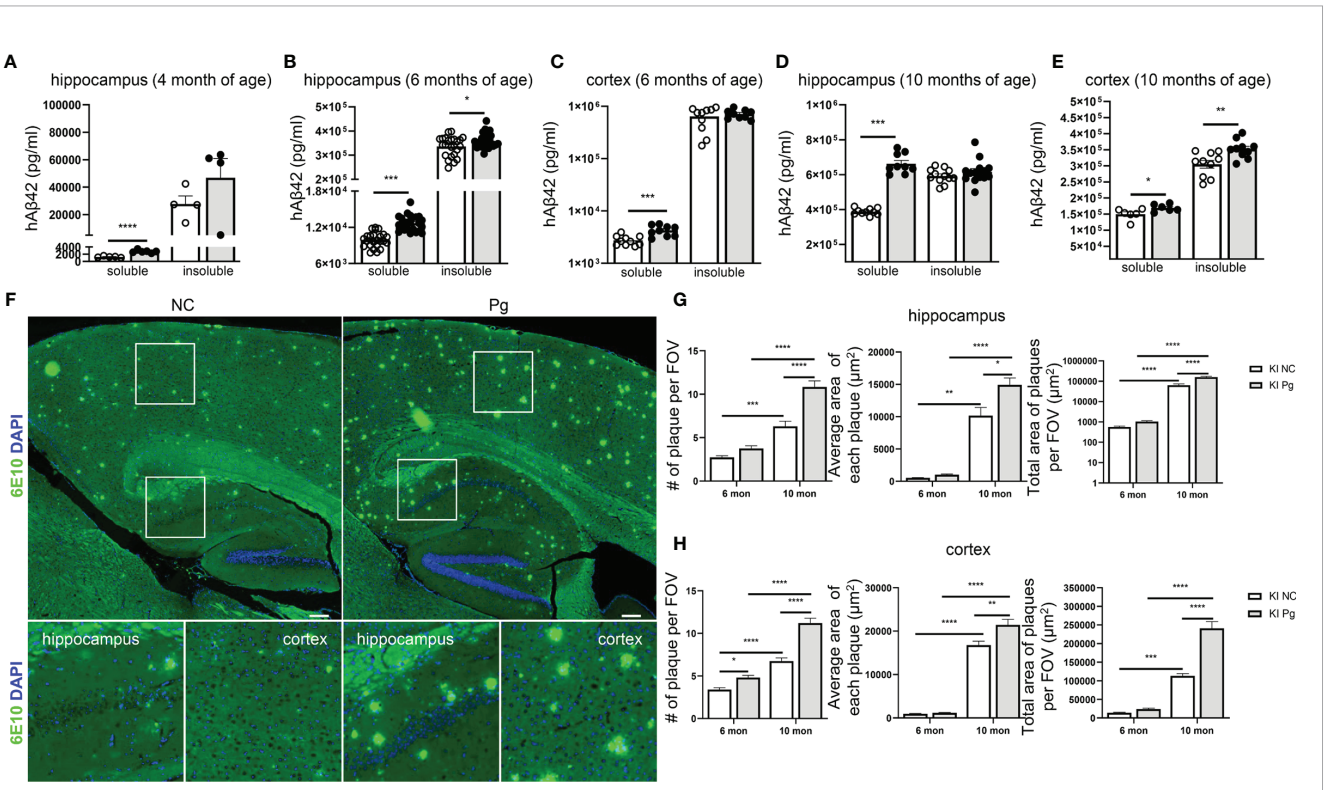

FIGURE 3 | Pg infection accelerates Aβ production and plaque formation in *App* KI mice. **(A–E)** Levels of soluble and insoluble hAβ42 in the brains of control and Pg-infected *App* KI mice at 4, 6 and 10 months of age. A, n=4-6/group; B, n=24/group; C-E, n=6-10/group. Samples were run in duplicate in ELISA. **(F)** Representative micrographs showing Aβ plaques formation in *App* KI mice at 10 months of age. Whole brain images were stitched with 30 series micrographs captured at 10 x objective using a KEYENCE BZ-800 microscope. Boxed areas were further enlarged. Aβ plaques were labeled with 6E10 (green) and cell nuclei were labeled with DAPI (blue). **(G, H)** Quantification of the number of Aβ plaques, average plaque size, and total plaque-occupied area per field of view (FOV) in the hippocampus **(G)** and cortex **(H)** of *App* KI mice at 6 and 10 months of age. Five representative regions of the cortex and hippocampus were captured at 40x objective from each brain section and quantified (n=5-7/group). Data are expressed as mean ± SEM. $^{*}P < 0.05$, $^{**}P < 0.01$, $^{***}P < 0.001$, $^{****}P < 0.0001$ by unpaired Student *t*-test **(A–E)**, or by two-way ANOVA followed with Tukey correction **(G, H)**.

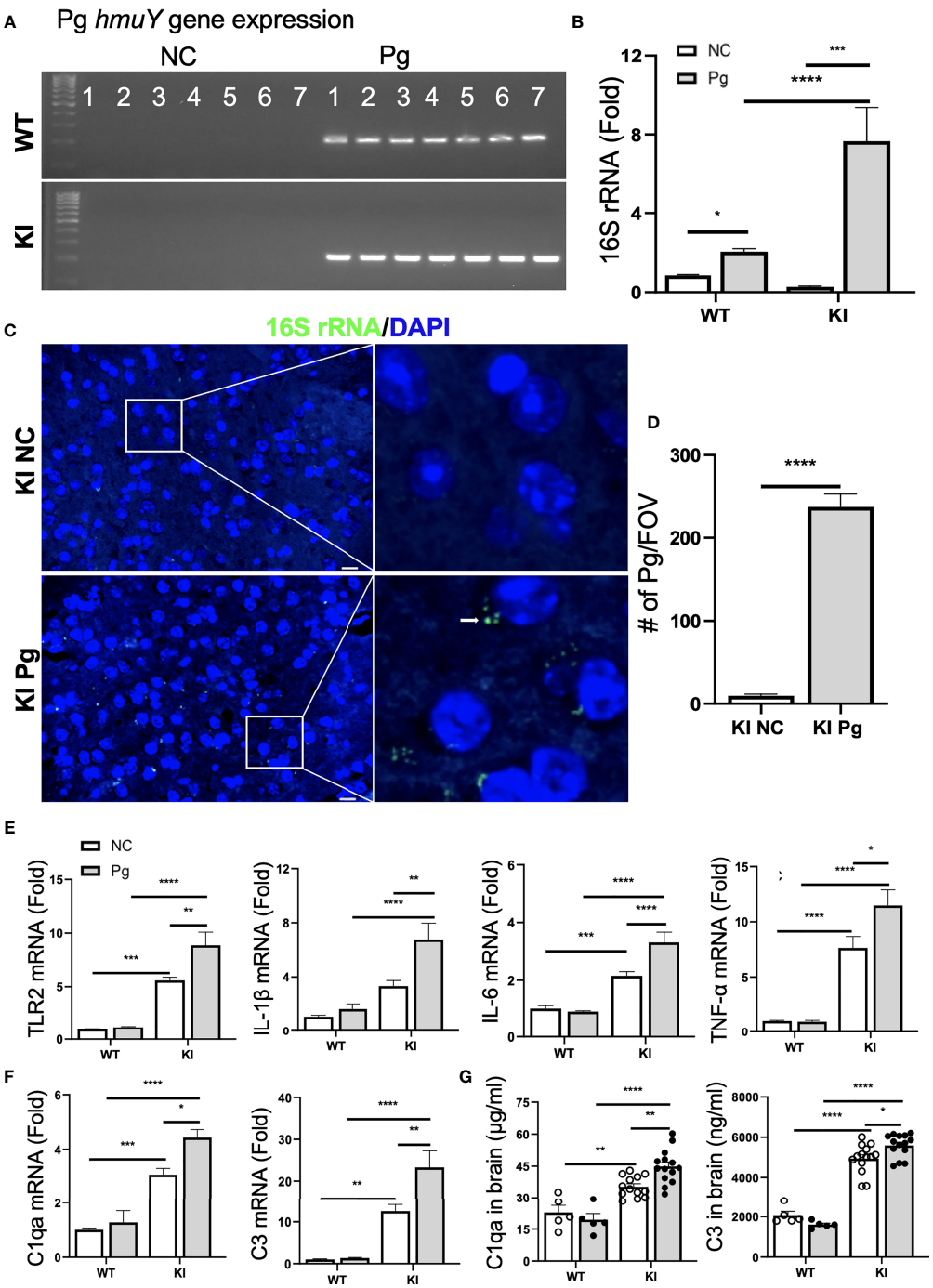

FIGURE 4 | Pg invades the brain and induces neuroinflammation and complement activation. **(A)** Pg-specific *hmuY* gene expression in brains from WT and *App* KI mice. **(B)** Pg-specific 16S rRNA expression in brains from WT and *App* KI mice. The levels of gene expression were normalized to GAPDH and shown as fold changes. Samples were run in duplicates (n=7/group). **(C)** Representative micrographs depicting intracellular localization of Pg in the cortex of brains from *App* KI mice. Pg were probed with 16S rRNA with FITC (green, arrowhead) and nuclei were labeled with DAPI (blue). Boxed areas were further enlarged. Scale bar, 10 μm. **(D)** Quantification of Pg in brain sections from non-infected and Pg-infected *App* KI mice. Five representative regions were captured at 40 x objective from each brain section and quantified (n=5-7/group); FOV, field of view. **(E)** The relative gene expression of inflammatory cytokines and TLR2 in brain tissues from WT and *App* KI mice. Samples were done in duplicates (n=5-7/group). **(F)** The relative gene expression of C1qa and C3 in brain tissues from WT and *App* KI mice. Samples were run in duplicates (n=5-7/group). **(G)** The levels of C1qa and C3 in the brains of WT and *App* KI mice. Samples were run in duplicates (WT mice, n=5-7/group; *App* KI mice, n=10-12/group). Data are expressed as mean ± SEM; $^{*}P < 0.05$, $^{**}P < 0.01$, $^{***}P < 0.001$, $^{****}P < 0.0001$ by two-way ANOVA followed with Tukey correction **(B, E–G)** or by unpaired Student *t*-test **(D)**.

of Pg-infected *App* KI mice was further ascertained by FISH using Pg specific 16S rRNA probe. Hybridization of the 16S rRNA probe to bacterial aggregates was located at the perinuclear regions of brain cells in Pg-infected *App* KI mice (**Figures 4C, D**). No Pg 16S rRNA was detected in non-infected *App* KI mice brains. These results demonstrate that upon the establishment of periodontal infection, Pg can access the brain and that AD mice are more susceptible to Pg brain invasion than WT mice.

Neuroinflammation is a critical component of neurodegenerative diseases like AD (41). Thus, we next determined how oral Pg infection affected the neuroinflammatory status of experimental mice. Without Pg infection, *App* KI mice showed significantly higher levels of TLR2 and inflammatory cytokine gene expression than WT mice (**Figure 4E**). Pg infection further enhanced the expression of these genes in the brains of *App* KI mice, while a minimal inflammatory response was observed in WT mice following Pg infection. Similar results were seen with C1qa and C3 gene and protein expression in the brains of WT and *App* KI mice. Non-infected *App* KI mice showed significantly higher levels of brain C1qa and C3 gene and protein expression than WT mice, and Pg infection further enhanced their expression in the brains of *App* KI mice (**Figures 4F, G**). However, minimal C1qa and C3 response was noted in the brains of WT mice following Pg infection. These results suggest that periodontal infection contribute significantly to the neuroinflammatory milieu established by AD possibly *via* activation of complement system.

Pg Infection Enhances Microglia Activation and Their Colocalization With C1q in *App* KI Mice

As the major immune cells in the CNS, microglia activation is an invariable feature of AD pathology, and activated microglia represent a major source of inflammatory factors in AD (42). We next assessed the activation of microglia and the spatial association between microglia and C1q in *App* KI mice. Pg infection significantly increased the number of $IBA1^+$ microglia in *App* KI mice (**Figures 5A–C**). In addition, a significant increase in the number of $C1qa^+IBA1^+$ cells was observed in Pg-infected *App* KI mice.

Pg Amplifies Aβ-Primed Microglia Activation *via* C1q

Given that AD mice exhibited neuroinflammation without Pg infection, and that Pg entered the brains of WT mice but induced minimal neuroinflammation compared to AD mice, we questioned if a potential interplay between Pg and Aβ could result in the increased neuroinflammation observed in AD mice. Primary microglia were cultured with different concentrations of Aβo, Pg, Aβo together with Pg, or pre-treated with Aβo followed by Pg infection. Interestingly, while Aβo alone at various doses induced very low levels of inflammatory cytokine and complement gene expression in microglia (**Figures 6A, B**), co-stimulation of microglia with Aβo and Pg at the same time decreased the gene expression of inflammatory cytokines as compared to Pg stimulation alone (**Figure 6A**). However, pre-

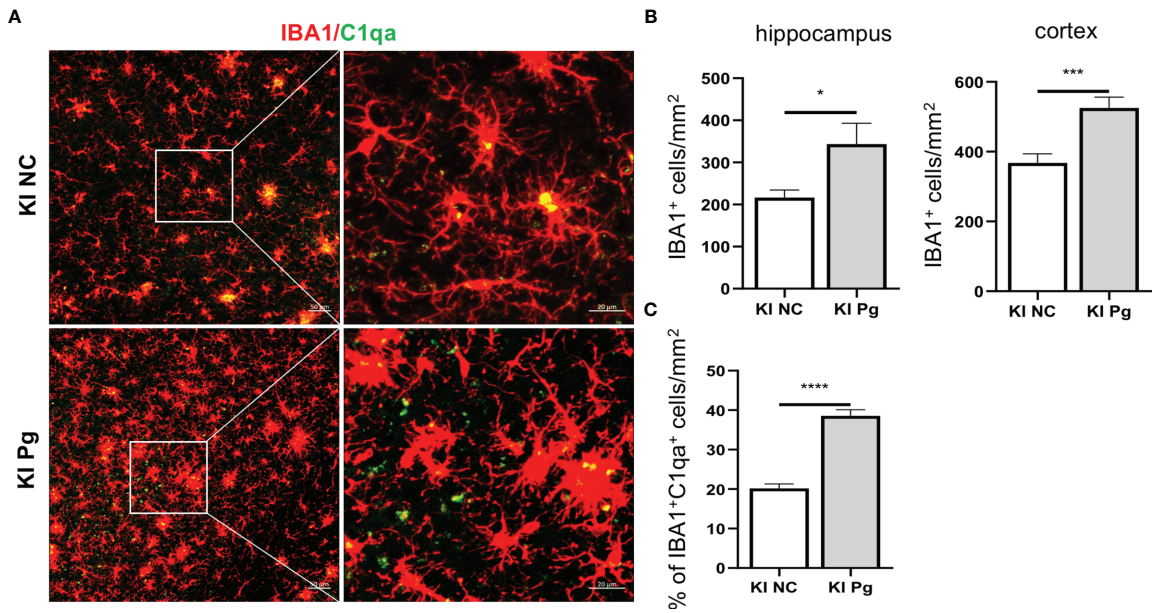

FIGURE 5 | Pg activates microglia in *App* KI mice and co-localize with complement C1q. Brain sections from 6-month-old non-infected and Pg-infected *App* KI mice were immune-stained with antibodies against IBA1and C1qa. **(A)** Representative Z-stack images of brain sections depicting the spatial association between microglia (red) and C1qa (green). **(B)** Quantification of $IBA1^+$ cells in the hippocampus and cortex regions. n=6-7 mice/group. **(C)** Percentage of $IBA1^+C1qa^+$ microglia in non-infected and Pg-infected *App* KI mice. Five representative micrographs of the cortex and hippocampus regions from each mouse were analyzed (n=5-7 mice/group). Data are expressed as mean ± SEM. $^*P < 0.05$, $^{***}P < 0.001$, $^{****}P < 0.0001$ by unpaired Students *t*-test.

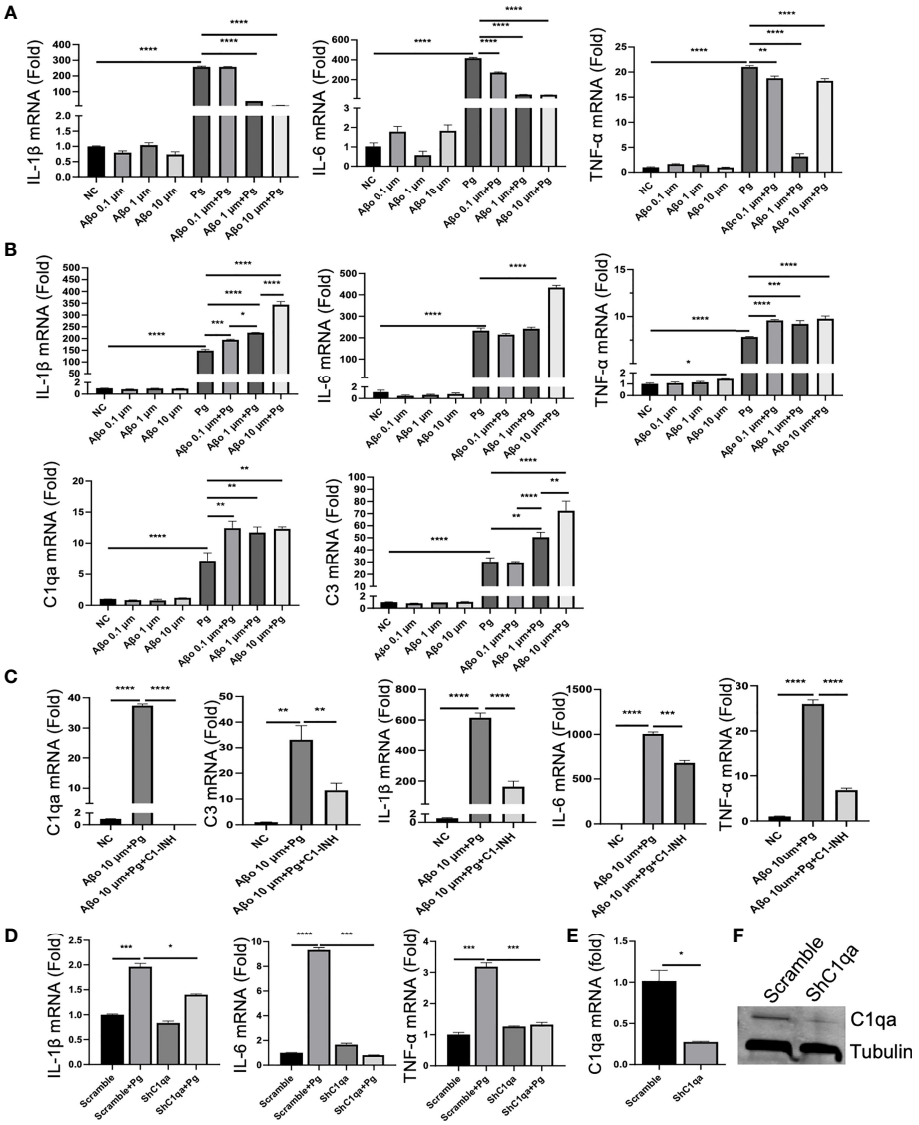

FIGURE 6 | Effect of Aβo and complement activation on Pg-induced microglial inflammatory responses. **(A, B)** Aβo on Pg-induced cytokine production and complement activation. Primary microglia were treated with Aβo (0.1, 1 or 10 μM), Pg (MOI=50), or co-stimulated with Aβo and Pg for 24 h **(A)**, or pretreated with Aβo for 6 h followed by Pg stimulation for 24 h **(B)**. Relative gene expression of IL-1β, IL-6, TNF-α, C1qa, and C3 was analyzed by RT-qPCR. **(C)** C1 inhibition on Pg-induced inflammatory gene expression by microglia. Primary microglia were untreated or pretreated with C1-INH for 4 h, and then treated with Aβo (10 μM) for 6 h followed by Pg (MOI=50) for 24 h. Relative gene expression of C1qa, C3, IL-1β, IL-6, and TNF-α in microglia were analyzed by RT-PCR**. (D)** Effect of C1qa depletion on Pg-induced cytokine gene expression by microglia. Primary microglia cells expressing scramble or C1qa shRNA vectors were treated with Pg (MOI=50) for 24 h. Relative gene expression of IL-1β, IL-6, TNF-α in microglia were analyzed by RT-PCR. Expression of C1qa mRNA **(E)** and protein **(F)** in primary microglia verified by RT-PCR and Western blot. Samples were run in duplicates. Data are expressed as mean ± SEM of three independent experiments; $^{*}P < 0.05$, $^{**}P < 0.01$, $^{***}P < 0.001$, $^{****}P < 0.0001$ by one-way ANOVA followed with Tukey correction.

treatment of microglia with Aβo significantly potentiated Pg-induced inflammatory cytokine and complement gene expression (**Figure 6B**).

To assess if the increased inflammatory response by Pg in Aβ-primed microglia was mediated by complement activation, microglia were pre-treated with C1-INH, a protease inhibitor of the classical complement component C1 (43), followed by Aβo and then Pg stimulation. Our results showed that C1-INH significantly decreased Pg-induced complement activation and cytokine production in Aβ-primed microglia (**Figures 6C, D**). To further verify if C1q spurs neuroinflammation in the presence of Pg, primary microglia were transfected with shC1qa or scramble vectors and then treated with Pg. Knock-down of C1qa significantly reduced Pg-induced inflammatory cytokine gene expression in microglia (**Figures 6D–F**). These results suggest that C1q plays a critical role in the amplification of microglia activation and neuroinflammation in AD mice following Pg infection.

Pg Infection Exacerbates Synapse Loss and the Colocalization of C1q With Synaptic Puncta in *App* KI Mice

One of the prominent pathological features of AD is the early loss of synapses (44). In addition, studies have shown that progressive brain C1q accumulation is associated with cognitive decline and memory impairment in aging, *via* microglia engulfment of the C1q-tagged synapses (45). Given the significantly increased brain C1q expression and remarkable memory deficits in *App* KI mice following Pg infection, we evaluated if synapses were altered as a result of periodontal infection, and its correlation with C1q expression. A significant loss of pre- and postsynaptic puncta (marked by SNAP25 and PSD95, respectively), as well as the colocalization of pre- and postsynaptic puncta, in the hippocampus and cortex of non-infected *App* KI mice were seen at 10 months of age compared to 6 months of age (**Figures 7A–D**). In addition, Pg infection significantly increased the loss of synaptic puncta in *App* KI mice at 6 and 10 months of age than their respective non-infected controls. Furthermore, a significant increase in the numbers of C1qa-labeled PSD95 puncta in the hippocampus and cortex was observed in non-infected and Pg-infected *App* KI

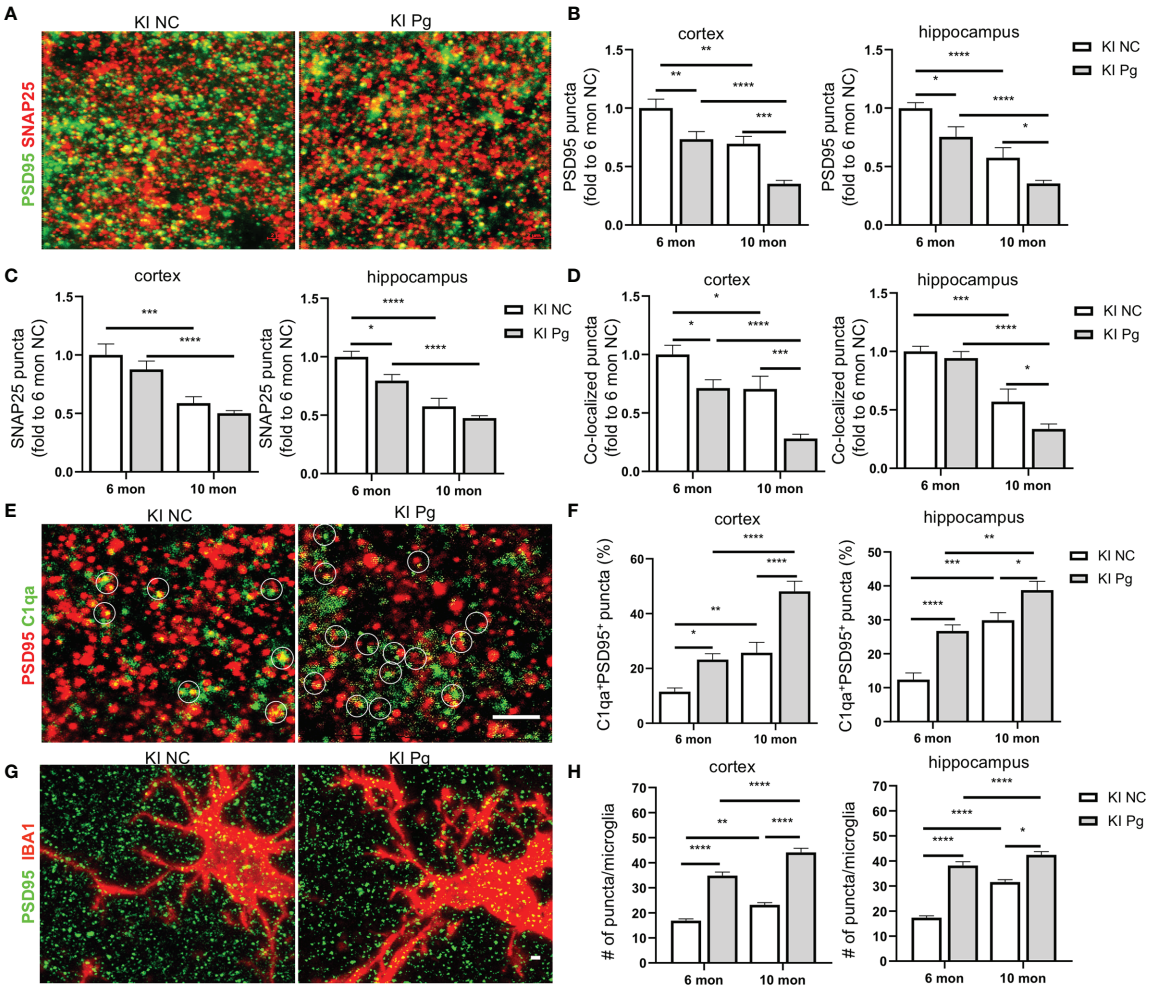

FIGURE 7 | Pg infection enhances microglial elimination of synapses in *App* KI mice. **(A)** Representative high magnification Z-stack images showing SNAP 25 (presynaptic marker, red) and PSD95 (postsynaptic marker, green) synaptic terminals in the cortex and hippocampus from non-infected and Pg-infected *App* KI mice at 10 months of age. **(B–D)** Quantification of PSD95 puncta **(B)**, SNAP25 puncta **(C)**, and the co-localized PSD95 and SNAP25 puncta **(D)** in the cortex and hippocampus CA1 regions from non-infected and Pg-infected *App* KI mice at 6 and 10 months of age. Scale bar: 2 µm. **(E)** Representative high magnification Z-stack images of C1qa (green) and PSD95 (red) co-stained puncta in the cortex and hippocampus of the brains from non-infected and Pg-infected *App* KI mice at 10 months of age. Circles show examples of C1qa puncta co-localized with PSD95 puncta. Scale bar: 4 µm. **(F)** Quantification of co-stained C1qa and PSD95 in the cortex and hippocampus CA1 regions from non-infected and Pg-infected *App* KI mice at 6 and 10 months of age. **(G)** Representative high magnification Z-stack images of subicular microglia (IBA1$^+$, red) co-stained with PSD95 (green) from non-infected and Pg-infected *App* KI mice at the 10 months of age, displaying elimination of synapses by microglia. Scale bar, 5 µm. **(H)** Quantification of engulfed PSD95 puncta density in microglia in the cortex and hippocampus CA1 regions of the brains from non-infected and Pg-infected *App* KI mice at 6 and 10 months of age. Data are expressed as mean ± SEM (n=4-7 mice/group). $^*P < 0.05$, $^{**}P < 0.01$, $^{***}P < 0.001$, $^{****}P < 0.0001$ by two-way ANOVA followed with Tukey correction.

mice at 10 months of age compared to that at 6 months of age, and Pg-infected *App* KI mice showed a significantly higher number of C1qa^{+}PSD95^{+} puncta than their non-infected controls at 6 months and 10 months of age (**Figures 7E, F**). Moreover, significant increase numbers of PSD95 puncta within microglial cell bodies was observed in the cortex and hippocampus of *App* KI mice at 10 months of age compared to those at 6 months of age, and Pg infection significantly increased the numbers at 6 and 10 months of age (**Figures 7G, H**). These results suggest that C1q and microglia communicate to regulate synapse pruning, and that periodontal infection potentiates C1q-mediated synapse engulfment by microglia.

Blocking C1qa Reduces Pg Induced Microglia-Mediated Synapse Loss *In Vitro*

To further confirm if the increased synapse removal by microglia in the presence of Pg was C1q dependent, primary microglia expressing C1qa shRNA or scramble vectors were co-cultured with primary neurons in the presence or absence of Pg, and the expression of PSD95 puncta in the co-cultures were analyzed. With scramble shRNA expression, PSD95 density in the co-cultures was reduced by ~50% following Pg stimulation (**Figures 8A, B**), demonstrating that Pg infection enhances the loss of synapses. However, with shC1qa expression, no significant loss of PSD95 was seen following Pg stimulation. Importantly, the number of PSD95 puncta in Pg-treated co-cultures with shC1qa expression was significantly higher than that in Pg-treated co-cultures with scramble shRNA expression, indicating that depletion of C1qa in microglia prevents Pg-induced synapse loss. We next verified the presence of PSD95 puncta within microglia in the co-cultures. Increased number of PSD95 puncta were observed within microglia expressing scramble vectors after Pg stimulation (**Figures 8A, C**). However, no increase in PSD95 puncta within microglia expressing shC1qa was seen following Pg stimulation. To further confirm these results, microglia cells were sorted out from the co-cultures by FACS. Pg infection led to an increased level of PSD95 expression in the microglial cell lysates from the co-cultures with scramble shRNA expression in microglia (**Figure 8D**). However, no increase in PSD95 expression was seen in the microglial cell lysates from the co-cultures with shC1qa expression. No NeuN (neuronal cell marker) signal was detected in any of the microglial cell lysates, indicating that there was no contamination of neurons in the sorted microglia and that the observed PSD95 intensity was due to microglial engulfment of neuronal synapses. Taken together, these results indicate that C1q expression in microglia is necessary for Pg-induced enhancement of synapse engulfment by microglia.

DISCUSSION

Increasing evidence suggests that periodontitis is associated with and may contributes to the development of AD. However, the

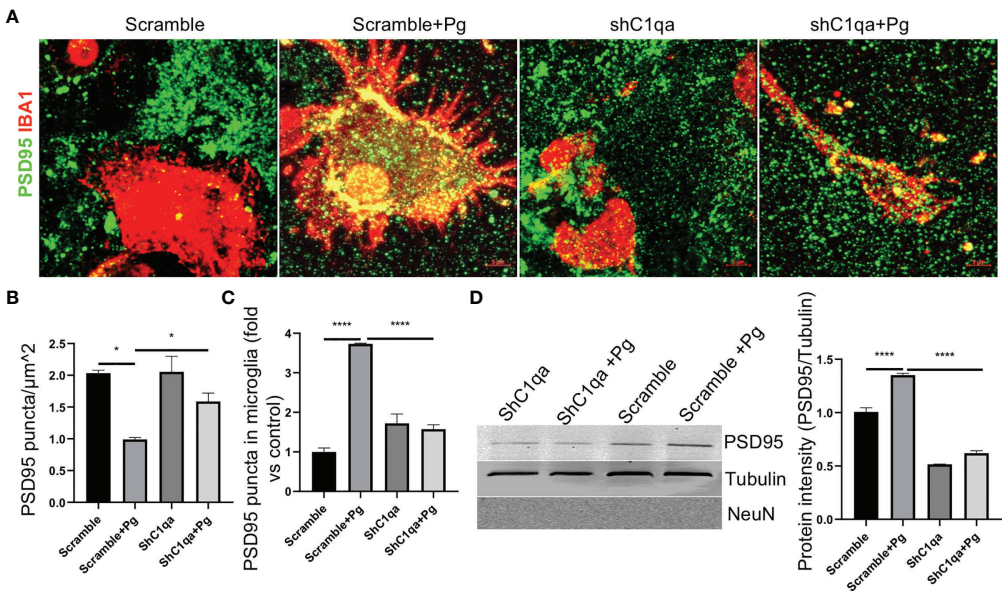

FIGURE 8 | Depletion of C1qa prevents Pg-induced synapse loss by microglia *in vitro*. **(A)** Representative Z-stack images of neuro-microglia (expressing shC1q or scramble vector) co-cultures in the presence or absence of Pg (MOI=50). Cultures were stained with IBA1 (red) and PSD95 (green). Scale bar: 5 μm. **(B, C)** Quantification of PSD95 puncta in the co-cultures **(B)** and in microglial cell bodies **(C)**. **(D)** Western blot analysis of PSD95 puncta in FACS-sorted IBA1^{+} microglia lysates from the co-cultures. NeuN, neuronal marker. Densitometric analysis was performed using ImageJ software, and normalized to tubulin and expressed as fold changes over scramble control. Data are expressed as mean ± SEM of three independent experiments. $^{*}P < 0.05$, $^{****}P < 0.0001$ by one-way ANOVA followed with Tukey correction.

mechanisms underlying such association have not yet been delineated. In the present study, we provide new evidence that the neuroinflamamtory staus established by AD, is greatly complicated by periodontal infection and the consequential entry of Pg into the brain *via* Aβ-primed microglial activation, thus unquestionably and significantly aggravating AD, and that Pg-induced brain overactivation of complement C1q is critical for periodontitis-associated acceleration of AD progression by amplifying microglial activation, neuroinflammation, and tagging synapses for microglial engulfment.

Periodontitis-related bacteremia, as well as the migration of Pg from gingival tissues to distant tissues *via* intravascular dissemination, has been reported in animal and human studies (46, 47). In addition, periodontitis may induce a systemic inflammatory state through mechanisms that include dissemination of pro-inflammatory cytokines (6). In this study, we were able to detect the presence of Pg in the brains of WT and AD mice following Pg infection. Importantly, a significantly higher amount of Pg were detected in the brains of AD mice than WT mice. One reason for the increased vulnerability of AD mice to Pg invasion of the brain may due to the increased BBB permeability related to increased activation of the innate immune response in the brains of AD mice, thus allowing for easier translocation of pathogens through the barrier (48). Along this line, we observed a pre-existing pro-inflammatory cytokine response in the brains of AD mice without Pg infection, and Pg infection further enhanced the neuroinflammation in AD mice.

Microglia are belived to be the main source of C1q in the brain (49), consistent with this notion, we found that Pg infection significantly increased the colocalization of C1q with microglia, and C1q plays an important role in Pg-induced inflammation in microglia. Previous studies have reported that the complement system is hyper-activated in the brain tissues from AD patients and mouse models (18, 19), inhibition or lack of complement components could ameliorate AD-relevant characters in multiple mouse models of AD (18, 50, 51). In addition, absence of C1q leads to less neuropathology in AD mice. On the other hand, activated complement fragments were abundant in the gingival crevicular fluids (GCF) and the chronically inflamed gingiva from patients with periodontitis, but were either undetectable or present in very low levels in the GCF and gingiva of healthy control individuals (52). Periodontal treatment that decreased clinical indices of periodontal inflammation has also been shown to decrease complement activity in GCF (53). Moreover, interception of the complement cascade protected mice and non-human primates from periodontitis (54). Thus, a dysregulated complement system may be a driver of chronic, non-resolving neuroinflammation in AD in the presence of periodontal infection.

Microglia are long-lived tissue-resident macrophages in the CNS (55). Like macorphages, microglia express pattern recognition receptors, e.g., TLRs, and can be activated by multiple exogeous TLR ligands (56). In addition, microglia are believed to possesse innate immune memeory after experiencing a primary "priming" or "desensitizing" stimulus, react with a stronger (immune training) or weaker (immune tolerance) immune response to a subsequent stimulus (57, 58). Pg mainly signals through TLR2 to induce periodontal inflammation and bone loss (59). Interestingly, TLR2 is also a primary receptor for Aβ peptides to trigger neuroinflammation (60). Thus, Aβ accumulation in the brain may underline the pre-existed brain TLR2 activation and neuroinflammation in AD mice in the absence of Pg infection. Interestingly, our studies showed that Aβo alone was unable to activate mciroglial cells *in vitro*. Yet, pretreatment of microglia cells with Aβo followed by Pg stimulation led to a significant increase in Pg-induced inflammatory response even when a very low amount of Aβo was used, which is consistent with our *in vivo* findings that Pg infection amplified compelement activation and neuroinflamamtion in AD mice. Therefore, it is likely that Aβ accumulation in AD mice may serve as a first "hit" to prime or train microglia, while Pg brain invasion as a second "hit" to activate the primed microglia, leading to exaggerated neuroinflamamtion in AD in the presence of periodontal infection. It is also possible that brain dissemination of Pg or inflammatory mediators can prime microglia for subsequent Aβ or inflammatory stimuation (61), which would suggest that periodontitis not only aggravates the severity of AD, but also increases the host susceptibility to AD.

It is important to point out that, in our study, minimal brain complement activation and neuroinflammation were seen in WT mice following Pg infection, despite Pg brain invasion. A possible explanation is that Aβ production in a healthy brain may help sequester the invading pathogens. In this regard, previous studies have shown that Aβ can protect culture cells from microbial infection by forming fibrils that entrap the pathogens and destroy cell membranes (62). In line with these observations, we found that *in vitro* co-stimulation of microglial cells with Aβo and Pg at the same time significantly impaired Pg-induced cytokine production.

Emerging research indicates that early and extra synapse loss is a predictor of cognitive impairment and the degree of synapse loss correlates most strongly with cognitive decline in AD (63). Several lines of evidence support the notion that synapse loss in AD is caused by complement-mediated synaptic pruning by microglia, and that C1q deficiency leads to less synapse loss and neuropathology in AD mice (18, 51, 64). Therefore, we reasoned that elevated complement and microglia activation induced by Pg infection would exacerbate synapse loss in AD mice. Indeed, we observed a significant loss of synapses and increased co-localization of C1q with synapses in AD mice following Pg infection. In addition, more synaptic puncta were observed within microglia following Pg infection, and this engulfment was prevented by depleting C1qa. However, how C1q-labeled synapses provide an "eat me" signal to microglia needs to be addressed in future studies. Furthermore, it will also be of interest to see if C1q inhibition or deficiency *in vivo* is sufficient to mitigate Pg-mediated acceleration of AD pathology.

In conclusion, we propose a "two-hit" model of periodontitis-associated aggravation of AD progression, with brain amyloid β accumulation as the first "hit", and Pg invasion of the brain as the

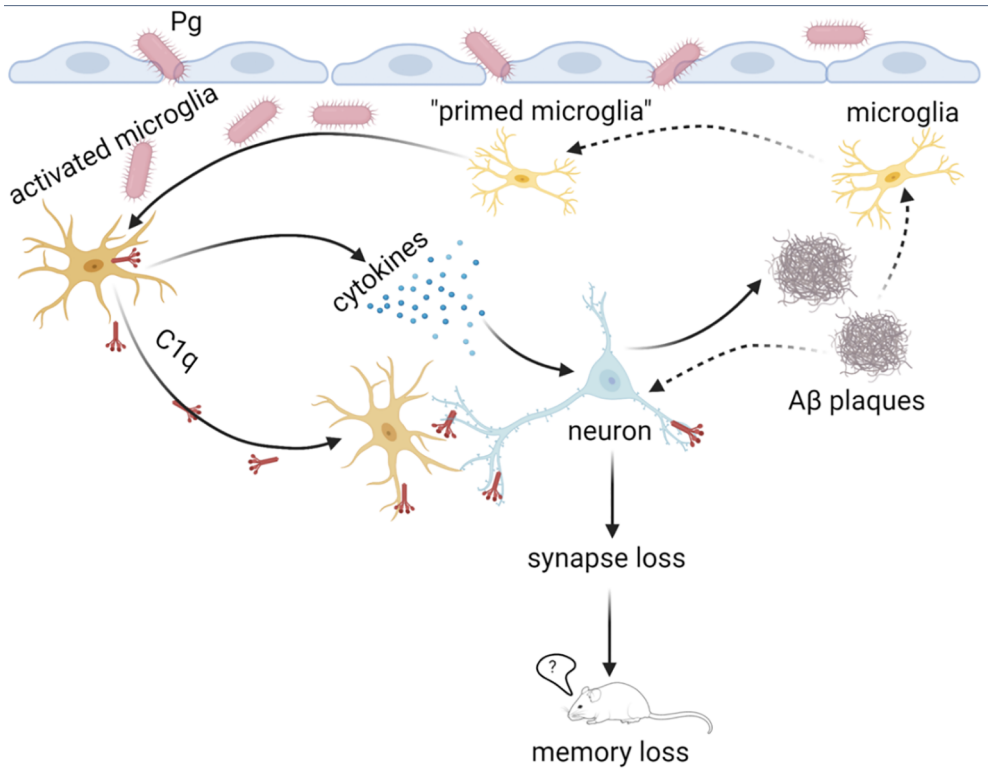

FIGURE 9 | Proposed "two-hit" model of AD progression in the presence of periodontitis. The accumulation of Aβ in the brain with AD may serve as the first "hit" to prime microglia and induce low levels of complement activation and neuroinflammation. In the presence of periodontitis, periodontal pathogens may invade the brain and serve as the second "hit" to amplify neuroinflammation of the Aβ-primed microglia and facilitate synapse loss. Complement C1q is critical for Pg-mediated acceleration of AD progression by tagging synapses for microglia engulfment. This image was created by Biorender.com.

second "hit" to facilitate microglial overactivation and synapse loss in AD in the presence of periodontitis (**Figure 9**). Furthermore, periodontitis-induced overactivation of complement C1q is critical in aggravating microglial priming and activation, leading to an exacerbated neurodegeneration in AD. Thus, simply reducing Aβ burden alone without eliminating periodontal infection may not completely break a vicious cycle formed by Aβ deposition, complement activation, and neuroinflammation in AD in the presence of periodontitis. Future studies will determine the regulation of microglia priming and if targeting certain complement components could ameliorate periodontitis and thus AD progression in the presence of periodontal infection. Knowledge obtained from these studies will fill the gap in our understanding of the association between periodontitis and AD, and will pave the way for targeting microbial etiology to ameliorate the clinical manifestations of AD and lower AD prevalence.

DATA AVAILABILITY STATEMENT

The original contributions presented in the study are included in the article/**Supplementary Material**. Further inquiries can be directed to the corresponding author.

ETHICS STATEMENT

The animal study was reviewed and approved by University of Alabama at Birmingham Institutional Animal Care and Use Committee.

AUTHOR CONTRIBUTIONS

PZ conceptualized and supervised the study. XH planned and performed the experiments, and analyzed data. ZL assisted with the animal experiments and WL assisted with imaging processing and data analysis. PZ and XH wrote the manuscript. JK, SM, SB, LP-M, QW, and ER provided expertise and resources, and critically reviewed the manuscript. TS and TCS provided the *App* KI mice. All authors read and approved the final manuscript.

FUNDING

This work was supported by National Institute of Dental and Craniofacial Research (NIDCR) grant DE026465 (to PZ). ZL was supported by a NIDCR training grant R90 DE023056. UAB Comprehensive Flow Cytometry Core is supported by NIH P30

AR048311 and P30 AI27667. UAB Behavior Assessment Core is supported by NIH P30 NS47466. Confocal images were taken at the UAB Comprehensive Neuroscience Center and the UAB Civitan International Research Center.

ACKNOWLEDGMENTS

We thank Gregory Harber for his technical assistance. We also thank Dr. Xin Xu from UAB Comprehensive Neuroscience Center for her help with the primary neuronal culture, and Dr. Yuechuan Chen from UAB Department of Oral & Maxillofacial Surgery for his help with construction of lentivirus vectors.

SUPPLEMENTARY MATERIAL

The Supplementary Material for this article can be found online at: https://www.frontiersin.org/articles/10.3389/fimmu.2022.816640/full#supplementary-material

REFERENCES

1. Bateman R. Alzheimer's Disease and Other Dementias: Advances in 2014. *Lancet Neurol* (2015) 14(1):4–6. doi: 10.1016/S1474-4422(14)70301-1
2. Chen Y, Dang M, Zhang Z. Brain Mechanisms Underlying Neuropsychiatric Symptoms in Alzheimer's Disease: A Systematic Review of Symptom-General and -Specific Lesion Patterns. *Mol Neurodegener* (2021) 16(1):38. doi: 10.1186/s13024-021-00456-1
3. Norton S, Matthews FE, Barnes DE, Yaffe K, Brayne C. Potential for Primary Prevention of Alzheimer's Disease: An Analysis of Population-Based Data. *Lancet Neurol* (2014) 13(8):788–94. doi: 10.1016/S1474-4422(14)70136-X
4. Association. As. 2020 Alzheimer's Disease Facts and Figures. *Alzheimers Dement* (2020) 16:391–460. doi: 10.1002/alz.12068
5. Lamont RJ, Hajishengallis G. Polymicrobial Synergy and Dysbiosis in Inflammatory Disease. *Trends Mol Med* (2015) 21(3):172–83. doi: 10.1016/j.molmed.2014.11.004
6. Hajishengallis G, Chavakis T. Local and Systemic Mechanisms Linking Periodontal Disease and Inflammatory Comorbidities. *Nat Rev Immunol* (2021) 21:426–40. doi: 10.1038/s41577-020-00488-6
7. Ide M, Harris M, Stevens A, Sussams R, Hopkins V, Culliford D, et al. Periodontitis and Cognitive Decline in Alzheimer's Disease. *PloS One* (2016) 11(3):e0151081. doi: 10.1371/journal.pone.0151081
8. Nascimento PC, Castro MML, Magno MB, Almeida A, Fagundes NCF, Maia LC, et al. Association Between Periodontitis and Cognitive Impairment in Adults: A Systematic Review. *Front Neurol* (2019) 10:323. doi: 10.3389/fneur.2019.00323
9. Kamer AR, Pirraglia E, Tsui W, Rusinek H, Vallabhajosula S, Mosconi L, et al. Periodontal Disease Associates With Higher Brain Amyloid in Normaly Elderly. *Neurobiol Aging* (2015) 36:627–33. doi: 10.1016/j.neurobiolaging.2014.10.038
10. Poole S, Singhrao SK, Kesavalu L, Curtis MA, Crean S. Determining the Presence of Periodontopathic Virulence Factors in Short-Term Postmortem Alzheimer's Disease Brain Tissue. *J Alzheimers Dis* (2013) 36(4):665–77. doi: 10.3233/JAD-121918
11. Dominy SS, Lynch C, Ermini F, Benedyk M, Marczyk A, Konradi A, et al. Porphyromonas Gingivalis in Alzheimer's Disease Brains: Evidence for Disease Causation and Treatment With Small-Molecule Inhibitors. *Sci Adv* (2019) 5(1):eaau3333. doi: 10.1126/sciadv.aau3333
12. Greenhalgh AD, David S, Bennett FC. Immune Cell Regulation of Glia During CNS Injury and Disease. *Nat Rev Neurosci* (2020) 21(3):139–52. doi: 10.1038/s41583-020-0263-9
13. Efthymiou AG, Goate AM. Late Onset Alzheimer's Disease Genetics Implicates Microglial Pathways in Disease Risk. *Mol Neurodegener* (2017) 12(1):43. doi: 10.1186/s13024-017-0184-x
14. Hajishengallis G, Reis ES, Mastellos DC, Ricklin D, Lambris JD. Novel Mechanisms and Functions of Complement. *Nat Immunol* (2017) 18(12):1288–98. doi: 10.1038/ni.3858
15. Ricklin D, Hajishengallis G, Yang K, Lambris JD. Complement: A Key System for Immune Surveillance and Homeostasis. *Nat Immunol* (2010) 11(9):785–97. doi: 10.1038/ni.1923
16. Hajishengallis G. Complement and Periodontitis. *Biochem Pharmacol* (2010) 80(12):1992–2001. doi: 10.1016/j.bcp.2010.06.017
17. Patters MR, Niekrash CE, Lang NP. Assessment of Complement Cleavage in Gingival Fluid During Experimental Gingivitis in Man. *J Clin Periodontol* (1989) 16(1):33–7. doi: 10.1111/j.1600-051x.1989.tb01609.x
18. Hong S, Beja-Glasser VF, Nfonoyim BM, Frouin A, Li S, Ramakrishnan S, et al. Complement and Microglia Mediate Early Synapse Loss in Alzheimer Mouse Models. *Science* (2016) 352(6286):712–6. doi: 10.1126/science.aad8373
19. Morgan BP. Complement in the Pathogenesis of Alzheimer's Disease. *Semin Immunopathol* (2018) 40(1):113–24. doi: 10.1007/s00281-017-0662-9
20. Veerhuis R. Histological and Direct Evidence for the Role of Complement in the Neuroinflammation of AD. *Curr Alzheimer Res* (2011) 8(1):34–58. doi: 10.2174/156720511794604589
21. Saito T, Matsuba Y, Mihira N, Takano J, Nilsson P, Itohara S, et al. Single App Knock-in Mouse Models of Alzheimer's Disease. *Nat Neurosci* (2014) 17(5):661–3. doi: 10.1038/nn.3697
22. Zhao Y, Li Z, Su L, Ballesteros-Tato A, Katz J, Michalek SM, et al. Characterization and Regulation of Osteoclast Precursors Following Chronic Porphyromonas Gingivalis Infection. *J Leukoc Biol* (2020) 108(4):1037–50. doi: 10.1002/jlb.1hi0620-230r
23. Poole S, Singhrao SK, Chukkapalli S, Rivera M, Velsko I, Kesavalu L, et al. Active Invasion of Porphyromonas Gingivalis and Infection-Induced Complement Activation in Apoe-/- Mice Brains. *J Alzheimers Dis* (2015) 43(1):67–80. doi: 10.3233/JAD-140315
24. Baker PJ, Dixon M, Roopenian DC. Genetic Control of Susceptibility to Porphyromonas Gingivalis-Induced Alveolar Bone Loss in Mice. *Infect Immun* (2000) 68(10):5864–8. doi: 10.1128/iai.68.10.5864-5868.2000
25. Lecourtier L, Antal MC, Cosquer B, Schumacher A, Samama B, Angst MJ, et al. Intact Neurobehavioral Development and Dramatic Impairments of Procedural-Like Memory Following Neonatal Ventral Hippocampal Lesion in Rats. *Neuroscience* (2012) 207:110–23. doi: 10.1016/j.neuroscience.2012.01.040
26. Shepherd JK, Grewal SS, Fletcher A, Bill DJ, Dourish CT. Behavioural and Pharmacological Characterisation of the Elevated "Zero-Maze" as an Animal Model of Anxiety. *Psychopharmacol (Berl)* (1994) 116(1):56–64. doi: 10.1007/BF02244871
27. West MJ. Regionally Specific Loss of Neurons in the Aging Human Hippocampus. *Neurobiol Aging* (1993) 14(4):287–93. doi: 10.1016/0197-4580(93)90113-p
28. Gage GJ, Kipke DR, Shain W. Whole Animal Perfusion Fixation for Rodents. *J Vis Exp* (2012) 65:3564. doi: 10.3791/3564
29. Chen Y, Peng Y, Che P, Gannon M, Liu Y, Li L, et al. Alpha(2A) Adrenergic Receptor Promotes Amyloidogenesis Through Disrupting APP-Sorla Interaction. *Proc Natl Acad Sci USA* (2014) 111(48):17296–301. doi: 10.1073/pnas.1409513111
30. Rajamohamedsait HB, Sigurdsson EM. Histological Staining of Amyloid and Pre-Amyloid Peptides and Proteins in Mouse Tissue. *Methods Mol Biol* (2012) 849:411–24. doi: 10.1007/978-1-61779-551-0_28
31. Potts EM, Coppotelli G, Ross JM. Histological-Based Stainings Using Free-Floating Tissue Sections. *J Vis Exp* (2020) 162:10.3791/61622. doi: 10.3791/61622
32. Ippolito DM, Eroglu C. Quantifying Synapses: An Immunocytochemistry-Based Assay to Quantify Synapse Number. *J Vis Exp* (2010) 45:2270. doi: 10.3791/2270
33. Gmiterek A, Wojtowicz H, Mackiewicz P, Radwan-Oczko M, Kantorowicz M, Chomyszyn-Gajewska M, et al. The Unique Hmuy Gene Sequence as a

Specific Marker of Porphyromonas Gingivalis. *PloS One* (2013) 8(7):e67719. doi: 10.1371/journal.pone.0067719
34. Maeda H, Fujimoto C, Haruki Y, Maeda T, Kokeguchi S, Petelin M, et al. Quantitative Real-Time PCR Using Taqman and SYBR Green for Actinobacillus Actinomycetemcomitans, Porphyromonas Gingivalis, Prevotella Intermedia, Tetq Gene and Total Bacteria. *FEMS Immunol Med Microbiol* (2003) 39(1):81–6. doi: 10.1016/S0928-8244(03)00224-4
35. Singhrao SK, Chukkapalli S, Poole S, Velsko I, Crean SJ, Kesavalu L. Chronic Porphyromonas Gingivalis Infection Accelerates the Occurrence of Age-Related Granules in Apoe(-)(/)(-) Mice Brains. *J Oral Microbiol* (2017) 9 (1):1270602. doi: 10.1080/20002297.2016.1270602
36. Barghorn S, Nimmrich V, Striebinger A, Krantz C, Keller P, Janson B, et al. Globular Amyloid Beta-Peptide Oligomer - a Homogenous and Stable Neuropathological Protein in Alzheimer's Disease. *J Neurochem* (2005) 95 (3):834–47. doi: 10.1111/j.1471-4159.2005.03407.x
37. Roque PJ, Costa LG. Co-Culture of Neurons and Microglia. *Curr Protoc Toxicol* (2017) 74:11 24 1–11 24 17. doi: 10.1002/cptx.32
38. Hilgenberg LG, Smith MA. Preparation of Dissociated Mouse Cortical Neuron Cultures. *J Vis Exp* (2007) 10):562. doi: 10.3791/562
39. DeTure MA, Dickson DW. The Neuropathological Diagnosis of Alzheimer's Disease. *Mol Neurodegener* (2019) 14(1):32. doi: 10.1186/s13024-019-0333-5
40. Chen GF, Xu TH, Yan Y, Zhou YR, Jiang Y, Melcher K, et al. Amyloid Beta: Structure, Biology and Structure-Based Therapeutic Development. *Acta Pharmacol Sin* (2017) 38(9):1205–35. doi: 10.1038/aps.2017.28
41. Heneka MT, Carson MJ, Khoury JE, Landreth GE, Brosseron F, Feinstein DL, et al. Neuroinflammation in Alzheimer's Disease. *Lancet Neurol* (2015) 14 (4):388–405. doi: 10.1016/s1474-4422(15)70016-5
42. Schafer DP, Stevens B. Microglia Function in Central Nervous System Development and Plasticity. *Cold Spring Harb Perspect Biol* (2015) 7(10): a020545. doi: 10.1101/cshperspect.a020545
43. Markovic SN, Inwards DJ, Frigas EA, Phyliky RP. Acquired C1 Esterase Inhibitor Deficiency. *Ann Intern Med* (2000) 132(2):144–50. doi: 10.7326/0003-4819-132-2-200001180-00009
44. Selkoe DJ. Alzheimer's Disease is a Synaptic Failure. *Science* (2002) 298 (5594):789–91. doi: 10.1126/science.1074069
45. Stephan AH, Madison DV, Mateos JM, Fraser DA, Lovelett EA, Coutellier L, et al. A Dramatic Increase of C1q Protein in the CNS During Normal Aging. *J Neurosci: Off J Soc Neurosci* (2013) 33(33):13460–74. doi: 10.1523/JNEUROSCI.1333-13.2013
46. Chukkapalli S, Rivera-Kweh M, Gehlot P, Velsko I, Bhattacharyya I, Calise SJ, et al. Periodontal Bacterial Colonization in Synovial Tissues Exacerbates Collagen-Induced Arthritis in B10 RIII Mice. *Arthritis Res Ther* (2016) 18 (1):161. doi: 10.1186/s13075-016-1056-4
47. Scannapieco FA. Periodontal Inflammation: From Gingivitis to Systemic Disease? *Compend Contin Educ Dent* (2004) 25(7 Suppl 1):16–25.
48. Varatharaj A, Galea I. The Blood-Brain Barrier in Systemic Inflammation. *Brain Behav Immun* (2017) 60:1–12. doi: 10.1016/j.bbi.2016.03.010
49. Fonseca MI, Chu SH, Hernandez MX, Fang MJ, Modarresi L, Selvan P, et al. Cell-Specific Deletion of C1qa Identifies Microglia as the Dominant Source of C1q in Mouse Brain. *J Neuroinflamm* (2017) 14(1):48. doi: 10.1186/s12974-017-0814-9
50. Fonseca MI, Ager RR, Chu SH, Yazan O, Sanderson SD, LaFerla FM, et al. Treatment With a C5ar Antagonist Decreases Pathology and Enhances Behavioral Performance in Murine Models of Alzheimer's Disease. *J Immunol* (2009) 183(2):1375–83. doi: 10.4049/jimmunol.0901005
51. Fonseca MI, Zhou J, Botto M, Tenner AJ. Absence of C1q Leads to Less Neuropathology in Transgenic Mouse Models of Alzheimer's Disease. *J Neurosci* (2004) 24(29):6457–65. doi: 10.1523/JNEUROSCI.0901-04.2004
52. Hajishengallis G, Maekawa T, Abe T, Hajishengallis E, Lambris JD. Complement Involvement in Periodontitis: Molecular Mechanisms and Rational Therapeutic Approaches. *Adv Exp Med Biol* (2015) 865:57–74. doi: 10.1007/978-3-319-18603-0_4
53. Beikler T, Peters U, Prior K, Eisenacher M, Flemmig TF. Gene Expression in Periodontal Tissues Following Treatment. *BMC Med Genomics* (2008) 1:30. doi: 10.1186/1755-8794-1-30
54. Hajishengallis G, Hajishengallis E, Kajikawa T, Wang B, Yancopoulou D, Ricklin D, et al. Complement Inhibition in Pre-Clinical Models of Periodontitis and Prospects for Clinical Application. *Semin Immunol* (2016) 28(3):285–91. doi: 10.1016/j.smim.2016.03.006
55. Prinz M, Erny D, Hagemeyer N. Ontogeny and Homeostasis of CNS Myeloid Cells. *Nat Immunol* (2017) 18(4):385–92. doi: 10.1038/ni.3703
56. Fiebich BL, Batista CRA, Saliba SW, Yousif NM, de Oliveira ACP. Role of Microglia Tlrs in Neurodegeneration. *Front Cell Neurosci* (2018) 12:329. doi: 10.3389/fncel.2018.00329
57. Zhang X, Kracht L, Lerario AM, Dubbelaar ML, Brouwer N, Wesseling EM, et al. Epigenetic Regualtion of Innate Immune Memory in Microglia. *bioRxiv* (2021). doi: 10.1101/2021.05.30.446351
58. Wendeln AC, Degenhardt K, Kaurani L, Gertig M, Ulas T, Jain G, et al. Innate Immune Memory in the Brain Shapes Neurological Disease Hallmarks. *Nature* (2018) 556(7701):332–8. doi: 10.1038/s41586-018-0023-4
59. Myneni SR, Settem RP, Connell TD, Keegan AD, Gaffen SL, Sharma A. TLR2 Signaling and Th2 Responses Drive Tannerella Forsythia-Induced Periodontal Bone Loss. *J Immunol* (2011) 187(1):501–9. doi: 10.4049/jimmunol.1100683
60. Liu S, Liu Y, Hao W, Wolf L, Kiliaan AJ, Penke B, et al. TLR2 Is a Primary Receptor for Alzheimer's Amyloid Beta Peptide to Trigger Neuroinflammatory Activation. *J Immunol* (2012) 188(3):1098–107. doi: 10.4049/jimmunol.1101121
61. Li JW, Zong Y, Cao XP, Tan L, Tan L. Microglial Priming in Alzheimer's Disease. *Ann Transl Med* (2018) 6(10):176. doi: 10.21037/atm.2018.04.22
62. Gosztyla ML, Brothers HM, Robinson SR. Alzheimer's Amyloid-Beta Is an Antimicrobial Peptide: A Review of the Evidence. *J Alzheimers Dis* (2018) 62 (4):1495–506. doi: 10.3233/JAD-171133
63. Spires-Jones TL, Hyman BT. The Intersection of Amyloid Beta and Tau at Synapses in Alzheimer's Disease. *Neuron* (2014) 82(4):756–71. doi: 10.1016/j.neuron.2014.05.004
64. Stevens B, Allen NJ, Vazquez LE, Howell GR, Christopherson KS, Nouri N, et al. The Classical Complement Cascade Mediates CNS Synapse Elimination. *Cell* (2007) 131(6):1164–78. doi: 10.1016/j.cell.2007.10.036

Conflict of Interest: SB is the CSO & Co-Founder of CNine Biosolutions, LLC.

The remaining authors declare that the research was conducted in the absence of any commercial or financial relationships that could be construed as a potential conflict of interest.

Publisher's Note: All claims expressed in this article are solely those of the authors and do not necessarily represent those of their affiliated organizations, or those of the publisher, the editors and the reviewers. Any product that may be evaluated in this article, or claim that may be made by its manufacturer, is not guaranteed or endorsed by the publisher.

frontiers | Frontiers in Immunology

TYPE Systematic Review
PUBLISHED 03 August 2022
DOI 10.3389/fimmu.2022.958273

OPEN ACCESS

EDITED BY
Peter Kraiczy,
Goethe University Frankfurt, Germany

REVIEWED BY
Eleni Gavriilaki,
G. Papanikolaou General Hospital, Greece
Péter Gál,
Research Centre for Natural Sciences, Hungary

*CORRESPONDENCE
Kristina Schulz
Kristina.schulz@unibas.ch

SPECIALTY SECTION
This article was submitted to Molecular Innate Immunity, a section of the journal Frontiers in Immunology

RECEIVED 31 May 2022
ACCEPTED 24 June 2022
PUBLISHED 03 August 2022

CITATION
Schulz K and Trendelenburg M (2022) C1q as a target molecule to treat human disease: What do mouse studies teach us?
Front. Immunol. 13:958273.
doi: 10.3389/fimmu.2022.958273

C1q as a target molecule to treat human disease: What do mouse studies teach us?

Kristina Schulz[1,2]* and Marten Trendelenburg[1,2]

[1]Laboratory of Clinical Immunology, Department of Biomedicine, University of Basel, Basel, Switzerland, [2]Division of Internal Medicine, University Hospital Basel, Basel, Switzerland

The complement system is a field of growing interest for pharmacological intervention. Complement protein C1q, the pattern recognition molecule at the start of the classical pathway of the complement cascade, is a versatile molecule with additional non-canonical actions affecting numerous cellular processes. Based on observations made in patients with hereditary C1q deficiency, C1q is protective against systemic autoimmunity and bacterial infections. Accordingly, C1q deficient mice reproduce this phenotype with susceptibility to autoimmunity and infections. At the same time, beneficial effects of C1q deficiency on disease entities such as neurodegenerative diseases have also been described in murine disease models. This systematic review provides an overview of all currently available literature on the C1q knockout mouse in disease models to identify potential target diseases for treatment strategies focusing on C1q, and discusses potential side-effects when depleting and/or inhibiting C1q.

KEYWORDS

C1q, complement, deficiency, knockout mouse, disease

Abbreviations: AD, Alzheimer's disease; ALS, amyotrophic lateral sclerosis; AMD, age-related macular degeneration; ANA, anti-nuclear antibody; APP, amyloid precursor protein; CNS, central nervous system; dLGN, dorsolateral geniculate nucleus; DNA, deoxyribonucleic acid; EEG, electroencephalography; EAE, experimental autoimmune encephalomyelitis; FLTD, frontotemporal lobar degeneration; GBM, glomerular basement membrane; GN, Glomerulonephritis; GRN, progranulin; GRP6, G protein-coupled receptor 6; I/R, ischemia/reperfusion; LN, lupus nephritis; LRP1B, lipoprotein receptor-related protein 1B; Ldlr, low-density lipoproteinreceptor; MAG, myelin associated glycoprotein; MBL, mannose-binding lectin; MOG, myelin oligodendrocyte glycoprotein; MPTP, 1-methyl-4-phenyl-1,2,3,6-tetrahydropyridine; MS, Multiple sclerosis; PE, preeclampsia; PFC, prefrontal cortex; PNS, peripheral nervous system; PrP^{c}, cellular prion protein; RGC, retinal ganglion cells; SCID, severe combined immunodeficiency disease; SLE, systemic lupus erythematosus; SOD1, superoxide dismutase 1; TBI, traumatic brain injury; TTR, transthyretin; TNF, tumor necrosis factor; wt, wild type.

Introduction

Complement protein C1q was first described in 1961 as the starter molecule of the classical pathway of the complement system. The complement system is an evolutionarily ancient set of about 50 proteins that is critically involved in host defense. An imbalance of complement is known to be related to the development of autoimmunity. Similarly, very rare cases of hereditary C1q deficiency in humans present clinically most notably with the autoimmune disease systemic lupus erythematosus (SLE) or SLE-like symptoms as well as recurrent bacterial infections (1). While this observation supports a protective role of C1q from the development of autoimmunity and infections, there are certain mouse disease models where the absence of C1q has beneficial effects (2–5). In these settings, C1q might function as a target molecule and its manipulation, for example a blockage by small molecules or specific antibodies, could be an effective treatment option. However, C1q is a highly versatile protein. It is well accepted that a number of non-canonical pathways exist: C1q not only triggers the avalanche of protease-activation involved in the classical complement pathway but can also interact directly with receptors thereby affecting numerous cellular processes from proliferation to induction of apoptosis (6, 7). The involvement of C1q is so broad and manifold that it is not straightforward to deduce its role in certain diseases and tissues, let alone the effect of its blockage or absence. Genetically engineered knockout mice provide the opportunity to gain important insights to this question.

C1q is composed of three different chains – A, B and C– which arrange into a hexameric structure resembling a bouquet of tulips (8). In 1998 Botto et al. created a C1qa knockout (C1qKO) mouse with the primary goal to study effects of C1q deficiency on autoimmunity (9). In the C1qKO mouse the expression of C1q is abrogated due to targeted deletion of the *C1qa* gene coding for the A chain that was isolated from the 129/sv genomic library (9). This systematic review provides a comprehensive overview of all studies up to date that employed the C1qKO mouse in the setting of a human disease model. It identifies potential target diseases for therapeutic intervention with C1q as a target molecule, and it illuminates potential side effects, when inhibiting C1q on a systemic level.

Methods

A database query of PubMed and Embase was performed with the search terms “complement C1q” and “mouse”. Broad search terms were chosen to avoid missing relevant publications. Peer-reviewed, PubMed-listed and/or Embase-listed publications written in English and published between 1998 and April 2022 were considered. Embase search was restricted to article type “article”. Removal of duplicates was automated based on DOI number using R software. Titles and abstracts were screened for inclusion criteria, namely usage of the C1qKO mouse in an *in vivo* disease model and/or addressing a human disease in an original research article (Figure 1). 177 publications remained for full text review. Criteria for exclusion were *in vitro* use only, no investigation of a human disease model, no use of the C1qKO mouse. One article was excluded due to retraction, another one as it was a case report. In addition, references of included studies were screened for relevant publications yielding four additional studies. In total, the databank search resulted in 145 publications. Publications were grouped according to disease mechanism and organ manifestation, respectively, yielding nine clusters. Each publication was evaluated with respect to disease outcome of the C1qKO mouse as compared to wild type (wt) control (Tables 1–3).

Results

1. C1q deficiency and diseases of the brain and retina

Most studies showing beneficial effects of C1q deficiency were performed in the immune-privileged brain and retina (**Table 1**). This is the disease cluster with the largest number of studies using the C1qKO mouse and a remarkable increase in publications in recent years.

1.1 C1q deficiency and neurodegenerative diseases of the retina

In 2007, Stevens et al. showed for the first time that C1q is involved in synaptic pruning in the developing brain as well as in neurodegeneration in the visual system, a prime system for studies on synaptic refinement (10). In the postnatal brain, retinal ganglion cells (RGC), which form the optic nerve with their axons, expressed C1q in the presence of immature astrocytes. C1q mainly localized to immature synapses in the downstream thalamic dorsolateral geniculate nucleus (dLGN). The physiological relevance of C1q for retinogeniculate refinement became apparent in C1qKO mice, that presented with reduced eye-specific segregation of RGC input onto dLGN. Knockout of the downstream complement component C3 in C3 knockout (C3KO) mice presented with a similar phenotype supporting complement activation as the underlying mechanism involved in this setting of synaptic pruning (10). Phosphatidylserine, which might act as a synaptic tag and serve as an “eat-me” signal, was elevated in the dLGN of C1qKO mice (150).

In glaucoma, neurons of the retina undergo neurodegeneration induced by elevated intra-ocular pressure. The DBA/2J mouse is a reproducible murine glaucoma model. Though not employing the

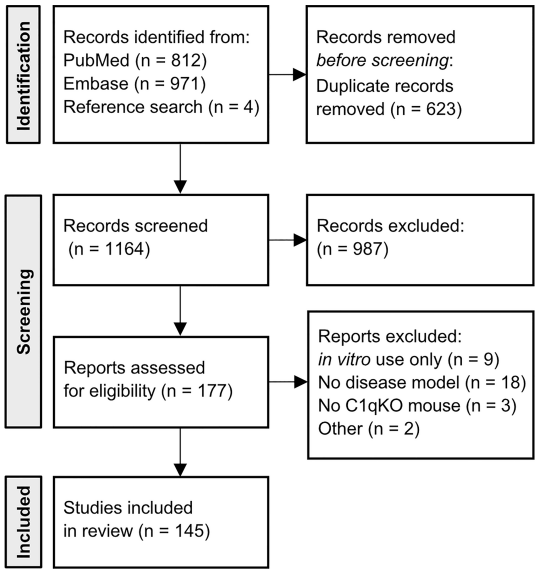

FIGURE 1
Flow diagram of included articles. Flowchart of number of included articles after database query of PubMed and Embase with search terms "complement C1q", AND "mouse". Four articles were included based on reference research of cited articles. Articles were initially screened by title and abstract to meet the inclusion criteria (*in vivo* use of C1qKO mouse, investigated disease model). 177 articles underwent full text review. Thirty-two publications did not fulfill the criteria.

C1qKO mouse in this section of the study, Stevens et al. provided evidence for C1q mediated synapse loss in the retina as an early crucial event in glaucoma, preceding axonal and thus optic nerve damage (10). In summary, this study demonstrated a prominent role of C1q in synapse elimination in the visual system during development as well as in the diseased state of neurodegeneration (10)

A number of studies of C1qKO mice confirmed detrimental effects of C1q in early stages of glaucoma (11–13) (Table 1). C1qKO mice showed markedly reduced optic nerve damage, an effect that faded with age (11). Early synaptic and dendritic atrophy of RGC was abolished in C1qKO mice and similarly could be preserved using pharmacological inhibition (13). A detailed study by Kumari et al. confirmed these results and identified a sex-dependency: only female C1qKO mice on a DBA/2NNia background had elevated intra-ocular pressure (12). The detailed time analysis supported the idea that the protective effect of C1q deficiency was restricted to early glaucoma and lost as the disease progressed (12). Taken together, these studies suggest C1q as a potential target only in very early stages of glaucoma before apparent axonal loss and thus clinical signs.

The effects of C1q deficiency on age-related macular degeneration (AMD) are less uniform (**Table 1**). AMD has a multifactorial genesis with polymorphisms in the complement system being one of the risk factors (151). The dry form is dominated by drusen and may transition to the wet form, characterized by an unfavorable increase in neovascularization. Photo-oxidative damage as a model for AMD showed a better long-term outcome in C1qKO mice (17). In particular microglia and macrophages had reduced levels of inflammasome activation (17). In contrast, several other models of AMD showed no influence by C1q deficiency. The rd1 mouse with a recessive mutation in the phosphodiesterase gene, is a model system to study photoreceptor degeneration and was employed to mimic early changes in AMD marked by rod cell death (14). Although C1q was highly expressed in retinas undergoing degeneration in the rd1 mouse, C1q deficiency affected neither the progression of the disease nor the clearance of photoreceptor-debris (14). Similarly, there was no clear effect of sole C1q deficiency in a model for wet AMD by laser-induced choroidal neovascularization (15). Unwanted neovascularization appeared to require complement amplification by the alternative pathway, as double knockout of the classical as well as the lectin pathway by C1qKO and mannose-binding lectin (MBL)KO caused equal protection as a factor B knockout (15). Also inflammation and microglial activation induced by immune complex-formation in the retina, a phenomenon associated with early AMD, remained unchanged in the C1qKO mouse (16).

Lastly, while C1q deficiency seems to be protective for neurodegenerative diseases of the retina, it aggravates retinal thinning during normal aging. This indicates that C1q and other complement components are important for retinal homeostasis during aging (18).

1.2 C1q deficiency and neurodegeneration

Brain C1q protein levels increase with age: while Stephan et al. reported a dramatic 300-fold increase in C1q protein levels detected by immunofluorescent signal in tissue slides of the aging mouse brain (29) other studies using novel monoclonal antibodies reported a moderate, less than two fold rise in brain homogenate (152). Normal aging brain was beneficially influenced by C1q deficiency, though effects on synaptic plasticity and memory were small and inconsistent across age-groups (29).

While the physiologically aging brain is known to show some functional constraints, one needs to distinguish a pathological loss of neurons occurring during neurodegeneration. The complement system is by now well accepted to have an influential role in this disease entity (153). Neurodegeneration is associated with neuronal cell death, synaptic loss, and neuroinflammation. Microglia and reactive A1 astrocytes are important cellular actors for all of these processes and both are intimately linked to C1q (31). Microglia, the local tissue macrophages, are a major source of C1q in the brain (154). Astrocytes, star-shaped glial cells, traditionally have mainly supportive functions for neuronal

TABLE 1 Overview of publications in the disease clusters CNS/PNS and retina, Ischemia and reperfusion and Liver diseases.

Disease entity	oc	Disease model	Gene manipulation and genetic background	Sex	Ref
CNS/PNS and retina					
Retina	-	pruning/glaucoma*	DBA/2J	f/m	(10)
	+	glaucoma	DBA/2J	f	(11)
	+	glaucoma	DBA/2NNia	f/m	(12)
	+	glaucoma	DBA/2J	f/m	(13)
	=	AMD	rd1	f/m	(14)
	=	AMD	$C1q^{-/-}$, $C1q^{-/-}MBL^{-/-}$	f/m	(15)
	=	AMD		f/m	(16)
	+	AMD		f/m	(17)
	-	retinal aging		f/m	(18)
Neuro-degeneration and aging	+	AD	$Q^{-/-}$, APPQ $^{-/-}$, $APPPS1Q^{-/-}$, C57BL/6, B6/SJL	f/m	(2)
	+	AD	APPQ $^{-/-}$, $APPPS1Q^{-/-}$, B6/SJL	f/m	(19)
	=	AD	$3xTgBUBC1q^{-/-}$, BUB/BnJ	f/m	(20)
	+	AD		f/m	(21)
	+	FTLD	$Grn^{-/-};C1q^{-/-}$	f/m	(22)
	+	FTLD	$Grn^{-/-};C1q^{-/-}$, $Grn^{-/-};C1q^{-/-};C3^{-/-}$	f/m	(23)
	=	ALS	$SOD1^{G37R}/C1q^{-/-}$	f/m	(24)
	+	ALS	*IL-1α*$^{-/-}$ *TNFα*$^{-/-}$ *C1q*$^{-/-}$, *IL-1α*$^{-/-}$ *TNFα*$^{-/-}$ *C1q*$^{-/-}$ *SOD1*^{G93A}	f/m	(25)
	=	M. Parkinson		m	(26)
	-	amyloid neuropathy	$mTTR^{-/-}hTTR^{Met30+/+}mC1q^{-/-}$, 129X1/SvJ/C57BL/6	f/m	(27)
	+	OIBP		f/m	(28)
	+	brain aging		f/m	(29)
CNS injury	=	TBI		f/m	(30)
	+	TBI	*C1q*$^{-/-}$, *IL-1α*$^{-/-}$ *Tnf*$^{-/-}$ *C1q*$^{-/-}$	f/m	(31)
	-	TBI		f/m	(32)
	-	TBI		f/m	(33)
	+	TBI		f/m	(34)
	+	injury by radiation	*C1qa*$^{FL/FL}$ *Cx3cr1*$^{CreERT2/WganJ}$	m	(35)
	+	spinal cord injury	BUB/BnJ	m	(36)
	=	spinal cord injury	BUB/BnJ	m	(37)
PNS injury	=	peripheral nerve lesion		f	(38)
	=	peripheral nerve lesion		f/m	(39)
Infection	+	prion disease	*C1qa*$^{-/-}$, *C1qa/H2-Bf/C2*$^{-/-}$	f/m	(3)
	+	prion disease		f	(4)
	=	prion disease		f/m	(40)
	=	HIV-and HAND		f/m	(41)
MS	+	MS		f/m	(42)
	=	MS		f/m	(43)
	+	MS	*C1q*$^{fl/fl}$;*TMEM-Cre*$^{ERT/+}$	f/m	(44)
Depression	-	depression		m	(45)
Epilepsy	-	epilepsy		f/m	(46)
	-	epilepsy	background n.s.	m	(47)
Ischemia and reperfusion					
H/I	+	H/I stroke		f/m	(5)
	+	H/I stroke		f/m	(48)
Stroke	=	ischemic stroke		f/m	(49)
	=	ischemic stroke		m	(50)
	+	ischemic stroke	$C1q/MBL^{-/-}$	m	(51)
I/R	+	retinal I/R		f/m	(52)
	=	GI I/R		m	(53)
	=	GI I/R		f/m	(54)
	+	GI I/R		f/m	(55)
	+	myocardial I/R	$C1q^{-/-}$, $C1q/fD^{-/-}$	m	(56)

(Continued)

TABLE 1 Continued

Disease entity	oc	Disease model	Gene manipulation and genetic background	Sex	Ref
	+	skeletal muscle I/R		f/m	(57)
	=	cutaneous I/R		m	(58)
		Liver diseases			
Liver toxicity	+	ALD		f	(59)
	+	ALD	*C1qa*$^{-/-}$, *C1qa/FD*$^{-/-}$	f	(60)
	+	hepatotoxicity		m	(61)
	=	hepatotoxicity		f	(62)
	+	NASH		m	(63)

Each cluster is subdivided according to disease and organ manifestation, respectively. Disease outcome (oc) of C1qKO mice compared to wt and/or C1q sufficient mice in the investigated disease model is given as "+" respectively turquoise =beneficial, "-" respectively ocher =detrimental, "=" respectively grey=no effect. The overall outcome on the disease entity is similarly color coded using lighter shades for ambiguous group results. Genetic modifications other than C1qKO and genetic background other than C57BL/6 are listed explicitly. In studies with several C1q deficient mice, all C1q deficient mice are listed. Sex as indicated in the study (f=female only, m=male only, f/m=mixed gender); if not mentioned explicitly by the study, mixed gender was assumed. AD, Alzheimer's disease; ALD, alcoholic liver disease; ALS, amyotrophic lateral sclerosis; AMD, age-related macular degeneration; APP, amyloid precursor protein; FLTD, frontotemporal lobar degeneration; GI I/R, gastrointestinal ischemia/reperfusion; H/I, hypoxia/ischemia; HAND HIV, associated neurocognitive disorder; I/R, Ischemia/reperfusion; MS, multiple sclerosis; NASH, non-alcoholic steatohepatitis; n.s., not specified; OIBP, obesity induced brain pathology; PNS, peripheral nervous system; TBI, traumatic brain injury. *in the Glaucoma part of the study no C1qKO mouse model was used; the outcome classification relates to synapse elimination.

metabolism and homeostasis, but can lose these features in the reactive A1 state. C1q is one of the factors which turn homeostatic functioning astrocytes into the reactive A1 state (31).

Alzheimer's disease (AD) is a prime example of a neurodegenerative disease histologically characterized by extracellular ß-amyloid plaques and intracellular tau tangles. Common murine models use genetic modifications leading to altered expression of the relevant proteins amyloid precursor protein (APP), presenilin 1 or 2 and/or tau. C1q has been shown to co-localize with ß-amyloid plaques (155). C1q deficiency did not alter plaque formation, but drastically reduced astrocytic reactivity in the vicinity of plaques causing reduced neuronal injury and thus improved neuronal integrity (2). Furthermore, ß-amyloid induced synapse loss was dependent upon C1q: intracerebral injection of oligomeric ß-amyloid did not induce synapse loss in C1qKO mice and, similarly, synapse loss could be prevented by concomitant application of an anti-C1q antibody (21). As expected, C1q levels in C1qKO APP mouse brains were undetectable. However, C3 levels were high both intracellularly, due to their expression by astrocytes, and extracellularly as the cleavage products C3b/iC3b on fibrillary amyloid plaques (19). It was reasoned that C3– probably activated *via* the alternative pathway– acted neuroprotectively (19). In contrast, another study showed neuroprotective effects of C1q *via* CREB induced low density lipoprotein receptor-related protein 1B (LRP1B) and G protein-coupled receptor 6 (GPR6) expression *in vitro* (20). LRP1B and GPR6 levels in young animals were significantly lower in C1q deficient 3xTgBUB Alzheimer mice. It was inferred that C1q acts neuroprotectively during the early phases (pre-plaque formation) of the disease, while detrimental effects of C1q occur *via* co-expression of C1r and C1s in late stages (20). However, the expression pattern of C1q only paralleled LRP1B and GPR6 levels in a very limited degree with levels most prominently elevated at >13 months of age (20). Thus, effects of C1q on AD may be complex and age dependent.

Frontotemporal lobar degeneration (FLTD) is a neurodegenerative disorder with symptoms most strikingly encompassing personality changes with blunting of emotions as well as the development of aphasia. The familiar form is known to be related to mutations in the progranulin gene (GRN), which causes protein aggregation. In the murine genetic model for FLTD using progranulin deficiency, two considerable studies showed C1q deficiency induced reduced neurotoxicity and synaptic pruning by microglia (22, 23). Importantly, C1q deficiency also mitigated phenotypical obsessive compulsive behaviors and premature mortality (22). Microglia, expressing high levels of the causal protein progranulin as well as lysosomal and complement genes, were the key players to induced synaptic pruning of preferentially inhibitory synapses in the ventral thalamus (22) and transitioned to an activated state in the GRN-knockout mouse model (23). Microgliosis was mitigated in double GRN- and C1qKO mice and near-completely rescued in the triple knockout for GRN, C1q, and C3. Similarly, pharmacological blocking of the complement membrane attack complex reduced neuronal cell death (23). Thus, C1q-mediated complement activation may underlie microglial transmitted neuronal cell death in this disease model.

Morbus Parkinson is characterized by a loss of dopaminergic neurons of the substantia nigra, which causes typical movement related symptoms like tremor, rigidity, and slowed gait but also cognitive deficits. There was no evidence for an effect of C1q deficiency on loss of nigral dopaminergic neurons, striatal dopaminergic fibers or dopamine levels in the murine Parkinson's disease model by 1-methyl-4-phenyl-1,2,3,6-

TABLE 2 Overview of publications in the disease clusters autoimmunity and infectiology.

Disease entity	oc	Disease model	Gene manipulation and genetic background	Sex	Ref
			Immunology		
Autoimmunity	-	C1qKO induced SLE	129/Ola, 129/Ola×C57BL/6 F2	f/m	(9)
	-	C1qKO induced SLE	129/Sv, 129/Sv×C57BL/6 F2	f/m	(64)
	-	C1qKO induced SLE		f/m	(65)
	-	C1qKO induced SLE	129/Sv, 129/Sv×C57BL/6, C57BL/6	f/m	(66)
	=	C1qKO induced SLE	*C1qa-/-* Ig^{HEL}, *C1qa-/-* Ig^{HEL}/sHEL	f/m	(67)
	-	C1qKO induced SLE	129/Ola×C57BL/6	f/m	(68)
	-	C1qKO induced SLE	129/Sv×C57BL/6, C57BL/6	f/m	(69)
	=	C1qKO induced SLE		f/m	(70)
	-	C1qKO induced SLE	C57BL/6.*C1q*$^{-/-}$, C57BL/6.*lpr/lpr.C1q*$^{-/-}$, MRL/Mp-*lpr/lpr.C1q*$^{-/-}$	f/m	(71)
	-	C1qKO induced SLE	MRL/Mp.*C1q*$^{-/-}$,	f/m	(72)
	-	Cq1KO induced SLE	129×B6 F_2	f	(73)
	-	Cq1KO induced SLE	C1q$^{-/-}$-Ig^{HEL}, C1q$^{-/-}$-Ig^{HEL}/mHEL-KK	f/m	(74)
	=	Cq1KO induced SLE	V_H3H9R/V_Lκ8R.MRL/Mp.*C1qa*$^{-/-}$, V_H3H9R.MRL/Mp.*C1qa*$^{-/-}$	f/m	(75)
	+	pristane induced SLE	BALB/c	f	(76)
	-	Cq1KO induced SLE		f	(77)
	-	Cq1KO induced SLE		f	(78)
	-	autoimmunity	MRL/Mp.*C1q*$^{-/-}$, C57BL/6.*C1q*$^{-/-}$	f	(79)
Autoimmune nephropathy	-	LN	*C1qa*$^{-/-}$, *C1qa/H2-Bf/C2*$^{-/-}$, 129/Sv×C57BL/6	f/m	(80)
	-	LN	*Sle1.C1q*$^{-/-}$, *Sle1.Mfge8*$^{-/-}$*C1q*$^{-/-}$	f/m	(81)
	=	LN		m	(82)
	-	Anti-GBM GN	C1qa$^{-/-}$, C1qa/H2-Bf/C2$^{-/-}$, 129/Sv×C57BL/6	f/m	(83)
	-	Anti-GBM GN	129/Sv×C57BL/6, C57BL/6	f/m	(84)
	=	Anti-GBM GN		f/m	(85)
	=	Cryoglobulinemic GN	BALB/c	f/m	(86)
	=	FSG sclerosis	BALB/c	f	(87)
	=	tubulointestinal fibrosis		m	(88)
Transplant rejection	-	transplant at rejection		f	(89)
	-	transplant at rejection	C57BL/6, BALBc	f	(90)
	-	transplant at rejection		f	(91)
Arthritis	=	arthritis	*C1q*$^{-/-}$, *C1q*$^{-/-}$/*MBL*$^{-/-}$	f/m	(92)
	+	arthritis	*C1q*$^{-/-}$/*Df*$^{-/-}$	f/m	(93)
Vaccination	=	anaphylaxis	129/SV	f/m	(94)
	=	rhesus prophylaxe		f/m	(95)
	+	immunoprophylaxis			(96)
	=	HSV- Impfung		f	(97)
	=	adenoviral vectors		f/m	(98)
	=	adenoviral vectors		m	(99)
	-	IBD	C1q/MBL$^{-/-}$	f/m	(100)
	+	sterile inflammation	C1q$^{-/-}$, C1q/fD$^{-/-}$	f/m	(101)
			Infectiology		
Bacterial infections	-	S. Pneumoniae		f/m	(102)
	-	S. Pneumoniae		f/m	(103)
	-	S. Pneumoniae septicaemie		f/m	(104)
	-	S. Pneumoniae meningitis		f/m	(105)
	-	S. Pneumoniae acute otitis		f/m	(106)
	-	S. Pneumoniae acute otitis		f/m	(107)
	-	S. Pneumoniae acute otitis		f/m	(108)
	-	S. Pyogenes septicaemie		f/m	(109)
	-	polymicrobial peritonitis	129/SV	m	(110)
	-	polymicrobial peritonitis	129/SV	f/m	(111)
	-	polymicrobial peritonitis		f/m	(112)
	-	Salmonella enterica	129/SV	m	(113)
	-	Borrelia burgdorferi		f/m	(114)

(Continued)

TABLE 2 Continued

Disease entity	oc	Disease model	Gene manipulation and genetic background	Sex	Ref
	-	Rickettsia austral is		f/m	(115)
New therapeutica	-	N. gonorrhoeae		f	(116)
	-	N. gonorrhoeae		f	(117)
	=	N. gonorrhoeae		f	(118)
	=	P. aeruginosa		m	(119)
Other pathogens	-	West Nile virus	$C1q^{-/-}$, $C1q \times fD^{-/-}$	f/m	(120)
	-	Malaria	129/Sv	f	(121)
	=	Nematode	–	f/m	(122)
	=	Cryptosporidium	–	f/m	(123)
	=	Candida albicans	–	f/m	(124)

Each cluster is subdivided according to disease and organ manifestation, respectively. Disease outcome (oc) of C1qKO mice compared to wt and/or C1q sufficient mice in the investigated disease model is given as "+" respectively turquoise =beneficial, "-" respectively ocher =detrimental, "=" respectively grey=no effect. The overall outcome on the disease entity is similarly color coded using lighter shades for ambiguous group results. Genetic modifications other than C1qKO and genetic background other than C57BL/6 are listed explicitly. In studies with several C1q deficient mice, all C1q deficient mice are listed. Sex as indicated in the study (f=female only, m=male only, f/m=mixed gender); if not mentioned explicitly by the study, mixed gender was assumed. FSG, focal segmental glomerulosclerosis; GBM, glomerular basement membrane; GN, Glomerulonephritis; HSV, herpes simplex virus; IBD, inflammatory bowel disease; LN, lupus nephritis; N., Neisseria; P., Pseudomonas aeruginosa; S., Streptococcus; SLE, systemic lupus erythematosus.

tetrahydropyridine (MPTP)-induced loss of nigral dopaminergic neurons (26). There is currently no study investigating potential behavioral differences also over a prolonged disease course.

Amyotrophic lateral sclerosis (ALS) is a severe neurodegenerative disorder characterized by a rapidly progressing loss of primary and secondary motor neurons leading eventually to death due to respiratory motor failure. In a murine disease model expressing mutated superoxide dismutase (SOD1), C1q deficiency alone only caused histological improvement such as decreased synaptic loss of cholinergic nerve terminals onto motor neurons, while leaving the clinical outcome and progression of the disease unaffected (24). However, the triple knockout of reactivating astrocytes A1 inducing factors Il-1α,TNFα and C1q affected gliosis positively leading to a marked extension of mouse survival (25).

Obesity-induced brain pathology is characterized by typical cerebrovascular and white matter signs, which are related to microglia phagocytosis. These are not present in obese C1qKO mice under a western diet (28).

In a model for amyloid neuropathy caused by aberrant transthyretin (TTR), amyloid depositions were exacerbated in C1qKO mice most likely due to decreased phagocytosis (27). Thus, in the field of neurodegenerative studies, this is the only clear exception to else overall beneficial effects of C1q deficiency (**Table 1**).

1.3 C1q deficiency and brain injury

Upon brain tissue damage, astrocytes are known to be reactivated and can form glial scar tissue. Liddelow et al. explored C1q involvement in the formation of reactive astrocytes by microglia (31). The release of C1q, Il-1α and TNFα from activated microglia triggered the formation of reactive astrocytes. A1 astroctyes lost their ability to support neurons and induced death of axotomized neurons in a model of optic nerve crush (31). A1 astrocytes are also of interest with respect to the above explored neurodegenerative diseases as A1 astrocytes – positive for C3 – have been shown to be present in human post-mortem tissue from a large number of neurodegenerative and neuroinflammatory diseases (31). While C1qKO mice still had the ability to form A1 astrocytes, this was strongly reduced in Il-1α and TNFα double knockouts and completely blocked in triple knockouts. With respect to optic nerve crush, RGC remained intact seven days after intervention in double and triple knockout mice as opposed to wt mice (31). As the effect was already present in the double knockout, the role of C1q for this outcome might be weak. Intravitreous treatment of wt mice with anti-C1q antibodies altered astroglia expression pattern only slightly, while the combination of anti-C1q, anti-TNFα and anti-Il-1α hindered A1 formation (31). In contrast, a different study showed that the treatment success of RGC axon regeneration after optic nerve injury critically depended upon the presence of C1q: While C1q deficiency alone did not change axon regeneration, it significantly reduced the regeneration in the presence of various pro-regenerative treatments (33). The route of delivery was critical for effects on regeneration: Anti-C1q antibody treatment was only hindering regeneration when delivered intranervally or systemically but not intravitreously. The authors inferred that blocking C1q and/or the absence of C1q caused reduced removal of myelin, with myelin being a growth-inhibitor for axon regeneration (33). Similarly, postinjury debris clearance was reduced in C1qKO as well as microglia-deficient Itgam KO mice when examining the dLGN after optic nerve crush, a setting of Wallerian degeneration (32). In contrast to Liddelow et al., C1q deficiency had no protective effect on RCG cell survival in this study (32). Thus, while data from the

TABLE 3 Overview of publications in the disease clusters Vascular diseases, Pregnancy, Cancer and Various.

Disease entity	oc	Disease model	Gene manipulation and genetic background	Sex	Ref
Vascular diseases					
Atherosclerosis	-	atherosclerosis	*C1q$^{-/-}$/Ldlr$^{-/-}$*	f	(125)
	-	atherosclerosis	*C1q.Ldlr$^{-/-}$, C1q.sIgM.Ldlr$^{-/-}$*	f	(126)
	-	woundhealing	–	f/m	(127)
	-	ALI	–	f	(128)
	-	primary hemostasis		f/m	(129)
Pregnancy					
Fetal loss	-	fetal loss		f	(130)
	+	fetal loss	C1q/fD $^{-/-}$	f	(131)
	=	fetal loss		f	(132)
PE	-	PE		f	(133)
	-	PE		f	(134)
	-	PE		f	(135)
Cancer					
Solid tumor	+	melanoma		f/m	(136)
	=	breast cancer	neuT^{+}-C1q$^{-/-}$, BALB/c	f	(137)
	+	ccRCC		f/m	(138)
Tumor therapy	-	immunotherapy		f/m	(139)
	=	immunotherapy		f/m	(140)
	=	immunotherapy		m	(141)
	-	immunotherapy	SCID/C1q$^{-/-}$	f	(142)
Various					
Skin	=	burn injury		f/m	(143)
	+	epidermolysis bullosa BALB/c		f/m	(144)
	+	muscle regeneration		f/m	(145)
Pulmo	-	COPD		f	(146)
	+	pulmonary fibrosis		f/m	(147)
	=	AA amyloidosis	C57B L 6×129/SV	f/m	(148)
	=	adipose inflammation		f	(149)

Each cluster is subdivided according to disease and organ manifestation, respectively. Disease outcome (oc) of C1qKO mice compared to wt and/or C1q sufficient mice in the investigated disease model is given as "+" respectively turquoise =beneficial, "-" respectively ocher =detrimental, "=" respectively grey=no effect. The overall outcome on the disease entity is similarly color coded using lighter shades for ambiguous group results. Genetic modifications other than C1qKO and genetic background other than C57BL/6 are listed explicitly. In studies with several C1q deficient mice, all C1q deficient mice are listed. Sex as indicated in the study (f=female only, m=male only, f/m=mixed gender); if not mentioned explicitly by the study, mixed gender was assumed. ALI, acute lung injury; AA, amyloid A protein; COPD, chronic obstructive pulmonary disease; PE, preeclampsia.

Liddelow et al. study point to a protective effect of C1q deficiency on RCG cell survival (31), Peterson et al. looked beyond effects on the retina itself and observed hampered axon regeneration in the absence of C1q (33)

In a recent study, a clear effect of C1q on secondary long term injury after traumatic brain injury (TBI) by cortical impact could be demonstrated: neuroinflammation and cell loss in the thalamus three weeks following injury in sensoricortex was markedly reduced in C1qKO mice and was similarly demonstrated by repetitive intraperitoneal (i.p.) application of anti-C1q antibodies (34). However, functional effects as measured on a shorter timescale (1-7 days post injury) by memory tests and motor performance were not present in C1qKO as well as C3KO mice undergoing a similar brain injury protocol; only C4 knockout (C4KO) mice presented with reduced motor deficiency (30).

Mice with flox-targeted absence of C1q in microglia undergoing cranial radiation induced brain injury showed reduced neuroinflammation and reduced synaptic loss when compared to wt mice (35). They presented clinically without cognitive deficit (35).

Outcomes in spinal cord injury were not uniform: while lesion volume was reduced in the C1qKO mice after spinal cord contusion (36) it was unchanged to wt after transection (37). Functionally there was a small but significant increase in fine locomotor recovery in C1qKO mice (36). In cell culture, C1q increased neurite growth by inhibiting repulsive signaling of myelin associated glycoprotein (MAG). Axons of C1qKO mice expressed increased turning after dorsal column transection but no gross effects on total sprouting or midline crossing were noted (37). The consequence of turning with respect to sensorimotor function remained unexplored (37).

In contrast to the central nervous system (CNS), there is no evidence so far for a crucial role of C1q in the peripheral nervous system (PNS): there was neither a difference in motor recovery or cell survival in unilateral facial nerve crush (39) nor in behavioral motor outcome and synaptic terminals of affected motoneurons by sciatic nerve crush (38). Synapse elimination in the PNS may instead involve Schwann cells and complement independent mechanisms (156).

1.4 C1q deficiency and epilepsy

Synaptic pruning, the process of synapse elimination of excessive synapses in the neonatal brain, occurs throughout the mammalian brain and is known to continue until early adulthood in humans. As mentioned above, in C1q deficient mice, synaptic pruning was disturbed and associated with dysfunctional synaptic refinement in the dLGN (10). Excessive glutamatergic inputs and epileptogenic activity in C1qKO mice with a behavioral phenotype of atypical absence seizure seen as "freezing" behavior was reported and would be in line with failed synaptic pruning on brain wide neuronal circuitry (46). Microscopic analysis confirmed anatomical changes, such as higher spine density on basal dendrites of layer Vb neurons in the sensorimotor cortex, which is most likely due to inadequate synaptic pruning (47). However, there is also evidence that the role of C1q in synaptic pruning cannot be generalized to all parts of the brain: C1q deficiency had neither an influence on synaptic pruning and development of normal hearing in the auditory system (157) nor on the primary visual cortex (158). With respect to epilepsy, electroencephalography (EEG) recordings were performed postnatally with the oldest animal being 60 days of age (46), and it remains unclear, whether epileptic EEG patterns and behavioral abnormalities persist in later adulthood. Similarly, while C1q is needed for synaptic refinement in dLGN during development (10), it is not required for later plasticity in the ocular dominance sensitive phase in primary visual cortex (159). Thus, it is possible that the effects of C1q deficiency are dependent on the developmental stage and the specific brain regions involved.

Although, a predisposition to epileptic seizures is not uncommon in inbred mouse strains (160), the occurrence of epilepsy in C1qKO mice has to be taken into account when interpreting results in other areas, in particular brain-connectivity related diseases like neurodegeneration, which might potentially be influenced by ongoing epilepsy.

From a translational point of view it is worth mentioning that, in contrast to the mouse model, neuropsychiatric lupus and epileptic seizures are a rather uncommon finding in C1q deficient humans with SLE (1, 161).

1.5 C1q deficiency and infectious diseases of the brain

The CNS is an immune privileged system: The blood brain barrier forms a border to the systemic circulation allowing only certain molecules and cells to enter the brain. Tissue grafts show prolonged survival, foreign antigens do not readily elicit an immune response.

In pneumococcal meningitis in complement deficient mice (C3 and C1qKO), a remarkable differential regulation of cytokines with systemic up-regulation and concomitant down-regulation in the CNS was observed (105). The down-regulation was associated with fewer intracranial complications such as intracranial pressure elevation and blood brain barrier disruption. However, overall there was a pronounced lethal outcome in the C1qKO mouse that was related to secondary blood spread and systemic actions (105).

In human immunodeficiency virus associated neurocognitive disorder synapse loss was accompanied by C1q depositions (41). However, C1q was not causally related, as knockout of C1q did not rescue synapse loss (41).

Prion diseases are a group of rare transmissible brain diseases with the infectious agent being an abnormally folded prion protein, which induces misfolding of their naturally occurring correctly folded counterpart cellular prion protein (PrP^C). Amyloid aggregates of misfolded proteins and vacuoles are micro- and macroscopic hallmarks of lethal prion diseases such as scrapie in sheep, bovine spongiform encephalopathy in cattle or Creutzfeldt-Jakob disease in human. The process of neuroinvasion, i.e. entering of the pathogen into the brain, was massively hampered in C1qKO mice (3, 4). While prion inoculation into brain tissue led to development of scrapie in all tested mice, peripheral i.p. inoculation resulted in markedly delayed disease expression (4) and did not cause pathological changes in C1qKO mice when only limited prion titres were inoculated (3). Mechanistically, antigen uptake by dendritic cells was affected. Thus, neuroinvasion of peripherally applied prion requires C1q, a transporter function that can be overcome by a high load of prion inocula.

The role of naturally abundant PrP^C is still less clear. Splenic PrP^C is upregulated in response to an immunological challenge by immune complexes or stomatitis virus, a C1q dependent effect which is absent in C1qKO mice (40).

1.6 C1q deficiency and inflammatory autoimmune diseases of the brain

Multiple sclerosis (MS) is an inflammatory autoimmune disease of the CNS with destruction of myelin sheaths. A widely used model to induce MS like symptoms in mice is the myelin oligodendrocyte glycoprotein (MOG) -experimental autoimmune encephalomyelitis (EAE) model, whereby MOG peptide is administered subcutaneously. C3 deficiency attenuated disease severity measured in a number of behavioral read outs, while lack of complement C1q *per se* did not change the disease course (43). However, flares, commonly seen after anti-MOG antibody application, were abolished in this model of MS in C1qKO mice (42). Microglia-targeted knockdown of C1q in an EAE model reduced microgliosis (44). Again, the clinical progression of the disease and clinical scoring remained unchanged. Interestingly, the application of a

specific C1q blocking antibody (ANX-M1.21) reduced IBA1-microglia/macrophages in the tested hippocampal region similarly, arguing for anti-C1q antibodies to potentially inhibit chronic inflammation in white matter (44).

1.7 C1q deficiency and depression

C1qKO mice show a pronounced learned helplessness behavior in response to an inescapable foot-shock paradigm, a well-established model to induce depressive-like behavior (45). Wt mice showed reduced C1q mRNA levels in the prefrontal cortex (PFC) in response to foot-shocks as compared to unshocked mice. Interestingly, levels of pro-inflammatory cytokines in the PFC were significantly increased in C1qKO mice independent of the shock paradigm (45). It remains uncertain, whether these increased cytokines relate to increased levels as seen in post-mortem brain samples of patients or merely reflect an altered balance in the C1qKO brain.

2. C1q deficiency and ischemia and reperfusion (I/R) injury

In diseases like stroke or myocardial infarction a period of hypoxia caused by e.g. a thrombus obviating the transport of blood and oxygen to the downstream tissue is often followed by reperfusion once the thrombus resolves either by itself or by means of medical intervention. This reperfusion is known to cause additional, so called reperfusional damage, with complement being known to play a role (162).

2.1 C1q deficiency in stroke and neonatal hypoxic brain injury

A model of hypoxic ischemic brain injury in neonatal mice mimicking birth complications showed repeatedly a clear detrimental effect of C1q (48). Besides ligation of the carotid artery, the pups were exposed to hypoxia by 8% O_2 over 15 min, as ligation alone does not reproducible cause tissue damage due to a pronounced collateral perfusion at this age. C1qKO mice presented with reduced infarction volume and better neurofunctional performance as compared to wt controls. Mitochondria in C1qKO mice had markedly reduced reactive oxygen species production even before the intervention, a difference that was no longer present in adulthood, pointing to a postnatally altered cell metabolism in the knockout model (48).

Results on brain ischemia in adult mice are less clear and show mostly little effect of C1q deficiency (49–51). Occlusion of the middle cerebral artery over 30-60 min followed by reperfusion caused slightly though non-significantly reduced infarct size in C1qKO mice as compared to wt controls (49). Application of C1 inhibitor (C1-INH) prior to occlusion reduced significantly infarct size, an effect even present in the C1qKO mice arguing strongly for a neuroprotective effect of C1-INH independent of the classical C1q-mediated complement pathway (49). Effects caused by binding of C1-INH to C3b or C4b seem plausible and match the finding of a protective effect of C3KO mice in stroke (50). Double knockout for the lectin and classical pathway protected from cerebral I/R injury (51). These data point to a dominant role of the lectin pathway. Similar to other settings, the study supports a critical amplification by the alternative pathway of an initial signal by the lectin or classical pathway for detrimental outcomes (51).

After acute ischemic injury of the retina, C1q deficiency prevented the loss of RGC and upregulation of microglia in retina as well as in the downstream superior colliculus (52). Retinal function was only initially rescued in C1qKO mice, but functional deficits did not differ by day 28 after I/R as compared to wt mice (52).

Thus, although prominently cited with respect to stroke models, the effects on infarct volume in neonatal studies (48) cannot be transferred to an I/R situation in adulthood (49–51) (**Table 1**). Aside from a different capacity for plastic changes, the neonatal brain has different metabolic capabilities and furthermore, as the authors point out, age dependent different functionality of complement pathways.

2.2 C1q deficiency and I/R injury in other organs

I/R injury in organs other than the brain is most prominently affected by the lectin pathway rather than C1q and the classical pathway. MBL null mice were protected from myocardial infarction by temporary ligation of the left-anterior descending coronary artery, while C1qKO mice had unchanged left ventricular function and infarction size compared to wt controls (56). Similarly, MBL deficiency had a protective outcome with respect to muscle necrosis in hind limb ischemia (57) and skin necrosis area in cutaneous I/R (58). Here, C1q deficiency showed a similar trend which was not significant (58).

MBL is also a key player for I/R injury in gastrointestinal ischemia (53–55). In regard to C1q deficiency there was evidence for protection from I/R injury in male but not female mice (55), an effect which might have been missed in other studies (54). While C1qKO mice were protected against remote pulmonary injury as a sign of reperfusional damage in the severe protocol of 2 h of hindlimb ischemia (57), this was not the case in the setting of 20 min of gastrointestinal I/R (53).

3. C1q deficiency and liver diseases

C1q deficiency alleviated drug- or ethanol-induced hepatoxicity reducing hepatocellular apoptosis, inflammation

and elevated liver enzymes in most cases (59–63). Protective effects of C1q deficiency on alcohol induced liver damage were modest overall. A detrimental effect of factor D deficiency was more pronounced and repeatedly shown, making factor D a protective factor (60, 62), and thus contrasting the commonly seen accelerating detrimental effect of alternative pathway activation. This may relate to high activation levels for adequate clearance of apoptotic cells or to the role of factor D as adipokine.

C1q deficient mice on a high fat diet as model for beginning non-alcoholic steatohepatitis became obese, but did not develop hepatic steatosis and insulin resistance pointing towards C1q as therapeutic target in obesity related glucose homeostasis derangements (63). Interestingly, there was no change in high fat diet-induced apoptosis of liver cells (63).

4. C1q and autoimmunity

4.1 The generation of the C1q knockout mouse: a model for autoimmunity

The complement system and particularly the early components of the classical pathway appear to play a paradoxical role in SLE, the prototype of an autoimmune disease: While flares of SLE are associated with increased complement activity and consumption, inherited deficiency of C1q is a major risk factor for the development of SLE (1, 163). In order to study effects of C1qKO on autoimmunity, Botto et al. created the C1qKO mouse in 1998 (9). In line with the clinical presentation of hereditary C1q deficiency in humans, C1q deficient mice developed anti-nuclear antibodies (ANA) in 55% of cases and glomerulonephritis (GN) in 25% of cases (9), features and distributions with remarkable similarity to human SLE. One striking finding was the high number of apoptotic cell bodies and blebs in the kidneys of C1qKO mice, which was present even in the absence of the development of GN. This fostered the *waste disposal hypothesis* as one – though not exclusive – explanation for the development of systemic autoimmunity (see 4.4) (164–166). Notably, already in the first impressive and very thorough description of the C1qKO mice, it became clear that the development of autoimmunity was dependent upon two aspects: genetic background and gender (9).

4.2 C1q deficiency as disease accelerator in the presence of lupus prone background genes

C1q deficiency itself does not necessarily cause autoimmunity as neither mice with a pure 129/Ola background (9) nor C57BL/6 mice (71) developed auto-antibodies. Only in the presence of a permissive lupus-prone genetic background, C1q deficiency caused accelerated autoimmunity. As mentioned above, the initial description by Botto et al. clearly pointed out that only mice on a mixed genetic background, namely the F2 generation 129/Ola×C57BL/6, showed substantial autoantibodies and GN, while none of the pure 129/Ola background mice developed GN (9). Following up on this finding, Bygrave et al. could show that a 129-derived segment on chromosome 1 in a B6 background was sufficient to have profound effects on autoimmunity leading to high ANA titres (167), thus showing that 129/Ola×C57BL/6 itself is a susceptible genetic background for autoimmunity. Notably, 129/Ola×C57BL/6 mice are widely employed to generate gene-targeted mice. The fundamental assumption underlying the investigation of knockout-models, namely that the null-gene is causally related to disease outcome, is therefore heavily confounded in complement knockout mice with respect to autoimmunity. In the presence of C1q deficiency, the 129-derived region on chromosome 1, as well as a region on chromosome 3 from the B6 could be confirmed to be linked to ANA expression (73). Similarly, regions on chromosome 7 of 129 and chromosome 13 of B6 mice were strongly linked to GN (73).

C1q deficiency accelerated the development of autoimmunity not only on a 129/Ola×C57BL/6 mixed genetic background but also on other lupus-prone genetic backgrounds. While in the setting of a nonpermissive background of C57BL/6 mice C1q deficiency did not induce autoimmunity, it did lead to an accelerated progress of disease in lupus prone MRL/Mp$^{+/+}$ animals (71). MRL/Mp$^{+/+}$ mice are the parent strain of the better known MRL/Mp-*lpr/lpr* mice but with intact *Fas* gene, nevertheless known to be prone to autoimmune features (168). When introducing a *Fas* deficiency by *lpr* mutation, disease acceleration by C1q deficiency did not occur. This is possibly due to the advanced severity of the disease in C57BL/6.*lpr/lpr* and MRL/Mp-*lpr/lpr* strains, which may not have allowed for the detection of accelerating effects (71).

C1q deficiency could be overcome by bone marrow transplantation, proving the monocyte/macrophage lineage as major source of C1q and at the same time offering a potential treatment option for SLE in C1q deficient patients (69, 169). In addition, bone marrow transplantation alleviated the autoimmune phenotype on a lupus prone MRL/Mp background (72). This study provided clear evidence for a causality of C1q deficiency for the observed autoimmunity.

Thus, it is not C1q deficiency *per se* that relates to autoimmunity. Rather C1q deficiency has the ability to accelerate autoimmune disease, when a lupus prone genetic background with a high tendency for autoimmunity is present (Table 2).

4.3 Gender affects autoimmune manifestations in C1qKO mice

In addition, an effect of gender on the development of autoimmunity was described by Botto et al.: When comparing

C1q sufficient mixed background controls to C1q deficient mice, a significant difference in ANA levels only existed between males. Control females on the mixed background already started off with high titres. An increased susceptibility to manifestation of autoimmunity in females was confirmed in double knockout mice for C1q and H2-Bf/C2$^{-/-}$ (80) as well as C1q deficiency in the lupus prone MRL/Mp background (71). Although this effect is particularly well described for autoimmunity on a lupus prone genetic background, it is still noteworthy that a large number of studies in C1qKO mice included in this review investigated female mice only (4, 11, 38, 59, 60, 62, 73, 76–79, 87, 97, 116, 125, 128, 146, 149, 170) while others only used male animals (26, 35–37, 45, 46, 50, 53, 61, 63, 88, 99, 110, 113, 119, 141) (Tables 1–3). Few studies evaluated specifically the differential gender effect (12, 24, 28, 55, 71, 80).

The gender specificity of autoimmunity is particularly exciting from a translational approach as human autoimmunity *per se* and SLE in particular clinically shows a clear gender effect with predominantly young female patients being affected (171).

4.4 Using murine C1q deficiency to understand underlying mechanisms of autoimmunity

Autoimmunity is characterized by auto-antibodies directed against self-antigens with the underlying mechanisms as to why autoimmunity arises in certain patients but also in certain mouse models being still a matter of debate. In the setting of C1q deficiency the striking amount of apoptotic cells (9), the fact that autoantibodies directed against proteins contained in apoptotic blebs as well as the well accepted role of C1q in the removal of cell debris has led to the *waste disposal hypothesis*: a prolonged exposure of the body to cell debris fuels antibody formation (164, 166, 172). Besides high numbers of apoptotic cells in kidneys with and without GN (9, 80), the rate of clearance of apoptotic cells was also reduced in C1qKO mice in a model of sterile peritonitis (66). While the involvement of C1q in the clearance of apoptotic cells is a robust finding and widely accepted, removal of apoptotic cells and induction of autoantibodies and GN were unchanged when apoptosis was induced by ultraviolet light in an attempt to mimic a sunburn-triggered SLE flare (70), indicating that the effect cannot be generalized to all tissues and disease settings. One study pointed to mainly lysed cells, such as those in necrotic tissue, as aggravating agent of autoimmunity in C1qKO mice, while intact apoptotic cells did have no effect (65).

Another – and not mutually exclusive –hypothesis on the role of C1q deficiency in the development of autoimmunity is a modulating influence of C1q on B and T cell autoreactivity (67, 77). The results of C1q deficiency on B cell autoreactivity were inconsistent ranging from increased positive selection of auto reactive B cells (74) to no clear effect (64, 67, 75). While effects on B cells are inconsistent, it is apparent that C1q deficiency has effects on T-cell responses and related cytokine levels as well as on dendritic cell antigen processing in the spleen (67, 77, 79, 173). A more recent comprehensive publication focused on the question as to why C1q but not C3 deficiency is critical for self-tolerance, showing that C1q specifically altered mitochondrial metabolism of T-cells (77). C1q deficiency led to a skew towards an effector CD8+ T-cell phenotype in response to chronic viral infection (77). Thus, self-tolerance in C1q deficiency may be lost due to an inadequate CD8+ T cell response to viral infection (77). An earlier report described chronically accelerated CD4+ T-cell activation and splenic monocytosis caused by C1q deficiency in a lupus prone genetic background (79). In addition, C1q was tightly linked to processing of immune complexes with splenic uptake of immune complexes being significantly reduced in C1q deficient mice (64, 68). Beyond effects on specific immune cells other mechanisms may also be of relevance. Molecular mimicry could be a link between epstein-barr virus infections and the formation of anti-C1q antibodies in SLE as shown in C1qKO mice (78).

In contrast to the great number of studies using C1q deficiency in lupus prone backgrounds to induce or accelerate autoimmunity, there is a single report showing alleviated autoimmunity in C1q deficiency (**Table 2**): when the SLE phenotype was induced by the i.p. injection of the oily substance pristane (76). In this setting, C1q deficiency surprisingly reduced auto-antibody titers and caused milder arthritis (76).

4.5 C1q deficiency in autoimmune nephropathies

4.5.1 Lupus nephritis is a typical feature in C1qKO mice

Lupus nephritis (LN) is a typical feature in C1qKO mice on a mixed genetic background (9, 80). LN is characterized by immune complex formation containing deoxyribonucleic acid (DNA) and anti-ds DNA immune complexes as well as C1q, laminin and other auto-antibody targets. While C1q deficiency was associated with an increase of apoptotic cells in kidneys, clearance did not require C3 activation (80). C1q deficiency also acted as disease accelerator in a polygenetic model of LN in which low complement was mimicked by C1q deficiency, autoantibody formation was induced by *Sle1* knockout (*Sle1*-KO) and defective clearance of apoptotic cells by *Mfge8* knockout (*Mfge8*-KO) (81). There was, however, no significant effect when comparing C1q sufficient *Sle1*-KO with C1q deficient *Sle1*-KO mice. In addition, anti-C1q antibodies are strongly associated with LN. In a model of LN by application of anti-glomerular basement membrane (GBM) antibodies as well as mouse anti-C1q antibodies, C1qKO mice did not show increased albuminuria (82), indicating that glomerular C1q-containing immune complexes are essential for disease manifestation in this setting.

4.5.2 Other autoimmune nephropathies

There are a variety of other forms of autoimmune nephropathies. Models of anti-GBM glomerulonephritis were overall aggravated by C1q deficiency (83–85) (Table 2). Anti-GBM antibody application led to severe glomerular thrombosis within four days of induction of disease in C1q-deficient mice compared to mild injury in wt controls (83). Again, C1q deficiency was only associated with increased nephritis susceptibility on a mixed genetic background but not on a pure C57BL/6 background (84, 85). Differences in susceptibility to glomerular inflammation were indeed so apparent in the investigated strains, that it could not be excluded, that the effect was caused by the background genes rather than the absence or presence of C1q (84).

Immune-complex glomerulonephritis induced by cryoglobulins remained unaltered by C1q deficiency (86). Furthermore, models which investigated sclerosis and fibrosis of the kidney remained unaffected by C1q deficiency (87, 88).

In summary, while in lupus prone strains C1q deficiency readily accelerates lupus nephritis (9, 80, 81), other forms of immune complex glomerulonephritis are not necessarily affected by C1q deficiency (86). Similarly, immune mediated nephritis induced by injection of anti-glomerular antibodies is deteriorated in certain mice strains but not on a non-permissive C57BL/6 background suggesting that the sole absence of C1q is not sufficient to cause disease but requires additional genetic and/or environmental factors (83–85).

4.6 C1q deficiency and tolerance induction in organ transplantation

Transplant rejection is associated with C3 deposition and related to complement activation (174). Counterintuitively, C1q as well as C3 appear to be protective with respect to allograft rejection as demonstrated by an earlier rejection of a solid organ transplant in C1qKO as well as C3KO mice (89–91). Intranasal tolerance induction failed in complement (C1q and C3) deficient mice (90). Importantly, models addressing T-cell specific graft responses (HY mismatched skin graft) showed faster rejection in C1q deficiency (90). Accepted grafted skin had increased mRNA levels of C1q (as well as C3 and interferon -γ), making an argument for a contribution of C1q to tolerance induction also with respect to grafted tissue (90).

4.7 C1q deficiency and arthritis

C1q deficiency alone did not change the outcome in a model of inflammatory arthritis induced by anti-collagen antibodies, instead the alternative pathway was responsible for driving the disease (92, 93). While factor D deficiency protected against disease manifestation, additional C1q deficiency did not result in further benefit (93).

4.8 C1q deficiency and vaccination

In models of vaccination (95, 97) and gene therapy vectors (98, 99), there was no major effect of C1q deficiency. Immunoprophylaxis by alloimmunization as performed e.g. in rhesus prophylaxis failed when performed at a timepoint of concomitant viral infection. This failure of immunoprophylaxis was complement dependent and C1qKO mice expressed successful alloimmunization under concomitant inflammation (96).

5. C1q deficiency and Infections

5.1 C1q deficiency aggravates bacterial infections

Complement is a cornerstone of innate immunity, giving rise to a rapid response to a number of pathogens. About 40% of patients with C1q deficiency present clinically with recurring severe bacterial infections (1). In agreement, the outcome of C1q deficient mice in studies on bacterial infections was exclusively negative (Table 2).

The encapsulated gram-positive diplococcus *Streptococcus pneumonia*, numerously studied in C1qKO mice, is the most common pathogen in human bacterial pneumonia and a highly relevant pathogen regarding meningitis (102–105, 108). In all investigated modes of infection (i.p., intranasal, intravenous, transtympal, intracysternal) C1q deficient mice presented with higher pathogen titers in tissue samples (102, 104–106, 108). Complement C3 and C1q protected against the spread of *Streptococcus pneumonia* into the blood, an effect which was even more pronounced in C3 deficient mice (104, 105). C1q deficiency (as well as factor B deficiency) reduced opsonization of *Streptococcus pneumoniae* in a model of otitis media (107) and phagocytosis triggered by activation of the classical pathway *via* IgM appeared to be the dominant route of defense against *Streptococcus pneumoniae* (102, 106). Protection against pneumococcal infections in a passive immunization model was dependent upon classical pathway activation, but not on a functional leukocytal Fc gamma receptor (103). The bacterium has developed specific virulence factors against complement like pneumolysin, which is expressed in certain strains of *Streptococcus pneumonia* and binds C1q (104). Counter intuitively, pneumolysin rather acted by activating than inhibiting the classical pathway, but the relation to decreased complement deposition on the bacterium remained unclear (104).

Although, it is the alternative pathway that is essential for the clearance of *Streptococcus pyogenes* infections, C1qKO mice also readily succumbed in *Streptococcus pyogenes* septicaemie due to inefficient phagocytosis (109). Similarly, C1qKO mice undergoing polymicrobial infection had greatly heightened mortality (94, 112), which was even inducible by low pathogen loads (110).

Many gram-negative bacteria are not susceptible to complement attacks due to the expression of complement regulators. However, possibly due to disturbed phagocytosis, C1qKO mice were unable to limit *Salmonella enterica* serovar Typhimurium growth with animal deaths starting to occur 6 days after transfection (113). Also infections with *Borrelia burgdorferi*, a tick transmissible spirochete, caused higher pathogen load in C1q deficiency, though clinical effects were comparatively mild (114). In this case, the pathomechanisms may relate to a delayed IgG class switch, altered T-cell response, and altered cytokine levels (114). Similarly, the pathogen burden in various organs during infections with *Rickettsia*, yet another intracellular pathogen transmitted among others by ticks, was significantly increased in C1qKO mice (115).

5.2 C1q deficiency and new antibacterial therapies

New antibacterial therapies against the increasingly drug-resistant *Neisseria gonorrhoeae*, a pathogen causing the sexually transmitted disease gonorrhoe, use chimeric antibodies with increased capability to form hexamers targeting specifically C1q and the complement pathway (116, 117), as well as other C1q independent virulence mechanism like sialylation of *Neisseria gonorrhoeae* lipooligosaccharides (118). The prophagocytic therapeutic effect of the pattern recognition receptor PTX3 against *Pseudomonas aerruginosa*, a pathogen associated with chronic lung infections, was similarly unchanged in C1qKO mice (119).

5.3 C1q deficiency and infections with other pathogens

The investigation of pathogens other than bacteria yielded mainly no effect of C1q deficiency on clinical outcome (122, 124) with the exceptions of negative outcomes in the infection with the malaria causing parasite *Plasmodium chabaudi chabaudi* (121) and the viral infection with West Nile virus (120) (**Table 2**). High viremia and mortality in C1qKO mice with spleens remaining virtually free of infectious virus again underpins the crucial role of C1q in transport and pathogen processing in this lymphoid organ (120, 121).

6. C1q deficiency and vessels

Atherosclerosis is a disease of the arterial vessel wall with a complex pathogenesis involving endothelial dysfunction, inflammatory, and immunological processes accompanying plaque formation. Apoptotic cells, while efficiently removed by activated macrophages in early lesions, are prominent in late lesions. Genetic knockout of low-density lipoproteinreceptor (LdlrKO) serves as a model of atherosclerosis. Lesion size and complexity is increased by additional C1q deficiency in LdlrKO mice kept on a high fat diet (125). IgM-Ldlr double knockout mice had even greater lesions, even when compared to triple knockout mice lacking IgM, Ldlr, and C1q (126). This observation supports IgM tagging of cholesterol with subsequent C1q-stimulated removal by macrophages as an important pathomechanism.

Angiogenesis, the formation of new vessels, is a tightly regulated mechanism physiologically occurring e.g. during wound healing. In skin wounds, vessel formation was found to be insufficient in C1qKO mice and could be restored upon the local application of C1q, suggesting a role of C1q as angiogenic factor for the treatment of chronic ulcera (127). C1qKO mice expressed altered lung vascular homeostasis with enhanced susceptibility of the pulmonary endothelium in response to injury (128).

Finally, the complement and coagulation cascades have been shown to interact at various levels (175) including the interaction of the two initiators von Willebrand factor and C1q (176, 177). The functional relevance of C1q in primary hemostasis was demonstrated by prolonged bleeding time of C1qKO mice in tail bleeding experiments (129).

7. C1q deficiency and pregnancy

C1q is present at the feto-maternal interface and has a promoting role for trophoblast invasion of the decidua (178). C1q deficiency was associated with smaller litter size, reduced fetal weight and increased frequency of fetal resorption (130). However, C1q deficiency is not related to fetal loss *per se* as there was no influence on fetal loss in a model of dysregulated uterine conditions induced by Il-2 primed T-cells directed against paternal antigens (132). Interestingly, litter size and fetal resorption was also not affected by C1q deficiency as compared to wt mice in this study (132), contradicting earlier findings (130).

Double knockout mice for C1q and factor D, i.e. defective classical and alternative pathways, were protected from fetal loss induced by antiphospholipid syndrome, a well-known clinical cause for miscarriage (131). This detrimental role of complement activation in fetal loss in antiphospholipid syndrome was further supported by robust C4 deposition at feto-maternal interface as well as in human tissue from SLE and/or antiphospholipid syndrome patients (131).

A robust and impressive phenotype of C1q deficiency is the development of preeclampsia (PE) characterized by hypertension, albuminuria, glomerular endotheliosis, and decreased levels of placental vascular endothelial growth factor (133–135). Development of PE relates to C1q deficiency of the fetus rather than the mother as it is also observed in C1q competent females carrying offspring from C1q deficient males (135). As in other models of PE, high-dose pravastatin treatment (amounts of 5 mg per day compared to 20-40 mg per day dosage commonly used in humans as lipid-lowering agent) could obviate the condition and restore trophoblast invasiveness

(135). PE caused persisting endothelial dysfunction for up to 6 months in C1q sufficient mothers and offspring as well as microglia activation in offspring, all of which responded to pravastatin treatment (133, 134).

8. C1q deficiency and cancer

C1q deficiency yielded conflicting effects in different cancer models (136–138) (Table 3). In a breast cancer model of Her2/neu transgenic (neuT) mice, C1q deficiency was associated with accelerated formation of lung metastases and intratumoral vessel formation, arguing for C1q as inhibitor of tumor angiogenesis (137). In contrast, a detailed study on implanted melanoma cells showed lower vascular density and fewer metastases as well as slowed down tumor growth and prolonged survival of C1q deficient mice (136). Human tissue expressed high levels of C1q in the stromal parenchyma at the tumor invading zone, arguing for C1q as a locally derived tumor promoting factor. Similarly, tumor vascularization was impaired in C1qKO mice in a model of lung carcinoma cells (138). Of note, the lung tumor cells were inoculated subcutaneously and thus in a similar microenvironment as the melanoma cells in the study by Bulla et al. (136). These results are not easy to reconcile with the breast cancer study (137). Besides a peculiar role of the skin as microenvironment for tumor growth or the effect of different background genes (BABLc versus B6) it is very likely that different cancer entities do not have comparable pathomechanisms of progression.

With respect to cancer treatment, B-cell depletion by the chimeric CD20 antibody rituximab appears to be critically dependent upon the presence of C1q (139), while mouse anti-CD20 antibody acted independently of C1q (140), a discrepancy which may relate to a species specificity of the used Fc segment. Unwanted toxic effects by high cytokine levels when using co-stimulatory small molecules were not affected by C1q deficiency (141). The synergistic effect of the combinatory therapy with trastuzumab and pertuzumab in hormone-receptor positive breast cancer was abolished in C1qKO mice (142).

9. Areas with limited evidence

In some disease models there are currently only singular studies employing C1qKO mice. Areas with beneficial effects of C1q deficiency include muscle regeneration in aged mice (145), sterile inflammation by i.p. administration of polyglycolic acid as present in degradation processes of absorbable sutures (101). Epidermolysis bullosa acquisita with subepidermal blisters induced by antibodies directed against collagen VII was most prominently influenced by the alternative pathway, while C1q deficiency only decreased the extent of skin disease at the end of the observation period (144).

Deleterious effects in C1q/MBL double-deficient mice were seen in inflammatory bowel disease modeled by dextran sulfate sodium-induced colitis (100). Effects of C1q on regulatory T cell differentiation also are related to a marked increase in lung inflammation in a mouse model for smoke induced chronic obstructive pulmonary disease (146). While the number of immune cells is unchanged in a model of silicate induced lung fibrosis, C1q deficiency was beneficial with respect to fibrotic changes (147). Conversely, intratracheal application of C1q in wt mice induced fibrotic changes (147).

In models of anaphylaxis (94), eschar formation after burn injury (143), and amyloidosis (148) there was no major effect of C1q deficiency. Inflammatory cytokines expressed in adipocytes in response to high ethanol feeding were reduced in C1q deficient mice with the number of apoptotic adipocytes remaining unchanged (149).

Discussion

C1q as target molecule to treat human disease

Are there diseases where C1q is harmful and a potential target protein to treat certain diseases? From an evolutionary perspective any protein in our body serves a purpose and can therefore in the first place be regarded as beneficial. In the case of C1q, this view is further underpinned by the evolutionarily conserved presence of C1q in many species. Clearly, when looking at immune defense and autoimmunity, C1q is not only beneficial but even critical. However, there may be circumstances where the presence of C1q becomes detrimental and the absence of C1q such as in the C1qKO mouse is beneficial. In the presented overview of disease-focused studies employing the C1qKO mouse, we identified neurodegenerative diseases, including glaucoma and secondary neurodegenerative processes after TBI, postexposure prophylaxis in prion disease and drug-induced liver inflammation as the most promising settings, in which an inhibition of C1q might be therapeutically valuable (Figure 2).

Most diseases with beneficial outcome in C1q deficiency can be summed up under the term sterile inflammation, while septic inflammation is associated with detrimental outcome in C1qKO mice. C1qKO mice had a beneficial outcome in response to application of substances (61), ethanol (60, 131), suture material (101) or amyloid plaques in neurodegeneration (2, 19). Even pristane induced SLE might be regarded in this context (76). In contrast to sterile inflammation, septic conditions caused by pathogens required the presence of C1q as seen by the detrimental outcomes of the C1qKO mouse (102–106, 108–

114) (Table 2). An exception to this rule is prion disease (3, 4), where C1q blockage may have great potential in postexposure prophylaxis.

Experimentally, C1q-blocking antibodies have been applied in a number of murine studies in recent years with promising results. Mainly neurological disease entities were tackled with main effects being shown on microglia: from potential synaptic rescue in transgenic Tau-P301S AD model mice (179) as well as wt mice challenged with intraventricular injection of soluble amyloid β oligomers (21) and neurolupus (180) to effects on microglia as a therapeutic approach to reduce chronic white matter inflammation in MS (44) and TBI (34). In mild TBI, C1q antibody application reduced secondary inflammatory neurodegeneration and protected against sleep pattern disruption and epileptogenic potentials (34). Interestingly, the i.p. application caused complete depletion of plasma C1q, while C1q levels in brain-homogenate – though significantly reduced – were detectable and remained above half of the control level, possibly also due to intracellular mostly microglial derived protein (34). Indeed, a number of clinical trials in humans have been undertaken to treat neurological as well as autoimmune diseases by delivering an anti-C1q antibody, which depletes and/or blocks serum C1q (181, 182). Currently these trials are in phase 2 for Guillain-Barré Syndrome, warm autoimmune hemolytic anemia, Huntington's disease and ALS (182). While treatment of Guillan-Barré Syndrome will be performed over a limited time period and a conference abstract reported promising results of a Phase 1b study on single-ascending-dose with respect to safety but also outcome (183), in the setting of Huntington's disease long term treatment might be necessary.

Based on the presented studies in animal models, there are several challenges arising when considering the treatment of diseases with anti-C1q directed antibodies. First, most relevant diseases would require treatment early on in the course of disease. This holds particularly true for glaucoma, one of the most promising candidates. Based on experimental data, anti-C1q blocking treatment might be required even before axonal damage and thus before symptom onset (12). Also with respect to neurodegenerative AD there is evidence for C1q being an early mediator of synapse loss (21). Second, treatment may be required over extended periods of time particularly in chronic diseases such as neurodegeneration and glaucoma. Third, a systemic blockage or depletion of C1q as a treatment could cause severe side effects, particularly if treatment is required over extended time periods. The main side effects to be expected under C1q depletion encompass elevated risk of infections, endangered pregnancy, and development of autoimmune phenomena. The outcome of C1qKO mice in models of bacterial infections is pronounced (Table 2) and the immunosuppressive effects of C1q depletion over longer time periods is likely to be relevant. When thinking of anti-C1q antibodies as a treatment for MS, as recently demonstrated in mice (44), the effects on pregnancy in this patient group need to be carefully considered. Autoimmunity in mice heavily depends on background genes in whose presence C1q deficiency may act as a disease accelerator. Possibly, only a limited number of individuals may be affected by autoimmune phenomena in response to prolonged systemic C1q inhibition. Nevertheless, the effect of C1q deficiency on autoimmunity seems to be more pronounced in human beings than in mice with about 77% of individuals with C1q deficiency developing SLE or SLE-like disease. In addition, anti-C1q antibodies targeted to the collagen-tail can aggravate immune complex nephritis in mice (82) and similarly therapeutic agents could aggravate ongoing immune processes in patients.

Current approaches use anti-C1q antibodies, which seem to cause a serum-depletion of C1q (181). This depletion, while being highly effective, is nevertheless the key to expected side effects. C1q is a highly functional and large molecule which poses the question of whether we can make use of its functionality. It is not unlikely that C1q expresses more than one functional domain that consequently mediates different downstream effects. There is the possibility, that specific cryptic epitopes relate to particular diseases and/or symptoms (184). Cryptic epitopes are hidden and only become exposed upon e.g. binding of specific target structures. A better understanding of these epitopes as well as downstream receptors and pathways would allow us to target therapies more precisely and avoid major side effects from unspecific depletion of this highly versatile molecule.

Limitations

The usage of C1qKO mice is an attractive tool to explore the causal relevance of the protein in *in vivo* models of disease. A mere correlation of C1q levels with disease manifestation may be misleading and unchanged disease manifestation in C1qKO mice can reveal missing causality (14, 43).

Though C1q knockout appears to be a very clean and clear-cut method to address the role of C1q, there are potential drawbacks to be considered. An evolutionarily conserved and highly relevant system like the complement cascade is bound to rely on multiple routes rather than on a single pathway/protein. Thus, it is possible that compensatory mechanisms come into play in the C1qKO mouse. The interactions of complement proteins are not as linear as often depicted on overview figures such that knocking out one player may have unexpected effects on other pathways (27). C1q might even have opposing effects on different mechanisms within a specific disease (20). Furthermore, when going into technical details it becomes clear, that the target gene cannot be knocked out without having some residual genetic information remaining. Specific 129 derived intervals on chromosome 1 were sufficient to have profound effects on autoimmunity namely the loss of tolerance to nuclear antigens (167), thus creating a major confounder. It is not

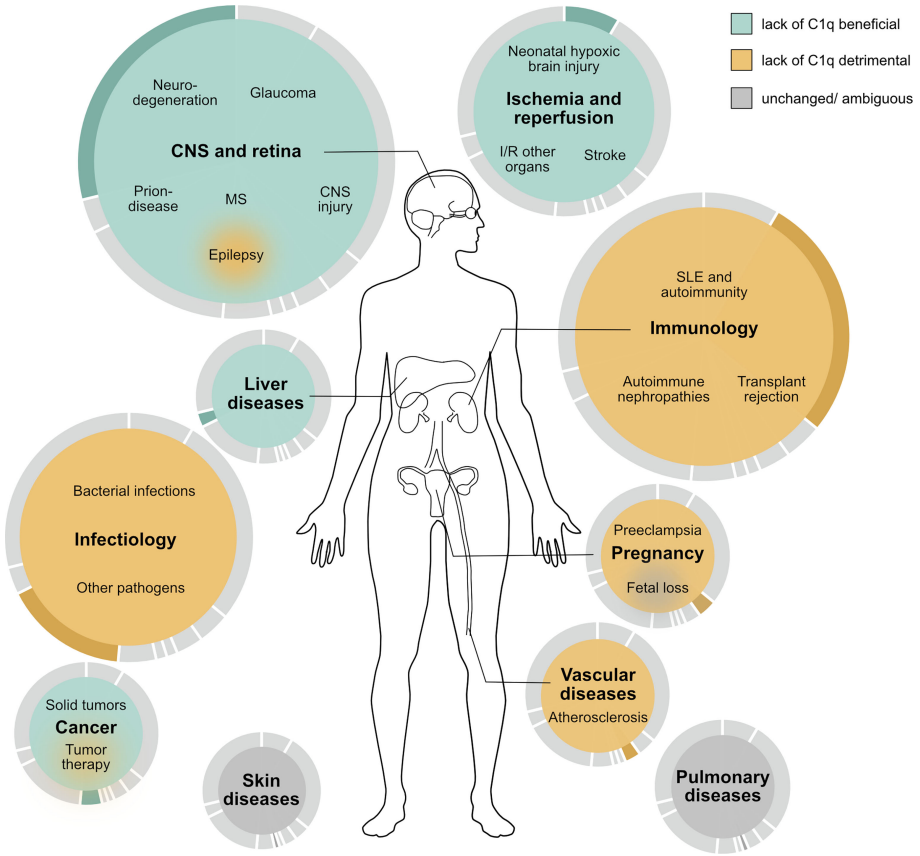

FIGURE 2
Schematic overview of the proposed effect of C1q deficiency on human disease based on the outcome of studies performed in murine disease models. Beneficial effects are colored in turquoise, detrimental in ocher, and outcomes without general trend or with ambiguous results in grey. The size of the colored area and the underlying pie chart illustrate the number of studies performed in the respective area. MS multiple sclerosis, I/R ischemia and reperfusion, SLE systemic lupus erythematosus.

always given, that the null-gene is exclusively causally related to disease outcome.

Second, there is the challenge of translating results from the mouse to the human, and vice versa modelling a human disease in a murine model. Disease models in mice are limited in various ways. In order to create a disease model, one must make certain assumptions on the causal origin of the disease to best mimic the disease. These assumptions might be misleading. Alternatively, the close observation of certain symptom sets in mice resembling features of human disease may lead to establishing a disease model. However, while symptoms may be similar, underlying pathomechanisms do not need to be. In addition, species differences like certain immunological features or levels of complement components may change pathomechanisms and hamper the transfer of murine outcomes into the human disease setting. Additionally, some diseases or symptoms may be utterly impossible to investigate in murine models e.g. aphasia in FTDL.

Finally, there are limitations in the design of this review. First, while we used broad search terms in our database query it is possible that we missed some publications. Second, negative results are not as regularly published as studies which are able to show an effect leading to a publication bias. Third, not all studies were designed to explore the outcome of C1qKO versus wt mice, which particularly limits the interpretation of studies using C1qKO in combination with another gene knockout.

Concluding remarks

The specific understanding of pathomechanisms in diseases involving the complement system has enabled us to apply targeted treatment. An example is paroxysmal nocturnal hemoglobinuria, which is caused by deficiency in CD55 and CD59, making red blood cells susceptible to complement-mediated lysis. Nowadays,

paroxysmal nocturnal hemoglobinuria can be successfully treated with the anti-C5 antibody eculizumab. C1q might be another upcoming target worthwhile exploring to treat or prevent for example neurodegenerative diseases, a disease entity with an immense socio-economic burden.

Several publications cited here made attempts to define good and bad players of the complement system. A quote from Benhar et al. seems applicable not only with respect to immune cells but all players of the immune-system: " *there are no 'good' or 'bad' immune cells; it is all a matter of their control and coordination* " (185). Indeed, it would make little sense from a biological perspective to have molecules or cells, which are under all circumstances "bad guys". As with anything in nature, it is often about maintaining the balance. This systematic review contributes to identifying those diseases, where C1q might be out of balance. First approaches today use anti-C1q antibodies, which seem to cause a serum-depletion and/or blocking of C1q (181). It is conceivable that a more specific targeting of specific epitopes of C1q may result in a therapeutic outcome with reduced systemic side effects. Future translational research is needed to evaluate adequate approaches to re-establish an equilibrium without causing side effects of the other extreme.

Data availability statement

The original contributions presented in the study are included in the article/Supplementary Material. Further inquiries can be directed to the corresponding author.

Author contributions

KS: drafting, conceptualizing, and editing. MT: conceptualization, reviewing, editing, and supervision. All authors contributed to the article and approved the submitted version.

Funding

MT is supported by a project grant of the Swiss National Science Foundation (SNSF) (320030_200423/1). KS is supported by the reglementary pool of the Division of Internal Medicine, University Hospital, Basel, Switzerland.

Acknowledgments

We thank Pascal Rabatscher, Claudia Donat and Eylül Tuncer for valuable input to the manuscript. We thank Shakuntala Savanthrapadian and Patricia Dietrich for editing.

Conflict of interest

The authors declare that the research was conducted in the absence of any commercial or financial relationships that could be construed as a potential conflict of interest.

Publisher's note

Supplementary material

The Supplementary Material for this article can be found online at: https://www.frontiersin.org/articles/10.3389/fimmu.2022.958273/full#supplementary-material

References

1. Stegert M, Bock M, Trendelenburg M. Clinical presentation of human C1q deficiency: how much of a lupus? *Mol Immunol* (2015) 67(1):3–11. doi: 10.1016/j.molimm.2015.03.007

2. Fonseca MI, Zhou J, Botto M, Tenner AJ. Absence of C1q leads to less neuropathology in transgenic mouse models of alzheimer's disease. *J Neurosci* (2004) 24(29):6457–65. doi: 10.1523/JNEUROSCI.0901-04.2004

3. Klein MA, Kaeser PS, Schwarz P, Weyd H, Xenarios I, Zinkernagel RM, et al. Complement facilitates early prion pathogenesis. *Nat Med* (2001) 7(4):488–92. doi: 10.1038/86567

4. Mabbott NA, Bruce ME, Botto M, Walport MJ, Pepys MB. Temporary depletion of complement component C3 or genetic deficiency of C1q significantly delays onset of scrapie. *Nat Med* (2001) 7(4):485–7. doi: 10.1038/86562

5. Ten VS, Sosunov SA, Mazer SP, Stark RI, Caspersen C, Sughrue ME, et al. C1q-deficiency is neuroprotective against hypoxic-ischemic brain injury in neonatal mice. *Stroke* (2005) 36(10):2244–50. doi: 10.1161/01.STR.0000182237.20807.d0

6. Nayak A, Ferluga J, Tsolaki AG, Kishore U. The non-classical functions of the classical complement pathway recognition subcomponent C1q. *Immunol Lett* (2010) 131(2):139–50. doi: 10.1016/j.imlet.2010.03.012

7. Thielens NM, Tedesco F, Bohlson SS, Gaboriaud C, Tenner AJ. C1q: A fresh look upon an old molecule. *Mol Immunol* (2017) 89:73–83. doi: 10.1016/j.molimm.2017.05.025

8. Kishore U, Reid KBM. C1q: structure, function, and receptors. *Immunopharmacology* (2000) 49(1–2):159–70. doi: 10.1016/S0162-3109(00)80301-X

9. Botto M, Dell'Agnola C, Bygrave AE, Thompson EM, Cook HT, Petry F, et al. Homozygous C1q deficiency causes glomerulonephritis associated with multiple apoptotic bodies. *Nat Genet* (1998) 19(1):56–9. doi: 10.1038/ng0598-56

10. Stevens B, Allen NJ, Vazquez LE, Howell GR, Christopherson KS, Nouri N, et al. The classical complement cascade mediates cns synapse elimination. *Cell* (2007) 131(6):1164–78. doi: 10.1016/j.cell.2007.10.036

11. Howell GR, Macalinao DG, Sousa GL, Walden M, Soto I, Kneeland SC, et al. Molecular clustering identifies complement and endothelin induction as early events in a mouse model of glaucoma. *J Clin Invest* (2011) 121(4):1429–44. doi: 10.1172/JCI44646

12. Kumari R, Astafurov K, Genis A, Danias J. Differential effects of C1qa ablation on glaucomatous damage in two sexes in DBA/2NNia mice. *PloS One* (2015) 10(11):1–20. doi: 10.1371/journal.pone.0142199

13. Williams PA, Tribble JR, Pepper KW, Cross SD, Morgan BP, Morgan JE, et al. Inhibition of the classical pathway of the complement cascade prevents early dendritic and synaptic degeneration in glaucoma. *Mol Neurodegener* (2016) 11 (1):1–13. doi: 10.1186/s13024-016-0091-6

14. Rohrer B, Demos C, Frigg R, Grimm C. Classical complement activation and acquired immune response pathways are not essential for retinal degeneration in the rd1 mouse. *Exp Eye Res* (2007) 84(1):82–91. doi: 10.1016/j.exer.2006.08.017

15. Rohrer B, Coughlin B, Kunchithapautham K, Long Q, Tomlinson S, Takahashi K, et al. The alternative pathway is required, but not alone sufficient, for retinal pathology in mouse laser-induced choroidal neovascularization. *Mol Immunol* (2011) 48(6–7):1–8. doi: 10.1016/j.molimm.2010.12.016

16. Murinello S, Mullins RF, Lotery AJ, Perry VH, Teeling JL. Fcγ receptor upregulation is associated with immune complex inflammation in the mouse retina and early agerelated macular degeneration. *Investig Ophthalmol Vis Sci* (2014) 55 (1):247–58. doi: 10.1167/iovs.13-11821

17. Jiao H, Rutar M, Fernando N, Yednock T, Sankaranarayanan S, Aggio-Bruce R, et al. Subretinal macrophages produce classical complement activator C1q leading to the progression of focal retinal degeneration. *Mol Neurodegener* (2018) 13(1):1–18. doi: 10.1186/s13024-018-0278-0

18. Mukai R, Okunuki Y, Husain D, Kim CB, Lambris JD, Connor KM. The complement system is critical in maintaining retinal integrity during aging. *Front Aging Neurosci* (2018) 10:1–12. doi: 10.3389/fnagi.2018.00015

19. Zhou J, Fonseca MI, Pisalyaput K, Tenner AJ. Complement C3 and C4 expression in C1q sufficient and deficient mouse models of alzheimer's disease. *J Neurochem* (2008) 106(5):2080–92. doi: 10.1111/j.1471-4159.2008.05558.x

20. Benoit ME, Hernandez MX, Dinh ML, Benavente F, Vasquez O, Tenner AJ. C1q-induced LRP1B and GPR6 proteins expressed early in Alzheimer disease mouse models, are essential for the C1q-mediated protection against amyloid- β neurotoxicity. *J Biol Chem* (2013) 288(1):654–65. doi: 10.1074/jbc.M112.400168

21. Hong S, Beja-Glasser VF, Nfonoyim BM, Frouin A, Li S, Ramakrishnan S, et al. Complement and microglia mediate early synapse loss in Alzheimer mouse models. *Science* (2016) 352(6286):712–6. doi: 10.1126/science.aad8373

22. Lui H, Zhang J, Makinson SR, Cahill MK, Kelley KW, Huang HY, et al. Progranulin deficiency promotes circuit-specific synaptic pruning by microglia *via* complement activation. *Cell* (2016) 165(4):921–35. doi: 10.1016/j.cell.2016.04.001

23. Zhang J, Velmeshev D, Hashimoto K, Huang YH, Hofmann JW, Shi X, et al. Neurotoxic microglia promote TDP-43 proteinopathy in progranulin deficiency. *Nature* (2020) 588(7838):459–65. doi: 10.1038/s41586-020-2709-7

24. Lobsiger CS, Boillée S, Pozniake C, Khan AM, McAlonis-Downes M, Lewcock JW, et al. C1q induction and global complement pathway activation do not contribute to ALS toxicity in mutant SOD1 mice. *Proc Natl Acad Sci U S A* (2013) 110(46):E4385–92. doi: 10.1073/pnas.1318309110

25. Guttenplan KA, Weigel MK, Adler DI, Couthouis J, Liddelow SA, Gitler AD, et al. Knockout of reactive astrocyte activating factors slows disease progression in an ALS mouse model. *Nat Commun* (2020) 11(1):1–9. doi: 10.1038/s41467-020-17514-9

26. Depboylu C, Schorlemmer K, Klietz M, Oertel WH, Weihe E, Höglinger GU, et al. Upregulation of microglial C1q expression has no effects on nigrostriatal dopaminergic injury in the MPTP mouse model of Parkinson disease. *J Neuroimmunol* (2011) 236(1–2):39–46. doi: 10.1016/j.jneuroim.2011.05.006

27. Panayiotou E, Fella E, Papacharalambous R, Malas S, Saraiva MJ, Kyriakides T. C1q ablation exacerbates amyloid deposition: a study in a transgenic mouse model of ATTRV30M amyloid neuropathy. *PloS One* (2017) 12(4):1–17. doi: 10.1371/journal.pone.0175767

28. Graham LC, Kocalis HE, Soto I, Howell GR. Deficiency of complement component c1q prevents cerebrovascular damage and white matter loss in a mouse model of chronic obesity. *eNeuro* (2020) 7(3):1–12. doi: 10.1523/ENEURO.0057-20.2020

29. Stephan AH, Madison DV, Mateos JM, Fraser DA, Lovelett EA, Coutellier L, et al. A dramatic increase of C1q protein in the CNS during normal aging. *J Neurosci* (2013) 33(33):13460–74. doi: 10.1523/JNEUROSCI.1333-13.2013

30. You Z, Yang J, Takahashi K, Yager PH, Kim HH, Qin T, et al. Reduced tissue damage and improved recovery of motor function after traumatic brain injury in mice deficient in complement component C4. *J Cereb Blood Flow Metab* (2007) 27 (12):1954–64. doi: 10.1038/sj.jcbfm.9600497

31. Liddelow SA, Guttenplan KA, Clarke LE, Bennett FC, Bohlen CJ, Schirmer L, et al. Neurotoxic reactive astrocytes are induced by activated microglia. *Nat* (2017) 541(7638):481–7. doi: 10.1038/nature21029

32. Norris GT, Smirnov I, Filiano AJ, Shadowen HM, Cody KR, Thompson JA, et al. Neuronal integrity and complement control synaptic material clearance by microglia after CNS injury. *J Exp Med* (2018) 215(7):1789–801. doi: 10.1084/jem.20172244

33. Peterson SL, Li Y, Sun CJ, Wong KA, Leung KS, de Lima S, et al. Retinal ganglion cell axon regeneration requires complement and myeloid cell activity within the optic nerve. *J Neurosci* (2021) 41(41):8508–31. doi: 10.1523/JNEUROSCI.0555-21.2021

34. Holden SS, Grandi FC, Aboubakr O, Higashikubo B, Cho FS, Chang AH, et al. Complement factor C1q mediates sleep spindle loss and epileptic spikes after mild brain injury. *Science* (2021) 373(6560):1–9. doi: 10.1126/science.abj2685

35. Markarian M, Krattli RP, Baddour JD, Alikhani L, Giedzinski E, Usmani MT, et al. Glia-selective deletion of complement c1q prevents radiation-induced cognitive deficits and neuroinflammation. *Cancer Res* (2021) 81(7):1732–44. doi: 10.1158/0008-5472.CAN-20-2565

36. Galvan MD, Luchetti S, Burgos AM, Nguyen HX, Hooshmand MJ, Hamers FPT, et al. Deficiency in complement C1q improves histological and functional locomotor outcome after spinal cord injury. *J Neurosci* (2008) 28(51):13876–88. doi: 10.1523/JNEUROSCI.2823-08.2008

37. Peterson SL, Nguyen HX, Mendez OA, Anderson AJ. Complement protein C1q modulates neurite outgrowth *in vitro* and spinal cord axon regeneration in vivo. *J Neurosci* (2015) 35(10):4332–49. doi: 10.1523/JNEUROSCI.4473-12.2015

38. Berg A, Zelano J, Stephan A, Thams S, Barres BA, Pekny M, et al. Reduced removal of synaptic terminals from axotomized spinal motoneurons in the absence of complement C3. *Exp Neurol* (2012) 237(1):8–17. doi: 10.1016/j.expneurol.2012.06.008

39. Akdagli S, Williams RA, Kim HJ, Yan Y, Mustapha M, Most SP. Facial nerve recovery in KBdB and C1q knockout mice: a role for histocompatibility complex 1. *Plast Reconstr Surg - Glob Open* (2016) 4(12):1–6. doi: 10.1097/GOX.0000000000001186

40. Lötscher M, Recher M, Hunziker L, Klein MA. Immunologically induced, complement-dependent up-regulation of the prion protein in the mouse spleen: Follicular dendritic cells versus capsule and trabeculae. *J Immunol* (2003) 170 (12):6040–7. doi: 10.4049/jimmunol.170.12.6040

41. Hammond JW, Qiu WQ, Marker DF, Chamberlain JM, Greaves-Tunnell W, Bellizzi MJ, et al. HIV Tat causes synapse loss in a mouse model of HIV-associated neurocognitive disorder that is independent of the classical complement cascade component C1q. *Glia* (2018) 66(12):2563–74. doi: 10.1002/glia.23511

42. Urich E, Gutcher I, Prinz M, Becher B. Autoantibody-mediated demyelination depends on complement activation but not activatory fc-receptors. *Proc Natl Acad Sci U S A* (2006) 103(49):18697–702. doi: 10.1073/pnas.0607283103

43. Hammond JW, Bellizzi MJ, Ware C, Qiu WQ, Saminathan P, Li H, et al. Complement-dependent synapse loss and microgliosis in a mouse model of multiple sclerosis. *Brain Behav Immun* (2020) 87:739–50. doi: 10.1016/j.bbi.2020.03.004

44. Absinta M, Maric D, Gharagozloo M, Garton T, Smith MD, Jin J, et al. A lymphocyte–microglia–astrocyte axis in chronic active multiple sclerosis. *Nat* (2021) 597(7878):709–14. doi: 10.1038/s41586-021-03892-7

45. Madeshiya AK, Whitehead C, Tripathi A, Pillai A. C1q deletion exacerbates stress-induced learned helplessness behavior and induces neuroinflammation in mice. *Transl Psychiatry* (2022) 12(50):1–8. doi: 10.1038/s41398-022-01794-4

46. Chu Y, Jin X, Parada I, Pesic A, Stevens B, Barres B, et al. Enhanced synaptic connectivity and epilepsy in C1q knockout mice. *Proc Natl Acad Sci U S A* (2010) 107(17):7975–80. doi: 10.1073/pnas.0913449107

47. Ma Y, Ramachandran A, Ford N, Parada I, Prince DA. Remodeling of dendrites and spines in the C1q knockout model of genetic epilepsy. *Epilepsia* (2013) 54(7):1232–9. doi: 10.1111/epi.12195

48. Ten VS, Yao J, Ratner V, Sosunov S, Fraser DA, Botto M, et al. Complement component C1q mediates mitochondria-driven oxidative stress in neonatal hypoxic – ischemic brain injury. *J. Neurosci.* (2010) 30(6):2077–87. doi: 10.1523/JNEUROSCI.5249-09.2010

49. De Simoni MG, Rossi E, Storini C, Pizzimenti S, Echart C, Bergamaschini L. The powerful neuroprotective action of C1-inhibitor on brain ischemia-reperfusion injury does not require C1q. *Am J Pathol* (2004) 164(5):1857–63. doi: 10.1016/S0002-9440(10)63744-3

50. Mocco J, Mack WJ, Ducruet AF, Sosunov SA, Sughrue ME, Hassid BG, et al. Complement component C3 mediates inflammatory injury following focal cerebral ischemia. (2006), 99(2):209–17. doi: 10.1161/01.RES.0000232544.90675.42

51. Elvington A, Atkinson C, Zhu H, Yu J, Stahl GL, Kindy MS. The alternative complement pathway propagates inflammation and injury in murine ischemic stroke. *J. Immunol.* (2012) 189:4640–47. doi: 10.4049/jimmunol.1201904

52. Silverman SM, Kim BJ, Howell GR, Miller J, John SWM, Wordinger RJ, et al. C1q propagates microglial activation and neurodegeneration in the visual axis following retinal ischemia/reperfusion injury. *Mol Neurodegener* (2016) 11(1):1–16. doi: 10.1186/s13024-016-0089-0

53. Hart ML, Ceonzo KA, Shaffer LA, Takahashi K, Rother RP, Reenstra WR, et al. Gastrointestinal ischemia-reperfusion injury is lectin complement pathway dependent without involving C1q. *J Immunol* (2005) 174(10):6373–80. doi: 10.4049/jimmunol.174.10.6373

54. Zhang M, Takahashi K, Alicot EM, Vorup-Jensen T, Kessler B, Thiel S, et al. Activation of the lectin pathway by natural IgM in a model of Ischemia/Reperfusion injury. *J Immunol* (2006) 177(7):4727–34. doi: 10.4049/jimmunol.177.7.4727

55. Wu M, Rowe JM, Fleming SD. Complement initiation varies by sex in intestinal ischemia reperfusion injury. *Front Immunol* (2021) 12:1–13. doi: 10.3389/fimmu.2021.649882

56. Walsh MC, Bourcier T, Takahashi K, Shi L, Busche MN, Rother RP, et al. Mannose-binding lectin is a regulator of inflammation that accompanies myocardial ischemia and reperfusion injury. *J Immunol* (2005) 175(1):541–6. doi: 10.4049/jimmunol.175.1.541

57. Chan RK, Ibrahim SI, Takahashi K, Kwon E, Mccormack M, Ezekowitz A, et al. The differing roles of the classical and mannose-binding lectin complement pathways in the events following skeletal muscle ischemia-reperfusion. *J Immunol* (2006) 177:8080–5. doi: 10.4049/jimmunol.177.11.8080

58. Peck CT, Strauß S, Stahl GL, Vogt PM, Busche MN. Mannose-binding lectin (MBL) and the lectin complement pathway play a role in cutaneous ischemia and reperfusion injury. *Innov Surg Sci* (2020) 5(1–2):43–51. doi: 10.1515/iss-2020-0017

59. Cohen JI, Roychowdhury S, McMullen MR, Stavitsky AB, Nagy LE. Complement and alcoholic liver disease: Role of C1q in the pathogenesis of ethanol-induced liver injury in mice. *Gastroenterology* (2010) 139(2):664–674.e1. doi: 10.1053/j.gastro.2010.04.041

60. McCullough RL, McMullen MR, Sheehan MM, Poulsen KL, Roychowdhury S, Chiang DJ, et al. Complement factor d protects mice from ethanol-induced inflammation and liver injury. *Am J Physiol Liver Physiol* (2018) 315(1):G66–79. doi: 10.1152/ajpgi.00334.2017

61. Kim SY, Son M, Lee SE, Park IH, Kwak MS, Han M, et al. High-mobility group box 1-induced complement activation causes sterile inflammation. *Front Immunol* (2018) 9:1–15. doi: 10.3389/fimmu.2018.00705

62. Cresci GA, Allende D, McMullen MR, Nagy LE. Alternative complement pathway component factor d contributes to efficient clearance of tissue debris following acute CCl4-induced injury. *Mol Immunol* (2015) 64(1):9–17. doi: 10.1016/j.molimm.2014.10.017

63. Hillian AD, McMullen MR, Sebastian BM, Rowchowdhury S, Kashyap SR, Schauer PR, et al. Mice lacking C1q are protected from high fat diet-induced hepatic insulin resistance and impaired glucose homeostasis. *J Biol Chem* (2013) 288(31):22565–75. doi: 10.1074/jbc.M113.465674

64. Cutler AJ, Botto M, Van Essen D, Rivi R, Davies KA, Gray D, et al. T Cell-dependent immune response in C1q-deficient mice: Defective interferon γ production by antigen-specific T cells. *J Exp Med* (1998) 187(11):1789–95. doi: 10.1084/jem.187.11.1789

65. Mevorach D. Opsonization of apoptotic cells: Implications for uptake and autoimmunity. *Ann N Y Acad Sci* (2000) 926:226–35. doi: 10.1111/j.1749-6632.2000.tb05615.x

66. Taylor PR, Carugati A, Fadok VA, Cook HT, Andrews M, Carroll MC, et al. A hierarchical role for classical pathway complement proteins in the clearance of apoptotic cells in vivo. *J Exp Med* (2000) 192(3):359–66. doi: 10.1084/jem.192.3.359

67. Cutler AJ, Cornall RJ, Ferry H, Manderson AP, Botto M, Walport MJ. Intact b cell tolerance in the absence of the first component of the classical complement pathway. *Eur J Immunol* (2001) 31(7):2087–93. doi: 10.1002/1521-4141(200107)31:7<2087::AID-IMMU2087>3.0.CO;2-C

68. Nash JT, Taylor PR, Botto M, Norsworthy PJ, Davies KA, Walport MJ. Immune complex processing in C1q-deficient mice. *Clin Exp Immunol* (2001) 123(2):196–202. doi: 10.1046/j.1365-2249.2001.01459.x

69. Petry F, Botto M, Holtappels R, Walport MJ, Loos M. Reconstitution of the complement function in C1q-deficient (C1qa –/–) mice with wild-type bone marrow cells. *J Immunol* (2001) 167(7):4033–7. doi: 10.4049/jimmunol.167.7.4033

70. Pickering MC, Fischer S, Lewis MR, Walport MJ, Botto M, Cook HT. Ultraviolet-radiation-induced keratinocyte apoptosis in C1q-deficient mice. *J Invest Dermatol* (2001) 117(1):52–8. doi: 10.1046/j.0022-202x.2001.01381.x

71. Mitchell DA, Pickering MC, Warren J, Fossati-Jimack L, Cortes-Hernandez J, Cook HT, et al. C1q deficiency and autoimmunity: The effects of genetic background on disease expression. *J Immunol* (2002) 168(5):2538–43. doi: 10.4049/jimmunol.168.5.2538

72. Cortes-Hernandez J, Fossati-Jimack L, Petry F, Loos M, Izui S, Walport MJ, et al. Restoration of C1q levels by bone marrow transplantation attenuates autoimmune disease associated with C1q deficiency in mice. *Eur J Immunol* (2004) 34(12):3713–22. doi: 10.1002/eji.200425616

73. Heidari Y, Bygrave AE, Rigby RJ, Rose KL, Walport MJ, Cook HT, et al. Identification of chromosome intervals from 129 and C57BL/6 mouse strains linked to the development of systemic lupus erythematosus. *Genes Immun* (2006) 7(7):592–9. doi: 10.1038/sj.gene.6364335

74. Ferry H, Potter PK, Crockford TL, Nijnik A, Ehrenstein MR, Walport MJ, et al. Increased positive selection of B1 cells and reduced b cell tolerance to intracellular antigens in c1q-deficient mice. *J Immunol* (2007) 178(5):2916–22. doi: 10.4049/jimmunol.178.5.2916

75. Fossati-Jimack L, Cortes-Hernandez J, Norsworthy PJ, Walport MJ, Cook HT, Botto M. C1q deficiency promotes the production of transgenic-derived IgM and IgG3 autoantibodies in anti-DNA knock-in transgenic mice. *Mol Immunol* (2008) 45(3):787–95. doi: 10.1016/j.molimm.2007.06.162

76. Carlucci F, Ishaque A, Ling GS, Szajna M, Sandison A, Donatien P, et al. C1q modulates the response to TLR7 stimulation by pristane-primed macrophages: Implications for pristane-induced lupus. *J Immunol* (2016) 196(4):1488–94. doi: 10.4049/jimmunol.1401009

77. Ling GS, Crawford G, Buang N, Bartok I, Tian K, Thielens NM, et al. C1q restrains autoimmunity and viral infection by regulating CD8+ T cell metabolism. *Science* (2018) 360(6388):558–63. doi: 10.1126/science.aao4555

78. Csorba K, Schirmbeck LA, Tuncer E, Ribi C, Roux-Lombard P, Chizzolini C, et al. Anti-C1q antibodies as occurring in systemic lupus erythematosus could be induced by an Epstein-Barr virus-derived antigenic site. *Front Immunol* (2019) 10:1–13. doi: 10.3389/fimmu.2019.02619

79. Trendelenburg M, Manderson AP, Fossati-Jimack L, Walport MJ, Botto M. Monocytosis and accelerated activation of lymphocytes in C1q-deficient autoimmune-prone mice. *Immunology* (2004) 113(1):80–8. doi: 10.1111/j.1365-2567.2004.01940.x

80. Mitchell DA, Taylor PR, Cook HT, Moss J, Bygrave AE, Walport MJ, et al. Cutting edge: C1q protects against the development of glomerulonephritis independently of C3 activation. *J Immunol* (1999) 162(10):5676–9.

81. Skopelja-Gardner S, Colonna L, Hermanson P, Sun X, Tanaka L, Tai J, et al. Complement deficiencies result in surrogate pathways of complement activation in novel polygenic lupus-like models of kidney injury. *J Immunol* (2020) 204(10):2627–40. doi: 10.4049/jimmunol.1901473

82. Trouw LA, Groeneveld TWL, Seelen MA, Duijs JMGJ, Bajema IM, Prins FA, et al. Anti C1q autoantibodies deposit in glomeruli but are only pathogenic in combination with glomerular C1q-containing immune complexes. *J Clin Invest* (2004) 114(5):679–88. doi: 10.1172/JCI200421075

83. Robson MG, Cook HT, Botto M, Taylor PR, Busso N, Salvi R, et al. Accelerated nephrotoxic nephritis is exacerbated in C1q-deficient mice. *J Immunol* (2001) 166(11):6820–8. doi: 10.4049/jimmunol.166.11.6820

84. Robson MG, Cook HT, Pusey CD, Walport MJ, Davies KA. Antibody-mediated glomerulonephritis in mice: The role of endotoxin, complement and genetic background. *Clin Exp Immunol* (2003) 133(3):326–33. doi: 10.1046/j.1365-2249.2003.02233.x

85. Otten MA, Groeneveld TWL, Flierman R, Rastaldi MP, Trouw LA, Faber-Krol MC, et al. Both complement and IgG fc receptors are required for development of attenuated antiglomerular basement membrane nephritis in mice. *J Immunol* (2009) 183(6):3980–8. doi: 10.4049/jimmunol.0901301

86. Trendelenburg M, Fossati-Jimack L, Cortes-Hernandez J, Turnberg D, Lewis M, Izui S, et al. The role of complement in cryoglobulin-induced immune complex glomerulonephritis. *J Immunol* (2005) 175(10):6909–14. doi: 10.4049/jimmunol.175.10.6909

87. Turnberg D, Lewis M, Moss J, Xu Y, Botto M, Cook HT. Complement activation contributes to both glomerular and tubulointerstitial damage in adriamycin nephropathy in mice. *J Immunol* (2006) 177(6):4094–102. doi: 10.4049/jimmunol.177.6.4094

88. Xavier S, Sahu RK, Landes SG, Yu J, Taylor RP, Ayyadevara S, et al. Pericytes and immune cells contribute to complement activation in tubulointerstitial fibrosis. *Am J Physiol - Ren Physiol* (2017) 312(3):F516–32. doi: 10.1152/ajprenal.00604.2016

89. Csencsits K, Burrell BE, Lu G, Eichwald EJ, Stahl GL, Bishop DK. The classical complement pathway in transplantation: Unanticipated protective effects of C1q and role in inductive antibody therapy. *Am J Transplant* (2008) 8(8):1622–30. doi: 10.1111/j.1600-6143.2008.02295.x

90. Baruah P, Simpson E, Dumitriu IE, Derbyshire K, Coe D, Addey C, et al. Mice lacking C1q or C3 show accelerated rejection of minor h disparate skin grafts and resistance to induction of tolerance. *Eur J Immunol* (2010) 40(6):1758–67. doi: 10.1002/eji.200940158

91. Fossati-Jimack L, Ling GS, Baudino L, Szajna M, Manivannan K, Zhao JC, et al. Intranasal peptide-induced tolerance and linked suppression: Consequences of complement deficiency. *Immunology* (2015) 144(1):149–57. doi: 10.1111/imm.12358

92. Banda NK, Takahashi K, Wood AK, Holers VM, Arend WP. Pathogenic complement activation in collagen antibody- induced arthritis in mice requires amplification by the alternative pathway. *J Immunol* (2007) 179(6):4101–9. doi: 10.4049/jimmunol.179.6.4101

93. Banda NK, Levitt B, Wood AK, Takahashi K, Stahl GL, Holers VM, et al. Complement activation pathways in murine immune complex-induced arthritis and in C3a and C5a generation *in vitro*: ORIGINAL ARTICLE. *Clin Exp Immunol* (2010) 159(1):100–8.

94. Windbichler M, Echtenacher B, Takahashi K, Ezekowitz RAB, Schwaeble WJ, Jensenius JC, et al. Investigations on the involvement of the lectin pathway of complement activation in anaphylaxis. *Int Arch Allergy Immunol* (2006) 141(1):11–23. doi: 10.1159/000094177

95. Bergström JJE, Heyman B. IgG suppresses antibody responses in mice lacking C1q, C3, complement receptors 1 and 2, or IgG fc-receptors. *PloS One* (2015) 10(11):1–11.

96. Escamilla-Rivera V, Santhanakrishnan M, Liu J, Gibb DR, Forsmo JE, Foxman EF, et al. Complement plays a critical role in inflammation-induced immunoprophylaxis failure in mice. *Front Immunol* (2021) 12:1–12. doi: 10.3389/fimmu.2021.704072

97. Visciano ML, Mahant AM, Pierce C, Hunte R, Herold BC. Antibodies elicited in response to a single cycle glycoprotein d deletion viral vaccine candidate bind C1q and activate complement mediated neutralization and cytolysis. (2021), 13(7):1–11. doi: 10.3390/v13071284

98. Appledorn DM, McBride A, Seregin S, Scott JM, Schuldt N, Kiang A, et al. Complex interactions with several arms of the complement system dictate innate and humoral immunity to adenoviral vectors. *Gene Ther* (2008) 15(24):1606–17. doi: 10.1038/gt.2008.114

99. Xu Z, Qiu Q, Tian J, Smith JS, Conenello GM, Morita T, et al. Coagulation factor X shields adenovirus type 5 from attack by natural antibodies and complement. *Nat Med* (2013) 19(4):452–7. doi: 10.1038/nm.3107

100. Schepp-Berglind J, Atkinson C, Elvington M, Qiao F, Mannon P, Tomlinson S. Complement-dependent injury and protection in a murine model of acute dextran sulfate sodium-induced colitis. *J Immunol* (2012) 188(12):6309–18. doi: 10.4049/jimmunol.1200553

101. Ceonzo K, Gaynor A, Shaffer L, Kojima K, Vacanti CA, Stahl GL. Polyglycolic acid-induced inflammation: Role of hydrolysis and resulting complement activation. *Tissue Eng* (2006) 12(2):301–8. doi: 10.1089/ten.2006.12.301

102. Brown JS, Hussell T, Gilliland SM, Holden DW, Paton JC, Ehrenstein MR, et al. The classical pathway is the dominant complement pathway required for innate immunity to streptococcus pneumoniae infection in mice. *Proc Natl Acad Sci U S A* (2002) 99(26):16969–74. doi: 10.1073/pnas.012669199

103. Saeland E, Vidarsson G, Leusen JHW, van Garderen E, Nahm MH, Vile-Weekhout H, et al. Central role of complement in passive protection by human IgG1 and IgG2 anti-pneumococcal antibodies in mice. *J Immunol* (2003) 170(12):6158–64. doi: 10.4049/jimmunol.170.12.6158

104. Yuste J, Botto M, Paton JC, Holden DW, Brown JS. Additive inhibition of complement deposition by pneumolysin and PspA facilitates streptococcus pneumoniae septicemia. *J Immunol* (2005) 175(3):1813–9. doi: 10.4049/jimmunol.175.3.1813

105. Rupprecht TA, Angele B, Klein M, Heesemann J, Pfister H-W, Botto M, et al. Complement C1q and C3 are critical for the innate immune response to streptococcus pneumoniae in the central nervous system. *J Immunol* (2007) 178(3):1861–9. doi: 10.4049/jimmunol.178.3.1861

106. Tong HH, Li YX, Stahl GL, Thurman JM. Enhanced susceptibility to acute pneumococcal otitis media in mice deficient in complement C1qa, factor b, and factor B/C2. *Infect Immun* (2010) 78(3):976–83. doi: 10.1128/IAI.01012-09

107. Li Q, Li YX, Stahl GL, Thurman JM, He Y, Tong HH. Essential role of factor b of the alternative complement pathway in complement activation and opsonophagocytosis during acute pneumococcal otitis media in mice. *Infect Immun* (2011) 79(7):2578–85. doi: 10.1128/IAI.00168-11

108. Tong HH, Lambert G, Li YX, Thurman JM, Stahl GL, Douthitt K, et al. Deletion of the complement C5a receptor alleviates the severity of acute pneumococcal otitis media following influenza a virus infection in mice. *PloS One* (2014) 9(4):e95160. doi: 10.1371/journal.pone.0095160

109. Yuste J, Ali S, Sriskandan S, Hyams C, Botto M, Brown JS. Roles of the alternative complement pathway and C1q during innate immunity to streptococcus pyogenes. *J Immunol* (2006) 176(10):6112–20. doi: 10.4049/jimmunol.176.10.6112

110. Celik I, Stover C, Botto M, Thiel S, Tzima S, Künkel D, et al. Role of the classical pathway of complement activation in experimentally induced polymicrobial peritonitis. *Infect Immun* (2001) 69(12):7304–9. doi: 10.1128/IAI.69.12.7304-7309.2001

111. Windbichler M, Echtenacher B, Hehlgans T, Jensenius JC, Schwaeble W, Männel DN. Involvement of the lectin pathway of complement activation in antimicrobial immune defense during experimental septic peritonitis. *Infect Immun* (2004) 72(9):5247–52. doi: 10.1128/IAI.72.9.5247-5252.2004

112. Dahlke K, Wrann CD, Sommerfeld O, Soßdorf M, Recknagel P, Sachse S, et al. Distinct different contributions of the alternative and classical complement activation pathway for the innate host response during sepsis. *J Immunol* (2011) 186(5):3066–75. doi: 10.4049/jimmunol.1002741

113. Warren J, Mastroeni P, Dougan G, Noursadeghi M, Cohen J, Walport MJ, et al. Increased susceptibility of C1q-deficient mice to salmonella enterica serovar typhimurium infection. *Infect Immun* (2002) 70(2):551–7. doi: 10.1128/IAI.70.2.551-557.2002

114. Zhi H, Xie J, Skare JT. The classical complement pathway is required to control borrelia burgdorferi levels during experimental infection. *Front Immunol* (2018) 9:1–12. doi: 10.3389/fimmu.2018.00959

115. Dahmani M, Cook JH, Zhu JC, Riley SP. Contribution of classical complement activation and IgM to the control of rickettsia infection. *Mol Microbiol* (2021) 116(6):1476–88. doi: 10.1111/mmi.14839

116. Shaughnessy J, Lewis LA, Zheng B, Carr C, Bass I, Gulati S, et al. Human factor h domains 6 and 7 fused to IgG1 fc are immunotherapeutic against neisseria gonorrhoeae. *J Immunol* (2018) 201(9):2700–9. doi: 10.4049/jimmunol.1701666

117. Gulati S, Beurskens FJ, de Kreuk BJ, Roza M, Zheng B, Deoliveira RB, et al. Complement alone drives efficacy of a chimeric antigonococcal monoclonal antibody. *PloS Biol* (2019) 17(6):1–29. doi: 10.1371/journal.pbio.3000323

118. Gulati S, Schoenhofen IC, Lindhout-Djukic T, Lewis LA, Moustafa IY, Saha S, et al. Efficacy of antigonococcal CMP-nonulosonate therapeutics require cathelicidins. *J Infect Dis* (2020) 222(10):1641–50. doi: 10.1093/infdis/jiaa438

119. Moalli F, Paroni M, Véliz Rodriguez T, Riva F, Polentarutti N, Bottazzi B, et al. The therapeutic potential of the humoral pattern recognition molecule PTX3 in chronic lung infection caused by pseudomonas aeruginosa. *J Immunol* (2011) 186(9):5425–34. doi: 10.4049/jimmunol.1002035

120. Mehlhop E, Diamond MS. Protective immune responses against West Nile virus are primed by distinct complement activation pathways. *J Exp Med* (2006) 203(5):1371–81. doi: 10.1084/jem.20052388

121. Taylor PR, Seixas E, Walport MJ, Langhorne J, Botto M. Complement contributes to protective immunity against reinfection by plasmodium chabaudi chabaudi parasites. *Infect Immun* (2001) 69(6):3853–9. doi: 10.1128/IAI.69.6.3853-3859.2001

122. Giacomin PR, Gordon DL, Botto M, Daha MR, Sanderson SD, Taylor SM, et al. The role of complement in innate, adaptive and eosinophil-dependent immunity to the nematode nippostrongylus brasiliensis. *Mol Immunol* (2008) 45(2):446–55. doi: 10.1016/j.molimm.2007.05.029

123. Petry F, Jakobi V, Wagner S, Tessema TS, Thiel S, Loos M. Binding and activation of human and mouse complement by cryptosporidium parvum (Apicomplexa) and susceptibility of C1q- and MBL-deficient mice to infection. *Mol Immunol* (2008) 45(12):3392–400. doi: 10.1016/j.molimm.2008.04.010

124. Held K, Thiel S, Loos M, Petry F. Increased susceptibility of complement factor B/C2 double knockout mice and mannan-binding lectin knockout mice to systemic infection with candida albicans. *Mol Immunol* (2008) 45(15):3934–41. doi: 10.1016/j.molimm.2008.06.021

125. Bhatia VK, Yun S, Leung V, Grimsditch DC, Benson GM, Botto MB, et al. Complement C1q reduces early atherosclerosis in low-density lipoprotein receptor-deficient mice. *Am J Pathol* (2007) 170(1):416–26. doi: 10.2353/ajpath.2007.060406

126. Lewis MJ, Malik TH, Ehrenstein MR, Boyle JJ, Botto M, Haskard DO. Immunoglobulin m is required for protection against atherosclerosis in low-density lipoprotein receptor-deficient mice. *Circulation* (2009) 120(5):417–26. doi: 10.1161/CIRCULATIONAHA.109.868158

127. Bossi F, Tripodo C, Rizzi L, Bulla R, Agostinis C, Guarnotta C, et al. C1q as a unique player in angiogenesis with therapeutic implication in wound healing. *Proc Natl Acad Sci U S A* (2014) 111(11):4209–14. doi: 10.1073/pnas.1311968111

128. Shah D, Romero F, Zhu Y, Duong M, Sun J, Walsh K, et al. C1q deficiency promotes pulmonary vascular inflammation and enhances the susceptibility of the lung endothelium to injury. *J Biol Chem* (2015) 290(49):29642–51. doi: 10.1074/jbc.M115.690784

129. Donat C, Kölm R, Csorba K, Tuncer E, Tsakiris DA, Trendelenburg M. Complement C1q enhances primary hemostasis. *Front Immunol* (2020) 11. doi: 10.3389/fimmu.2020.01522

130. Agostinis C, Bulla R, Tripodo C, Gismondi A, Stabile H, Bossi F, et al. An alternative role of C1q in cell migration and tissue remodeling: Contribution to trophoblast invasion and placental development. *J Immunol* (2010) 185(7):4420–9. doi: 10.4049/jimmunol.0903215

131. Cohen D, Buurma A, Goemaere NN, Girardi G, Le Cessie S, Scherjon S, et al. Classical complement activation as a footprint for murine and human antiphospholipid antibody-induced fetal loss. *J Pathol* (2011) 225(4):502–11. doi: 10.1002/path.2893

132. Moldenhauer LM, DIener KR, Hayball JD, Robertson SA. An immunogenic phenotype in paternal antigen-specific CD8 + T cells at embryo implantation elicits later fetal loss in mice. *Immunol Cell Biol* (2017) 95(8):705–15. doi: 10.1038/icb.2017.41

133. Sutton EF, Gemmel M, Brands J, Gallaher MJ, Powers RW. Paternal deficiency of complement component C1q leads to a preeclampsialike pregnancy in wild-type female mice and vascular adaptations postpartum. *Am J Physiol - Regul Integr Comp Physiol* (2020) 318(6):R1047–57. doi: 10.1152/ajpregu.00353.2019

134. Garrett N, Pombo J, Umpierrez M, Clark JE, Simmons M, Girardi G. Pravastatin therapy during preeclampsia prevents long-term adverse health effects in mice. *JCI Insight* (2018) 130(4):126567. doi: 10.1172/jci.insight.120147

135. Singh J, Ahmed A, Girardi G. Role of complement component C1q in the onset of preeclampsia in mice. *Hypertension* (2011) 58(4):716–24. doi: 10.1161/HYPERTENSIONAHA.111.175919

136. Bulla R, Tripodo C, Rami D, Ling GS, Agostinis C, Guarnotta C, et al. C1q acts in the tumour microenvironment as a cancer-promoting factor independently of complement activation. *Nat Commun* (2016) 7(10346):1–11. doi: 10.1038/ncomms10346

137. Bandini S, Macagno M, Hysi A, Lanzardo S, Conti L, Bello A, et al. The non-inflammatory role of C1q during Her2/neu-driven mammary carcinogenesis. *Oncoimmunology* (2016) 5(12):1–13. doi: 10.1080/2162402X.2016.1253653

138. Roumenina LT, Daugan MV, Noe R, Petitprez F, Vano YA, Sanchez-Salas R, et al. Tumor cells hijack macrophage-produced complement C1q to promote tumor growth. *Cancer Immunol Res* (2019) 7(7):1091–105. doi: 10.1158/2326-6066.CIR-18-0891

139. Di Gaetano N, Cittera E, Nota R, Vecchi A, Grieco V, Scanziani E, et al. Complement activation determines the therapeutic activity of rituximab in vivo. *J Immunol* (2003) 171(3):1581–7. doi: 10.4049/jimmunol.171.3.1581

140. Uchida J, Hamaguchi Y, Oliver JA, Ravetch JV, Poe JC, Haas KM, et al. The innate mononuclear phagocyte network depletes b lymphocytes through fc receptor-dependent mechanisms during anti-CD20 antibody immunotherapy. *J Exp Med* (2004) 199(12):1659–69. doi: 10.1084/jem.20040119

141. Schabowsky RH, Elpek KG, Madireddi S, Sharma RK, Yolcu ES, Bandura-Morgan L, et al. A novel form of 4-1BBL has better immunomodulatory activity than an agonistic anti-4-1BB ab without ab-associated severe toxicity. *Vaccine* (2009) 28(2):512–22. doi: 10.1016/j.vaccine.2009.09.127

142. Tsao L-C, Crosby EJ, Trotter TN, Wei J, Wang T, Yang X, et al. Trastuzumab/pertuzumab combination therapy stimulates antitumor responses through complement-dependent cytotoxicity and phagocytosis. *JCI Insight* (2022) 7(6):1–18. doi: 10.1172/jci.insight.155636

143. Møller-Kristensen M, Hamblin MR, Thiel S, Jensenius JC, Takahashi K. Burn injury reveals altered phenotype in mannan-binding lectin-deficient mice. *J Invest Dermatol* (2007) 127(6):1524–31. doi: 10.1038/sj.jid.5700748

144. Mihai S, Chiriac MT, Takahashi K, Thurman JM, Holers VM, Zillikens D, et al. The alternative pathway of complement activation is critical for blister induction in experimental epidermolysis bullosa acquisita. *J Immunol* (2007) 178 (10):6514–21. doi: 10.4049/jimmunol.178.10.6514

145. Naito AT, Sumida T, Nomura S, Liu ML, Higo T, Nakagawa A, et al. Complement C1q activates canonical wnt signaling and promotes aging-related phenotypes. *Cell* (2012) 149(6):1298–313. doi: 10.1016/j.cell.2012.03.047

146. Yuan X, Chang CY, You R, Shan M, Gu BH, Madison MC, et al. Cigarette smoke–induced reduction of C1q promotes emphysema. *JCI Insight* (2019) 4 (13):1–17. doi: 10.1172/jci.insight.124317

147. Ogawa T, Shichino S, Ueha S, Ogawa S, Matsushima K. Complement protein C1q activates lung fibroblasts and exacerbates silica-induced pulmonary fibrosis in mice. *Biochem Biophys Res Commun* (2022) 603:88–93. doi: 10.1016/j.bbrc.2022.02.090

148. Hutchinson WL, Herbert J, Botto M, Pepys MB. Classical and alternative pathway complement activation are not required for reactive systemic AA amyloid deposition in mice. *Immunology* (2004) 112(2):250–4. doi: 10.1111/j.1365-2567.2004.01881.x

149. Sebastian BM, Roychowdhury S, Tang H, Hillian AD, Feldstein AE, Stahl GL, et al. Identification of a cytochrome P4502E1/Bid/C1q-dependent axis mediating inflammation in adipose tissue after chronic ethanol feeding to mice. *J Biol Chem* (2011) 286(41):35989–97. doi: 10.1074/jbc.M111.254201

150. Scott-Hewitt N, Perrucci F, Morini R, Erreni M, Mahoney M, Witkowska A, et al. Local externalization of phosphatidylserine mediates developmental synaptic pruning by microglia. *EMBO J* (2020) 39(16):1–20. doi: 10.15252/embj.2020105380

151. Rohrer B. Anaphylatoxin signaling in retinal pigment and choroidal endothelial cells: Characteristics and relevance to age-related macular degeneration. *Adv Exp Med Biol* (2018) 1074:45–51. doi: 10.1007/978-3-319-75402-4_6

152. Byrne RAJ, Torvell M, Daskoulidou N, Fathalla D, Kokkali E, Carpanini SM, et al. Novel monoclonal antibodies against mouse C1q: characterisation and development of a quantitative elisa for mouse C1q. *Mol Neurobiol* (2021) 58 (9):4323–36. doi: 10.1007/s12035-021-02419-5. (0123456789).

153. Schartz ND, Tenner AJ. The good, the bad, and the opportunities of the complement system in neurodegenerative disease. *J Neu Roinflamm* (2020) 17 (1):1–25. doi: 10.1186/s12974-020-02024-8

154. Fonseca MI, Chu SH, Hernandez MX, Fang MJ, Modarresi L, Selvan P, et al. Cell-specific deletion of C1qa identifies microglia as the dominant source of C1q in mouse brain. *J Neuroinflamm* (2017) 14(1):1–15. doi: 10.1186/s12974-017-0814-9

155. Rupprecht C, Sarker RSJ, Rammes G. Morphological representation of c1q in the aging central nervous system. *Pharmacopsychiatry* (2022). doi: 10.1055/a-1704-8260

156. Wilton DK, Dissing-Olesen L, Stevens B. Neuron-glia signaling in synapse elimination. *Annu Rev Neurosci* (2019) 42:107–27. doi: 10.1146/annurev-neuro-070918-050306

157. Calton MA, Lee D, Sundaresan S, Mendus D, Leu R, Wangsawihardja F, et al. A lack of immune system genes causes loss in high frequency hearing but does not disrupt cochlear synapse maturation in mice. *PloS One* (2014) 9(5):1–10. doi: 10.1371/journal.pone.0094549

158. Cong Q, Soteros BM, Huo A, Li Y, Tenner AJ, Sia GM. C1q and SRPX2 regulate microglia mediated synapse elimination during early development in the visual thalamus but not the visual cortex. *Glia* (2022) 70(3):451–65. doi: 10.1002/glia.24114

159. Welsh CA, Stephany CÉ, Sapp RW, Stevens B. Ocular dominance plasticity in binocular primary visual cortex does not require C1q. *J Neurosci* (2020) 40 (4):769–83. doi: 10.1523/JNEUROSCI.1011-19.2019

160. Löscher W, Russell JF, Thomas NF. The relevance of inter- and intrastrain differences in mice and rats and their implications for models of seizures and epilepsy wolfgang. vol. 73. *Epilepsy Behav* (2018) 73:214–35.

161. van Schaarenburg RA, Magro-Checa C, Bakker JA, Teng YKO, Bajema IM, Huizinga TW, et al. C1q deficiency and neuropsychiatric systemic lupus erythematosus. *Front Immunol* (2016) 7:1–8. doi: 10.3389/fimmu.2016.00647

162. Banz Y, Rieben R. Role of complement and perspectives for intervention in ischemia-reperfusion damage. *Ann Med* (2012) 44(3):205–17. doi: 10.3109/07853890.2010.535556

163. Bao L, Cunningham PN, Quigg RJ. Complement in lupus nephritis: New perspectives. *Kidney Dis* (2015) 1(2):91–9. doi: 10.1159/000431278

164. Walport MJ, Davies KA, Botto M. C1q and systemic lupus erythematosus. *Immunobiology* (1998) 199(2):265–85. doi: 10.1016/S0171-2985(98)80032-6

165. Walport MJ. Advances in immunology between innate and adaptive. *English J* (2001) 344(15):1140–4.

166. Manderson AP, Botto M, Walport MJ. The role of complement in the development of systemic lupus erythematosus. *Annu Rev Immunol* (2004) 22:431–56. doi: 10.1146/annurev.immunol.22.012703.104549

167. Bygrave AE, Rose KL, Cortes-Hernandez J, Warren J, Rigby RJ, Terence Cook H, et al. Spontaneous autoimmunity in 129 and C57BL/6 mice-implications for autoimmunity described in gene-targeted mice. *PloS Biol* (2004) 2(8):1081–90. doi: 10.1371/journal.pbio.0020243

168. Bigler C, Hopfer H, Danner D, Schaller M, Mihatsch MJ, Trendelenburg M. Anti-C1q autoantibodies do not correlate with the occurrence or severity of experimental lupus nephritis. *Nephrol Dial Transplant* (2011) 26(4):1220–8. doi: 10.1093/ndt/gfq558

169. Arkwright PD, Riley P, Hughes SM, Alachkar H, Wynn RF. Successful cure of C1q deficiency in human subjects treated with hematopoietic stem cell transplantation. *J Allergy Clin Immunol* (2014) 133(1):265–7. doi: 10.1016/j.jaci.2013.07.035

170. Trendelenburg M, Lopez-Trascasa M, Potlukova E, Moll S, Regenass S, Frémeaux-Bacchi V, et al. High prevalence of anti-C1q antibodies in biopsy-proven active lupus nephritis. *Nephrol Dial Transplant* (2006) 21(11):3115–21. doi: 10.1093/ndt/gfl436

171. Tsokos GC. Systemic lupus erythematosus. *N Engl J Med* (2011) 10 (365):2110–21. doi: 10.1056/NEJMra1100359

172. Walport MJ. Complement. second of two parts. *English J* (2001) 344 (15):1140–4.

173. Baruah P, Dumitriu IE, Malik TH, Cook HT, Dyson J, Scott D, et al. C1q enhances IFN-7 production by antigen-specific T cells *via* the CD40 costimulatory

pathway on dendritic cells. *Blood* (2009) 113(15):3485–93. doi: 10.1182/blood-2008-06-164392

174. Cernoch M, Viklicky O. Complement in kidney transplantation. *Front Med* (2017) 4:1–11. doi: 10.3389/fmed.2017.00066

175. Markiewski MM, Nilsson B, Nilsson Ekdahl K, Mollnes TE, Lambris JD. Complement and coagulation: strangers or partners in crime? *Trends Immunol* (2007) 28(4):184–92. doi: 10.1016/j.it.2007.02.006

176. Donat C, Thanei S, Trendelenburg M. Binding of von willebrand factor to complement C1q decreases the phagocytosis of cholesterol crystals and subsequent IL-1 secretion in macrophages. *Front Immunol* (2019) 10:1–11. doi: 10.3389/fimmu.2019.02712

177. Kölm R, Schaller M, Roumenina LT, Niemiec I, Kremer Hovinga JA, Khanicheh E, et al. Von Willebrand factor interacts with surface-bound C1q and induces platelet rolling. *J Immunol* (2016) 197(9):3669–79. doi: 10.4049/jimmunol.1501876

178. Agostinis C, Tedesco F, Bulla R. Alternative functions of the complement protein C1q at embryo implantation site. *J Reprod Immunol* (2017) 119:74–80. doi: 10.1016/j.jri.2016.09.001

179. Dejanovic B, Huntley MA, De Mazière A, Meilandt WJ, Wu T, Srinivasan K, et al. Changes in the synaptic proteome in tauopathy and rescue of tau-induced synapse loss by C1q antibodies. *Neuron* (2018) 100(6):1322–1336.e7. doi: 10.1016/j.neuron.2018.10.014

180. Han X, Xu T, Ding C, Wang D, Yao G, Chen H, et al. Neuronal NR4A1 deficiency drives complement-coordinated synaptic stripping by microglia in a mouse model of lupus. *Signal Transduct Target Ther* (2022) 7(1):1–16. doi: 10.1038/s41392-021-00867-y

181. Lansita JA, Mease KM, Qiu H, Yednock T, Sankaranarayanan S, Kramer S. Nonclinical development of ANX005: A humanized anti-C1q antibody for treatment of autoimmune and neurodegenerative diseases. *Int J Toxicol* (2017) 36(6):449–62. doi: 10.1177/1091581817740873

182. Annexon. clinical pipeline. (2022).

183. Papri N, Islam Z, Jahan I, Kroon H-A, Humphriss E, Sankaranarayanan S, et al. 2020 Peripheral nerve society virtual event. vol. 25, ANX005, a C1q inhibitor, for treatment of Guillain-Barré syndrome: Phase 1b study results. (2020), 508–9.

184. Kleer JS, Rabatscher PA, Weiss J, Leonardi J, Vogt SB, Kieninger-grä A, et al. Epitope-speci fi c anti-C1q autoantibodies in systemic lupus erythematosus. *Front. Immunol* (2022) 12:1–12.

185. Benhar I, London A, Schwartz M. The privileged immunity of immune privileged organs: The case of the eye. *Front Immunol* (2012) 3:1–6. doi: 10.3389/fimmu.2012.00296

frontiers | Frontiers in Immunology

TYPE Original Research
PUBLISHED 05 September 2022
DOI 10.3389/fimmu.2022.968206

OPEN ACCESS

EDITED BY
Dimitrios C. Mastellos,
National Centre of Scientific Research Demokritos, Greece

REVIEWED BY
Trent M. Woodruff,
The University of Queensland, Australia
Maartje G. Huijbers,
Leiden University Medical Center, Netherlands

*CORRESPONDENCE
Eva-Maria Nichols
eva-maria.x.nichols@gsk.com

SPECIALTY SECTION
This article was submitted to Molecular Innate Immunity, a section of the journal Frontiers in Immunology

RECEIVED 13 June 2022
ACCEPTED 19 July 2022
PUBLISHED 05 September 2022

CITATION
Lekova E, Zelek WM, Gower D, Spitzfaden C, Osuch IH, John-Morris E, Stach L, Gormley D, Sanderson A, Bridges A, Wear ER, Petit-Frere S, Burden MN, Priest R, Wattam T, Kitchen SJ, Feeney M, Davis S, Morgan BP and Nichols E-M (2022) Discovery of functionally distinct anti-C7 monoclonal antibodies and stratification of anti-nicotinic AChR positive Myasthenia Gravis patients.
Front. Immunol. 13:968206.
doi: 10.3389/fimmu.2022.968206

Discovery of functionally distinct anti-C7 monoclonal antibodies and stratification of anti-nicotinic AChR positive Myasthenia Gravis patients

Eleonora Lekova[1], Wioleta M. Zelek[2], David Gower[3], Claus Spitzfaden[4], Isabelle H. Osuch[1], Elen John-Morris[1], Lasse Stach[3], Darren Gormley[1], Andrew Sanderson[5], Angela Bridges[5], Elizabeth R. Wear[1], Sebastien Petit-Frere[1], Michael N. Burden[3], Richard Priest[3], Trevor Wattam[3], Semra J. Kitchen[1], Maria Feeney[1], Susannah Davis[3], B. Paul Morgan[2] and Eva-Maria Nichols[1*]

[1]Immunology Research Unit, GlaxoSmithKline Research & Development (GSK R&D), Stevenage, United Kingdom, [2]Division of Infection and Immunity and Dementia Research Institute, Systems Immunity Research Institute, School of Medicine, Cardiff University, Wales, United Kingdom, [3]Medicinal Science and Technology, Biopharm Discovery, GlaxoSmithKline Research & Development (GSK R&D), Stevenage, United Kingdom, [4]Medicines, Science and Technology, Protein Cellular and Structural Sciences (PCSS) Structural and Biophysical Sciences, GlaxoSmithKline Research & Development (GSK R&D), Stevenage, United Kingdom, [5]Medicines, Science and Technology, Protein Cellular and Structural Sciences (PCSS) Protein and Cellular Sciences, GlaxoSmithKline Research & Development (GSK R&D), Stevenage, United Kingdom

Myasthenia Gravis (MG) is mediated by autoantibodies against acetylcholine receptors that cause loss of the receptors in the neuromuscular junction. Eculizumab, a C5-inhibitor, is the only approved treatment for MG that mechanistically addresses complement-mediated loss of nicotinic acetylcholine receptors. It is an expensive drug and was approved despite missing the primary efficacy endpoint in the Phase 3 REGAIN study. There are two observations to highlight. Firstly, further C5 inhibitors are in clinical development, but other terminal pathway proteins, such as C7, have been relatively understudied as therapeutic targets, despite the potential for lower and less frequent dosing. Secondly, given the known heterogenous mechanisms of action of autoantibodies in MG, effective patient stratification in the REGAIN trial may have provided more favorable efficacy readouts. We investigated C7 as a target and assessed the *in vitro* function, binding epitopes and mechanism of action of three mAbs against C7. We found the mAbs were human, cynomolgus monkey and/or rat cross-reactive and each had a distinct, novel mechanism of C7 inhibition. TPP1820 was effective in preventing experimental MG in rats in both prophylactic and therapeutic dosing regimens. To enable identification of MG patients that are likely to respond to C7 inhibition, we developed a patient stratification assay and showed in a small cohort of MG patients (n=19) that 63% had significant complement

activation and C7-dependent loss of AChRs in this *in vitro* set up. This study provides validation of C7 as a target for treatment of MG and provides a means of identifying patients likely to respond to anti-C7 therapy based on complement-activating properties of patient autoantibodies.

KEYWORDS

myasthenia gravis, autoantibodies, terminal pathway, MAC assembly, complement C7, myasthenia gravis patient stratification, complement therapy

Introduction

The complement system plays an important role in innate and adaptive immune response and tissue homeostasis and is broadly involved in both common and rare diseases (1). Activation of the complement system through one of three pathways, alternative, lectin and classical, results in formation of a C3 convertase, cleaving C3 into C3a and C3b. The latter facilitates clearance of microorganisms and immune complexes through opsonization as well as initiating formation of the C5 convertase on the cell surface. Cleavage of C5 by C5 convertases initiates the terminal pathway and results in generation of C5a, a potent anaphylatoxin and C5b, which rapidly binds C6, C7, C8 and multiple molecules of C9 to form the membrane attack complex (MAC) (2). The MAC mediates lysis of microorganisms in infection and tissue damage and inflammation in disease (2, 3).

The 2007 FDA approval of Eculizumab (Soliris, Alexion Pharmaceuticals), an anti-C5 monoclonal antibody, for the treatment of Paroxysmal Nocturnal Hemoglobinuria (PNH), presented a significant milestone in the field of complement therapeutics (4, 5). Treatment with Eculizumab requires high, bi-weekly i.v. doses of 1200mg for the treatment of PNH and atypical Hemolytic Uremic Syndrome (aHUS) (4), with an annual per-patient cost of ~$400,000. While many therapeutic concepts and modalities have been explored across the entire complement cascade, relatively few have progressed into clinical development and the terminal pathway remains a focus point (6). Notably, very few approaches have explored other terminal pathway targets, despite the potential for lower, less frequently administered doses. Three C6 antibodies, including Regenemab, CP010 (unpublished pre-clinical candidate, Regenesance), have been described and more recently, a panel of potent C7 and C5b7 inhibitors was described that highlights the potential of lower dosing compared to targeting C5 (7, 8). An important consideration, not specific for anti-complement therapies, but relevant for all high-priced drugs that have potentially serious side-effects that need to be carefully managed, is the need for mechanism-based patient stratification to identify those patients who have a high likelihood of an adequate response.

In 2017, Eculizumab was also approved for the treatment of refractory Myasthenia Gravis (MG), an autoantibody-mediated disease characterized by disrupted cholinergic transmission due to decreased numbers of acetylcholine receptor (AChR) at the neuromuscular junction (NMJ), resulting in weakness and lack of muscular control (9). Before the approval, treatment options for patients were limited to general immune-suppressive drugs and off-label use of Rituximab for B cell depletion (10). Autoantibodies against the muscle nicotinic AChR are detectable by radioimmunoassay in 80 - 90% of MG patients and contribute directly to the MG pathology. In autoantibody-mediated disease, complement activation is driven through Fc effector function of the autoantibodies. The classical pathway can be effectively activated by immune-complex associated IgA, IgM and IgG (2). The importance of complement activation, *via* autoantibodies of the IgG1 and IgG3 subtypes, is well documented in MG (11–13). The serum AChR autoantibody titers in different patients do not correlate with disease severity, which is likely due to the heterogeneity of antibodies and their effector functions, and antibodies have been shown to reduce the number of AChR by at least three mechanisms: endocytosis/degradation mediated *via* antibody receptor crosslinking, functional blockade of acetylcholine binding sites, and complement-mediated AChR loss (14–16). Autoantibody-mediated complement deposition and tissue damage, leading to AChR loss, appears to be one of the main pathological mechanisms as demonstrated by the efficacy of Eculizumab in a phase 2 trial in AChR-antibody positive patients with generalized MG (17). However, the primary efficacy endpoint was missed in the phase 3 REGAIN study (NCT01997229), assessing the safety and efficacy of Eculizumab in anti-AChR antibody-positive refractory generalized myasthenia gravis (13). A possible explanation for this could be that patients were not stratified.

Here, we describe the *in vitro* and *in vivo* characterization of a new anti-C7 monoclonal antibody and provide insights into tractable, functionally relevant epitopes on C7. We show that the antibody ablates disease in rodent MG models and describe a novel method for patient stratification that highlights the heterogeneity of complement-dependence in MG and enables

categorization of nicotinic AChR autoantibody positive patients according to complement-dependent loss of AChR.

Materials and methods

Anti-C7 antibody generation and scale up and purification of TPP1820

Immunizations and antibody discovery

All animal studies were ethically reviewed and carried out in accordance with Animals (Scientific Procedures) Act 1986 and the GSK Policy on the Care, Welfare and Treatment of Animals. Transgenic mice expressing a human V-gene repertoire, were immunized with human C7 protein purified from normal human serum (Complement Technology, Inc). B-cells enriched from the spleen and lymph node tissues were used for hybridoma fusion and direct single B-cell sorting. For the sorting cells were stained with a combination of fluorescently labelled antibodies against B cell markers. Memory and plasma blast B cells were labelled with B220-PECy7, IgM-BV605 and CD43-FITC, plasma cells with B220-PECy7 and CD138-PE. Contaminating cells were excluded by gating out cells positive for CD3, CD93, CD11c, Ter-119 and Gr1, all conjugated to PerCPCy5.5. Antigen specific B-cells and CD138+ plasma cells were single cell sorted using the BD FACS Aria III (Becton Dickinson). To identify C7 binding memory or plasma blast cells the cells were incubated with a biotinylated version of the human protein isolated from human plasma. C7 binding was visualized using streptavidin-PE and streptavidin-APC. cDNA was synthesized from the sorted B-cells and used for V-gene amplification by PCR. Cognate VH and VL chains were then cloned into the Adimab yeast-based platform (Adimab, LLC) and clonal yeast populations with concomitant HC and LC expression and human C7 binding were isolated by FACS, expressed and purified. Antibody clones derived from both the hybridoma and B-cell sorting methods were characterized and selected based on their binding affinity, inhibitory potency in the classical pathway hemolysis assay and epitope diversity.

Antibody optimization by generation and selection of random mutagenesis libraries

Affinity maturation libraries were built for the selected, functional anti-C7 antibodies by diversifying each of the complementary determining regions (CDRs) 1, 2, and 3 of the heavy- and light-chain variable region (VH and VL) genes. Random mutations restricted to the CDRs were introduced by splice-overlap-extension (SOE) PCR using degenerate oligonucleotides synthesized with mixtures of nucleotide bases with a bias towards the wild-type nucleotide. Antibodies were selected from the affinity maturation libraries using the Adimab platform according to the protocols developed by Adimab, LLC. Human C7 protein was biotinylated *via* amine coupling, magnetic bead selections were performed using streptavidin beads from Miltenyi (MACS®) and FACS selections were performed on the BD FACS Aria III (Becton Dickinson). Cells from the yeast maturation libraries which showed improved antigen binding over the parental antibodies were bulk sorted and plated on agar plates for single colony isolation and sequencing.

TTP1820 scale up and purification

The monoclonal antibodies were obtained by transient expression in HEK293-6E cells. Supernatants were collected after 10 days, sterile filtered and the antibodies affinity purified using MabSelect SuRe columns on the Akta Xpress system. Purity and integrity of the purified mAbs was confirmed by analytical size exclusion chromatography and SDS-PAGE. Endotoxin levels were confirmed to be below 0.75 EU/mL using an EndoSafe endotoxin reader (Charles River Laboratories).

Affinity measurement by surface plasmon resonance

Surface plasmon resonance experiments were performed on a Biacore 8K instrument (Cytiva) using HBS-EP+ (Teknova) at pH 7.4 as a running buffer. For the SPR chip, Protein A (Pierce) was immobilized on a CM5 chip (Cytiva) using a Biacore amine coupling kit (Cytiva) according to the manufacturer's instructions. Multi-cycle kinetics experiments were run as follows. Antibodies were diluted in running buffer to 0.5µg/ml and captured on the sample flow cells of all channels at a flow rate of 10 µL/min for 60s. Antigen was flowed over both flow cells of all channels at a flow rate of 30µl/min for 180s followed by a 600s dissociation time. The chip surface was regenerated between cycles using 50mM NaOH for 30s at a flow rate of 30µL/min. Antigen concentrations used were 0, 0.39, 1.56, 6.25 and 25nM. The data was analyzed in the Biacore analysis software to a 1:1 binding model using local Rmax and double referencing. Off-rates fitted as slower than $1x10^{-5}$ 1/s and too slow to be fitted reliably were manually adjusted to $1x10^{-5}$ 1/s. Antigens used were human complement C7 (Complement Tech) and cyno complement C7 purified from cynomolgus serum (Seralab).

Hemolysis assays

Sheep erythrocytes (TCS Biosciences) were prepared for assay with gentle washing in CFD (Complement Fixation Diluent, Oxoid Ltd) followed by sensitization with a complement fixation antibody (Amboceptor, Siemens Healthcare) for 30min at 37°C. Control antibodies included were an in-house anti-C5 and disabled anti-C5 antibody (both isotype matched with test mAbs, human Fc-disabled IgG1κ) for human serum and a mouse anti-C7 mAb (Quidel), mouse IgG1κ was used for the rat serum, in addition to the isotype control for the test antibodies. There was no cyno cross-reactive

positive control available at the time of the experiments, therefore only the test antibody isotype control was included. Serial dilutions of test antibodies, along with positive and negative control antibodies as above, were prepared in CFD and 50µL added to the wells of a 96-well U-bottomed assay plate (Greiner Bio-One). Pooled normal human serum (or rat serum/cyno serum) was diluted in CFD to a concentration previously determined to elicit 80% lysis of sheep erythrocytes and 50µL were added to the wells of the assay plate containing the serially diluted test molecules. 50µL of diluted serum was also added to wells containing an equal volume of CFD to determine maximum complement induced lysis. The plate was then incubated on ice for 30min. Following incubation, 50µL of sensitized sheep erythrocytes were added to all wells of the assay plate and also to wells containing 100µL of water only (to give 100% lysis control) and wells containing 100µL of CFD only (to give 0% lysis control). The plate was then incubated at 37°C for 30 min to allow complement mediated lysis of the cells to take place. Following lysis, the plate was centrifuged at 500g for 3 min and supernatants transferred to a Maxisorp 96-Well Flat-Bottom Assay Plate (Nunc). Absorbance was measured at 405nm on a Molecular Devices SpectraMax M5 plate reader. The percentage hemolysis was calculated as = 100 x (Test sample at 405nm - A405nm 0% lysis control)/(A405nm 100% lysis control - A405nm 0% lysis control). Dose response curves for the test and control antibodies were derived in GraphPad Prism (v 5.01) using a four-parameter logistic curve fit and EC50 values determined.

HDX-MS

Hydrogen Deuterium Exchange Mass Spectometry (HDX-MS) was used to determine the C7 binding epitopes of TPP1657, TPP1653 and in the case of TPP1820, the parental molecule TPP1651 was included as TPP1820 was derived later through affinity maturation. Based on our previous experience the epitope in daughter clones does not change as a result of our affinity maturation process, protection patterns tend to be more pronounced. Full experimental details, method and supporting experimental data are located in Supplementary File 1 which contains Table S1 (HDX Experimental Data Summary), Table S2 (Table of peptides with statistically significant protection) and Figure S1 (Sequence coverage and redundancy), Figure S2 (Differential fractional uptake and time course data vs. peptide ID), Figure S3 (Woods plots) and Figure S4 (Volcano plot analysis).

MAC assembly and elucidating anti-C7 antibody mechanism of action using Bio-Layer Interferometry (BLI) technology

BLI experiments were performed on an OctetRed384 instrument (Fortebio) using phosphate buffer saline IgG free (PBSF) buffer. Anti-mouse capture (AMC) biosensors (Fortebio) were equilibrated in PBSF (10 min shaking 200xg) then 133nM anti-C6 monoclonal antibody (Quidel) or 133nM mouse IgG1,κ isotype control (GlaxoSmithKline) were loaded onto the AMC biosensors (600s). Following a PBSF wash step (30 seconds), 100nM of C5b6, C7, C8 and C9 (Complement Technologies) were added to the AMC biosensors sequentially (time varied between 300-800s depending on the protein being assessed). PBSF only controls were included for each protein addition step of forming the complex and represent the negative controls. To determine whether the anti-C7 mAbs prevent C5b6:C7 or C7:C8 interactions binding of C7 in the presence or absence of 2nM or 200nM anti-C7 antibody to previously captured C5b6 biosensors was evaluated (800 seconds). Subsequent steps then sequentially assessed the ability of C7, C8 or C9 complement proteins to bind to the AMC biosensors (800s). In all experiments a PBSF buffer only control, representing a reference biosensor, was included. To subtract background noise, values for the reference biosensor was subtracted from the sample biosensor values. When elucidating anti-C7 antibody method of action, all traces were aligned to the beginning of the addition of C7 step.

Passive experimental autoimmune Myasthenia Gravis in rats

To measure *in vivo* effects and prophylactic therapeutic efficacy of TPP1820, Lewis rats (150 – 180g) were obtained from Charles River Laboratories (Edinburgh, UK) and allowed to acclimatize for one week. Disease was then induced by subcutaneous administration of anti-Acetylcholine receptor (AChR) mAb35 at 1mg/kg in PBS. MAb35 binds the main immunogenic region of AChR, activating complement and damaging the neuromuscular junction endplates, causing severe muscle weakness. Animals were assessed frequently post-disease initiation for weight loss and clinical symptoms (0, no disease; 1, loss of tail tone and reduced grip strength in back legs; 2, loss of grip in front legs; 3, hind limb weakness and wasting; 4, loss of grip and hind limb paralysis; 5, moribund). The grip strength was assessed by allowing the rat to grip a standard gridded metal cage-top with its rear or forepaws then gently lifting the rat – a healthy rat lifts the lid (0), a weakened rat lifts but loses its grip (1,2), a paralysed rat cannot grip at all (3,4). mAb35-injected rats were split into two groups: Group 1 (n = 8) was treated with mAb TPP1820 at 40 mg/kg dose (standard dose for anti-complement mAb used in animal models, comparable to bolus dose of ~20mg/kg of Eculizumab for initiation of therapy) given by intraperitoneal injection at time zero. Group 2 (n = 8) received an isotype control antibody GRITS 53541 (control EAMG) at the same time, route and dose. All animals were humanely killed by CO_2 asphyxiation either when weight loss exceeded 20% of starting weight, clinical score exceeded 3 (Home Office license requirements), or at 48 hours (h) post-disease induction. Blood was taken for serum assays at 0, 24 and

48h (or at time of euthanasia if earlier). For the therapeutic efficacy of TPP1820, mAb35-injected rats were split into two groups: Group 1 (n = 8) was treated with test mAb TPP1820 at 40 mg/kg dose (standard dose for anti-complement mAb used in rodent models) given by intraperitoneal injection 16h post-induction of EAMG. Group 2 (n = 8) received an isotype control antibody (GRITS 53541) at the same times, routes and doses. Rats were humanely killed at the end point of the experiment at 48h post-induction, or earlier if clinical score exceeded 3 or weight loss exceeded 20%. Blood was taken for serum assays at 0, 24 and 48h (or at time of kill if earlier).

All animal studies were ethically reviewed and carried out in accordance with Animals (Scientific Procedures) Act 1986 and the GSK Policy on the Care, Welfare and Treatment of Animals.

Measurement of plasma TCC in rats

Maxisorp plates (Nunc, Loughborough, UK) were coated with rabbit anti-rat C9 IgG (in house; 10μg/ml in bicarbonate buffer, pH 9.6) at 4°C overnight; wells were blocked (1h at 37°C with 3% BSA in PBS), washed once in PBS containing 0.05% Tween 20 (PBS-T). Standard curves of zymosan-activated normal rat serum (serial dilution series staring at 1 in 5) and rat serum samples diluted 1 in 50 in 1% BSA-PBS, 20mM EDTA were added in duplicate and incubated overnight at 4°C. Wells were washed with PBS-T 3X, then incubated (2h, room temperature (RT)) with monoclonal 12C3 anti- rat/mouse C5b-9 (in house; 5μg/ml in PBS-T). After washing, wells were incubated (1h, RT) with biotinylated donkey anti-Mouse IgG (1:2000 in PBS-T; Jackson ImmunoResearch #715-005-150). After washing, Streptavidin-HRP (1:2000 in PBS-T; R&D Systems, # 890803) was added and incubated 30 minutes at RT. After washing, plates were developed using o-phenylenediamine dihydrochloride (SIGMAFAST; Sigma-Aldrich, St Louis, MO) and absorbance (492 nm) was measured. Protein concentrations (Units/ml) of serum samples were automatically calculated by reference to the standard curve using GraphPad Prism (GraphPad, La Jolla, CA, USA).

Ex vivo hemolysis assay

The assay system comprised optimally antibody-sensitized sheep erythrocytes (ShEA) incubated with rat serum (NRS) dilutions in HEPES-based buffer supplemented with Ca^{2+} and Mg^{2+} cations (assay buffer) (SOP in (18)). Sheep blood was from TCS Bioscience and anti-ShE antiserum (#ORLC25, Siemens Amboceptor) was from Cruinn Diagnostics (Dublin, UK). In an initial *in vitro* assay, a serum dilution was selected to give ~75-90% hemolysis of ShEA at end point (30min at 37°C; typically, 2-5% NRS) in the absence of inhibitor. Test and positive control mAb were then titrated in a broad range of concentrations (in triplicate) into the NRS dilutions (100μL) in the wells of a U-welled microtiter plate and ShEA (100μL) at the appropriate dilution in assay buffer added and incubated for 30min at 37°C. Plates were centrifuged, supernatants removed to a flat-well microtiter plate and absorbances measured spectrophometrically. Percent hemolysis was calculated for each well by comparison with 0 and 100% lysis controls. Hemolytic activity in sera from the experimental animals were tested in essentially the same assay; rat serum dilutions (10-0%, in triplicate, 100μL per well in assay buffer) were made in the wells of a U-welled microtiter plate and ShEA (100μL) in assay buffer were added and incubated for 30min at 37°C. Plates were centrifuged, supernatants removed to a flat-welled microtiter plate and absorbances measured spectrophometrically (A405) and % lysis calculated for each sample.

Hemolytic activity in IgG-depleted NHS was tested as described above but using complement fixation diluent (CFD) (Oxoid Ltd.) rather than HBS buffer. The percentage hemolysis was calculated as = 100 x (A405 nm test sample - A405 nm 0% lysis control)/(A405 nm 100% lysis control - A405 nm 0% lysis control). The NHS hemolysis dose-response curves were plotted in GraphPad Prism v7 and analyzed using a four-parameter logistic curve fit to calculate the EC50 concentrations.

Plasmid generation

AChRαβ & AChRδε plasmids: cDNAs for the α1/β1 and δ/ε subunits of human nAChR were cloned into the dual expression vectors pBiCIH and pBiCIN respectively. pBiCIH and pBiCIN are hygromycin and neomycin resistant derivatives of the bi-cistronic vector pCIN5 (19), modified by insertion of a SV40-promoter-polyadenylation signal cassette to allow expression of a second gene insert. In pBiCIH and pBiCIN, the α1 and δ subunits are expressed from the CMV promoter as bi-cistronic inserts linked to the selectable marker by an IRES element; the β1 and ε subunits are expressed from the SV40 promoter.

Rapsyn plasmid: The pCIP4 plasmid backbone (made internally) contains an IRES element upstream of the puromycin resistance cassette, allowing stable selection of cell lines. The Rapsyn gene (NM_005055) was synthesized at GenScript, then subcloned into pCIP4 using NotI and BamHI restriction sites.

Transient cell transfection

ARPE-19 CD46, CD55, CD59 KO cells were available as a suitable tool cell line as they are susceptible to complement attack, without the need of blocking antibodies to the above complement regulatory proteins. The cells were cultured in DMEM/F12 + GlutaMAX medium (Invitrogen), supplemented with 10% HI-FBS (Invitrogen), 15mM HEPES (Invitrogen), and 1X MEM-NEAA (Invitrogen) (complete culture medium).

Generation of these cells is described in Supplementary File 2. Due to the biolicensing terms of the CRISPR reagents, this cell line cannot be made available and a protocol to replicate the effect of complement regulator deficiency is included in Supplementary File 2. One day before transfection, the cells were seeded in 96-well black glass-bottom plates (Greiner) at a cell density of 20,000 cells/well in complete culture medium and incubated overnight at 37°C, 5% CO_2, high humidity. Lipofectamine/DNA lipid complexes were prepared in Opti-MEM™ Medium (Invitrogen) according to the manufacturer's instructions: 0.2µg total DNA and 0.15µL lipofectamine was used per well. The following plasmids were added at a molar ratio of 1:1:1 (0.055µg pCIP4-huRapsyn, 0.074µg pBiCIH-hnAChRα1β1, and 0.071µg pBiCIN-hnAChRδε per well). The culture medium from the wells was aspirated and replaced with lipofectamine/DNA lipid complex, pre-diluted 1 in 10 in complete culture medium. The cells were incubated for 24h at 37°C, 5% CO_2, high humidity.

Quantification of AChR expression on transfected cells

The cells were blocked following transfection with 200µL/well of complete culture medium + 1% BSA (staining buffer) for 15 – 30 min at 37°C, 5% CO_2, high humidity, then stained with 50µL/well Alexa Fluor™ 647 conjugated α-Bungarotoxin (AF647 α-Bungarotoxin; Invitrogen) at 2.5µg/ml in staining buffer and incubated for 30 min at 37°C, 5% CO_2, high humidity. The cells were washed twice with 200µL/well of PBS and fixed for 10 min at RT with 50µL/well of 10% Formalin (Sigma), washed twice with 200µL/well of PBS and stained with a solution, containing 10 Units/ml Alexa Fluor™ 488 Phalloidin (actin stain, Invitrogen) and 1µg/ml Hoechst 33342 (nuclear stain, Invitrogen). The cells were incubated for 30min at 37°C, 5% CO_2, high humidity, and washed 2x with 200µL/well PBS. PBS was added to the wells at 100µL/well and images were captured on an InCell 2200 or InCell 6000 imager (GE Healthcare), using a 10X objective. Images were analyzed using Columbus v2.8 (Perkin Elmer). The following image analysis algorithm was used. The fluorescence from the DAPI channel (Hoechst 33342 stain) was used to find the nuclei. The fluorescence from the FITC channel (Alexa Fluor™ 488 Phalloidin stain) was then used to identify the cytoplasm and draw the cell perimeter. Spots of clustered surface AChR were identified within each cell, based on the AF647 α-Bungarotoxin (Cy5) fluorescence, and various spot parameters were calculated. The sum of the spot fluorescence per cell was used to set the threshold for identifying "AChR Pos Cells". The % positive cells was calculated by dividing the number of positive cells by the total number of cells, multiplied by 100. The data was plotted in GraphPad Prism v7.05.

Human sample collection

Myasthenia Gravis patient plasma samples were purchased from Tissue Solutions (Glasgow, UK). These patients were confirmed as anti-nicotonic AChR positive based on a autoanitobdy titre determined by immunoassay (see Table S3 for patient details).

Pooled control plasma was prepared from blood obtained from healthy volunteers at GSKs internal blood donation unit. 100mL of EDTA anti-coagulated blood was obtained per donor from six donors in total. The blood was centrifuged for 10 min at 2000xg, 4°C and the plasma supernatants were transferred to clean 50mL falcon tubes which were centrifuged again for 5 min at 2000 x g, 4°C. All plasma supernatants from all donors were pooled into a sterile reservoir, aliquoted into sterile Eppendorf tubes, and stored at -80°C.

Pooled normal human serum (NHS) was prepared from blood obtained from healthy volunteers at GSKs internal blood donation unit. Blood was collected from 10 healthy volunteers in serum separator tubes (S-Monovette® 7.5ml Z-Gel, Sarstedt) and processed to preserve complement activity. The blood was left to clot at RT for 20 – 30min, then the tubes were immersed in ice water to contract the clots and centrifuged for 10min at 2000xg at 4°C. The serum supernatants from all tubes were pooled into a 50 ml Falcon tube. The tube was centrifuged for 5min at 2000xg, 4°C. The supernatant was transferred into a fresh reservoir, aliquoted and frozen immediately at -80°C.

The human biological samples described were sourced ethically and their research use was in accord with the terms of the informed consents under an IRB/EC approved protocol.

ELISA for quantification of patient autoantibody titers in-house

The Anti-Acetylcholine Receptor ELISA (IgG) kit from Euroimmun (catalogue number EA 1435-9601 G) was used for quantification of patient autoantibody titers in-house. The plasma test samples were thawed at RT and diluted 1:26 in sample buffer. The 1:26 sample dilutions were considered as neat samples on the standard curve, and controls were also diluted 1:26. Some of the samples which had higher titers were further diluted and dilution factor from this step was used when calculating the sample concentrations from the standard curve. The absorbance was read at 450 nm and 650 nm on a PHERAstar FSX. The data analysis was carried in the PHERAstar FSX MARS Software v3.20 R2: the blank and 650 nm values were subtracted from all wells and a standard curve was plotted and analyzed using a four-parameter logistic curve-fit. The unknown sample concentrations were calculated using the four-parameter logistic equation and multiplied by the dilution factor (if applicable). Each sample was tested in three

independent experiments and the mean of the three experiments was calculated.

Immunoglobulin (Ig)-depletion of normal human serum

The pooled NHS was depleted of immunoglobulins using Protein A/G agarose (Thermo Scientific) in order to remove natural antibodies that may bind to the cells and cause non-specific MAC deposition. 15mL Protein A/G agarose resin was used per 3.5mL NHS. The resin was washed three times with 35mL PBS and placed on ice. The NHS was thawed in a water bath at 37°C, mixed with the resin and incubated for 30min in a 4°C cold cabinet on a roller mixer. The NHS/resin suspension was centrifuged for 2min at 1000xg, 0°C. The supernatant was aliquoted in Eppendorf tubes and immediately frozen at -80°C. Except for the assay validation data, all MG experiments reported used Ig-depleted NHS as source of complement.

MSD assay for human immunoglobulin

To confirm whether immunoglobulin depletion was successful, NHS and Ig-depleted NHS were tested for IgG, IgA, and IgM levels using a commercial immunoassay kit (Human/NHP Isotyping Panel 1 kit, Meso Scale Discovery). NHS samples were assayed at dilutions ranging from 1/20 – 1/1,562,500 (1/5 serial dilution intervals) according to the manufacturer's instructions. The data was analyzed using the MSD Discovery Workbench Software v4.0.12. The background (Blank values) was subtracted from all samples/standards (ECL Signal - Blank). A standard curve was generated by plotting the "ECL Signal – Blank" values against the concentration and analyzed using a four-parameter logistic curve-fit, including a 1/Y2 weighting function. The unknown sample concentrations were calculated using the four-parameter logistic equation and multiplied by the dilution factor where applicable.

Patient autoantibody binding assay

The transfected cells were blocked with 200µL/well of complete culture medium + 1% BSA and a 1/40 dilution of TruStain FcR block (Biolegend) for 30-60min at 37°C. MG and control plasma samples were thawed and incubated in a heat-block for 30-45min at 56°C to heat-inactivate complement. The heat-inactivated samples were diluted 1/10 in complete culture medium and added to the blocked wells at 50µL/well. The plates were incubated for 30min at 37°C, 5% CO_2, 95% humidity. The wells were washed twice with 200µL/well of PBS and stained with 2.5µg/ml AF647 α- Bungarotoxin, combined with 20µg/ml of either Cy3 Donkey Anti-human IgG, Fcγ specific, or Cy3 Donkey Anti-human IgM, Fc5µ specific, or Cy3 Donkey Anti-human IgA, α chain specific (all Jackson ImmunoResearch). The plates were incubated for 30min at 37°C, 5% CO_2, high humidity and washed twice with 200µL/well of PBS. The cells were fixed for 10min at RT with 50µL/well of 10% Formalin (Sigma), then washed and stained with 1µg/ml Hoechst 33342 (nuclear stain) + 10 Units/ml AF488 Phalloidin (actin stain) for 30min at 37°C, 5% CO_2, high humidity. The wells were then washed, filled with 100µL/well PBS and imaged on an InCell 6000 imager (GE Healthcare), using a 10X objective. Images were analyzed using Columbus v2.8 (Perkin Elmer). The following image analysis algorithm was used. The fluorescence from the DAPI channel (Hoechst 33342 stain) was used to find the nuclei. The fluorescence from the FITC channel (Alexa Fluor™ 488 Phalloidin stain) was then used to identify the cytoplasm and draw the cell perimeter. Spots of clustered surface AChR were identified within each cell, based on the AF647 α- Bungarotoxin (Cy5) fluorescence, and various spot parameters were calculated. The sum of the spot fluorescence per cell was used to set the threshold for identifying "AChR Pos Cells" (Cy5) and "Anti-human Immunoglobulin Pos Cells" (dsRed). The % positive cells was calculated by dividing the number of positive cells by the total number of cells, multiplied by 100. The same calculation was used for the % negative cells but using the number of negative cells. To correct for non-AChR specific immunoglobulin binding, the % Immunoglobulin positive cells within the AChR negative cell population were subtracted (background corrected). The average background-corrected values from three independent experiments (except for MG patient 1 where there was only sufficient sample for one experiment) were plotted in GraphPad Prism v7.03, where samples were classed into the following four categories, based on the average percentage of positive cells: between 0% - 15% (-), between 15% - 40% (+), between 40% - 65% (++), between 65% - 100% (+++). Statistical analysis was carried out in GraphPad Prism v7.05, using a repeated measures 1way ANOVA without correction, with Dunnet's multiple comparison test, comparing the means (n=3 experiments) of each plasma sample to the mean of the pooled control plasma sample. For MG Patient 1 (n=1 experiment, 2 replicates) the mean of the two replicates was compared to the mean of the two pooled control plasma replicates from the same experiment using an unpaired t-test.

Complement-mediated AChR loss and MAC deposition assays

The transfected cells were blocked with 200µL/well of complete culture medium + 1% BSA and a 1/40 dilution of TruStain FcR block for 30-60 min at 37°C. MG and control plasma samples were thawed and incubated in a heat-block for 30-45 min at 56°C to inactivate complement. The heat-inactivated samples were diluted 1/10 in complete culture

medium. A 10µg/ml mAb35 (Rat anti-AChR tool Ab, Genetex) solution was also prepared in culture medium. The blocking solution from the plates was aspirated and the diluted MG plasma samples or controls were added to the cells and incubated for 30min at 37°C, 5% CO_2, high humidity. The wells were washed twice with 180µL/well of PBS and the anti-C7 blocking antibody or the corresponding isotype control antibody (both at 20µg/ml in culture medium) added to the appropriate wells at 50µL/well. Culture medium alone was added to control wells. Ig-depleted NHS aliquots were quickly thawed in a water bath at 37°C and placed on ice prior to dilution to 30% in culture medium immediately before addition to the plates (50µL/well). Culture medium alone was added to control wells. The plates were incubated for 2.5-3h at 37°C, 5% CO_2, high humidity, washed twice with 180µL/well of PBS and stained with 50µL/well of 2.5µg/ml AF647 α-Bungarotoxin + 10µg/ml polyclonal Rabbit anti-C5b9 antibody (Abcam) in staining buffer (culture medium + 1% BSA) for 30 min at 37° C, 5% CO_2, high humidity. The wells were washed twice with 180µL/well of PBS and fixed with 50µL/well of 10% Formalin for 10min at RT, the washed again as above. A staining cocktail was prepared, containing 1µg/ml Hoechst 33342 (nuclear stain) + 10 Units/ml AF488 Phalloidin (actin stain) + 1/200 dilution of PE Donkey Anti-Rabbit secondary antibody (Jackson ImmunoResearch) in staining buffer and added to the wells at 50µL/well. The plates were incubated for 30min at 37°C, 5% CO_2, high humidity (95%), washed twice with 180µL/well of PBS, 100µL/well PBS added, and the plates were imaged on an InCell 6000 imager using a 10X magnification. Images were analyzed using Columbus v2.8 (Perkin Elmer). The following image analysis algorithm was used. The fluorescence from the DAPI channel (Hoechst 33342 stain) was used to find the nuclei. The fluorescence from the FITC channel (Alexa Fluor™ 488 Phalloidin stain) was then used to identify the cytoplasm and draw the cell perimeter. Fluorescent spots of clustered surface AChR (Cy5 fluorescence) and deposited MAC (dsRed fluorescence) were identified within each cell, and various spot parameters were calculated. The sum of the spot fluorescence per cell was used to set the threshold for identifying "AChR Pos Cells" and "MAC Pos Cells". The % positive cells was calculated by dividing the number of positive cells by the total number of cells, multiplied by 100. The "AChR Pos Cell Population: % MAC Pos Cells" was calculated by dividing the AChR/MAC double positive cells by the total number of AChR positive cells, multiplied by 100. To be able to class patients into different categories based on levels of AChR loss and MAC deposition, a "fold change relative to NHS treatment" ratio was calculated for all treatment conditions to normalize the data from different experiments, by dividing each treatment value by the NHS-treatment value for that plate. For the AChR readout the classification was as follows: 1 – 0.8 (-), 0.8 – 0.6 (+), 0.6 – 0.3 (++). For the MAC readout the classification was as follows: 1 – 1.3 (-), 1.3 – 1.8 (+), 1.8 – 2.3 (++), 2.3 – 3.5 (+++). The % positive cells values were plotted in GraphPad Prism v7.05 and statistical analysis was performed using a repeated measures 1way ANOVA without correction, using Tukey's multiple comparisons test. For patient categories 1, 2, and 4, the average of all donors within the category was analyzed. For individual donors (except Patient 1), statistical analysis was performed on the average of n=3 experiments, each carried out in duplicate. For MG Patient 1 (category 3) (n=1 experiment, 2 replicates) an unpaired t-test was used to compare the mean of duplicates between conditions.

Correlation between ELISA anti-AChR titers, IgG cell binding to AChR and MAC deposition

A two-tailed, non-parametric Spearman correlation with 95% confidence interval was calculated in GraphPad Prism v7.05 between the following pairs of sample sets: IgG cell binding to AChR vs. MAC deposition on the AChR positive cells, IgG cell binding to AChR vs. ELISA anti-AChR titres, and ELISA anti-AChR titres vs. MAC deposition on the AChR positive cells. The values used for IgG cell binding were the background corrected fluorescent intensity averages of 3 replicates for all samples, except for MG Patient 1, where the average of two replicates from one experiment was used as there was not enough sample for further repeats. The values used for MAC deposition on the AChR positive cells were the "MG Plasma + NHS" fluorescent intensity averages of 3 replicates for all samples, except for MG Patient 1, where the average of two replicates from one experiment was used as there was not enough sample for further repeats. The values used to calculate the correlations for the ELISA anti-AChR titres were the average of 3 replicates for all samples, except for MG Patient 1, where the titer provided in the supplier datasheet was used as there was not enough sample to re-test in-house.

Results

Novel function-blocking anti-C7 mAbs show distinct C7 binding epitopes and mechanism of action

Functional anti-C7 antibodies were discovered by immunization of transgenic mice, that have a diverse human V-gene repertoire, combined with standard hybridoma techniques and B-cell sorting methods. 397 antibodies were screened by Surface Plasmon Resonance (SPR) to measure human C7 binding affinity (Kd), functional blockers were subsequently identified in a single dose classical pathway hemolysis assay (>30). Selected antibodies were grouped according to epitope bins using a sandwich Surface Plasmon

Resonance (SPR) based method. The top seven functional, epitope diverse antibodies, were optimized for affinity and potency. Affinity optimization was achieved using the Adimab yeast-based platform, improved binders were selected from mutagenesis libraries generated by introducing random diversity into the CDRs of the heavy- and light-chain-variable genes. A total of 649 sequence unique antibodies were screened by Surface Plasmon Resonance for C7 binding. The optimization campaign delivered a hit panel of high-affinity and high-potency antibodies (with single-digit nanomolar IC50 potencies in the hemolysis assay). The antibodies were purified, stability and biophysical properties evaluated (data not shown) and further characterized functionally as described below.

A diverse panel of antibodies, that represented four distinct epitope bins determined by SPR, was selected from the hits using binding and affinity data to human and cyno C7. Three representative clones (TPP1657, TPP1653 and TPP1820 or its parental clone TPP1651) were included in the present work. Species cross-reactivity of the three mAbs was assessed using classical pathway hemolysis assays (CP CH50) using normal human, rat and cyno sera. In hemolysis assays using normal human and cyno serum, TPP1657 and TPP1820 showed comparable function with IC50s below 2nM for both species, while TPP1653 had IC50s of 2.6nM and 2.4nM for human and cyno, respectively (Figures 1A, B, D). TPP1657 was particularly potent in cyno serum with an IC50 of 0.47nM. TPP1657 and TPP1820 also inhibited rat C7, displaying IC50s of 3nM and 1.8nM, respectively; TPP1653 did not cross-react with rat (Figures 1C, D). SPR showed binding of all three mAbs to human and cyno C7 with high affinities in the pM range, with exception of TPP1657 which had an affinity for human C7 off 2nM (Figure 1D).

The three mAbs were determined to be in separate epitope bins by competitive ELISA (data not shown). HDX-MS was applied to determine the C7 binding epitopes of TPP1657, TPP1653 and in the case of TPP1820, the parental molecule TTP1651 was included. For this, mAb/C7 complexes or free C7 were deuterium labelled, the reactions quenched, and samples subjected to mass spectrometry. Protected peptides, indicative of binding epitopes on C7, were determined by comparing peptide uptake plots for complexed and free C7 (Supplementary File 1). Epitopes for three different domains of human C7 were identified for the mAbs (Figure 1E). The protection patterns returned imply that the epitope for TPP1820 is in the C-terminal FIM domains (residues 717-746) (Figure 1F). TPP1653 binds to residues 335-362 and 393-408 of the MAC pore forming (MACPF) region (Figure 1F). TPP1657 epitope includes the LDLRA and possibly the bottom of the MACPF (residues 90-110 and 175-185) (Figure 1F).

To further assess the mechanism of action of the mAbs, a bio-layer-interferometry assay (Octet system) was developed to model stepwise assembly of the MAC on AMC biosensors. For this C5b6 was captured on the sensors and dipped sequentially into C7 with an excess of anti-C7 mAb, isotype control or without antibody, followed by C8 and C9 (Figure 2A). In this assay, no binding response was measured upon dipping the C5b6 coated sensors in TPP1820/C7 mix demonstrating that the antibody blocked C7 binding into the complex (Figure 2B). In contrast, a partial binding response to C7 (~60% of max response in controls) was recorded in presence of 200nM TPP1653, but no further response upon addition of C8 (Figure 2C). The TPP1657 binding response was comparable to the control conditions, demonstrating no impact of antibody on complex binding; however, no further response was measured upon addition of C8, showing that the antibody prevented C8 binding the C5b-7 complex (Figure 2D).

TPP1820 is an effective therapeutic for experimental Myasthenia Gravis in rats

Rats treated with the isotype control mAb, either at the time of disease initiation or 16h post-initiation, developed progressive disease and lost weight as expected in the model. In contrast, rats treated with TPP1820 at the time of induction showed no clinical disease and steady weight gain over the course of the experiments (Figures 3A, a) and b)). When treatment with mAb TPP1820 was delayed to 16h post-initiation, early disease was evident at 24h but this was significantly lower than in controls and stabilized with even lower disease scores and significantly greater weight gain compared to controls at 48h (Figures 3B, a) and b)). TPP1820 given at 40mg/kg completely inhibited serum lytic activity at 24 and 48h; treatment with the control mAb did not inhibit lytic activity (Figures 3A, c), 3B, c)). Serum levels of the complement activation product TCC were significantly elevated at 24 and 48h in controls compared to TPP1820-treated rats ($P<0.0001$); TCC levels in TPP1820-treated rats did not change over the time course (Figures 3A, d), 3B, d)).

Robust Myasthenia Gravis patient stratification assay reproduces MG disease biology *in vitro* using tool anti-AChR antibody mAb35

In order to make the case for a complement-targeted therapy in MG and identify patients appropriate for such a therapy, an assay system was sought that enabled stratification of MG patients according to the complement-activating ability of their anti-nicotinic AChR autoantibodies, differentiating them from MG patients with only ligand-blocking or crosslinking anti-AChR antibodies that do not activate complement and would not be amenable to complement therapies (Figure 4A). For this, a previously established CD46, CD55, CD59 triple knock out ARPE19 cell line (Gormley et al, manuscript in preparation) was transiently co-transfected with three plasmids, encoding for AChR subunits α1 & β1 (plasmid 1), δ & ϵ (plasmid 2) and the Rapsyn gene (plasmid 3) (Figure 4B). The presence of assembled AChR on the transfected cells was confirmed by staining with AF647-labelled α-Bungarotoxin. α-Bungarotoxin only stained cells co-transfected with plasmids 1 &

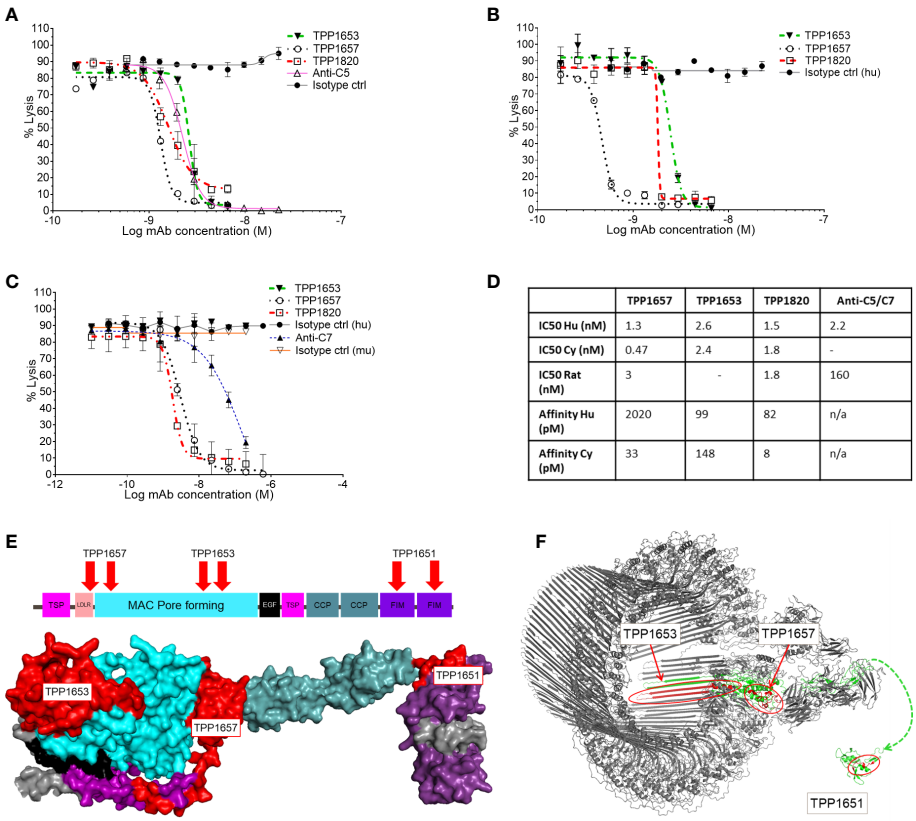

	TPP1657	TPP1653	TPP1820	Anti-C5/C7
IC50 Hu (nM)	1.3	2.6	1.5	2.2
IC50 Cy (nM)	0.47	2.4	1.8	-
IC50 Rat (nM)	3	-	1.8	160
Affinity Hu (pM)	2020	99	82	n/a
Affinity Cy (pM)	33	148	8	n/a

FIGURE 1
Functional characterization of an anti-C7 monoclonal antibody and HDX-MS epitope mapping. Classical pathway sheep haemolysis assays were used to test the function of TPP1653 (closed triangle), TPP1657 (open circle) and TPP1820 (open square) in normal human serum, comparing to isotype matched active (open triangle) and disabled anti-C5 (closed circle) control antibodies **(A)**. Activity in normal cyno serum was relative to an isotype control for test antibodies only **(B)** and activity in rat was relative to an anti-C7 control and relative human and mouse isotype controls **(C)**. The haemolysis data are representative of several independent experiments. The affinity of the mAbs for human and cyno C7 was measured by SPR **(D)**. **(E)** Diagram of the domain structure of C7 and space filling model of the homologous part of the C6 crystal structure (res. 50-913) representative of the open conformation of C7 (Aleshin et al., 2012; PDB code 3T5O). The model is colour coded by domain. HDX epitopes of TPP1653, TPP1657 and the parent molecule TPP1651 of TPP1820 are coloured red. **(F)** Cryo-EM structure of the membrane attack complex (Menny et al., 2018; PDB code 6H04) and NMR structure of the FIM domain of C7 (Phelan et al., 2009; PDB code 2WCY). The C7 moiety of the complex is shown in green. Significant HDX Protection patterns of TPP1651, 1653 and 1657 were mapped in red. A dashed line linking N693 of the MAC structure to N693 of the first FIM domain indicates the context of the two structures.

2, encoding for AChRα1β1 and AChRδϵ respectively (Figure 4C), or co-transfected with plasmids 1, 2 and 3, encoding for AChRα1β1, AChRδϵ and Rapsyn respectively (Figure 4B), but not cells which were transfected individually with either plasmid 1 (AChRα1β1) (Figure 4D) or plasmid 2 (AChRδϵ) (Figure 4E), or untransfected (Figure 4F). α-Bungarotoxin has two binding sites, which are between the α1 and δ and the α1 and ϵ subunits of AChR (20). Since the AChR pairs that provide the binding site for α-Bungarotoxin were on different plasmids, the results above confirm the expression of AChR subunits α1, δ, ϵ directly and of subunit β1 indirectly, in the double and triple transfected cells. AChR subunits α1, δ, ϵ were confirmed directly by α-Bungarotoxin binding. The β1 subunit was confirmed indirectly as it was on the same plasmid backbone and under the same SV40 promoter (Figure S5) as the ϵ subunit. The lack of binding of α-Bungarotoxin to cells, transfected with either AChRα1β1 only or cells transfected with AChRδϵ only, further confirms the specificity of the reagent to fully assembled AChR. As expected, the presence of the Rapsyn gene led to AChR clustering (Figure 4B), which was not the case for cells, transfected with all four AChR subunits α1β1δϵ, but without Rapsyn where the α-Bungarotoxin staining was homogenous (Figure 4C). Pooled serum from healthy donors depleted of immunoglobulins, used as a source of complement in the assay, had minimal residual IgG, IgA and IgM (Figure 4G), retained complement hemolytic activity albeit reduced (Ig-Depl NHS EC50 1.08% compared to NHS EC50 0.29%) (Figure 4H) and showed minimal non-specific binding to transfected cells, contrasting with the high non-specific immunoglobulin binding from NHS (Figures 4I, J). The triple-

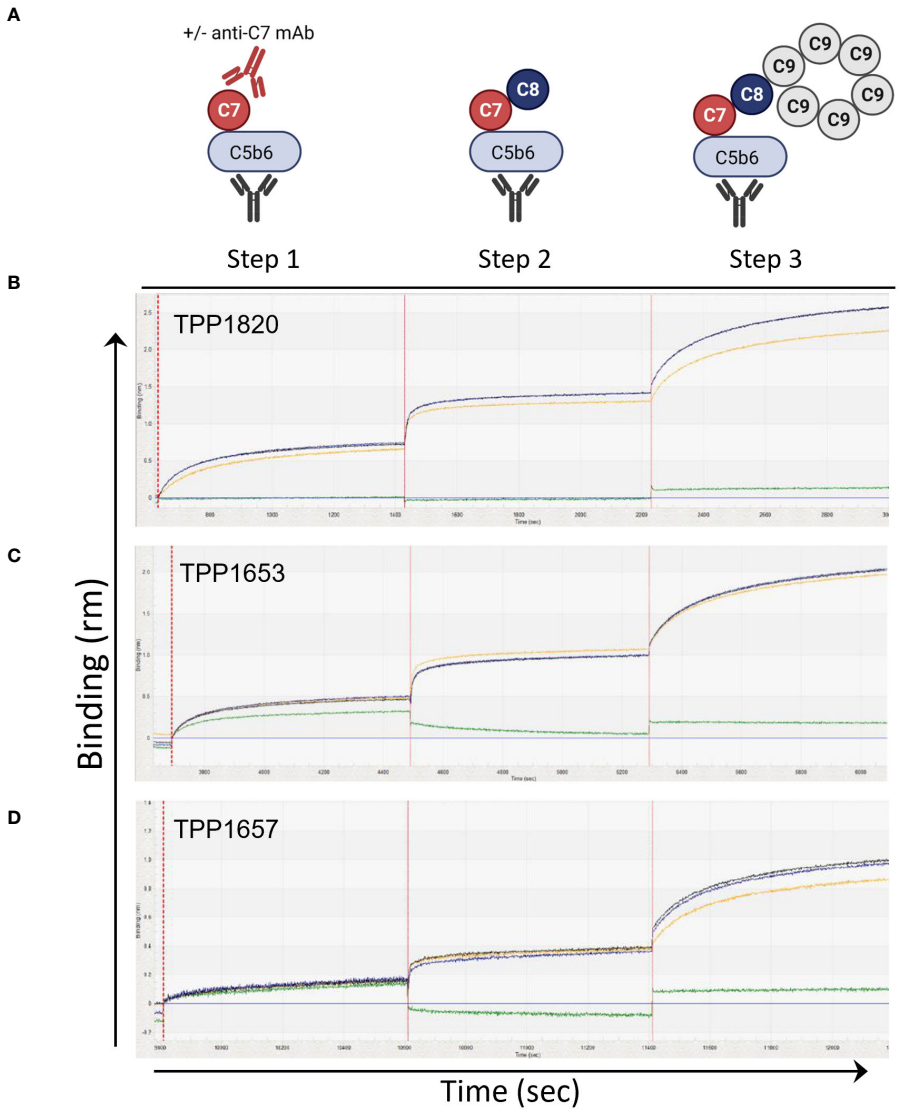

FIGURE 2
Assembly of the MAC complex using BLI technology – determine anti-C7 antibody mechanism of action. The sensograms demonstrate the assembly of MAC in the presence of absence of anti-C7 antibodies TPP1653, TPP1657 and TPP1820 following C5b6 capture onto AMC sensor (previous capture of anti-C6 mAb and C5b6 binding are not shown). Sensograms for each anti-C7 antibody evaluated are aligned to the C7/anti-C7 antibody addition step and the data has been reference subtracted (reference = αC6 mAb and C5b6 only, lighter blue trace). **(A)** Schematic representation of assembly MAC and evaluating anti-C7 mechanism of action. **(B)** 200nM and 2 nM of antibody TPP1820, **(C)** TPP1653, **(D)** and TPP1657 were pre-incubated with 100nM C7 then the C5b6 captured AMC biosensors were dipped into C7/anti-C7 wells (step 1) before sequential addition into the C8 (step 2) and C9 wells (step 3). Traces were compared to the positive controls with anti-C7 antibody absent or to the hIgG1k isotype control (black and darker blue traces respectively). This figure represents 1 of the 3 experiments conducted.

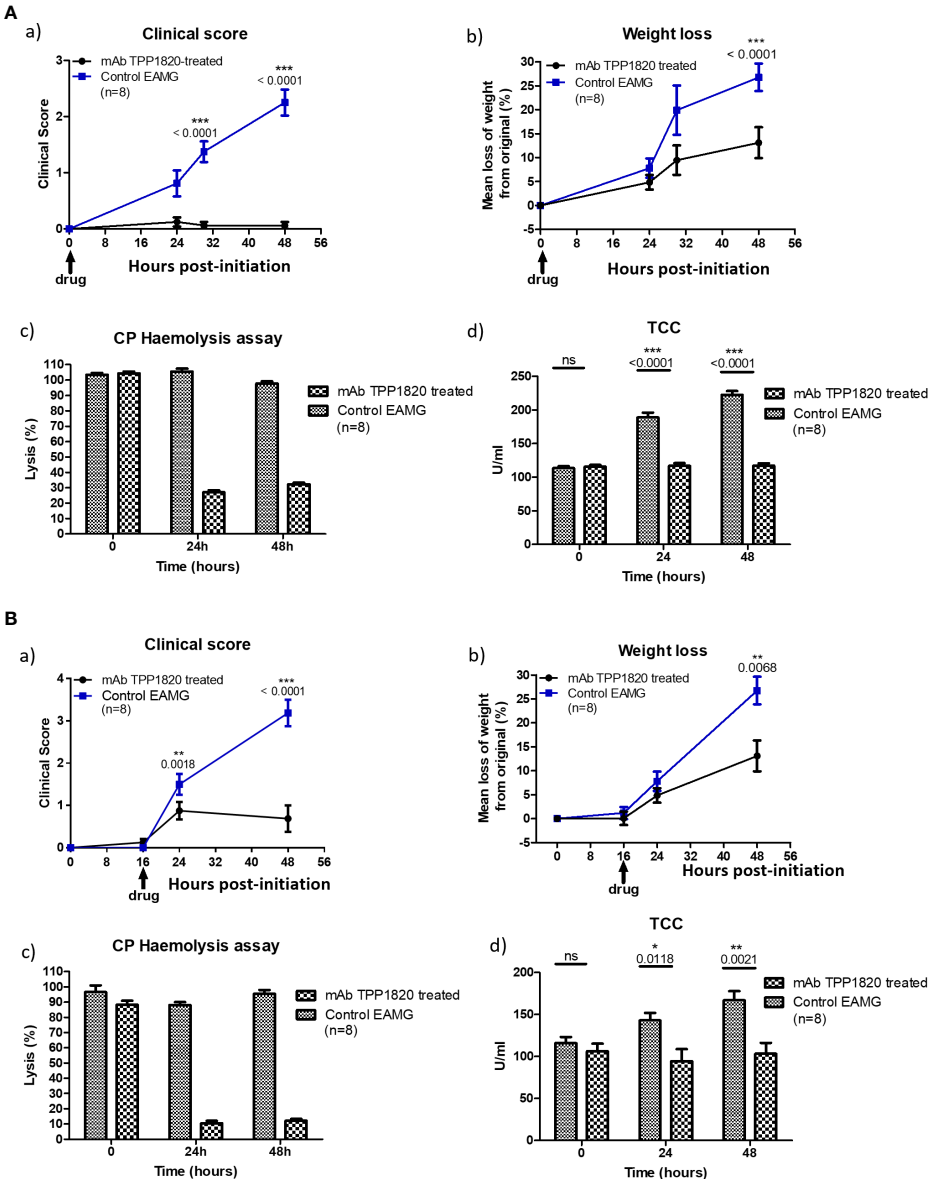

FIGURE 3
Therapeutic effect of monoclonal antibody (mAb) TPP1820 in experimental autoimmune myasthenia gravis (EAMG). TPP1820 or an isotype control IgG was administered either at the time of EAMG induction (time 0; 3A) or 8 hours after disease induction (3B) with 8 rats in each group in each experiment. Clinical score, assessed as described below, and weight change were monitored (**A**, a) - b) and **B**, a) - b)). In both experiments, control EAMG animals rapidly developed muscle weakness reaching clinical scores of three or four; in contrast, TPP1820-treated rats showed minimal clinical disease across the time course. In both experiments, control animals showed reduced weight gain or even weight loss, while TPP1820-treated animals continued to gain weight over the experiment. All animals were bled pre-induction and at 24 and 48 hours for measurement of serum hemolytic activity and terminal complement complex levels (**A**, c) - d) and **B**, c) - d)). Hemolytic activity remained high in control EAMG animals in both experiments, while TPP1820-treated rats showed markedly reduced hemolytic activity at 24 and 4h hours in both experiments. In control rats, there was an increase in TCC levels at 24 and 48hr; in contrast, TP1820-treated rats showed no increase in TCC levels in either experiment. Differences in TCC levels between the groups were significant at 24 and 48 hours in each experiment. Results are means of determinations from eight TPP1820-treated and eight isotype control-treated EAMG animals in each experiment. Error bars represent SD. Clinical disease was scored as follows: 1. Reduced grip strength in front legs and floppy tail; 2. loss of grip in back legs; 3. loss of grip and hind limb weakness and wasting; 4. loss of grip and hind limb paralysis; 5. moribund. *p <0.05, **p <0.01, ***p <0.001, ns = not significant.

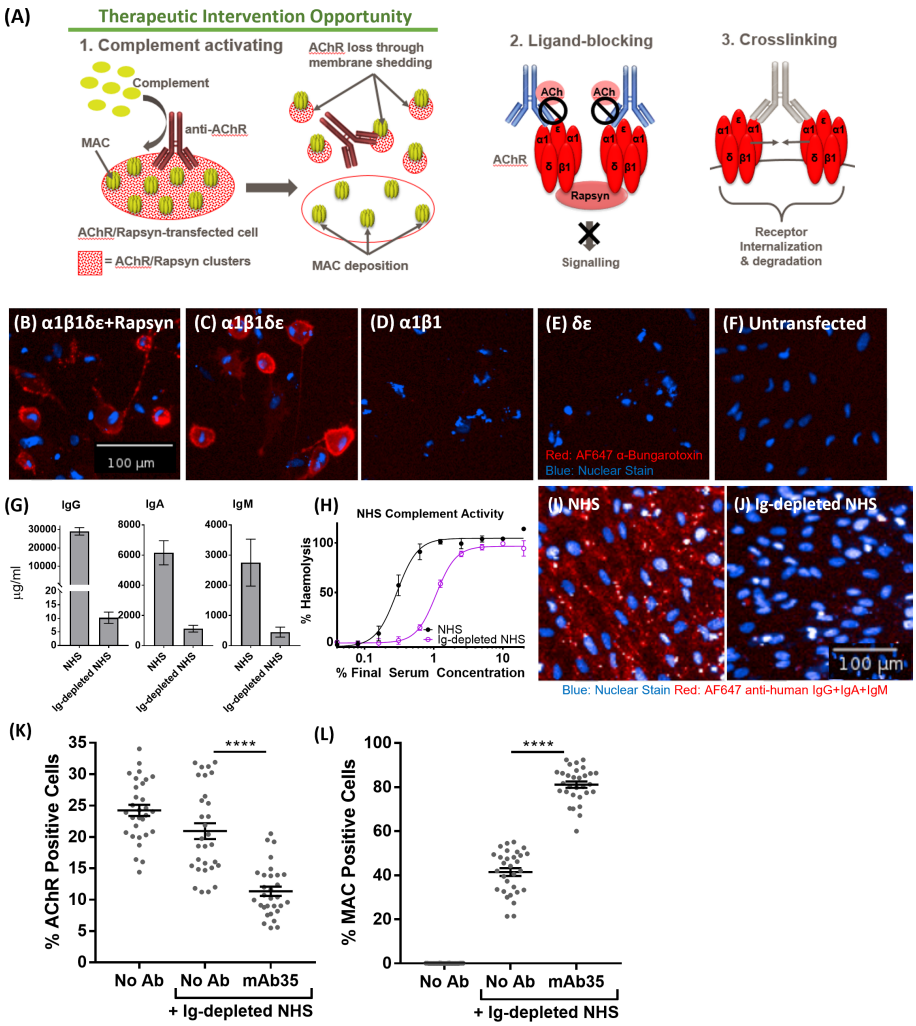

FIGURE 4
(A) Schematic representation of Myasthenia Gravis disease biology driven by anti-AChR autoantibodies. **(B–F)** AF647 α-Bungarotoxin (in red) and nuclear stain (in blue) binding to cells transfected with AChRα1β1δε+Rapsyn **(B)**, AChRα1β1δε **(C)**, AChRα1β1 **(D)**, AChRδε **(E)**, Untransfected control cells **(F, G)** IgG, IgA, and IgM quantification of immunoglobulin-depleted vs. non-depleted NHS. **(H)** Haemolytic activity of immunoglobulin-depleted vs. non-depleted NHS. **(I)** Binding profile (IgG+IgA+IgM binding) of non-depleted NHS to transfected cells (blue: nuclear stain; red: AF647 anti-human IgG+IgA+IgM). **(J)** Binding profile (IgG+IgA+IgM binding) of immunoglobulin (Ig)-depleted NHS to transfected cells (blue: nuclear stain; red: AF647 anti-human IgG+IgA+IgM). **(K)** AChR decrease in AChR+Rapsyn-transfected cells incubated with tool anti-AChR antibody mAb35 in the presence of Ig-depleted NHS (n = 30) (One-way ANOVA (GraphPad Prism), Tukey's multiple comparisons test). **(L)** Increased MAC deposition in AChR positive cells, incubated with tool anti-AChR antibody mAb35 in the presence of Ig-depleted NHS (n = 30) (One-way ANOVA (GraphPad Prism), Tukey's multiple comparisons test). All NHS used and referred to in the remainder of the paper is Ig-depleted NHS. ****p <0.0001.

transfected cells were then incubated with the rat anti-human AChR tool antibody mAb35, washed and incubated with Ig-depleted NHS. AChR expression was detected using α-Bungarotoxin and MAC deposition using a C5b-9 antibody (Figures 4K, L). Compared to Ig-depleted NHS only, mAb35 in the presence of Ig-depleted NHS showed a significant decrease ($p<0.0001$) in AChR positive cells (Figure 4K) and a significant increase ($p<0.0001$) in MAC deposition within the AChR positive cell population (Figure 4L).

MG patient autoantibodies display heterogenous binding to AChR on the cell surface

We screened MG patient plasma samples for IgG binding to the AChR+Rapsyn transfected cells; bound IgG was detected using Cy3-labelled anti-human IgG; AF647-labelled α-Bungarotoxin was used to stain the AChR clusters. Figure 5A summarizes IgG binding to the AChR positive cells corrected by

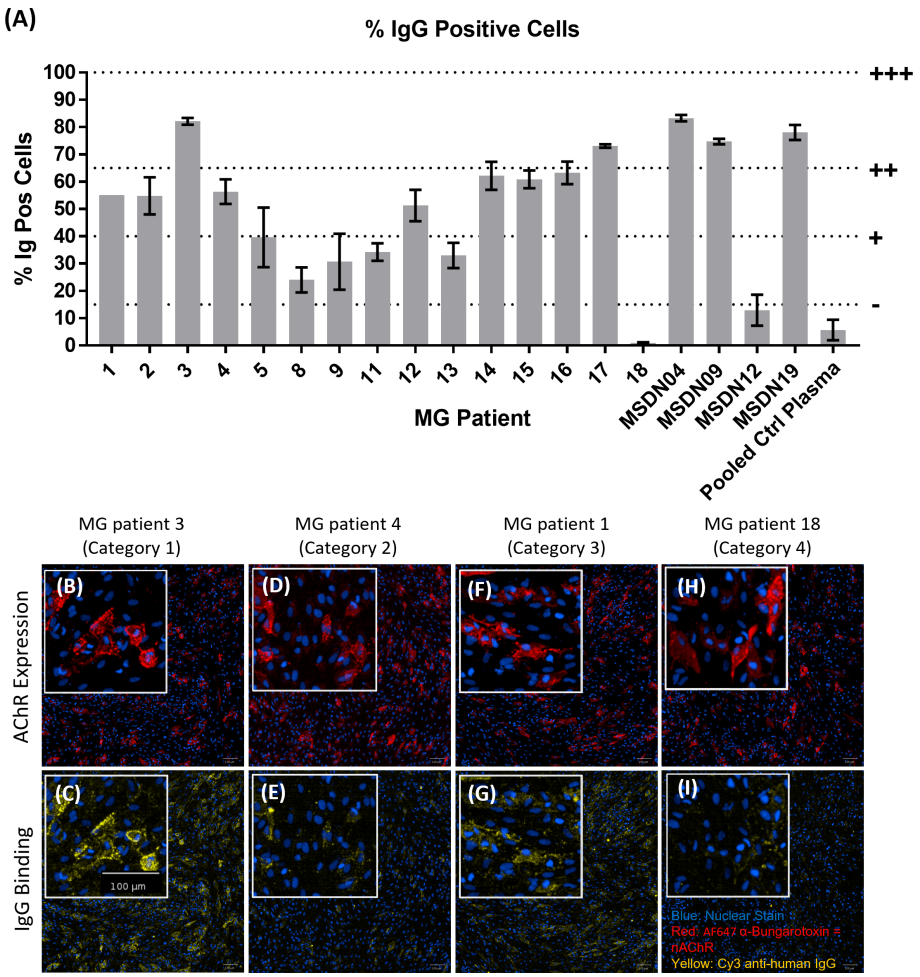

FIGURE 5
MG patient autoantibody binding pattern to AChR+Rapsyn transfected cells. **(A)** Image analysis summary graph, showing % IgG Positive cells. The bars represent the Mean ± SEM, n = 3 experiments, except for MG Patient 1 where n=1 experiment due to insufficient sample volume to perform additional repeats. Statistical significance was obtained using one-way ANOVA with Dunnet's multiple comparison test, comparing the mean (n = 3 experiments) of each plasma sample to the mean of the pooled control plasma sample, except for MG Patient 1 (n = 1 experiment, 2 replicates), where statistical significance was obtained using an unpaired t-test, comparing the mean of the two MG patient 1 replicates to the mean of the two pooled control plasma replicates from the same experiment. **(B–I)** Representative images from each patient category showing AChR expression **(B, D, F, H)** and patient IgG binding **(C, E, G, I)**, with nuclear stain in blue, AF647 α-Bungarotoxin in red and Cy3 Anti-Human IgG in yellow. **(B, C)** MG Patient 3 (Category 1), **(D, E)** MG Patient 4 (Category2), **(F, G)** MG Patient 1 (Category 3), **(H, I)** MG Patient 18 (Category 4).

subtracting background IgG binding to AChR negative cells. MG patients 3, 17, MSDN04, MSDN09, and MSDN19 showed strong binding to AChR - between 65% - 100% IgG positive cells (+++). MG patients 1, 2, 4, 12, 14, 15 and 16 showed moderate binding to AChR - between 40% - 65% IgG positive cells (++). MG patients 5, 8, 9, 11, and 13 showed low binding to AChR - between 15% - 40% IgG positive cells (+). MG patients 18 and MSDN12, as well as the pooled control plasma showed borderline to no binding to AChR - between 0% - 15% IgG positive cells (-). Figures 5B-I shows example images of cell staining with patient sera, representing different categories as summarized in Table 1. MG patient 3 (category 1) showed strong binding of IgG to the cell surface which followed the same binding pattern as α-Bungarotoxin (Figures 5B, C). MG patient 4 (category 2) and MG patient 1 (category 3) showed moderate binding of IgG to the cell surface in the same binding pattern as α-Bungarotoxin (Figures 5D–G). For MG patient 18, minimal background binding of IgG to the cell surface was visible, which was randomly spread, not following the same binding pattern as α-Bungarotoxin and was not picked-up by the analysis software algorithm (Figures 5H, I). All MG plasma samples, except for Patient 8, Patient 18, and patient MSDN12, showed statistically significant binding to the cells as compared to pooled control plasma (p-values ranging from 0.04 to <0.0001).

C7 inhibition significantly reduced AChR loss mediated by complement-activating autoantibodies *in vitro*

The patient stratification assay was then validated with MG patient plasma as the source of anti-AChR autoantibodies (Figure 6). Representative images of AChR expression (Figures 6A, C, E, F) and MAC deposition (Figures 6B, D, F, H) show that, compared to pooled control plasma + NHS (Figures 6A, B), plasma from MG patient 3 + NHS (Figures 6C, D) showed a decrease in AChR staining (Figure 6C), accompanied by an increase in MAC deposition (Figure 6D). The presence of the anti-C7 antibody (TPP1820, referred to as "anti-C7 antibody"), in MG patient 3 plasma + NHS (Figures 6E, F) prevented the AChR loss and MAC deposition, but an isotype control antibody (Figures 6G, H) did not. The image analysis summary graphs (n=3 experiments) (Figures 6I, J) show that compared to NHS alone or pooled control plasma + NHS, plasma from MG patient 3 + NHS lead to a statistically significant decrease in % AChR positive cells with $p = 0.0009$ and 0.0006 respectively (Figure 6I), as well as a statistically significant increase in MAC deposition within the AChR positive cell population with $p = 0.0002$ and 0.0009 respectively (Figure 6J). Addition of the anti-C7 antibody completely prevented the AChR loss (Figure 6I) and MAC deposition (Figure 6J), whereas addition of an isotype control did not have any effect.

Categorization of patient plasma according to complement dependent AChR loss

MG patient plasmas were grouped into four categories based on degree of IgG cell binding, ability to cause AChR loss and MAC deposition, and whether these can be blocked by the anti-C7 antibody (Table 1). The mean of all patient plasmas from each category was plotted and analyzed in GraphPad Prism (Figure 7). The in-house anti-AChR ELISA testing showed similar autoantibody titers as compared to the titers provided by the supplier (for samples where this information was available); however, there were discrepancies for some of the samples between autoantibody IgG binding to AChR on the transfected cells and ELISA antibody titers and therefore only the IgG cell binding data was taken into consideration when categorizing the patients as the patient autoantibodies would have bound to AChR on the cell surface, rather than plate-surface bound AChR.

Patient samples from category 1 showed high (++) AChR loss that was fully or partially blocked by the anti-C7 antibody,

TABLE 1 Myasthenia Gravis patient categories according to how the patient Ig mediates AChR loss, MAC deposition and effect of C7 inhibition.

MG Patient	AChR Loss	AChR Loss blocked by anti-C7 Ab?	MAC Deposition	IgG Cell Binding	Anti-AChR Titre (nmol/L)	Category
2	++	**Yes**	+	++	5.43	1
3	++	**Yes**	++	+++	143.49	1
14	++	**Yes**	+	++	13.65	1
15	++	**Yes**	+	++	12.09	1
16	++	**Yes**	+	++	23.60	1
17	++	**Yes**	++	+++	67.52	1
MSDN04	++	**Yes (Partially)**	+++	+++	130.32	1
MSDN09	++	**Yes**	+++	+++	1.78	1
MSDN19	++	**Yes (Partially)**	+++	+++	53.84	1
4	+	**Yes**	-	++	4.80	2
12	+	**Yes**	-	++	10.13	2
13	+	**Yes**	-	+	3.80	2
1	-	**N/A**	-	++	18.40	3
5	-	**N/A**	-	+	16.28	4
8	-	**N/A**	-	+	2.18	4
9	-	**N/A**	-	+	3.21	4
11	-	**N/A**	-	+	4.37	4
18	-	**N/A**	-	-	41.89	4
MSDN12	-	**N/A**	+	-	<Detection Range	4
Pooled Ctrl Plasma	-	**N/A**	-	-	<Detection Range	N/A
Max Scale	++		+++	+++		

N/A, not applicable.

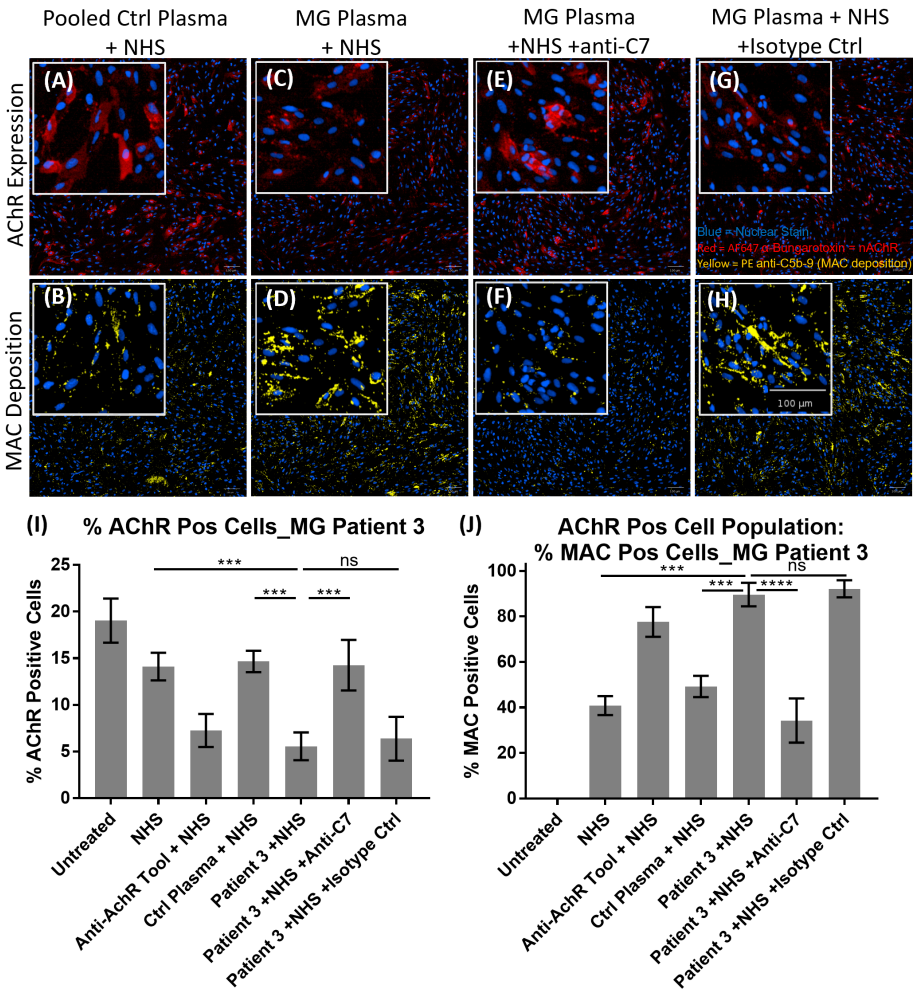

FIGURE 6
Example of MG patient plasma tested in the AChR loss and MAC deposition assay. **(A–H)** Representative images from MG patient 3 showing AChR expression **(A, C, E, G)** and MAC deposition **(B, D, F, H)**, with nuclear stain in blue, AF647 α-Bungarotoxin in red and PE anti-C5b-9 in yellow. "NHS" refers to Ig-depleted NHS in this figure. **(A, B)** Pooled control plasma + NHS, **(C, D)** MG Plasma + NHS, **(E, F)** MG Plasma + NHS +anti-C7, **(G, H)** MG Plasma + NHS +Isotype Ctrl. **(I, J)** Image analysis summary graphs for MG patient 3, showing % AChR positive cells **(I)** and % MAC positive cells within the AChR positive cell population **(J)**. The bars represent the Mean ± SEM, n = 3 experiments. Statistical significance was obtained using a repeated measures one-way ANOVA without correction, using Tukey's multiple comparisons test. ***p <0.001, ****p <0.0001, ns, not significant.

low (+) to high (+++) MAC deposition and moderate (++) to high (+++) IgG cell binding (Table 1 and Figures 5A–C). When comparing NHS or pooled control plasma + NHS with MG plasma + NHS, patient samples from category 1 showed a statistically significant ($p<0.0001$) decrease in AChR expression (Figure 7A) and a statistically significant ($p<0.0001$) increase in MAC deposition (Figure 7B), which were blocked by the anti-C7 antibody, but not the isotype control antibody.

Patient samples from category 2 showed low (+) AChR loss that was fully blocked by the anti-C7 antibody, no detectable (-) MAC deposition and low (+) to moderate (++) IgG cell binding (Table 1 and Figures 5A, D, E). MG plasma samples from category 2 + NHS showed a statistically significant decrease in AChR expression when compared to NHS alone ($p=0.0003$) or pooled control plasma + NHS ($p=0.0014$) (Figure 7C) and a statistically significant increase in MAC deposition when compared to NHS alone ($p=0.0003$), but not pooled control plasma + NHS (ns) (Figure 7D). The anti-C7 antibody, but not the isotype control antibody fully blocked the AChR loss (Figure 7C) and MAC deposition was blocked to below the detection level with NHS alone (Figure 7D).

Only one sample fitted into category 3; because of limited sample it was tested in a single experiment in duplicate. The profile comprised moderate (++) IgG binding to the AChR on the cells (Table 1 and Figures 5A, F, G), but no significant AChR loss or MAC deposition, whereas the anti-AChR tool antibody did show a significant AChR loss ($p=0.017$) (Figures 7E, F,

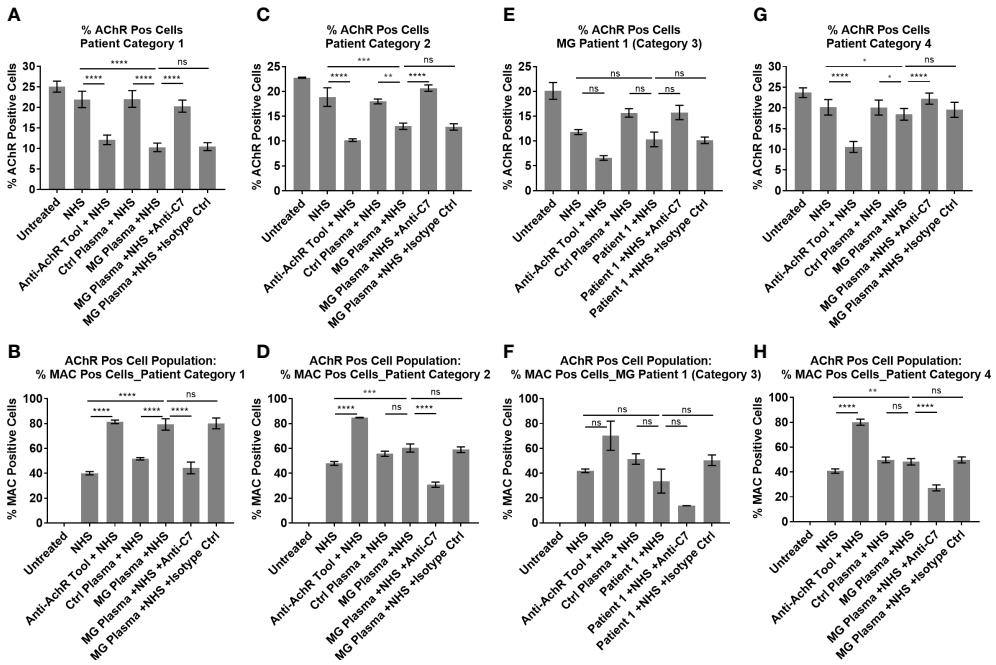

FIGURE 7
Patient Ig-mediated loss of AChR and MAC deposition - plotted means of Myasthenia Gravis patient categories, showing % AChR positive cells **(A, C, E, G)** and % MAC positive cells within the AChR positive cell population **(B, D, F, H)**. **(A, B)** Patient category 1, Mean ± SEM, n = 9 patients (mean of 3 experiments per patient, with two replicates each), **(C, D)** Patient category 2, Mean ± SEM, n = 3 patients (mean of 3 experiments per patient, with two replicates each), **(E, F)** Patient category 3, Mean ± SD, n = 2 replicates (1 patient, n = 1 experiment), **(G, H)** Patient category 4, Mean ± SEM, n = 7 patients (mean of 3 experiments per patient, with two replicates each). Statistical significance was obtained using a repeated measures one-way ANOVA without correction, using Tukey's multiple comparisons test, except for category 3 where an ordinary ANOVA was used without pairing. *p <0.05, **p <0.01, ***p <0.001, ****p <0.0001, ns = not significant.

Figure S10). There was no information on disease score provided by the supplier for this sample.

Patient samples from category 4 showed no detectable (-) AChR loss, no MAC deposition and no (-) or low (+) IgG cell binding (Table 1 and Figures 5A, H, I). MG plasma samples from category 4 + NHS did not show any biologically significant changes compared to NHS alone or control plasma + NHS for the AChR loss and MAC deposition readouts, but did show a statistically significant decrease in AChR expression (p=0.0333 when compared to NHS alone, p=0.0449 when compared to pooled control plasma + NHS) (Figure 7G) and MAC deposition (p=0.0097 when compared to NHS alone; not significant when compared to pooled control plasma + NHS) (Figure 7H). Inclusion of the anti-C7 antibody, but not the isotype control reduced MAC deposition to below the level seen with NHS alone (Figure 7H).

Statistically significant correlation was observed when comparing IgG cell binding vs. MAC deposition ($r = 0.8$, $p < 0.0001$ Figure S14A and Table S4), IgG cell binding vs. anti-AChR antibody titers ($r = 0.5965$, $p = 0.007$, Figure S14B and Table S4), anti-AChR antibody titers vs. MAC deposition ($r = 0.4684$, $p = 0.0431$, Figure S14C and Table S4).

Discussion

The role of complement in human disease has been well described and many therapeutic concepts developed to target the system and harness the clear potential for therapeutic benefit in diverse diseases with significant unmet patient need (6, 21); however, few candidates have successfully progressed past Phase III clinical trials to approval. Two of the contributing factors are the choice of target and adequate patient stratification.

Therapies in the terminal pathway space have been focused on C5 (Eculizumab/Ravalizumab, Alexion Pharmaceuticals; Crovalimab, Roche; Zilucoplan, UCB) and, apart from a few recent examples, including C6 (Regenemab, CP010), other terminal pathway targets have received little attention (7, 8). The Eculizumab experience in PNH highlighted that not only the high target concentration and turnover, but also target-mediated drug disposition are contributing factors for the high dosing requirements. A mechanistic blind spot of C5 inhibition was highlighted with the identification of "C3 bypass" cleavage of C5 which allows C5 cleavage to occur in patients despite stoichiometrically adequate C5-inhibition (22). There are also variants of C5 that have been shown to have reduced or no

binding to Eculizumab (23). Inhibition of the terminal pathway at a different point, such as C7, would overcome this and has additional advantages. Compared to C5, effective inhibition of C7 may be achieved at lower, less frequent doses *via* a subcutaneous route due to the lower plasma concentration and a likely more predictable, stable target concentration as C7 is not an acute phase reactant (24). Inhibition of C7 would also allow generation of C5a, which may have important safety implications as it would retain host defense and homeostatic functions of this fragment (25, 26).

In the present work, we report the characterization of three molecules from a discovery campaign that selected C7 inhibiting mAbs. In CP CH50 using normal human, cyno and rat sera, all three mAbs showed inhibition of human and cyno complement mediated lysis (Figures 1A, B) while TPP1657 and TPP1820 additionally inhibited rat serum (Figure 1C). The affinities of the mAbs for human and cyno C7 determined by SPR were mainly in the pM range (Figure 1D). In a previous report of four novel anti-C7 mAbs, reported affinities correlated with IC50 values in a comparable hemolysis assay (8). The two more potent mAbs from this study, with affinities of ~1nM, had comparable IC50 values to the mAbs in the present report where there was no apparent correlation between affinity and IC50 values. In terms of affinity and *in vitro* efficacy, the point of diminishing returns for C7 inhibition may therefore lie at affinities of ~1nM with further differences in efficacy driven by each mAb's unique mechanism of action.

We used HDX-MS to map the C7 epitopes of the mAbs (Figure 1E) and further elucidated the mechanism of action for each mAb using a BLI assay to model the stepwise assembly of the MAC (Figure 2A). Three distinct epitopes, with different mechanisms of action were identified. TPP1820 bound the FIM domains (Figure 1E) and prevented binding of C7 to C5b6 in the BLI assay (Figure 2B). The C7 FIM domains bind the C345C domain of C5 in the C5b6 complex, a critical step in MAC formation (27–29). TPP1653 bound the pore-forming MACPF domain (Figure 1F); mapping of the HDX protection patterns on the MAC structure (Figure 1G) suggested that the transition of region 335-362 from disordered loop to structured β-sheet, and its move away from the 393-408 pattern, were the critical steps in inhibition of MAC formation by TPP1653. In the BLI assay, TPP1653 partially inhibited binding of C7 to C5b6, but not C8 binding to C5b7 (Figure 2C). These data support the mechanism suggested by the HDX-MS data (Figure 1G) as the β-hairpin is only unfolded after binding to C5b6, rendering the C5b7 complex lipophilic (30, 31). This means that TPP1653 likely prevents the critical initial anchoring of C5b7 to the cell membrane, thus preventing formation of MAC but not the soluble TCC. TPP1657 binds an epitope on the LDLRA domain (Figure 1H), possibly bridging the bottom of the MAC pore-forming domain; the BLI assay showed that TPP1657 inhibited C8 binding to C5b7 (Figure 2D). This is a novel finding as the importance of the C7 LDLRA domain for C8 binding had not been shown previously. These data provide the first description of functionally relevant epitopes on C7 that are tractable for inhibition.

TPP1820 was selected for an *in vivo* study due to the better potency in the rat hemolysis assay. (Figure 1C). Passive experimental MG (EAMG) in rats, induced by injection of a complement-fixing anti-AChR mAb (mAb35), is a well-established model replicating acute clinical features of the human disease (32, 33). TPP1820, given prophylactically at the time of disease induction or therapeutically 16h post-disease induction, significantly suppressed clinical disease in the EAMG model in comparison to isotype control treated animals when assessed at 24, 30 and 48 hr (Figures 3A, B). These findings are in line with previous reports of C5 and C7 inhibition in this model (8, 34, 35). As the data presented are derived from a single, high-dose study it is not possible to draw any comparative conclusions on the efficacy of TPP1820 versus other mAbs that were previously assessed in this model. Nonetheless, these data show that C7 inhibition, prophylactically or therapeutically during acute pathology, protects rats from developing experimental MG and provides further validation of C7 as a target in MG.

MG is a heterogenous disease, both at the level of auto-antigen (AChR, muscle-specific kinase (MuSK), LDL receptor related protein 4 (LRP4/agrin)) and within each serological subtype (36). For anti-AChR positive MG, this has been highlighted in the Eculizumab REGAIN study which failed to show a statistically significant difference between Eculizumab and placebo (13). To address the issue of patient stratification and facilitate future trial design, we developed a cell-based patient stratification assay and undertook a proof of concept study in small cohort of patients (n=19). The assay reproduced MG disease biology *in vitro* and showed that 12 out of 19 patients (patient categories 1 + 2) had clear C7-dependent loss of AChRs (Table 1), identifying a subset of patients with pronounced complement involvement and therefore likely to benefit from terminal pathway complement therapy. Potential alternative mechanisms in the other seven patients were not evaluated due to heterogeneity and limited samples. Patient IgG binding and MAC deposition showed a stronger correlation than autoantibody titers and MAC deposition, suggesting that cell binding is a more meaningful measure than the antibody titre (Figure S14). Patient IgG binding also correlated with autoantibody titers, however two obvious outliers were observed in the small patient cohort tested here. A recent study by Obaid et al. showed a similar level of heterogeneity of MG patient Ig ability to cause MAC formation in a larger cohort and similar trend to correlation of autoantibody cell binding and MAC deposition (37). While we applied our assay to a smaller cohort, we titrated the levels of normal NHS to sub-lytic levels to prevent lysis of cells impacting quantification of MAC deposition and AChR loss which may result in higher sensitivity in our system. This assay provides a useful tool for

patient stratification and as well as identifying the most relevant patients for MAC-targeting therapies but is also applicable to testing of inhibitors upstream of MAC, e.g. C1q and C3.

However, the complexity of the cell-based assay we developed presents challenges for its use in a clinical setting in the present form. A flow cytometry assay using stably transfected cells and detecting C3/MAC deposition may be more practical. Here, the assay system developed by Obaid et al, is more suited. The complement regulator deficient ARPE-19 were chosen as tool to interrogate the MAC-dependent mechanisms and the ability to perform reproducible transfection, similar to the choice of HEK cells by Obaid et al, 2022 (37). If assay throughput was less of a requirement, primary cells or a myoblast cell line, would be preferred over an epithelial line for physiological relevance. Plomp et al, used murine hemi-diaphragms to model the complement activation using a tool anti-AChR mAb and the downstream functional effects, but the setup is less well suited to a clinical setting (38). It is important to emphasize that we are unable to assess the predictive value of this *in vitro* system and verify the exact disease mechanism in patients. For this, the assay would require validation using e.g. historical patient samples that have received anti-complement or other therapies with associated response/non-response data. Inclusion of a cohort of patient samples with an unrelated autoimmune disease would confirm specificity of our assay beyond the healthy donor plasma included here.

In conclusion, we characterized a set of novel anti-C7 monoclonal antibodies, and provided novel insights into tractable, functionally relevant epitopes on C7 and further validation of C7 as target for MG. With view to improved clinical trial design, we report a proof of concept patient stratification assay, developed to assess the heterogeneity of complement-dependence in MG. Taken together, these findings are relevant to future development and testing of new complement therapies in MG and other terminal pathway mediated pathologies, to facilitate bringing the right drug to the right patient with the associated benefits of faster and better treatment outcomes for patients and lowered burden on healthcare systems for society.

Data availability statement

The raw data supporting the conclusions of this article will be made available by the authors, without undue reservation. Anti-C7 mAbs can be made available under MTA to repeat the in vitro experiments. The CRISPR edited APRE-19 cell line cannot not be shared due to licensing limitations. A protocol to replicate the effect of the regulator k/o is included as supplementary file.

Ethics statement

Ethical review and approval was not required for the study on human participants in accordance with the local legislation and institutional requirements. The patients/participants provided their written informed consent to participate in this study. All animal experiments were approved by the Committee for Animal Care, Welfare and Use committee. All animal studies were ethically reviewed and carried out in accordance with European Directive 2010/63/EEC and the GSK Policy on the Care, Welfare and Treatment of Animals.

Author contributions

E-MN, SD, BM, MF, TW, and SK contributed to design of the study and supervised. EL, WZ, DGow, CS, IO, LS, DGorm, AS, AB, EW, RP, MB, and SP-F performed experiments, analysis, and statistical analysis. MF and E-MN performed review of data integrity. EL and E-MN wrote the first draft of the study. All authors contributed to the article and approved the submitted version.

Funding

BM and WZ would like acknowledge UK Dementia Research Institute and Alzheimer's Research Race Against Dementia Fellowship.

Acknowledgments

BM is supported by the UK Dementia Research Institute (UK-DRI), funded in part by the Medical Research Council. WZ is a Race Against Dementia Fellow and UK-DRI Future Leader Fellow. The authors would like to acknowledge the expert contributions of Joselli Silva O'Hare, Victoria Martin and Irene Sanjuan-Nandin in the *in vivo* campaign and selections.

Conflict of interest

EL, DGow, CS, IO, LS, DGorm, AS, AB, EW, MB, TW, RP, SK, MF, SD, E-MN are employees and shareholders of GSK. SP-F is an employee of GSK.

The remaining authors declare that the research was conducted in the absence of any commercial or financial relationships that could be construed as a potential conflict of interest.

Publisher's note

Supplementary material

The Supplementary Material for this article can be found online at: https://www.frontiersin.org/articles/10.3389/fimmu.2022.968206/full#supplementary-material

SUPPLEMENTARY FILE 1
Containing supplementary data and methods for the HDX-MS and BLI experiments:

SUPPLEMENTARY FILE 2
Generation of complement regulator deficient ARPE-19 cells and protocol for inhibition of complement regulators in lieu of the cell line.

SUPPLEMENTARY FILE 3
Containing supplementary data for the MG patient stratification assay.

SUPPLEMENTARY FIGURE 5
Plasmid maps of pBiCIH-hnAChRα1β1 and pBiCIN-hnAChRδε, created in SnapGene 5.3.2.

SUPPLEMENTARY FIGURE 6
Plasmid map of PCIP4_Rapsyn, created in SnapGene 5.3.2.

References

1. Cedzynski M, Thielens NM, Mollnes TE, Vorup-Jensen T. Editorial: The role of complement in health and disease. *Front Immunol* (2019) 10:1869. doi: 10.3389/fimmu.2019.01869

2. Walport MJ. Complement. first of two parts. *N Engl J Med* (2001) 344 (14):1058–66. doi: 10.1056/NEJM200104053441406

3. Morgan BP, Walters D, Serna M, Bubeck D. Terminal complexes of the complement system: new structural insights and their relevance to function. *Immunol Rev* (2016) 274(1):141–51. doi: 10.1111/imr.12461

4. Hillmen P, Young NS, Schubert J, Brodsky RA, Socie G, Muus P, et al. The complement inhibitor eculizumab in paroxysmal nocturnal hemoglobinuria. *N Engl J Med* (2006) 355(12):1233–43. doi: 10.1056/NEJMoa061648

5. Hillmen P, Risitano AM, Peffault de Latour R. Pegcetacoplan versus eculizumab in PNH. reply. *N Engl J Med* (2021) 385(18):1725–6. doi: 10.1056/NEJMc2106424

6. Morgan BP, Harris CL. Complement, a target for therapy in inflammatory and degenerative diseases. *Nat Rev Drug Discovery* (2015) 14(12):857–77. doi: 10.1038/nrd4657

7. Lin K, Zhang L, Kong M, Yang M, Chen Y, Poptic E, et al. Development of an anti-human complement C6 monoclonal antibody that inhibits the assembly of membrane attack complexes. *Blood Adv* (2020) 4(9):2049–57. doi: 10.1182/bloodadvances.2020001690

8. Zelek WM, Morgan BP. Monoclonal antibodies capable of inhibiting complement downstream of C5 in multiple species. *Front Immunol* (2020) 11:612402. doi: 10.3389/fimmu.2020.612402

9. Drachman DB. Myasthenia gravis. *N Engl J Med* (1994) 330(25):1797–810. doi: 10.1056/NEJM199406233302507

10. Keller CW, Pawlitzki M, Wiendl H, Lunemann JD. Fc-receptor targeted therapies for the treatment of myasthenia gravis. *Int J Mol Sci* (2021) 22(11):05755–05772. doi: 10.3390/ijms22115755

11. Engel AG, Lambert EH, Howard FM. Immune complexes (IgG and C3) at the motor end-plate in myasthenia gravis: ultrastructural and light microscopic localization and electrophysiologic correlations. *Mayo Clin Proc* (1977) 52(5):267–80.

12. Engel AG. The immunopathological basis of acetylcholine receptor deficiency in myasthenia gravis. *Prog Brain Res* (1979) 49:423–34. doi: 10.1016/S0079-6123(08)64654-3

13. Howard JF Jr., Utsugisawa K, Benatar M, Murai H, Barohn RJ, Illa I, et al. Safety and efficacy of eculizumab in anti-acetylcholine receptor antibody-positive refractory generalised myasthenia gravis (REGAIN): a phase 3, randomised, double-blind, placebo-controlled, multicentre study. *Lancet Neurol* (2017) 16 (12):976–86. doi: 10.1016/S1474-4422(17)30369-1

14. Drachman DB. Myasthenia gravis (first of two parts). *N Engl J Med* (1978) 298(3):136–42. doi: 10.1056/NEJM197801192980305

15. Drachman DB, Adams RN, Josifek LF, Self SG. Functional activities of autoantibodies to acetylcholine receptors and the clinical severity of myasthenia gravis. *N Engl J Med* (1982) 307(13):769–75. doi: 10.1056/NEJM198209233071301

16. Howard FM Jr., Lennon VA, Finley J, Matsumoto J, Elveback LR. Clinical correlations of antibodies that bind, block, or modulate human acetylcholine receptors in myasthenia gravis. *Ann NY Acad Sci* (1987) 505:526–38. doi: 10.1111/j.1749-6632.1987.tb51321.x

17. Howard JF Jr., Barohn RJ, Cutter GR, Freimer M, Juel VC, Mozaffar T, et al. A randomized, double-blind, placebo-controlled phase II study of eculizumab in patients with refractory generalized myasthenia gravis. *Muscle Nerve* (2013) 48 (1):76–84. doi: 10.1002/mus.23839

18. Zelek WM. Measuring total classical pathway and activities of individual components of the mouse complement pathway. *Bio Protoc* (2021) 11(19):e4175. doi: 10.21769/BioProtoc.4175

19. Expression and analysis of recombinant ion channels. In: *From structural studies to pharmacological screening, 1st ed*. New Jersey: Wiley.

20. Vincent A. Unravelling the pathogenesis of myasthenia gravis. *Nat Rev Immunol* (2002) 2(10):797–804. doi: 10.1038/nri916

21. Garred P, Tenner AJ, Mollnes TE. Therapeutic targeting of the complement system: From rare diseases to pandemics. *Pharmacol Rev* (2021) 73(2):792–827. doi: 10.1124/pharmrev.120.000072

22. Harder MJ, Kuhn N, Schrezenmeier H, Hochsmann B, von Zabern I, Weinstock C, et al. Incomplete inhibition by eculizumab: mechanistic evidence for residual C5 activity during strong complement activation. *Blood* (2017) 129 (8):970–80. doi: 10.1182/blood-2016-08-732800

23. Nishimura J, Yamamoto M, Hayashi S, Ohyashiki K, Ando K, Brodsky AL, et al. Genetic variants in C5 and poor response to eculizumab. *N Engl J Med* (2014) 370(7):632–9. doi: 10.1056/NEJMoa1311084

24. Wurzner R, Joysey VC, Lachmann PJ. Complement component C7. assessment of *in vivo* synthesis after liver transplantation reveals that hepatocytes do not synthesize the majority of human C7. *J Immunol* (1994) 152(9):4624–9.

25. Klos A, Tenner AJ, Johswich KO, Ager RR, Reis ES, Köhl J. The role of the anaphylatoxins in health and disease. *Mol Immunol* (2009) 46(14):2753–66. doi: 10.1016/j.molimm.2009.04.027

26. Sinno H, Malhotra M, Lutfy J, Jardin B, Winocour S, Brimo F, et al. Complements c3 and c5 individually and in combination increase early wound strength in a rat model of experimental wound healing. *Plast Surg Int 2013* (2013) p:243853. doi: 10.1155/2013/243853

27. DiScipio RG. Formation and structure of the C5b-7 complex of the lytic pathway of complement. *J Biol Chem* (1992) 267(24):17087–94. doi: 10.1016/S0021-9258(18)41897-2

28. Thai CT, Ogata RT. Complement components C5 and C7: recombinant factor I modules of C7 bind to the C345C domain of C5. *J Immunol* (2004) 173 (7):4547–52. doi: 10.4049/jimmunol.173.7.4547

29. Hadders MA, et al. Assembly and regulation of the membrane attack complex based on structures of C5b6 and sC5b9. *Cell Rep* (2012) 1(3):200–7. doi: 10.1016/j.celrep.2012.02.003

30. DiScipio RG, et al. The structure of human complement component C7 and the C5b-7 complex. *J Biol Chem* (1988) 263(1):549–60. doi: 10.1016/S0021-9258(19)57427-0

31. Menny A, et al. CryoEM reveals how the complement membrane attack complex ruptures lipid bilayers. *Nat Commun* (2018) 9(1):5316. doi: 10.1038/s41467-018-07653-5

32. Engel AG, et al. Experimental autoimmune myasthenia gravis: a sequential and quantitative study of the neuromuscular junction ultrastructure and electrophysiologic correlations. *J Neuropathol Exp Neurol* (1976) 35(5):569–87. doi: 10.1097/00005072-197609000-00008

33. Tzartos S, et al. Passive transfer of experimental autoimmune myasthenia gravis by monoclonal antibodies to the main immunogenic region of the acetylcholine receptor. *J Neuroimmunol* (1987) 15(2):185–94. doi: 10.1016/0165-5728(87)90092-0

34. Chamberlain-Banoub J, et al. Complement membrane attack is required for endplate damage and clinical disease in passive experimental myasthenia gravis in Lewis rats. *Clin Exp Immunol* (2006) 146(2):278–86. doi: 10.1111/j.1365-2249.2006.03198.x

35. Zelek WM, Taylor PR, Morgan BP. Development and characterization of novel anti-C5 monoclonal antibodies capable of inhibiting complement in multiple species. *Immunology* (2019) 157(4):283–95. doi: 10.1111/imm.13083

36. Fichtner ML, et al. Autoimmune pathology in myasthenia gravis disease subtypes is governed by divergent mechanisms of immunopathology. *Front Immunol* (2020) 11:776. doi: 10.3389/fimmu.2020.00776

37. Obaid AH, et al. Heterogeneity of acetylcholine receptor autoantibody-mediated complement activity in patients with myasthenia gravis. *Neurol Neuroimmunol Neuroinflamm* (2022) 9(4). doi: 10.1212/NXI.0000000000001169

38. Plomp JJ, et al. A bioassay for neuromuscular junction-restricted complement activation by myasthenia gravis acetylcholine receptor antibodies. *J Neurosci Methods* (2022) 373:109551. doi: 10.1016/j.jneumeth.2022.109551

frontiers | Frontiers in Immunology

TYPE Mini Review
PUBLISHED 12 September 2022
DOI 10.3389/fimmu.2022.979414

OPEN ACCESS

EDITED BY
Fumitaka Shimizu,
Yamaguchi University School of Medicine, Japan

REVIEWED BY
Shiyou Chen,
University of Missouri, United States

*CORRESPONDENCE
Horea Rus
hrus@umaryland.edu

SPECIALTY SECTION
This article was submitted to Multiple Sclerosis and Neuroimmunology, a section of the journal Frontiers in Immunology

RECEIVED 27 June 2022
ACCEPTED 22 August 2022
PUBLISHED 12 September 2022

CITATION
Tatomir A, Cuevas J, Badea TC, Muresanu DF, Rus V and Rus H (2022) Role of RGC-32 in multiple sclerosis and neuroinflammation – few answers and many questions.
Front. Immunol. 13:979414.
doi: 10.3389/fimmu.2022.979414

Role of RGC-32 in multiple sclerosis and neuroinflammation – few answers and many questions

Alexandru Tatomir[1,2], Jacob Cuevas[1], Tudor C. Badea[3], Dafin F. Muresanu[2], Violeta Rus[4] and Horea Rus[1,5*]

[1]Department of Neurology, University of Maryland, School of Medicine, Baltimore, MD, United States, [2]Department of Neurosciences, "Iuliu Hatieganu" University of Medicine and Pharmacy, Cluj-Napoca, Romania, [3]Research and Development Institute, Faculty of Medicine, Transylvania University of Brasov, Brasov, Romania, [4]Department of Medicine, Division of Rheumatology and Clinical Immunology, University of Maryland, School of Medicine, Baltimore, MD, United States, [5]Neurology Service, Baltimore Veterans Administration Medical Center, Baltimore, MD, United States

Recent advances in understanding the pathogenesis of multiple sclerosis (MS) have brought into the spotlight the major role played by reactive astrocytes in this condition. Response Gene to Complement (RGC)-32 is a gene induced by complement activation, growth factors, and cytokines, notably transforming growth factor β, that is involved in the modulation of processes such as angiogenesis, fibrosis, cell migration, and cell differentiation. Studies have uncovered the crucial role that RGC-32 plays in promoting the differentiation of Th17 cells, a subtype of $CD4^+$ T lymphocytes with an important role in MS and its murine model, experimental autoimmune encephalomyelitis. The latest data have also shown that RGC-32 is involved in regulating major transcriptomic changes in astrocytes and in favoring the synthesis and secretion of extracellular matrix components, growth factors, axonal growth molecules, and pro-astrogliogenic molecules. These results suggest that RGC-32 plays a major role in driving reactive astrocytosis and the generation of astrocytes from radial glia precursors. In this review, we summarize recent advances in understanding how RGC-32 regulates the behavior of Th17 cells and astrocytes in neuroinflammation, providing insight into its role as a potential new biomarker and therapeutic target.

KEYWORDS

RGC-32, multiple sclerosis, EAE (experimental autoimmune encephalomyelitis), radial glia, neuroinflammation, astrocyte, Th17

10.3389/fimmu.2022.979414

Introduction

Recent years have brought an appreciable increase in our understanding of the pathogenesis of multiple sclerosis (MS), an autoimmune, demyelinating disorder of the central nervous system (CNS) with a potentially huge socioeconomic impact (1).

MS pathogenesis results from the combined action of multiple effectors, including autoreactive myelin-specific T and B cells, pro-inflammatory cytokines, macrophages, microglia, astrocytes, and the complement system (2–4). A central role is played by $CD4^+$ T cells, which are thought to be primed in the periphery against myelin-specific antigens and then to migrate into the CNS, where they launch an inflammatory cascade against myelin and oligondedrocytes (OLG), leading to demyelination and eventually, in the chronic progressive phases, to axonal loss and neurodegeneration (5).

Astrocytes play vital roles in regulating physiological processes necessary for maintaining CNS homeostasis, such as synaptogenesis, neurotransmitter clearance, ion and water balance, formation and maintenance of the blood-brain barrier (BBB) and regulation of blood flow (6, 7). Astrocytes are also critical players in the pathogenesis of MS and its murine model, experimental autoimmune encephalomyelitis (EAE) by sustaining key pathological processes involved in disease initiation and progression (8–10).

First isolated from rat OLG stimulated by sublytic complement activation, RGC-32 was found to be induced by a number of growth factors, hormones, and cytokines, such as transforming growth factor (TGF)-β (11–13). RGC-32 modulates a number of cellular processes, including cell cycle regulation, cell migration, cellular differentiation, and fibrosis, and influences pathological processes such as carcinogenesis, metabolic disorders, atherosclerosis, and autoimmunity (13–15). Our work has demonstrated that RGC-32 plays an important role in the pathogenesis of EAE by regulating the differentiation of Th17 cells (16) as well as the ability of astrocytes to undergo reactive changes (17–19).

In this mini-review, we seek to summarize the most recent advances in understanding the contribution of RGC-32 to multiple sclerosis and neuroinflammation, as well as its ability to regulate astrocyte and Th17 cell biology.

Abbreviations: AGM, axonal guidance molecules; BBB, blood-brain barrier; CNS, central nervous system; CTGF, connective tissue growth factor; EAE, experimental autoimmune encephalomyelitis; ECM, extracellular matrix; EPHA7, ephrin receptor type 7A; GM-CSF, granulocyte macrophage colony-stimulating factor; FBN, fibrillin; FBLN, fibulin; GFAP, glial fibrillary acidic protein; HSPG2, heparan sulfate proteoglycan 2; HOPX, homeodomain-only protein homeobox; KO, knockout; MMP, matrix metalloproteinase; MS, multiple sclerosis; PLAUR, plasminogen activator, urokinase receptor; PLXNA1, plexin A1; RGC-32, response gene to complement 32; SPOCK3, Sparc/osteonectin, cwcv and kazal-like domains proteoglycan 3; STAT3, signal transducer and activator of transcription 3; STC1, stanniocalcin-1; VEGF, vascular endothelial growth factor; VCAN, versican; WDFY1, WD repeat and FYVE domain-containing protein 1; WT, wild type.

Th17 cells and their role in MS

Th17 cells differentiate from naïve $CD4^+$ T cells in the presence of IL-6 and TGF-β (20). They have high pathogenic potential in light of their ability to generate pro-inflammatory cytokines, including IL-17, IL-21, IL-22 and granulocyte macrophage colony-stimulating factor (GM-CSF) (20, 21). IL-17 is particularly effective in promoting BBB disruption and in recruiting immune cells into the CNS (22, 23), while GM-CSF is highly pro-inflammatory and augments the recruitment of peripheral immune cells into the CNS (23, 24).

RGC-32 as a key regulator of Th17 cell differentiation

Using an RGC-32 knock-out (KO) mouse model, we have been able to demonstrate that RGC-32 promotes the differentiation of Th17 cells both *in vitro* and *in vivo*. When compared to wild-type (WT) cells, $CD4^+$ cells isolated from RGC-32 KO mice express lower levels of IL-17, as well as some of the transcription factors necessary for Th17 differentiation, including retinoic acid receptor-related orphan receptor gamma t (RORγt), B cell–activating transcription factor (BATF), and interferon regulatory factor 4 (IRF4) under Th17-polarizing conditions (16). On the other hand, we have observed that the differentiation of Th1, Th2, and Tregs is not affected by the lack of RGC-32. Further analysis has revealed a defect in SMAD2 and AKT phosphorylation in RGC-32 KO $CD4^+$ cells, suggesting that RGC-32 preferentially facilitates the differentiation of Th17 cells in a TGF-β-dependent and independent manner (16).

Moreover, we have observed that RGC-32 KO mice develop a milder EAE phenotype than do their WT counterparts, with a lower clinical score at the peak of disease (day 14). Immunohistochemical analysis has revealed a smaller inflammatory infiltrate and fewer demyelination foci in the spinal cords of RGC-32 KO mice, and a lower number of $IL\text{-}17^+$ and $GM\text{-}CSF^+$ cells (16).

Interestingly, one study has shown that overexpression of RGC-32 in peripheral blood mononuclear cells (PBMC) isolated from patients with dilated cardiomyopathy augments the number of Th17 cells (25). We have also shown that B and T cells from patients with systemic lupus erythematous exhibit higher levels of RGC-32 and that overexpression of RGC-32 in

human naïve $CD4^+$ T cells augments the expression of IL-17 (26). These studies provide evidence of RGC-32's role in the differentiation of human Th17 cells.

RGC-32 as a blood-based biomarker in MS

The first evidence for a potential role of RGC-32 in MS came from experiments showing that RGC-32 is present in MS plaques in perivascular and parenchymal areas and co-localizes with $CD3^+$ and $CD68^+$ cells, indicating that inflammatory cells express RGC-32 in MS brains (27). In addition, astrocytes have also been found to express RGC-32 (27).

RGC-32 is also expressed in PBMC isolated from patients with relapsing-remitting MS (RRMS). The mRNA levels of RGC-32 are significantly lower in patients with relapses than in stable patients or in patients who do not respond to glatiramer acetate (GA) (28). Furthermore, RGC-32 can potentially serve as a reliable biomarker in MS, with a 90% probability of detecting relapses and 85% probability of correctly predicting responses to GA therapy (28). Moreover, *in vitro* experiments have shown that silencing RGC-32 in PBMC leads to decreased levels of Fas ligand (FasL) and SIRT1, key regulators of apoptosis, suggesting that RGC-32 can regulate immune cell survival by influencing FasL and SIRT1 expression (27).

Collectively, these results suggest that RGC-32 is a novel regulator of the diffrentiation of Th17 cells, making it a potential new therapeutic target in autoimmunity (Figure 1).

Astrocyte emerges as an important contributor to the development and progression of MS and EAE

The morphological and molecular changes undergone by astrocytes after brain injury are collectively called reactive astrocytosis (29). Most experts in the field consider this a continuum phenomenon of transformations that can range from subtle changes in gene expression and cell metabolomics to gross morphological changes, such as cellular hypertrophy, with glial scar sitting at the extreme endpoint on this axis (30–32).

Reactive astrocytes are capable of mounting and perpetuating cellular processes leading to neuroinflammation and tissue remodeling (33). While they can exert both beneficial and detrimental effects by gain of function or loss of normal physiological properties, the net result is estimated to be pathogenic, and reactive astrocytes are currently seen as being a major contributor to MS pathogenesis (8, 34, 35).

RGC-32 regulates the ability of astrocytes to undergo reactive changes during EAE

We have shown that the levels of glial fibrillary acidic protein (GFAP), a universal marker for reactive astrocytosis, are significantly lower in the spinal cords of RGC-32 KO mice than in WT mice under both normal conditions and in acute EAE. We have found similar results in cultured neonatal brain astrocytes, with RGC-32 KO cells having lower levels of GFAP than WT cells (18).

Our team has also observed that RGC-32 KO astrocytes from the spinal cord white matter of mice with acute EAE display an elongated, bipolar morphology, reminiscent of radial glia and astrocyte progenitors, while the WT astrocytes near the inflammatory infiltrate have a reactive phenotype with body hypertrophy and process branching (17, 18). Interestingly, the number of cells that are positive for vimentin and fatty acid binding protein 7 (FABP7) and display radial glia morphology is significantly higher in RGC-32 KO mice than in WT mice on both day 0 and day 14 (18). These two markers are normally expressed by astrocyte lineage cells during brain development but can persist in mature astrocytes and adult radial glia (36–39). Their expression is increased in reactive astrocytes following brain injury (40, 41). We have observed that $vimentin^+$ and $FABP7^+$ radial cells have a much broader distribution in RGC-32 KO mice, whereas in WT mice they are distributed mostly around inflammatory infiltrates (18), suggesting that these cells are more likely radial glia and immature astrocytes in RGC-32 KO mice, whereas in WT mice they are vimentin- and FABP7-re-expressing reactive astrocytes. Moreover, RGC-32 KO spinal cord astrocytes display a higher proliferative index, as measured by the expression of the proliferation marker Ki-67 (18). Collectively, these results suggest that astrocytes lacking RGC-32 have an immature phenotype and display an intrinsic inability to respond to inflammation, to upregulate GFAP, and to undergo the morphological changes associated with glial scar formation at the peak of EAE (Figure 2).

The immature phenotype of RGC-32 KO astrocytes translates into an impaired expression of gliotic scar components and growth factors

Glial scar plays a major role in the evolution of inflammatory lesions. While during the acute phase it might play a beneficial role by fencing the inflammatory infiltrate in and thus avoiding its spread into healthy tissue, during chronic phases it might have a rather detrimental role by inhibiting remyelination and axonal regeneration (42). However, recent

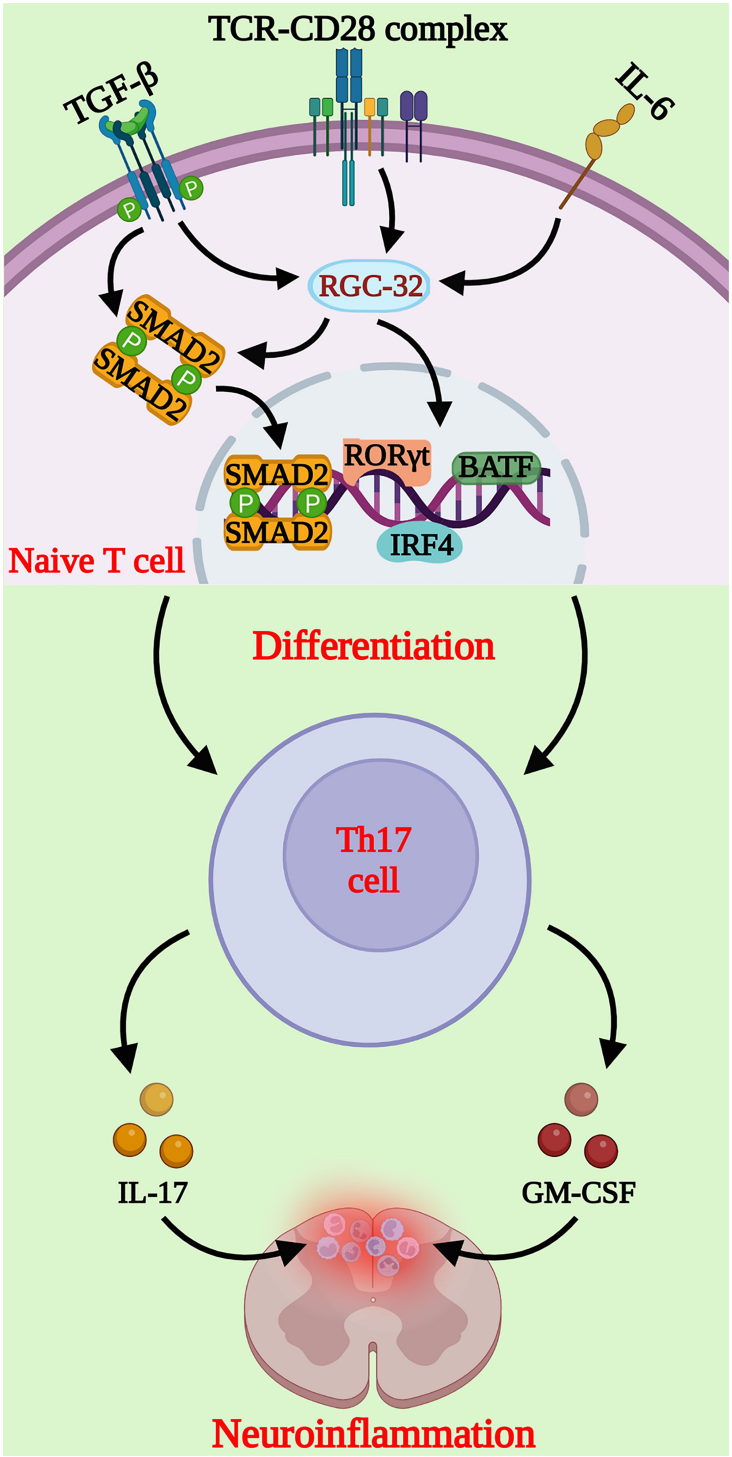

FIGURE 1
Schematic representation of the molecular pathways regulated by RGC-32 during Th17 cell differentiation. RGC-32 is upregulated in naïve $CD4^+$ T cells cultured under Th17 differentiating conditions. Our studies showed that lack of RGC-32 impairs the expression of critical transcription factors involved in Th17 cell differentiation, such as the master regulator RORγt, IRF4 and BATF. The phosphorylation of SMAD2 downstream of TGF-β receptor activation might be one of the major pathways positively regulated by RGC-32 during Th17 cells generation. Th17 cells play a major role in neuroinflammatory changes at the peak of EAE mediated primarily by IL-17 and GM-CSF, that exert important chemotactic properties. (Created with BioRender.com).

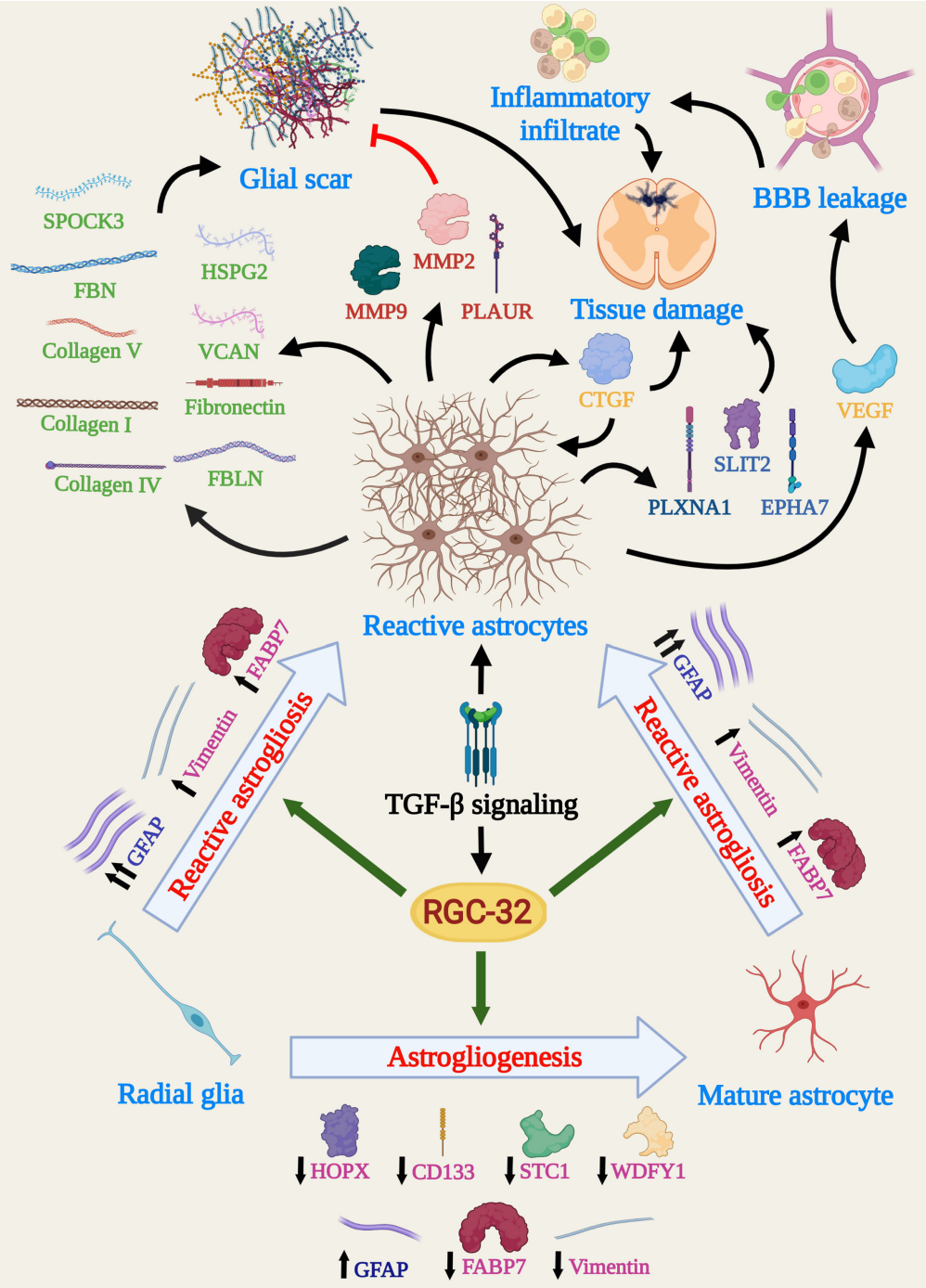

FIGURE 2
Schema depicting the main molecular and cellular processes influenced by RGC-32 in astrocytes during EAE. Data show that RGC-32 plays a major role in driving changes specific to reactive astrocytosis, such as cellular hypertrophy and glial scar formation, by favoring GFAP upregulation and synthesis of ECM components. The secretion of growth factors and AGM with BBB leakage and tissue damage potential point to a mainly pathogenic role of RGC-32, at least during acute EAE. On the other hand, RGC-32 seems to have astrogliogenic potential, since a lack of RGC-32 results in a higher number of radial glia and astrocyte precursors in adult mice. Since adult radial glial cells are a major source of reactive astrocytes in the spinal cords during EAE, it is also highly possible that RGC-32 favors this direct transition. (Created with BioRender.com).

advances have challenged this view and demonstrated that the glial scar can contribute to axonal regeneration (43, 44).

In vitro experiments have demonstrated that RGC-32 KO brain astrocytes stimulated with TGF-β produce lower levels of extracellular matrix (ECM) components such as pro-collagen I, IV, and V; fibronectin; fibrillin; and fibulin, as well as proteoglycan core proteins such as heparan sulfate proteoglycan 2 (HSPG2), versican (VCAN), and testican (SPOCK3) (17, 19). Mechanistically, RGC-32 physically associates with the transcription factor SMAD3 and is translocated to the nucleus through a process that requires SMAD3 phosphorylation and RhoA-Rho kinase activation (17). Moreover, RGC-32 KO astrocytes synthesize higher levels of enzymes involved in ECM remodeling, for example, matrix metalloproteinases (MMPs) 2 and 9, the plasminogen activator urokinase receptor (PLAUR), and tissue inhibitor of metalloproteinases 1 (TIMP1) (18). These findings point to an important role for RGC-32 in glial scar formation and remodeling.

Reactive astrocytes secrete a multitude of growth factors, with some of them having neurotrophic, reparatory effects, and others being pro-inflammatory, leading to tissue destruction (10, 45). RGC-32 KO neonatal brain astrocytes stimulated with TGF-β synthesize and/or secrete lower levels of growth factors such as connective tissue growth factor (CTGF), insulin-like growth factor 1 (IGF1), IGF binding proteins (IGFBP) 2, 3, and 6, vascular endothelial growth factor A (VEGF-A) and platelet-derived growth factor AA (PDGF-AA), than do their WT counterparts (18).

Among these proteins, VEGF and CTGF deserve special attention. VEGF plays a particular role in MS pathogenesis by facilitating BBB leakage, vascular remodeling, and immune cell trafficking (46). CTGF has been found to participate in astrocyte differentiation and activation, being able to drive reactive changes in astrocytes in an autocrine manner (47, 48). We have shown that a lack of RGC-32 impairs CTGF synthesis not only in cultured astrocytes but also in spinal cords, since RGC-32 KO mice display lower levels of $CTGF^+$ astrocytes during acute EAE (18). To our knowledge, these results are the first to show that RGC-32 acts upstream of CTGF, making this molecule a major component of the TGF-β-RGC-32-CTGF axis in astrocytes.

RGC-32 profoundly alters the transcriptomic landscape of brain astrocytes

In a quest to decipher the molecular networks underlying RGC-32's ability to regulate astrocytic maturation and reactivity, we have performed next-generation RNA sequencing on brain astrocytes purified from WT and RGC-32 KO mice, under basal conditions and after TGF-β stimulation. We found that a lack of RGC-32 has a significant impact on the transcriptomic programs normally associated with brain development, neurogenesis, cell motility, and cell projection (19). Of special note is the fact that the differential regulation of pathways ontologically related to cell motility suggests that RGC-32 may be involved in astrocyte migration, as we have already described for other cell types such as endothelial cells and vascular smooth muscle cells (49, 50).

Functional enrichment analysis has shown that many pathways impaired by lack of RGC-32 are associated with processes such as neurogenesis and nervous system development (19). Connectivity analysis has further revealed a particular network of interconnected molecules involved in axonal guidance that is differentially regulated only in WT astrocytes (19). These axonal guidance molecules (AGM) play vital roles during brain development, providing axons with cues for normal wiring (51). In adult brains, reactive astrocytes are a major pool for AGM synthesis and secretion and, thanks to their ability to inhibit axonal regeneration and to regulate the immune system, AGM are thought to play an important role in MS pathogenesis (52–54). RGC-32 KO astrocytes have lower mRNA levels of AGM family members such as ephrin receptor A type 7 (EPHA7), plexin A1 (PLXNA1), and Slit guidance ligand 2 (SLIT2) (19). On a similar note, we have found a lower number of EPHA7/GFAP-double positive cells in the spinal cords of RGC-32 KO mice during peak EAE (19). These findings suggest the idea that the differential regulation of AGM, particularly by EPHA7, may be another major pathway by which RGC-32 facilitates reactive astrogliosis during neuroinflammation.

RGC-32 - a missing link in astrogliogenesis?

Astrocytes are derived from radial glia, cells with pluripotent properties. In the developing spinal cord, radial glia produce intermediate precursors in the ventricular zone, which then migrate toward the mantle zone, where they proliferate before differentiating into mature astrocytes, particularly the so-called fibrous astrocytes (55, 56). A number of radial glia persist during adulthood and can serve as a pool for the generation of reactive astrocytes during EAE (57).

Immunohistochemical studies using homeodomain-only protein homeobox (HOPX), CD133, stanniocalcin-1 (STC1), and WD repeat and FYVE domain-containing protein 1 (WDFY1), four markers expressed by neural stem progenitors and radial glia (58–61), have shown that spinal cords from RGC-32 KO mice display a greater number of $HOPX^+$, $CD133^+$, $STC1^+$, and $WDFY1^+$ cells than do WT mice during acute EAE, further supporting the conclusion that in the absence of RGC-32, astrocytes remain at the stage of radial glia and progenitors (19). Furthermore, our study was the first to show that spinal cord radial

glia express STC1 and WDFY1 and that their number and morphology are affected during EAE in an RGC-32 dependent manner (19). Interestingly, a recent study has found that RGC-32 is necessary for the self-renewal of neural stem cells and that a lack of RGC-32 favors neurogenesis in an *in vitro* cerebral organoid model (62).

Finally, we have shown that down-regulation of RGC-32 in cultured astrocytes reduces the nuclear translocation of signal transducer and activator of transcription 3 (STAT3) (18), which plays a key role in the gliogenic switch by activating promoters of astrocytic-specific genes such as GFAP (63).

Taken together, all these results suggest that RGC-32 may play a role in conferring on neural stem progenitors an astrogliogenic fate, thus regulating the transition of radial glia toward mature and/or reactive astrocytes, at least in the spinal cord (Figure 2).

Future directions

Despite the abovementioned promising results, some questions still remain concerning exactly how RGC-32 modulates neuroinflammation:

1) How do astrocyte heterogeneity and species differences affect RGC-32 expression and function?

Astrocyte heterogeneity is a well-analyzed topic, and differences exist not only between species but also between spinal cord and brain astrocytes in the same species (64, 65). Therefore, in order for us to have a broader picture, additional studies are needed to determine whether our *in vivo* results can be replicated in adult mouse brains. Conversely, the transcriptomic profile of RGC-32 KO brain astrocytes should be compared with that of RGC-32 KO spinal cord astrocytes.

Similarly, in order to obtain a glimpse into the differences and similarities in RGC-32 function between mouse and human astrocytes, one should perform studies using normal human brain tissue as well as tissue isolated from MS patients to analyze the expression of proteins and genes found to be the most differentially regulated by RGC-32.

2) What are the other cytokines with a potential impact on the regulation of RGC-32 expression?

During acute EAE, a cocktail of various cytokines and chemokines acts at the site of inflammation (66). Therefore, a major question is: what effect(s) do other cytokines have on RGC-32 expression, beyond TGF-β? One study has reported that RGC-32 transcript are reduced by pro-inflammatory cytokines in purified brain astrocytes (67). Thus, it would be interesting to find out how the net effect of pro-inflammatory and anti-inflammatory cytokines might regulate RGC-32 expression in MS and EAE. This question leads us to wonder whether RGC-32 expression might ultimately be linked to various types of reactive astrocytes, such as the recently described pro-inflammatory, neurotoxic A1 and anti-inflammatory, protective A2 phenotypes (68), and whether the end results of anti- and pro-inflammatory influences can affect RGC-32 in such a way as to skew the balance of astrocyte reactivity toward one phenotype or another.

3) What role does RGC-32 play in other cell types?

RGC-32's role in other cell types beyond the astrocyte is a fully pertinent research question to pursue. One study has found that RGC-32's expression is activated in OLG precursor cells and promotes their proliferation after spinal cord injury (69). While we have already shown that sublytic C5b-9 can affect the OLG cell cycle by activating SIRT1 (70), additional studies are necessary to clearly delineate how RGC-32 might affect OLG during neuroinflammation and whether it might play any role in remyelination.

Microglia are CNS-resident cells with an instrumental role in driving neuroinflammation (71). Evidence suggests that RGC-32 regulates macrophage differentiation and functions in various pathologies (72–74), and since macrophages share the same developmental origin as microglia (75), we assume that RGC-32 also plays an important role in these cells. In fact, RGC-32 has been shown to be expressed by cells with a microglial morphology in MS brains (27). Thus, further studies should shed light on this issue and will help to complete the cellular and molecular puzzle centered around RGC-32 in MS and related inflammatory diseases.

Conclusions

Understanding how exactly astrocytes interact with their environment and which molecular switches are activated at any particular point in time or space after CNS injury is crucial to decipher their pathogenic potential. RGC-32 has emerged so far as a new factor regulating astrocyte biology, since it intervenes along the whole axis of reactive astrogliosis, influencing not only the transcriptomic network but also the sheer gross morphology of reactive astrocytes. Its role in modulating other cells with crucial role in

neuroinflammation, such as Th17 cells, make RGC-32 a reliable target for understanding and eventually treating MS and related diseases.

Author contributions

AT, VR, and HR designed the study. AT, JC, TB, DM, VR, and HR wrote the manuscript. All authors contributed to the article and approved the submitted version.

Funding

This work was supported in part by a grant from Veterans Administration Merit Award (I01BX001458 to HR), by a RO1 NS42011 grant (to HR) and by PN-III-P4-PCE-2021-0333 grant, from UEFISCDI, Romania (TB).

Acknowledgments

We thank Dr. Deborah McClellan for editing this manuscript.

Conflict of interest

The authors declare that the research was conducted in the absence of any commercial or financial relationships that could be construed as a potential conflict of interest.

Publisher's note

References

1. Dobson R, Giovannoni G. Multiple sclerosis - a review. *Eur J Neurol* (2019) 26:27–40. doi: 10.1111/ene.13819

2. Nicol B, Salou M, Laplaud D-A, Wekerle H. The autoimmune concept of multiple sclerosis. *Presse Med* (2015) 44:e103–12. doi: 10.1016/j.lpm.2015.02.009

3. Mallucci G, Peruzzotti-Jametti L, Bernstock JD, Pluchino S. The role of immune cells, glia and neurons in white and gray matter pathology in multiple sclerosis. *Prog Neurobiol* (2015) 127-128:1–22. doi: 10.1016/j.pneurobio.2015.02.003

4. Martin R, Sospedra M, Rosito M, Engelhardt B. Current multiple sclerosis treatments have improved our understanding of MS autoimmune pathogenesis. *Eur J Immunol* (2016) 46:2078–90. doi: 10.1002/eji.201646485

5. Engelhardt B, Comabella M, Chan A. Multiple sclerosis: Immunopathological heterogeneity and its implications. *Eur J Immunol* (2022) 52:869–81. doi: 10.1002/eji.202149757

6. Sofroniew MV, Vinters HV. Astrocytes: Biology and pathology. *Acta Neuropathol* (2010) 119:7–35. doi: 10.1007/s00401-009-0619-8

7. Verkhratsky A, Nedergaard M. Physiology of astroglia. *Physiol Rev* (2018) 98:239–389. doi: 10.1152/physrev.00042.2016

8. Brambilla R. The contribution of astrocytes to the neuroinflammatory response in multiple sclerosis and experimental autoimmune encephalomyelitis. *Acta Neuropathol* (2019) 137:757–83. doi: 10.1007/s00401-019-01980-7

9. Yi W, Schluter D, Wang X. Astrocytes in multiple sclerosis and experimental autoimmune encephalomyelitis: Star-shaped cells illuminating the darkness of CNS autoimmunity. *Brain Behav Immun* (2019) 80:10–24. doi: 10.1016/j.bbi.2019.05.029

10. Aharoni R, Eilam R, Arnon R. Astrocytes in multiple sclerosis-essential constituents with diverse multifaceted functions. *Int J Mol Sci* (2021) 22:5904. doi: 10.3390/ijms22115904

11. Badea TC, Niculescu FI, Soane L, Shin ML, Rus H. Molecular cloning and characterization of RGC-32, a novel gene induced by complement activation in oligodendrocytes. *J Biol Chem* (1998) 273:26977–81. doi: 10.1074/jbc.273.41.26977

12. Vlaicu SI, Cudrici C, Ito T, Fosbrink M, Tegla CA, Rus V, et al. Role of response gene to complement 32 in diseases. *Arch Immunol Ther Exp (Warsz)* (2008) 56:115–22. doi: 10.1007/s00005-008-0016-3

13. Vlaicu SI, Tatomir A, Anselmo F, Boodhoo D, Chira R, Rus V, et al. RGC-32 and diseases: The first 20 years. *Immunol Res* (2019) 67:267–79. doi: 10.1007/s12026-019-09080-0

14. Vlaicu SI, Tatomir A, Rus V, Rus H. Role of C5b-9 and RGC-32 in cancer. *Front Immunol* (2019) 10:1054. doi: 10.3389/fimmu.2019.01054

15. Vlaicu S, Tatomir A, Fosbrink M, Nguyen V, Boodhoo D, Cudrici C, et al. RGC-32' dual role in smooth muscle cells and atherogenesis. *Clin Immunol* (2022) 238:109020. doi: 10.1016/j.clim.2022.109020

16. Rus V, Nguyen V, Tatomir A, Lees JR, Mekala AP, Boodhoo D, et al. RGC-32 promotes Th17 cell differentiation and enhances experimental autoimmune encephalomyelitis. *J Immunol* (2017) 198:3869–77. doi: 10.4049/jimmunol.1602158

17. Tatomir A, Tegla CA, Martin A, Boodhoo D, Nguyen V, Sugarman AJ, et al. RGC-32 regulates reactive astrocytosis and extracellular matrix deposition in experimental autoimmune encephalomyelitis. *Immunol Res* (2018) 66:445–61. doi: 10.1007/s12026-018-9011-x

18. Tatomir A, Beltrand A, Nguyen V, Boodhoo D, Mekala A, Cudrici C, et al. RGC-32 regulates generation of reactive astrocytes in experimental autoimmune encephalomyelitis. *Front Immunol* (2021) 11:608294. doi: 10.3389/fimmu.2020.608294

19. Tatomir A, Beltrand A, Nguyen V, Courneya J-P, Boodhoo D, Cudrici C, et al. RGC-32 acts as a hub to regulate the transcriptomic changes associated with astrocyte development and reactive astrocytosis. *Front Immunol* (2021) 12:705308. doi: 10.3389/fimmu.2021.705308

20. Patel DD, Kuchroo VK. Th17 cell pathway in human immunity: Lessons from genetics and therapeutic interventions. *Immunity* (2015) 43:1040–51. doi: 10.1016/j.immuni.2015.12.003

21. Bettelli E, Korn T, Oukka M, Kuchroo VK. Induction and effector functions of T(H)17 cells. *Nature* (2008) 453:1051–7. doi: 10.1038/nature07036

22. Kuwabara T, Ishikawa F, Kondo M, Kakiuchi T. The role of IL-17 and related cytokines in inflammatory autoimmune diseases. *Mediators Inflammation* (2017) 2017:3908061. doi: 10.1155/2017/3908061

23. Yasuda K, Takeuchi Y, Hirota K. The pathogenicity of Th17 cells in autoimmune diseases. *Semin Immunopathol* (2019) 41:283–97. doi: 10.1007/s00281-019-00733-8

24. Pierson ER, Goverman JM. GM-CSF is not essential for experimental autoimmune encephalomyelitis but promotes brain-targeted disease. *JCI Insight* (2017) 2:e92362. doi: 10.1172/jci.insight.92362

25. Li B, Zhou W, Tang X, Wang W, Pan J, Tan M. Response gene to complement-32 promotes the imbalance of Treg/Th17 in patients with dilated cardiomyopathy. *Cell Physiol Biochem* (2017) 43:1515–25. doi: 10.1159/000481975

26. Talpos-Caia A, Tatomir A, Nguyen V, Cudrici CD, Rednic S, Rus HG, et al. Response gene to complement-32 expression is upregulated in lupus T cells and promotes IL-17A expression. *Lupus* (2018) 5(Suppl 2):A1–A81. doi: 10.1136/lupus-2018-lsm.17

27. Tegla CA, Cudrici CD, Azimzadeh P, Singh AK, R3 T, Khan A, et al. Dual role of response gene to complement-32 in multiple sclerosis. *Exp Mol Pathol* (2013) 94:17–28. doi: 10.1016/j.yexmp.2012.09.005

28. Kruszewski AM, Rao G, Tatomir A, Hewes D, Tegla CA, Cudrici CD, et al. RGC-32 as a potential biomarker of relapse and response to treatment with glatiramer acetate in multiple sclerosis. *Exp Mol Pathol* (2015) 99:498–505. doi: 10.1016/j.yexmp.2015.09.007

29. Sofroniew MV. Molecular dissection of reactive astrogliosis and glial scar formation. *Trends Neurosci* (2009) 32:638–47. doi: 10.1016/j.tins.2009.08.002

30. Escartin C, Galea E, Lakatos A, O'Callaghan JP, Petzold GC, Serrano-Pozo A, et al. Reactive astrocyte nomenclature, definitions, and future directions. *Nat Neurosci* (2021) 24:312–25. doi: 10.1038/s41593-020-00783-4

31. Escartin C, Guillemaud O, Carrillo-de Sauvage MA. Questions and (Some) answers on reactive astrocytes. *Glia* (2019) 67:2221–47. doi: 10.1002/glia.23687

32. Sofroniew MV. Astrocyte reactivity: Subtypes, states, and functions in CNS innate immunity. *Trends Immunol* (2020) 41:758–70. doi: 10.1016/j.it.2020.07.004

33. Giovannoni F, Quintana FJ. The role of astrocytes in CNS inflammation. *Trends Immunol* (2020) 41:805–19. doi: 10.1016/j.it.2020.07.007

34. Correale J, Farez MF. The role of astrocytes in multiple sclerosis progression. *Front Neurol* (2015) 6:180. doi: 10.3389/fneur.2015.00180

35. Linnerbauer M, Wheeler MA, Quintana FJ. Astrocyte crosstalk in CNS inflammation. *Neuron* (2020) 108:608–22. doi: 10.1016/j.neuron.2020.08.012

36. Sundholm-Peters NL, Yang HKC, Goings GE, Walker AS, Szele FG. Radial glia-like cells at the base of the lateral ventricles in adult mice. *J Neurocytol* (2004) 33:153–64. doi: 10.1023/B:NEUR.0000029654.70632.3a

37. Barry D, McDermott K. Differentiation of radial glia from radial precursor cells and transformation into astrocytes in the developing rat spinal cord. *Glia* (2005) 50:187–97. doi: 10.1002/glia.20166

38. Petit A, Sanders AD, Kennedy TE, Tetzlaff W, Glattfelder KJ, Dalley DA, et al. Adult spinal cord radial glia displays a unique progenitor phenotype. *PloS One* (2011) 6:e24538. doi: 10.1371/journal.pone.0024538

39. Ebrahimi M, Yamamoto Y, Sharifi K, Kida H, Kagawa Y, Yasumoto Y, et al. Astrocyte-expressed FABP7 regulates dendritic morphology and excitatory synaptic function of cortical neurons. *Glia* (2016) 64:48–62. doi: 10.1002/glia.22902

40. Xue P, Chen L, Lu X, Zhang J, Bao G, Xu G, et al. Vimentin promotes astrocyte activation after chronic constriction injury. *J Mol Neurosci* (2017) 63:91–9. doi: 10.1007/s12031-017-0961-6

41. Kamizato K, Sato S, Shil SK, Umaru BA, Kagawa Y, Yamamoto Y, et al. The role of fatty acid binding protein 7 in spinal cord astrocytes in a mouse model of experimental autoimmune encephalomyelitis. *Neuroscience* (2019) 409:120–9. doi: 10.1016/j.neuroscience.2019.03.050

42. Cregg JM, DePaul MA, Filous AR, Lang BT, Tran A, Silver J. Functional regeneration beyond the glial scar. *Exp Neurol* (2014) 253:197–207. doi: 10.1016/j.expneurol.2013.12.024

43. Adams KL, Gallo V. The diversity and disparity of the glial scar. *Nat Neurosci* (2018) 21:9–15. doi: 10.1038/s41593-017-0033-9

44. Bradbury EJ, Burnside ER. Moving beyond the glial scar for spinal cord repair. *Nat Commun* (2019) 10:3879. doi: 10.1038/s41467-019-11707-7

45. Bozic I, Savic D, Lavrnja I. Astrocyte phenotypes: Emphasis on potential markers in neuroinflammation. *Histol Histopathol* (2021) 36:267–90. doi: 10.14670/HH-18-284

46. Girolamo F, Coppola C, Ribatti D, Trojano M. Angiogenesis in multiple sclerosis and experimental autoimmune encephalomyelitis. *Acta Neuropathol Commun* (2014) 2:84. doi: 10.1186/s40478-014-0084-z

47. Mendes FA, Coelho-Aguiar JM, Kahn SA, Reis AH, Dubois LG, Romão LF, et al. Connective-tissue growth factor (CTGF/CCN2) induces astrogenesis and fibronectin expression of embryonic neural cells. *In Vitro. PloS One* (2015) 10: e0133689. doi: 10.1371/journal.pone.0133689

48. Lu M, Yan XF, Si Y, Chen XZ. And astrocyte-mediated inflammatory response in culture conditions. *Inflammation* (2019) 42:1693–704. doi: 10.1007/s10753-019-01029-7

49. Fosbrink M, Cudrici C, Tegla CA, Soloviova K, Ito T, Vlaicu S, et al. Response gene to complement 32 is required for C5b-9 induced cell cycle activation in endothelial cells. *Exp Mol Pathol* (2009) 86:87–94. doi: 10.1016/j.yexmp.2008.12.005

50. Vlaicu SI, Tatomir A, Boodhoo D, Ito T, Fosbrink M, Cudrici C, et al. Rgc-32 is expressed in the human atherosclerotic arterial wall: Role in C5b-9-Induced cell proliferation and migration. *Exp Mol Pathol* (2016) 101:221–30. doi: 10.1016/j.yexmp.2016.09.004

51. Giger RJ, Hollis 2ER, Tuszynski MH. Guidance molecules in axon regeneration. *Cold Spring Harb Perspect Biol* (2010) 2:a001867. doi: 10.1101/cshperspect.a001867

52. Bolsover S, Fabes J, Anderson PN. Axonal guidance molecules and the failure of axonal regeneration in the adult mammalian spinal cord. *Restor Neurol Neurosci* (2008) 26:117–30.

53. Lotfi R, Nasiri Kalmarzi R, Rajabinejad M, Hasani S, Zamani F. The role of immune semaphorins in the pathogenesis of multiple sclerosis: Potential therapeutic targets. *Int Immunopharmacol* (2021) 95:107556. doi: 10.1016/j.intimp.2021.107556

54. Lee WS, Lee WH, Bae YC, Suk K. Axon guidance molecules guiding neuroinflammation. *Exp Neurobiol* (2019) 28:311–9. doi: 10.5607/en.2019.28.3.311

55. Molofsky AV, Deneen B. Astrocyte development: A guide for the perplexed. *Glia* (2015) 63:1320–9. doi: 10.1002/glia.22836

56. Akdemir ES, Huang AY, Deneen B. Astrocytogenesis: Where, when, and how. *F1000Res* (2020) 9:233. doi: 10.12688/f1000research.22405.1

57. Bannerman P, Hahn A, Soulika A, Gallo V, Pleasure D. Astrogliosis in EAE spinal cord: Derivation from radial glia, and relationships to oligodendroglia. *Glia* (2007) 55:57–64. doi: 10.1002/glia.20437

58. Li Y, He ZC, Zhang XN, Liu Q, Chen C, Zhu Z, et al. Stanniocalcin-1 augments stem-like traits of glioblastoma cells through binding and activating NOTCH1. *Cancer Lett* (2018) 416:66–74. doi: 10.1016/j.canlet.2017.11.033

59. Yeo IJ, Park MH, Son DJ, Kim JY, Nam KT, Hyun BK, et al. Prdx6 inhibits neurogenesis through downregulation of WDFY1-mediated Tlr4 signal. *Mol Neurobiol* (2019) 56:3132–44. doi: 10.1007/s12035-018-1287-2

60. Zweifel S, Marcy G, Lo Guidice Q, Li D, Heinrich C, Azim K, et al. Hopx defines heterogeneity of postnatal subventricular zone neural stem cells. *Stem Cell Rep* (2018) 11:770–83. doi: 10.1016/j.stemcr.2018.08.006

61. Yang C, Pu S, Zhu H, Qin W, Zhao H, Guo Z, et al. Identification and functional characterization of CD133(+)GFAP(+)CD117(+)Sca1(+) neural stem cells. *Mol Cell Biochem* (2022) 477:897–914. doi: 10.1007/s11010-021-04339-3

62. Guo Z, Chen M, Chao Y, Cai C, Liu L, Zhao L, et al. RGCC balances self-renewal and neuronal differentiation of neural stem cells in the developing mammalian neocortex. *EMBO Rep* (2021) 22:e51781. doi: 10.15252/embr.202051781

63. Hong S, Song MR. STAT3 but not STAT1 is required for astrocyte differentiation. *PloS One* (2014) 9:e86851. doi: 10.1371/journal.pone.0086851

64. Yoon H, Walters G, Paulsen AR, Scarisbrick IA. Astrocyte heterogeneity across the brain and spinal cord occurs developmentally, in adulthood and in response to demyelination. *PloS One* (2017) 12:e0180697. doi: 10.1371/journal.pone.0180697

65. Yang Y, Jackson R. Astrocyte identity: evolutionary perspectives on astrocyte functions and heterogeneity. *Curr Opin Neurobiol* (2019) 56:40–6. doi: 10.1016/j.conb.2018.11.006

66. Kurschus FC. T Cell mediated pathogenesis in EAE: Molecular mechanisms. *BioMed J* (2015) 38:183–93. doi: 10.4103/2319-4170.155590

67. Hasel P, Rose IVL, Sadick JS, Kim RD, Liddelow SA. Neuroinflammatory astrocyte subtypes in the mouse brain. *Nat Neurosci* (2021) 24:1475–87. doi: 10.1038/s41593-021-00905-6

68. Liddelow SA, Barres BA. Reactive astrocytes: Production, function, and therapeutic potential. *Immunity* (2017) 46:957–67. doi: 10.1016/j.immuni.2017.06.006

69. Doi T, Ogata T, Yamauchi J, Sawada Y, Tanaka S, Nagao M. Chd7 collaborates with Sox2 to regulate activation of oligodendrocyte precursor cells after spinal cord injury. *J Neurosci* (2017) 37:10290–309. doi: 10.1523/JNEUROSCI.1109-17.2017

70. Tatomir A, Rao G, Boodhoo D, Vlaicu SI, Beltrand A, Anselmo F, et al. Histone deacetylase SIRT1 mediates C5b-9-Induced cell cycle in oligodendrocytes. *Front Immunol* (2020) 11:619. doi: 10.3389/fimmu.2020.00619

71. Woodburn SC, Bollinger JL, Wohleb ES. The semantics of microglia activation: neuroinflammation, homeostasis, and stress. *J Neuroinflamm* (2021) 18:258. doi: 10.1186/s12974-021-02309-6

72. Tang R, Zhang G, Chen SY. Response gene to complement 32 protein promotes macrophage phagocytosis *via* activation of protein kinase c pathway. *J Biol Chem* (2014) 289:22715–22. doi: 10.1074/jbc.M114.566653

73. Sun C, Chen SY. RGC32 promotes bleomycin-induced systemic sclerosis in a murine disease model by modulating classically activated macrophage function. *J Immunol* (2018) 200:2777–85. doi: 10.4049/jimmunol.1701542

74. Zhao P, Wang B, Zhang Z, Zhang W, Liu Y. Response gene to complement 32 expression in macrophages augments paracrine stimulation-mediated colon cancer progression. *Cell Death Dis* (2019) 10:776. doi: 10.1038/s41419-019-2006-2

75. Saijo K, Glass CK. Microglial cell origin and phenotypes in health and disease. *Nat Rev Immunol* (2011) 11:775–87. doi: 10.1038/nri3086

frontiers | Frontiers in Immunology

TYPE Brief Research Report
PUBLISHED 26 January 2023
DOI 10.3389/fimmu.2023.1086673

OPEN ACCESS

EDITED BY
Zvi Fishelson,
Tel Aviv University, Israel

REVIEWED BY
Antonio Torsello,
University of Milano-Bicocca, Italy
József Dobó,
Hungarian Academy of Sciences (MTA), Hungary

*CORRESPONDENCE
Trent M. Woodruff
t.woodruff@uq.edu.au

SPECIALTY SECTION
This article was submitted to Molecular Innate Immunity, a section of the journal Frontiers in Immunology

RECEIVED 01 November 2022
ACCEPTED 12 January 2023
PUBLISHED 26 January 2023

CITATION
Li XX, Lee JD, Lee HS, Clark RJ and Woodruff TM (2023) TLQP-21 is a low potency partial C3aR activator on human primary macrophages. *Front. Immunol.* 14:1086673. doi: 10.3389/fimmu.2023.1086673

TLQP-21 is a low potency partial C3aR activator on human primary macrophages

Xaria X. Li, John D. Lee, Han S. Lee, Richard J. Clark and Trent M. Woodruff*

School of Biomedical Sciences, The University of Queensland, St. Lucia, Australia

TLQP-21 is a 21-amino acid neuropeptide derived from the VGF precursor protein. TLQP-21 is expressed in the nervous system and neuroendocrine glands, and demonstrates pleiotropic roles including regulating metabolism, nociception and microglial functions. Several possible receptors for TLQP-21 have been identified, with complement C3a receptor (C3aR) being the most commonly reported. However, few studies have characterised the activity of TLQP-21 in immune cells, which represent the major cell type expressing C3aR. In this study, we therefore aimed to define the activity of both human and mouse TLQP-21 on cell signalling in primary human and mouse macrophages. We first confirmed that TLQP-21 induced ERK signalling in CHO cells overexpressing human C3aR, and did not activate human C5aR1 or C5aR2. TLQP-21 mediated ERK signalling was also observed in primary human macrophages. However, the potency for human TLQP-21 was 135,000-fold lower relative to C3a, and only reached 45% at the highest dose tested (10 μM). Unlike in humans, mouse TLQP-21 potently triggered ERK signalling in murine macrophages, reaching near full activation, but at ~10-fold reduced potency compared to C3a. We further confirmed the C3aR dependency of the TLQP-21 activities. Our results reveal significant discrepancy in TLQP-21 C3aR activity between human and murine receptors, with mouse TLQP-21 being consistently more potent than the human counterpart in both systems. Considering the supraphysiological concentrations of hTLQP-21 needed to only partially activate macrophages, it is likely that the actions of TLQP-21, at least in these immune cells, may not be mediated by C3aR in humans.

KEYWORDS

TLQP-21, Complement C3a, C3aR, C5aR1, C5aR2

Introduction

VGF (non-acronym) is a large neuropeptide precursor (~68 kDa) classified as a member of the extended granin protein family (1). VGF is cleaved by the prohormone convertases such as prohormone convertase (PC) 1/3 and PC2 to generate a variety of bioactive peptides of low molecular weights (2). Among them, TLQP-21 is a 21-residue peptide derived from the *C*-terminus (residues 556-576) of the VGF precursor protein (3). Using the expression of VGF mRNA as a proxy, past studies have suggested the expression of TLQP-21 in the central

and peripheral nervous system and in several neuroendocrine glands including the pancreas, adrenal medullar and pituitary, however, further investigation using more specific molecular tools are needed to confirm these findings (2–4). TLQP-21 possesses pleiotropic roles in physiology and cell biology, including reducing obesity by decreasing food intake and/or increasing energy expenditure; potentiating adrenergic-induced lipolysis in adipocytes; modulating gastric contractility and acid secretion; reproduction; nociception; neuroprotection and modulation of microglia functions (2, 3).

In recent years, three possible binding targets of TLQP-21 have been identified: the globular C1q receptor (5, 6), heat shock cognate 71 kDa protein A8 (HSPA8) and the complement C3a receptor (C3aR) (1, 7), with C3aR being the most extensively studied (2, 8). C3aR is a classical G protein-coupled receptor which is the cognate receptor for the complement peptide C3a (9). From a cell signalling perspective, TLQP-21 ligation to cells activates phospholipase C (PLC)-β mediated generation of diacylglycerol (DAG) and inositol 1,4,5-trisphosphate (IP_3), which subsequently triggers extracellular signal-regulated kinase (ERK)1/2 phosphorylation and intracellular calcium mobilisation (10). These signalling pathways have been demonstrated in Chinese hamster ovary (CHO), 3T3-L1 and murine adipocytes, RAW264.7 macrophages and primary murine microglia to be dependent on C3aR (6, 11–14).

C3aR is expressed by all leukocytes of myeloid origin, such as neutrophils, dendritic cells, microglia and macrophages, and has been shown to modulate multiple aspects of immune cell signalling and functions in response to C3a (9, 15). However, despite this widespread expression of C3aR on myeloid cells, there is a general lack of studies examining the effect of TLQP-21 on these immune cells. Therefore, in the present study, we aimed to define the pharmacological activity of TLQP-21 on the cell signalling of human and murine primary macrophages. Human TLQP-21 (hTLQP-21) and mouse TLQP-21 (mTLQP-21) harbour 24% (5 out of 21) difference in their amino acid sequences (2, 7). Considering the differential activities of the two molecules as reported previously (16, 17), both hTLQP-21 and mTLQP-21 were synthesised, and comparatively analysed. We identified that both versions of TLQP-21 induced ERK signalling in primary human and murine macrophages at relatively high concentrations compared to C3a. Signalling by TLQP-21 was C3aR-dependent, with mouse TLQP-21 being consistently more potent in both mouse and human cells, relative to the human peptide. In view of the relatively low C3aR activity of human TLQP-21 we observed on macrophages, this action of TLQP-21 may not be physiologically relevant in human peripheral immune cells such as macrophages.

Abbreviations: BMDM, bone marrow-derived macrophage; BRET, bioluminescence resonance energy transfer; BSA, bovine serum albumin; C3aR, C3a receptor; C5aR1, C5a receptor 1; CHO, Chinese hamster ovary cells; CHO-C3aR, Chinese hamster ovary cells stably expressing C3aR; CHO-C5aR1, Chinese hamster ovary cells stably expressing C5aR1; DMEM, Dulbecco's Modified Eagle's Medium; ERK1/2, extracellular signal-regulated kinase 1/2; FBS, foetal bovine serum; hC3a, human C3a; HEK293, human embryonic kidney 293 cells; HMDM, human monocyte-derived macrophage; hTLQP-21, human TLQP-21; mC3a, mouse C3a; mTLQP-21, mouse TLQP-21; RT, room temperature; S.E.M., standard error of the mean; SFM, serum-free medium.

Materials and methods

Ligands and materials

Human C5a, human TLQP-21 (TLQPPSALRRRHYHHALPPSR) and mouse TLQP-21 (TLQPPASSRRRHFHHALPPAR) were synthesized by Fmoc-based solid phase peptide synthesis using previously described methods (18, 19). The C3aR inhibitor, SB290157 trifluoroacetate salt, and purified human C3a were purchased from Merck (Perth, Australia). Recombinant mouse C3a was purchased from R&D Systems (Minneapolis, USA). Bovine serum albumin (BSA) was purchased from Merck (Perth, Australia). For cell culture, trypsin-EDTA, HBSS, HEPES, Dulbecco's Modified Eagle's Medium (DMEM), phenol-red free DMEM, Ham's F12, Iscove's Modified Dulbecco's Medium, RPMI-1640 and Penicillin-Streptomycin were purchased from Thermo Fisher Scientific (Melbourne, Australia). Dulbecco's phosphate-buffered saline was purchased from Lonza (Melbourne, Australia). Stocks of TLQP-21 were reconstituted in water at 1 mM. All ligand dilutions were prepared in serum-free medium (SFM) containing 0.1% BSA.

Cell culture

Cell lines for this study were cultured as previously described (20). Non-transfected CHO-K1 cells or CHO cells stably expressing the human C3aR (CHO-C3aR; Product # ES-730-C, PerkinElmer, Melbourne, Australia) were maintained in Ham's F12 medium containing 10% foetal bovine serum (FBS), 100 IU/ml penicillin and 100 µg/ml streptomycin, with additional 400 µg/ml G418 (*In vivo*Gen, San Diego, USA) added for CHO-C3aR cell culture. HEK293 cells were maintained in DMEM medium containing 10% FBS, 100 IU/ml penicillin and 100 µg/ml streptomycin. All cell lines were maintained in T175 flasks (37°C, 5% CO_2) and subcultured at 80-90% confluency using 0.05% trypsin-EDTA in DPBS.

HMDMs were generated and cultured as previously described (20), with experiments approved by The University of Queensland Human Research Ethics Committee. Briefly, human buffy coat blood from anonymous healthy donors was obtained through the Australian Red Cross Blood Service (Brisbane, Australia). Human CD14+ monocytes were isolated from blood using Lymphoprep density centrifugation (STEMCELL, Melbourne, Australia) followed by CD14+ MACS magnetic bead separation (Miltenyi Biotec, Sydney, Australia). The isolated monocytes were differentiated for 7 days in Iscove's Modified Dulbecco's Medium supplemented with 10% FBS, 100 IU/ml penicillin, 100 µg/ml streptomycin and 15 ng/ml recombinant human macrophage colony stimulating factor (BioLegend, San Diego, USA) on 10 mm square dishes (Bio-strategy, Brisbane, Australia). Non-adherent cells were removed by washing with DPBS, and the adherent differentiated HMDMs were harvested by gentle scraping.

Mouse bone marrow-derived macrophages (BMDMs) were obtained and cultured as previously described (20, 21). All experiments using mice were approved by the University of Queensland animal ethics committee. Wild-type and $C3aR^{-/-}$ mice on a C57BL/6J genetic background (n = 3) were sacrificed by cervical

dislocation. The tibia was removed and sterilised. Upon removal of both epiphyses, bone marrow cells were harvested by flushing the central cavity with complete RPMI-1640 medium using a 10 ml syringe attached to a 25-gauge needle. Cells were then cultured in complete RPMI-1640 medium (containing 10 % FBS, 100 IU/ml penicillin, 100 µg/ml streptomycin) supplemented with 100 ng/ml recombinant human macrophage colony stimulating factor on 10 mm square dishes. Mature adherent macrophages for assays were harvested on day 6-7 by gentle scraping.

Phospho-ERK1/2 assays

Ligand-induced ERK1/2 phosphorylation was assessed using the AlphaLISA *Surefire Ultra* p-ERK1/2 (Thr202/Tyr204) kit (PerkinElmer, Melbourne, Australia) following the manufacturer's protocol as previously described (18, 20, 22). Briefly, CHO-K1, CHO-C3aR, CHO-C5aR1, HMDMs (50,000/well) or BMDMs (90,000/well) were seeded in tissue culture-treated 96-well plates (Corning, Corning, USA) for 24 h and serum-starved overnight. All ligand dilutions were prepared in serum-free medium (SFM) containing 0.1% BSA. For inhibition assays, cells were pre-treated with the following ligands (5 µM SB290157, or respective concentrations of hC3a, mC3a, hC5a, hTLQP-21, and mTLQP-21) or the solvent-only control for 30 min before agonist (hC3a, hTLQP-21 and mTLQP-21) addition. The concentration and identity of the ligands are described in detail in the figure legends. For stimulation, cells were treated with ligands at the indicated concentrations for 10 min at RT and then immediately lysed using AlphaLISA lysis buffer on a microplate shaker (450 rpm, 10 min). For the detection of phospho-ERK1/2 content, cell lysate (5 µL/well) was transferred to a 384-well ProxiPlate (PerkinElmer, Melbourne, Australia) and added to the donor and acceptor reaction mix (2.5 µL/well, respectively), followed by a 2-h incubation at RT in the dark. On a Tecan Spark 20M (Tecan, Männedorf, Switzerland), the plate was measured using standard AlphaLISA settings.

BRET assays measuring β-arrestin 2 recruitment to C5aR2

The C5a-mediated β-arrestin 2 recruitment to C5aR2 was measured using bioluminescence resonance energy transfer (BRET)-based assay using methods described elsewhere (20, 22, 23). Briefly, HEK293 cells were transiently transfected with β-arrestin 2-NanoLuc (Nluc) and human C5aR2-Venus constructs using XTG9 (Roche, Sydney, Australia) for 24 h. Transfected cells were then seeded (100,000/well) onto white 96-well plates (Corning, New York, USA) in phenol-red free DMEM containing 5% FBS overnight. For BRET assay, cells were firstly incubated with the substrate Endurazine (1:200, Promega, Sydney, Australia) for 2 h (37°C, 5% CO_2). All ligands were prepared in SFM containing 0.1% BSA. On a Tecan Spark 20M microplate reader (Tecan, Männedorf, Switzerland) (37°C), the BRET light emissions (460-485 and 520-545 nm) were continuously monitored for 24 reads with respective ligands (C5a, hTLQP-21, m-TLQP-21) and vehicle control (medium) added after the first 4 reads. The ligand-induced BRET ratio was calculated by subtracting the emission ratio of Venus (520-545 nm)/Nluc (460-485 nm) of the vehicle-treated wells from that of the ligand-treated wells, and the data at 40 min post ligand addition was used for the plotting of concentration-response curves.

Data collection, processing and analysis

All experiments were conducted in triplicates and repeated on three separate occasions unless otherwise specified. Data was analysed using GraphPad software (Prism 9.1). Data from each individual repeat was normalised accordingly (as specified in the figure legends) before being combined and expressed as mean ± standard error of the mean (S.E.M.) unless otherwise described. For all dose-response studies, logarithmic concentration-response curves were plotted using combined data and analysed to determine the respective potency values. Statistical analysis was performed using two-way ANOVA with Dunnett's *post hoc* analysis. Donor-matched comparisons were made for HMDM experiments. Differences were deemed significant when $p < 0.05$.

Results

hTLQP-21 and mTLQP-21 activate ERK signalling in CHO-K1 and CHO-C3aR cells

We first tested hTLQP-21 and mTLQP-21 in CHO-K1 cells to confirm the prior reported agonistic activities of these peptides in this cell line. Receptor-induced ERK1/2 phosphorylation was used as a readout. Plasma-derived human C3a (hC3a) significantly triggered ERK1/2 phosphorylation in CHO-K1 cells (Figures 1A, C), confirming the expression of endogenous C3aR in these cells (7). A significant reduction in ERK1/2 phosphorylation was observed at higher C3a concentrations, similar to the previous reported data for primary human macrophages (18). Both human and mouse versions of TLQP-21 triggered ERK signalling in CHO-K1 cells, albeit with lower efficacy and potency relative to hC3a. We next examined the ERK-inducing activities of TLQP-21 in CHO cells overexpressing human C3aR (Figures 1B, C; Table 1). hC3a potently and dose-dependently triggered ERK1/2 phosphorylation in CHO-C3aR cells (EC_{50} = 0.15 nM). Both hTLQP-21 and mTLQP-21 acted as full agonists relative to C3a on this signalling pathway, with mTLQP-21 being ~ 7-fold more potent than hTLQP-21 (EC_{50} = 83.6 nM for mTLQP-21 and 587 nM for hTLQP-21, respectively). Notably, the relative efficacy of C3a-induced ERK signalling in CHO-K1 cells was 2.6-fold lower than that in CHO-C3aR cells (2.7- versus 7.3-fold baseline for CHO-K1 and CHO-C3aR, respectively; Figure 1C). This is likely attributed to the much lower endogenous C3aR expression in the non-transfected CHO cells (7, 20).

TLQP-21 does not activate human C5aR1 or C5aR2

We have previously reported the promiscuous activity of complement receptor peptides across the three closely related

10.3389/fimmu.2023.1086673

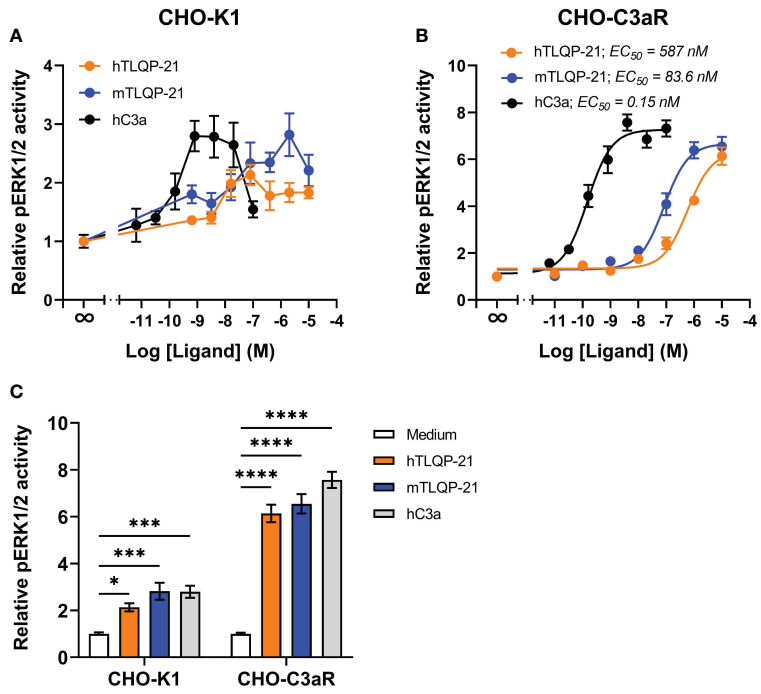

FIGURE 1
hTLQP-2 and mTLQP-21 activate ERK signalling in CHO-K1 and CHO-C3aR cells. hTLQP-21, mTLQP-21 and plasma-derived human C3a were tested in **(A)** non-transfected CHO-K1 or **(B)** CHO cells stably expressing human C3aR. CHO cells were serum-starved overnight and then stimulated with various ligands for 10 min before being lysed. The phospho-ERK1/2 content in the lysate was measured and expressed as fold-baseline before being combined. The maximum relative pERK1/2 activity induced by each ligand is shown in **(C)**. Data represent mean ± S.E.M. of triplicate measurements from 3-4 independent experiments (n = 3-4). Two-way ANOVA with Dunnett's *post hoc* analysis. *$P < 0.05$, ***$P < 0.001$, ****$P < 0.0001$. Ligand treated versus medium treated cells for each cell line.

anaphylatoxin receptors C3aR, C5aR1 and C5aR2 (9, 20). We therefore next examined if TLQP-21 may also demonstrate bioactivity at C5a receptors. C5aR1 is a classical GPCR, which, upon activation, recruits $G\alpha_i$ and $G\alpha_{16}$, and triggers ERK1/2 phosphorylation (9, 22). However, C5aR2, being a non-canonical GPCR, does not couple to the common classes of G proteins and is devoid of the classical G protein-mediated signalling activities (24–26). We therefore measured ligand-induced β-arrestin 2 recruitment as a readout for C5aR2 activation, utilising a BRET assay previously established in HEK293 cells (23, 27). Both human and mouse TLQP-21, up to 10 μM, did not trigger significant ERK1/2 activation in CHO cells overexpressing human C5aR1 (Figure 2A), nor could we detect any induced C5aR2-mediated β-arrestin 2 recruitment in the BRET assay (Figure 2B). Therefore, among the three complement receptors examined, the activity of TLQP-21 on C3aR is likely to be selective.

TLQP-21 triggers C3aR-dependent ERK signalling in human monocyte-derived macrophages

Next, we aimed to determine the effect of TLQP-21 treatment in primary human monocyte-derived macrophages (HMDMs), which is an established and widely used model of resting tissue macrophages that expresses high levels of endogenous human C3aR (20, 28, 29). We stimulated the cells with different concentrations of hTLQP-21

TABLE 1 Summary of potencies and activities of TLQP-21 tested on CHO-C3aR, HMDM and BMDM.

	CHO-C3aR			HMDM			BMDM		
	EC_{50} (nM)	$logEC_{50}$ ± SE	% C3a activity ± SE	EC_{50} (nM)	$logEC_{50}$ ± SE	% C3a activity ± SE	EC_{50} (nM)	$logEC_{50}$ ± SE	% C3a activity ± SE
C3a	0.15	-9.8 ± 0.1	100 ± 2.8	0.11	-9.9 ± 0.1	100 ± 6.2	8.4	-8.1 ± 0.1	100 ± 4.1
hTLQP-21	587.0	-6.2 ± 0.1	87.0 ± 3.5	14820	-4.8 ± 0.9	45.3 ± 10	401	-6.4 ± 0.2	63.3 ± 4.2
mTLQP-21	83.6	-7.1 ± 0.1	91.8 ± 2.7	2846	-5.5 ± 0.2	93.5 ± 18	96.5	-7.0 ± 0.3	80.1 ± 5.1

Potencies and efficacies of human and mouse TLQP-21 were determined in CHO-C3aR, HMDM and BMDM cells using phospho-ERK1/2 assays. Data were normalised to fold baseline before combined for analysis (n = 3-4).

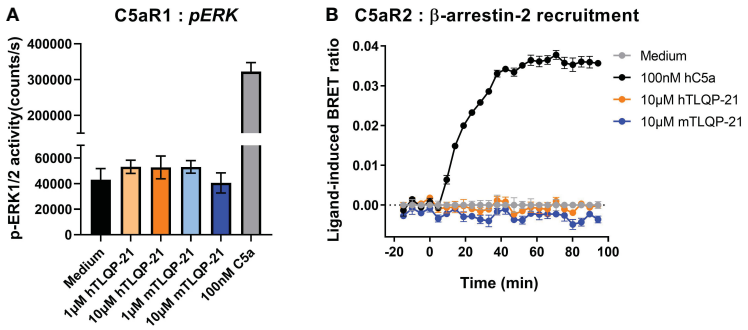

FIGURE 2
hTLQP-2 and mTLQP-21 do not activate human C5aR1 or C5aR2. **(A)** CHO cells stably expressing human C5aR1 were serum-starved overnight and then stimulated with various ligands for 10 min before being lysed. The phospho-ERK1/2 content in the lysate was measured and expressed as counts/s. **(B)** HEK293 cells were transiently transfected using C5aR2-Venus and β-arrestin 2-nanoluc BRET pairs for 24 hours, and seeded overnight. Filtered light emissions between 460-485 nm (nanoluc) and 520-545 nm (Venus) were continually monitored for 90 min, with respective ligands (mTLQP-21 and hTLQP-21, 10 μM; hC5a, 100 nM) added at the 0 min time point. Data are expressed as ligand-induced BRET (Venus/nanoLuc emission) ratios. Data represent mean ± S.E.M. of triplicate measurements from a single experiment.

and mTLQP-21 and then detected the phosphorylated ERK1/2 content in the cell lysate. Expectedly, human C3a potently induced ERK1/2 phosphorylation in HMDMs with an EC_{50} of 0.11 nM (Figure 3A; Table 1). Both versions of TLQP-21 triggered ERK signalling in HMDMs, but with greatly reduced potencies (by 25,000- to 135,000-fold) in comparison to hC3a (estimated EC_{50} = 2.8 μM for mTLQP-21 and 14.8 μM for hTLQP-21 respectively). In addition, whilst mTLQP-21 at 10 μM triggered up to 93% of the hC3a-induced level, the ERK signalling activity induced by hTLQP-21 only reached 45%. In order to examine whether this low-potency TLQP-21 induced ERK activation was dependent on C3aR, we pre-treated HMDMs with the C3aR antagonist SB290157 (30). A 5 μM concentration of SB290157 was chosen to avoid any C3aR or C5aR2 agonistic effect (20). SB290157 significantly inhibited hTLQP-21 and mTLQP-21 induced ERK signalling in HMDMs by 70-90 % (Figure 3B). The antagonising activity of SB290157 was more potent towards mTLQP-21 induced ERK activation (to 16% of the control level) than that of hTLQP-21 (to 29% of the control level), and dependent on the concentration of TLQP-21 tested. Notably, under control conditions, 10 μM mTLQP-21 only reached 40% of the C3a induced activity (Figure 3B) rather than the 93% as identified in Figure 3A. This discrepancy is likely caused by the different C3aR expression levels between individual human donors (29), which could affect the relative activities of the ligands amongst separate experiments.

To further validate the C3aR dependency of TLQP-21 in human macrophages, we conducted a desensitization assay using hC3a, based on the concept that any TLQP-21 binding to C3aR would impede hC3a from binding and activating C3aR, and the ERK1/2 phosphorylation triggered by TLQP-21 would desensitise subsequent ERK signalling triggered by hC3a. We observed that pre-treating cells with both versions of TLQP-21 significantly dampened hC3a-induced ERK signalling, with mTLQP-21 being consistently more potent than hTLQP-21 (Figure 3C). This inhibitory effect is likely to be competitive as it could be overcome by increasing the concentration of hC3a (ranging from 80-90% inhibition for 1 nM hC3a and 30-50% for 100 nM hC3a). In homologous desensitisation control experiments (Figure 3D), as expected, pretreating cells with hC3a, hTLQP-21 and mTLQP-21 significantly dampened the subsequent ERK activity triggered by these ligands. No similar TLQP-21 mediated inhibition was observed for hC5a-indued ERK1/2 activity (Figure 3E), indicating the inhibitory activity of TLQP-21 was C3aR-specific rather than towards basal activities of the cell. Based on these data, we conclude that both human and mouse TLQP-21 induce C3aR-mediated ERK signalling in HMDMs.

TLQP-21 triggers C3aR-dependent ERK signalling in murine bone marrow-derived macrophages

We next assessed if TLQP-21 similarly activated ERK signalling in murine primary bone marrow-derived macrophages. Recombinant mouse C3a dose-dependently triggered ERK1/2 phosphorylation in BMDMs (EC_{50} = 8.4 nM) (Figure 4A; Table 1). Both hTLQP-21 and mTLQP-21 induced ERK signalling in BMDMs (EC_{50} = 96.5 nM for mTLQP-21 and 401 nM for hTLQP-21 respectively), with mTLQP-21 being ~4-fold more potent than hTLQP-21, consistent with the trends observed in CHO-C3aR and HMDMs (Figure 1B, 3A). Neither mTLQP-21 nor hTLQP-21 achieved full activation of C3aR relative to mC3a (63% and 80% for hTLQP-21 and mTLQP-21 respectively). Notably, both TLQP-21 species demonstrated an ~40-fold improvement in potency at murine C3aR (in BMDMs) relative to human C3aR (in HMDMs). The TLQP-21-induced ERK signalling was abolished in C3aR-deficient BMDMs (Figure 4B), indicating that the ERK-activating effect was entirely C3aR-dependent. Thus, TLQP-21 similarly activates C3aR-dependent ERK signalling in BMDMs.

Discussion

TLQP-21 is a neuropeptide with important endocrine and enteroendocrine functions demonstrated by multiple groups (2, 3). Several studies have reported the complement receptor C3aR as an endogenous receptor for TLQP-21 (3, 7, 8, 13, 16). However, few have

10.3389/fimmu.2023.1086673

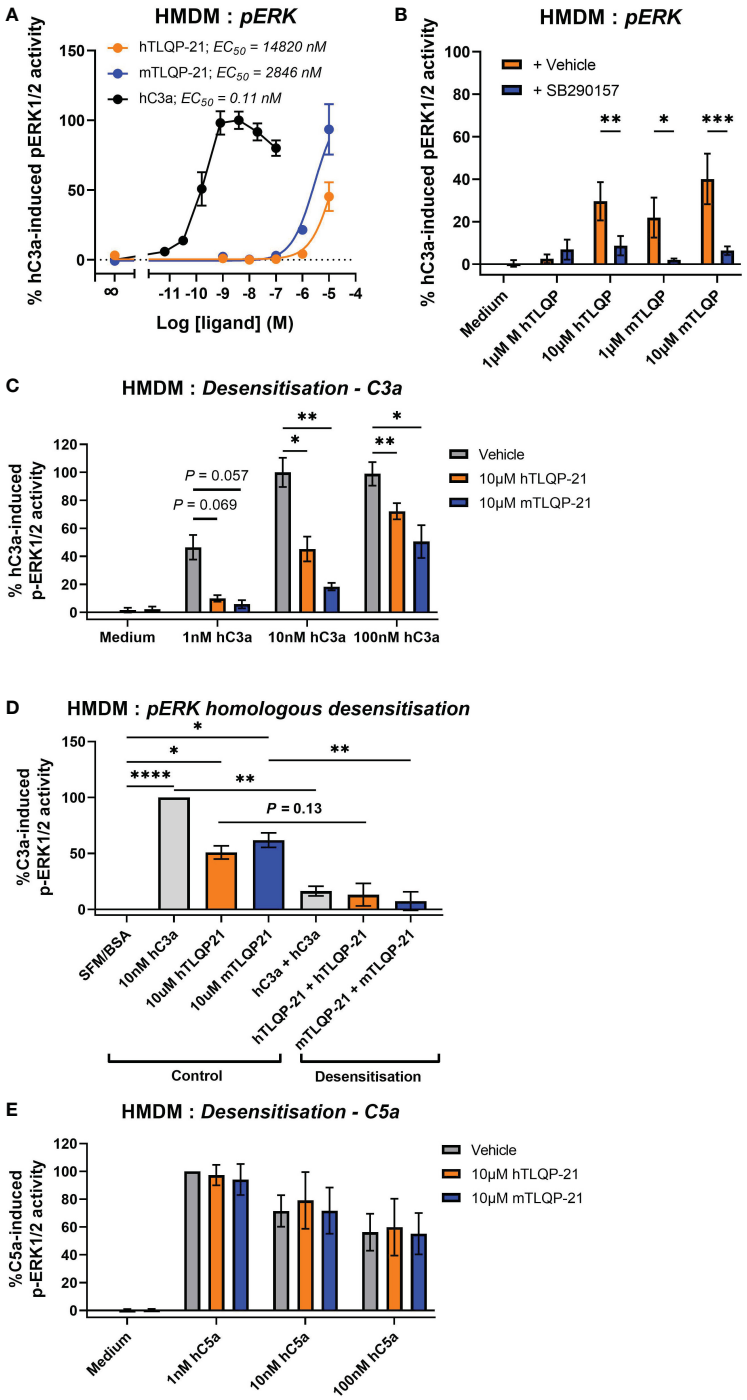

FIGURE 3
Agonistic and antagonistic activities of hTLQP-21 and mTLQP-21 in human monocyte-derived macrophages. Serum-starved HMDMs (50,000/well) were **(A)** stimulated with medium or respective ligands at the indicated concentrations for 10 min and then lysed, or **(B)** pre-treated with 5 μM SB290157 for 30 min prior to stimulation. **(C)** HMDMs were pre-treated with 10 μM hTLQP-21 or mTLQP-21 for 30 min before being stimulated with respective concentrations of human C3a. **(D)** HMDMs were pre-treated with 10 nM hC3a, 10 μM hTLQP-21 or mTLQP-21 for 30 min before being stimulated with the same concentrations of the above ligands for 10 min and then lysed. **(E)** HMDMs were pre-treated with 10 μM hTLQP-21 or mTLQP-21 for 30 min before being stimulated with respective concentrations of human C5a for 10 min and then lysed. The phospho-ERK1/2 content in the cell lysate was measured and normalised to the maximum hC3a/hC5a-induced levels before being combined. Data represent mean ± S.E.M. of triplicate measurements using cells from 4 independent donors (n = 4). Two-way ANOVA with Dunnett's *post hoc* analysis. *$P < 0.05$, **$P < 0.01$, ***$P < 0.001$, ****$P < 0.0001$. Ligand pre-treated *versus* vehicle treated donor-matched cells.

10.3389/fimmu.2023.1086673

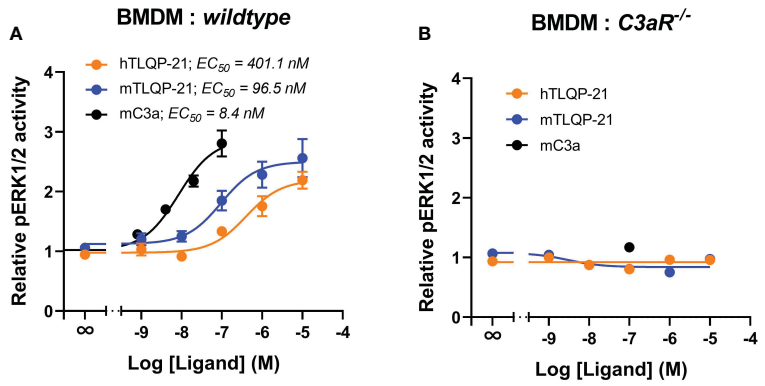

FIGURE 4
TLQP-21 triggers ERK signalling through C3aR in murine bone marrow-derive macrophages. BMDMs (90,000/well) from *wildtype mice* **(A)** or with *C3aR knockout mice* **(B)**, were serum-starved overnight and then stimulated with respective ligands at the indicated concentrations for 10 min. The phospho-ERK1/2 content in the cell lysate was measured and normalised to the medium only-treated levels before being combined. Data represent mean ± S.E.M. of triplicate measurements using cells from 3 mice (n = 3).

explored the potential actions of TLQP-21 on immune cells, despite the wide expression of C3aR on these cells (9). Therefore, the primary goal of this study was to characterise the signalling activities of this peptide in primary macrophages, which could allow us to infer whether any of the reported physiological functions of TLQP-21 might be mediated by immune cells in a C3aR-dependent fashion.

First, we validated the signalling activities of our in-house synthesised TLQP-21 on native CHO-K1 cells. In accordance with previous studies (7, 17), both human and mouse TLQP-21 significantly induced ERK1/2 phosphorylation in CHO-K1 cells, with mouse TLQP-21 being marginally more efficacious relative to the human version. Unexpectedly, the ERK signalling activity fell at higher concentrations of TLQP-21, which might reflect the unique characteristic of C3aR-mediated signalling activities in primary cells, as previously observed (18).

On CHO-C3aR cells, which artificially express a high density of human C3aR to enable robust pharmacological characterisation (20), both TLQP-21 peptides behaved as full agonists relative to human C3a. This, together with the lack of activity of TLQP-21 on CHO-C5aR1 cells, provides evidence the ERK signalling activity caused by TLQP-21 was mediated by C3aR rather than the highly conserved C5aR1. TLQP-21 is unlikely to activate other endogenous receptors expressed by CHO cells, either, considering the negligible ERK activity triggered by the ligand. However, this will need to validated in future experiments. The relative potencies of the two versions of TLQP-21 on CHO-C3aR, with the mTLQP-21 being ~ 7-fold more potent than hTLQP-21, are consistent with previous reported data (refer to Figure 5, in Sahu et al. (16)). One possible explanation for the lower potency of hTLQP-21, is that the human peptide has a partially unfolded structure in the presence of hC3aR, whilst mTLQP-21 retains a strong helical structure (16). In addition, by contrast to hTLQP-21, mTLQP-21 possesses a S20A substitution, which confers increased hydrophobicity of the peptide and thereby enhances its binding affinity to the hydrophobic C3aR binding pocket (16, 17). Interestingly, despite the several instances of ligand promiscuity between C3aR and C5a receptors as observed previously (20, 31, 32), we did not observe any significant activity of TLQP-21 on human C5aR2, which adds to the evidence that the action of TLQP-21 was likely to be C3aR-specific.

Previously, TLQP-21 has been shown to induce calcium mobilisation in murine RAW264.7 cells and primary murine microglia (6, 12, 13). However, only mouse TLQP-21 was used in these studies and to the best of our knowledge, no data is available for the potential activity of TLQP-21 in human immune cells. Here, in primary HMDMs, human C3a demonstrated comparable and potent ERK-inducing activities in both HMDMs and CHO-C3aR cells. However, by contrast to hC3a, the agonistic activity of TLQP-21 peptides was markedly weaker in HMDMs relative to CHO-C3aR, with EC_{50} values in the high micromolar range, and neither peptide triggered full activation (agonism), relative to hC3a. Next, we sought to decipher if the induced ERK signalling activity was mediated through C3aR. Because of the impracticality of knocking out C3aR in primary human macrophages, we used SB290157 as a pharmacological tool to block C3aR, which we have demonstrated to be a viable approach in HMDMs (20, 30). SB290157 significantly inhibited C3a-induced ERK signalling, to less than 20% of the untreated level. Considering that SB290157 at the concentration used does not exhibit any detectable agonist activity on C5aR1 or C3aR (20), the observed dampening effect on ERK signalling was likely caused by SB290157 inhibiting C3aR. Next, in our receptor desensitization assay, pre-treating HMDMs with both versions of TLQP-21 was able to dampen C3a-induced ERK1/2 phosphorylation, and expectedly, mTLQP-21 was consistently more potent than hTLQP-21 for all concentrations of hC3a tested. The TLQP-21 mediated inhibitory effect could be overcome by adding higher concentrations of hC3a. Because no such inhibition was observed for C5a-mediated ERK signalling in the same cells, the inhibitory action of TLQP-21 was unlikely to be caused by any non-specific inhibitory actions of the peptide on the cell signalling of HMDMs. Further, the competitive behaviour observed between TLQP-21 and C3a possibly indicate that TLQP-21 and C3a bind to a similar binding site on C3aR, potentially involving D417, R161, and R340 in the C3aR binding motif interacting with the *C*-terminal arginine of TLQP-21 and C3a (16). Together, this provides evidence that TLQP-21 induces ERK1/2 phosphorylation in human macrophages through C3aR.

Human C3aR shares 65% similarity with its murine counterpart. However, the extracellular loop II of human and murine C3aR, which is required for C3a binding, only shares a 45% sequence identity (33). Considering a large number of TLQP-21 studies are performed in mouse models, we examined the signalling activities of TLQP-21 on murine C3aR using murine primary bone marrow-derived macrophages. Consistent with our previous findings in CHO-C3aR and HMDMs and in literature (2, 17), mTLQP-21 more potently induced ERK signalling than hTLQP-21. Neither hC3a, nor the TLQP-21 peptides caused any significant ERK signalling activity in C3aR-deficient cells, confirming the C3aR-specificity of the signalling actions of TLQP-21 in mouse cells.

In this study, by measuring the cell signalling activities of TLQP-21 in native CHO-K1, CHO-C3aR and primary human and murine macrophages, we validated that TLQP-21 also activates and signals through C3aR in a primary immune cell setting. Consistent with previous publications, murine TLQP-21 was more potent than human TLQP-21 on both human and mouse C3aR, and both peptides demonstrated improvement in potency on murine C3aR relative to human C3aR (8, 16). This could be explained by the increased hydrophobicity of the mC3aR binding pocket relative to hC3aR (ILVMS, 59% hydrophobicity for mC3aR versus VSLVC, 53% hydrophobicity for hC3aR), which enables more favourable interaction with *C*-terminal motif of TLQP-21 (PPAR for mTLQP-21 and PPSR for hTLQP-21) (16).

Notably, mTLQP-21 demonstrated a moderate potency in the submicromolar range and close-to-full agonistic potency on mouse BMDMs. By contrast, hTLQP-21 is a weak activator of human C3aR in HMDMs, with a high micromolar potency and only reaching ~50% of the C3a-induced level at the highest dose tested (10 μM). In the physiological context, the plasma concentration of TLQP-21 are reported to be 70 pmol/ml (70 nM) in mouse and 80–90 pmol/ml (80-90 nM) in healthy humans, but much lower in tissues such as the pancreas (34–36). This suggests that in the human system, physiological concentrations of human TLQP-21 acting through C3aR, are unlikely to elicit any significant response (i.e., less than 5% of C3a activity based on our data), at least in peripheral blood macrophages. Indeed, on a molar potency level, hTLQP-21 was ~135,000-fold less active than C3a, which would necessitate a remarkably high local concentration of the parent molecule VGF in order for this peptide to be functional at C3aR *in vivo*. Similar discrepant actions of mTLQP-21 and hTLQP-21 were also reported by Sahu et al. (16), where only mTLQP-21, but not the human counterpart, significantly potentiated 10 nM isoproterenol-induced lipolysis in human adipocytes. The current study is, nevertheless, limited by the primary focus on macrophages. It would be interesting to explore in future experiments whether the weak and partial C3aR activity of hTLQP-21 also holds in other C3aR-expressing cells that may be in close vicinity to VGF-expressing cells within the peripheral and central nervous systems. Further, it is necessary to assess cell signalling pathways other than ERK1/2 phosphorylation, such as cAMP signalling, intracellular calcium mobilisation and β-arrestin recruitment, to gain a more wholistic view of C3aR activity following TLQP-21 ligation. These explorative studies would also help to provide a mechanistic explanation for the partial activity of TLQP-21 on C3aR, and the differential responses between human and mouse C3aR. Alternative signalling pathways in cells other than macrophages (e.g., neutrophils, epithelial cells, neuronal cells), may account for the physiological activity of TLQP-21 reported in the literature.

Importantly, the potential effects of administering TLQP-21 *in vivo* have been explored in a range of mouse models, to explore the biological functions of TLQP-21 in food intake, metabolism, gastric contractility and acid secretion, reproduction, nociception, neuroprotection and modulation of microglia functions (2, 3). Nevertheless, few have examined or validated the biological effects of TLQP-21 in a relevant human system, such as by using human primary cells, tissues or organoids. Considering the large discrepancy in potency and efficacy between hTLQP-21 (on hC3aR) and mTLQP-21 (on mC3aR) in macrophages, further studies are needed to validate if the physiological functions of TLQP-21 observed in mouse models can be translated into human biology. Indeed, one of the major physiological functions of TLQP-21, as reported by several groups, is to modulate microglia functions, which subsequently has implications in β-Amyloid plaque clearance, Alzheimer's disease neuropathy and nociception (6, 11, 12, 37). As human primary microglia cell models and 3D cultures become more widely available (38–40), it would be informative to examine any modulatory effect of TLQP-21 in these human systems.

In sum, this study characterised the signalling activities of TLQP-21 on human and murine primary macrophages and demonstrated the ability of both human and mouse TLQP-21 to activate C3aR-dependent ERK signalling, with the mouse TLQP-21 being consistently more potent than the human counterpart. TLQP-21 confers important physiological functions. However, considering the supraphysiological concentrations of hTLQP-21 needed to only partially activate human macrophages, it is conceivable that any immune actions of TLQP-21 are mediated by pathways other than C3aR in humans.

Data availability statement

The raw data supporting the conclusions of this article will be made available by the authors, without undue reservation.

Ethics statement

The studies involving human participants were reviewed and approved by The University of Queensland Human Research Ethics Committee. The patients/participants provided their written informed consent to participate in this study. The animal study was reviewed and approved by The University of Queensland Animal Ethics Committee.

Author contributions

TW and XL conceived the project and designed the research. XL performed the research, analysed data and wrote the first paper draft with assistance from TW. JL generated the murine cells used in this study. HL and RC synthesised the TLQP-21 peptides and other key

reagents for the study. All authors contributed to the article and approved the submitted version.

Funding

This work was supported by National Health and Medical Research Council of Australia (NHMRC) [Grant APP1118881 to TW and RC].

Acknowledgments

We would like to acknowledge Australian Red Cross Lifeblood and human donors for providing the cells used in these studies.

Conflict of interest

The authors declare that the research was conducted in the absence of any commercial or financial relationships that could be construed as a potential conflict of interest.

Publisher's note

References

1. Akhter S, Chakraborty S, Moutinho D, Álvarez-Coiradas E, Rosa I, Viñuela JE, et al. The human VGF-derived bioactive peptide TLQP-21 binds heat shock 71 kDa protein 8 (HSPA8)on the surface of SH-SY5Y cells. *PloS One* (2017) 12(9):e0185176. doi: 10.1371/journal.pone.0185176

2. Sahu BS, Nguyen ME, Rodriguez P, Pallais JP, Ghosh V, Razzoli M, et al. The molecular identity of the TLQP-21 peptide receptor. *Cell Mol Life Sci* (2021) 78(23):7133–44. doi: 10.1007/s00018-021-03944-1

3. Bresciani E, Possenti R, Coco S, Rizzi L, Meanti R, Molteni L, et al. TLQP-21, a VGF-derived peptide endowed of endocrine and extraendocrine properties: Focus on *in vitro* calcium signaling. *Int J Mol Sci* (2019) 21(1):130. doi: 10.3390/ijms21010130

4. Turolla E, Valtorta S, Bresciani E, Fehrentz J-A, Giuliano L, Stucchi S, et al. Study of the tissue distribution of TLQP-21 in mice using [18F]JMV5763, a radiolabeled analog prepared *via* [18F]aluminum fluoride chelation chemistry. *Front Pharmacol* (2018) 9:1274. doi: 10.3389/fphar.2018.01274

5. Chen Y-C, Pristerà A, Ayub M, Swanwick RS, Karu K, Hamada Y, et al. Identification of a receptor for neuropeptide VGF and its role in neuropathic pain. *J Biol Chem* (2013) 288(48):34638–46. doi: 10.1074/jbc.M113.510917

6. Elmadany N, de Almeida Sassi F, Wendt S, Logiacco F, Visser J, Haage V, et al. The VGF-derived peptide TLQP21 impairs purinergic control of chemotaxis and phagocytosis in mouse microglia. *J Neurosci* (2020) 40(17):3320–31. doi: 10.1523/JNEUROSCI.1458-19.2020

7. Hannedouche S, Beck V, Leighton-Davies J, Beibel M, Roma G, Oakeley EJ, et al. Identification of the C3a receptor (C3AR1) as the target of the VGF-derived peptide TLQP-21 in rodent cells. *J Biol Chem* (2013) 288(38):27434–43. doi: 10.1074/jbc.M113.497214

8. Akhter MS. A comparative review on TLQP-21 receptors: rodent versus human. *In Vivo* (2020) 3:5. doi: 10.5455/jabet.2020.d102

9. Klos A, Wende E, Wareham KJ, Monk PNInternational Union of Basic and Clinical Pharmacology. LXXXVII. Complement peptide C5a, C4a, and C3a receptors. . *Pharmacol Rev* (2013) 65(1):500. doi: 10.1124/pr.111.005223

10. Molteni L, Rizzi L, Bresciani E, Possenti R, Passeri PP, Ghè C, et al. Pharmacological and biochemical characterization of TLQP-21 activation of a binding site on CHO cells. *Front Pharmacol* (2017) 8(167):167–78. doi: 10.3389/fphar.2017.00167

11. Gaamouch FE, Audrain M, Lin W-J, Beckmann ND, Jiang C, Hariharan SP, et al. VGF-derived peptide TLQP-21 modulates microglial function through C3aR1 signaling pathways and reduces neuropathology in 5xFAD mice. *Mol Neurodegener* (2020) 15(1):4. doi: 10.1186/s13024-020-0357-x

12. Doolen S, Cook J, Riedl MS, Kitto KF, Kohsaka S, Honda CN, et al. Complement 3a receptor in dorsal horn microglia mediates pronociceptive neuropeptide signaling. *Glia* (2017) 65(12):1976–89. doi: 10.1002/glia.23208

13. Molteni L, Rizzi L, Bresciani E, Meanti R, Fehrentz J-A, Verdié P, et al. STIM proteins and orai Ca2+ channels are involved in the intracellular pathways activated by TLQP-21 in RAW264.7 macrophages. *Front Pharmacol* (2018) 9. doi: 10.3389/fphar.2018.01386

14. Cero C, Razzoli M, Han R, Sahu BS, Patricelli J, Guo Z, et al. The neuropeptide TLQP-21 opposes obesity via C3aR1-mediated enhancement of adrenergic-induced lipolysis. *Mol Metab* (2017) 6(1):148–58. doi: 10.1016/j.molmet.2016.10.005

15. Coulthard LG, Woodruff TM. Is the complement activation product C3a a proinflammatory molecule? re-evaluating the evidence and the myth. *J Immunol* (2015) 194(8):3542. doi: 10.4049/jimmunol.1403068

16. Sahu BS, Rodriguez P, Nguyen ME, Han R, Cero C, Razzoli M, et al. Peptide/Receptor Co-evolution explains the lipolytic function of the neuropeptide TLQP-21. *Cell Rep* (2019) 28(10):2567–80.e6. doi: 10.1016/j.celrep.2019.07.101

17. Cero C, Vostrikov VV, Verardi R, Severini C, Gopinath T, Braun PD, et al. The TLQP-21 peptide activates the G-protein-coupled receptor C3aR1 *via* a folding-upon-binding mechanism. *Structure* (2014) 22(12):1744–53. doi: 10.1016/j.str.2014.10.001

18. Li XX, Clark RJ, Woodruff TM. C5aR2 activation broadly modulates the signaling and function of primary human macrophages. *J Immunol* (2020) 205(4):ji2000407. doi: 10.4049/jimmunol.2000407

19. Gorman DM, Li XX, Payne CD, Cui CS, Lee JD, Rosengren KJ, et al. Development of synthetic human and mouse C5a: Application to binding and functional assays *In vitro* and *In vivo*. *ACS Pharmacol Transl Sci* (2021) 4(6):1808–17. doi: 10.1021/acsptsci.1c00199

20. Li XX, Kumar V, Clark RJ, Lee JD, Woodruff TM. The "C3aR antagonist" SB290157 is a partial C5aR2 agonist. *Front Pharmacol* (2020) 11(2241):591398. doi: 10.1101/2020.08.01.232090

21. Davies JQ, Gordon S. Isolation and culture of murine macrophages. In: Helgason CD, Miller CL, editors. *Basic cell culture protocols*. Totowa, NJ: Humana Press (2005). p. 91–103.

22. Li XX, Lee JD, Massey NL, Guan C, Robertson AAB, Clark RJ, et al. Pharmacological characterisation of small molecule C5aR1 inhibitors in human cells reveals biased activities for signalling and function. *Biochem Pharmacol* (2020) 180:114156. doi: 10.1016/j.bcp.2020.114156

23. Croker DE, Halai R, Kaeslin G, Wende E, Fehlhaber B, Klos A, et al. C5a2 can modulate ERK1/2 signaling in macrophages *via* heteromer formation with C5a1 and [beta]-arrestin recruitment. *Immunol Cell Biol* (2014) 92(7):631–9. doi: 10.1038/icb.2014.32

24. Li XX, Lee JD, Kemper C, Woodruff TM. The complement receptor C5aR2: A powerful modulator of innate and adaptive immunity. *J Immunol* (2019) 202(12):3339. doi: 10.4049/jimmunol.1900371

25. Pandey S, Maharana J, Li XX, Woodruff TM, Shukla AK. Emerging insights into the structure and function of complement C5a receptors. *Trends Biochem Sci* (2020) 45(8):693–705. doi: 10.1016/j.tibs.2020.04.004

26. Pandey S, Kumari P, Baidya M, Kise R, Cao Y, Dwivedi-Agnihotri H, et al. Intrinsic bias at non-canonical, β-arrestin-coupled seven transmembrane receptors. *Mol Cell* (2021) 81:4605–4621.e11. doi: 10.1101/2021.02.02.429298

27. Croker DE, Monk PN, Halai R, Kaeslin G, Schofield Z, Wu MCL, et al. Discovery of functionally selective C5aR2 ligands: Novel modulators of C5a signalling. *Immunol Cell Biol* (2016) 94(8):787–95. doi: 10.1038/icb.2016.43

28. Lacey DC, Achuthan A, Fleetwood AJ, Dinh H, Roiniotis J, Scholz GM, et al. Defining GM-CSF– and Macrophage-CSF–dependent macrophage responses by *In vitro* models. *J Immunol* (2012) 188(11):5752. doi: 10.4049/jimmunol.1103426

29. Mommert S, Aslan D, Ratz L, Stark H, Gutzmer R, Werfel T. The anaphylatoxin C3a receptor expression on human M2 macrophages is down-regulated by stimulating the histamine H4 receptor and the IL-4 receptor. *J Innate Immun* (2018) 10(4):349–62. doi: 10.1159/000490426

30. Ames RS, Lee D, Foley JJ, Jurewicz AJ, Tornetta MA, Bautsch W, et al. Identification of a selective nonpeptide antagonist of the anaphylatoxin C3a receptor that demonstrates antiinflammatory activity in animal models. *J Immunol* (2001) 166(10):6341. doi: 10.4049/jimmunol.166.10.6341

31. Halai R, Bellows-Peterson ML, Branchett W, Smadbeck J, Kieslich CA, Croker DE, et al. Derivation of ligands for the complement C3a receptor from the c-terminus of C5a. *Eur J Pharmacol* (2014) 745:176–81. doi: 10.1016/j.ejphar.2014.10.041

32. Li XX, Clark RJ, Woodruff TM. Anaphylatoxin receptor promiscuity for commonly used complement C5a peptide agonists. *Int Immunopharmacol* (2021) 100:108074. doi: 10.1016/j.intimp.2021.108074

33. Chao T-H, Ember JA, Wang M, Bayon Y, Hugli TE, Ye RD. Role of the second extracellular loop of human C3a receptor in agonist binding and receptor function *. *J Biol Chem* (1999) 274(14):9721–8. doi: 10.1074/jbc.274.14.9721

34. Corda G, Noli B, Manconi B, Brancia C, Pellegrini M, Naro F, et al. TLQP-21 changes in response to a glucose load. *Tissue Cell* (2021) 68:101471. doi: 10.1016/j.tice.2020.101471

35. Brancia C, Noli B, Boido M, Pilleri R, Boi A, Puddu R, et al. TLQP peptides in amyotrophic lateral sclerosis: Possible blood biomarkers with a neuroprotective role. *Neuroscience* (2018) 380:152–63. doi: 10.1016/j.neuroscience.2018.03.023

36. Guo ZK, Sahu BS, He R, Finan B, Cero C, Verardi R, et al. Clearance kinetics of the VGF-derived neuropeptide TLQP-21. *Neuropeptides* (2018) 71:97–103. doi: 10.1016/j.npep.2018.06.003

37. Cho K, Jang Y-J, Lee S-J, Jeon Y-N, Shim Y-L, Lee J-Y, et al. TLQP-21 mediated activation of microglial BV2 cells promotes clearance of extracellular fibril amyloid-β. *Biochem Biophys Res Commun* (2020) 524(3):764–71. doi: 10.1016/j.bbrc.2020.01.111

38. Etemad S, Zamin RM, Ruitenberg MJ, Filgueira L. A novel *in vitro* human microglia model: Characterization of human monocyte-derived microglia. *J Neurosci Methods* (2012) 209(1):79–89. doi: 10.1016/j.jneumeth.2012.05.025

39. Ryan KJ, White CC, Patel K, Xu J, Olah M, Replogle JM, et al. A human microglia-like cellular model for assessing the effects of neurodegenerative disease gene variants. *Sci Transl Med* (2017) 9(421):eaai7635. doi: 10.1126/scitranslmed.aai7635

40. Albornoz EA, Amarilla AA, Modhiran N, Parker S, Li XX, Wijesundara DK, et al. SARS-CoV-2 drives NLRP3 inflammasome activation in human microglia through spike protein. *Mol Psychiatry* (2022). doi: 10.1038/s41380-022-01831-0

frontiers | Frontiers in Cellular Neuroscience

TYPE Original Research
PUBLISHED 22 March 2023
DOI 10.3389/fncel.2023.1094106

OPEN ACCESS

EDITED BY
Iliana Michailidou,
Leiden University Medical Center (LUMC), Netherlands

REVIEWED BY
Nawal Bahia El Idrissi,
Maastricht University, Netherlands
Paschalis Theotokis,
University General Hospital of Thessaloniki AHEPA, Greece

*CORRESPONDENCE
Owain W. Howell
✉ o.w.howell@swansea.ac.uk

†These authors have contributed equally to this work

SPECIALTY SECTION
This article was submitted to Cellular Neuropathology, a section of the journal Frontiers in Cellular Neuroscience

RECEIVED 09 November 2022
ACCEPTED 07 February 2023
PUBLISHED 22 March 2023

CITATION
Evans R, Watkins LM, Hawkins K, Santiago G, Demetriou C, Naughton M, Dittmer M, Rees MI, Fitzgerald D, Morgan BP, Neal JW and Howell OW (2023) Complement activation and increased anaphylatoxin receptor expression are associated with cortical grey matter lesions and the compartmentalised inflammatory response of multiple sclerosis. *Front. Cell. Neurosci.* 17:1094106. doi: 10.3389/fncel.2023.1094106

Complement activation and increased anaphylatoxin receptor expression are associated with cortical grey matter lesions and the compartmentalised inflammatory response of multiple sclerosis

Rhian Evans[1†], Lewis M. Watkins[1†], Kristen Hawkins[1], Gabriella Santiago[1], Constantinos Demetriou[1], Michelle Naughton[2], Marie Dittmer[3], Mark I. Rees[4], Denise Fitzgerald[2], B. Paul Morgan[5], James W. Neal[1] and Owain W. Howell[1*]

[1]Faculty of Medicine, Health and Life Sciences, Swansea University Medical School, Swansea, United Kingdom, [2]The Wellcome-Wolfson Institute for Experimental Medicine, Queen's University Belfast, Belfast, United Kingdom, [3]Centre for Experimental Medicine, Queen's University Belfast, Belfast, United Kingdom, [4]Faculty of Medicine and Health, The University of Sydney, Darlington, NSW, Australia, [5]School of Medicine, UK Dementia Research Institute Cardiff and Systems Immunity Research Institute, Cardiff University, Cardiff, United Kingdom

Background: The extent of cortical pathology is an important determinant of multiple sclerosis (MS) severity. Cortical demyelination and neurodegeneration are related to inflammation of the overlying leptomeninges, a more inflammatory CSF milieu and with parenchymal microglia and astroglia activation. These are all components of the compartmentalised inflammatory response. Compartmentalised inflammation is a feature of progressive MS, which is not targeted by disease modifying therapies. Complement is differentially expressed in the MS CSF and complement, and complement receptors, are associated with demyelination and neurodegeneration.

Methods: To better understand if complement activation in the leptomeninges is associated with underlying cortical demyelination, inflammation, and microglial activation, we performed a neuropathological study of progressive MS (n = 22, 14 females), neuroinflammatory (n = 8), and non-neurological disease controls (n = 10). We then quantified the relative extent of demyelination, connective tissue inflammation, complement, and complement receptor positive microglia/macrophages.

Results: Complement was elevated at the leptomeninges, subpial, and within and around vessels of the cortical grey matter. The extent of complement C1q immunoreactivity correlated with connective tissue infiltrates, whilst activation products C4d, Bb, and C3b associated with grey matter demyelination, and C3a receptor 1+ and C5a receptor 1+ microglia/macrophages closely apposed C3b labelled cells. The density of C3a receptor 1+ and C5a receptor 1+ cells was increased at the expanding edge of subpial and leukocortical lesions. C5a

receptor 1+ cells expressed TNFα, iNOS and contained puncta immunoreactive for proteolipid protein, neurofilament and synaptophysin, suggesting their involvement in grey matter lesion expansion.

Interpretation: The presence of products of complement activation at the brain surfaces, their association with the extent of underlying pathology and increased complement anaphylatoxin receptor positive microglia/macrophages at expanding cortical grey matter lesions, could represent a target to modify compartmentalised inflammation and cortical demyelination.

KEYWORDS

complement, demyelination, leptomeninges, microglia, inflammation

Introduction

Cortical demyelination and neurodegeneration are associated with a more severe and disabling multiple sclerosis (MS) (Calabrese et al., 2015; Absinta et al., 2020). Infiltrates of immune cells in the leptomeningeal and perivascular spaces, which are a feature of the broader compartmentalised inflammatory response that characterises established MS (Lassmann, 2019), associate with the extent of cortical pathology (Magliozzi et al., 2007; Reynolds et al., 2011; Lassmann, 2019; Kee et al., 2022). These cellular infiltrates represent an intrathecal source of soluble cytokines and inflammatory signals, which may activate microglia and astrocytes, so they become damaging to myelin or directly cytotoxic to neurons in the subpial and perivascular tissues (Gardner et al., 2013; Magliozzi et al., 2019b). Recognising the biological pathways associated with cortical pathology and compartmentalised inflammation will be important to guide future attempts to target such clinically meaningful aspects of MS pathology.

Inflammation of the leptomeninges and perivascular space is associated with gradients of tissue injury, detectable on advanced MRI and at autopsy, that represent substantial neuronal and glial alterations, and are most pronounced in the subpial tissue but extend through the depth of the cortical grey matter (GM) (Peterson et al., 2001; Magliozzi et al., 2010; Mainero et al., 2015; Griffiths et al., 2020; Junker et al., 2020). A transcriptomic and biochemical signature of inflammation, enriched for cytokines that support tissue-homing and lymphoid neogenesis, alongside complement proteins, characterise the cerebrospinal fluid (CSF) of cases with more extensive cortical GM lesions at diagnosis. A finding replicated in cases characterised by extensive cortical demyelination and leptomeningeal inflammation at post-mortem (Magliozzi et al., 2018, 2019a,b, 2020). Complement proteins (including C1q, C3), activation products (C4d) and their receptors, including anaphylatoxin receptors (C3aR1 and C5aR1), are located at subpial, leukocortical, white matter (WM) and deep GM areas in MS, where they associate with the extent of myelin and neuronal loss (Breij et al., 2008; Barnett et al., 2009; Ingram et al., 2014; Michailidou et al., 2015, 2017; Watkins et al., 2016; Loveless et al., 2018; Cooze et al., 2022). The concentration of complement proteins in the CSF differs between MS and non-inflammatory controls and between MS subtypes, disease severity and outcome (Aeinehband et al., 2015; Håkansson et al., 2020). Complement and complement receptors are essential to B: T-cell co-stimulation, monocyte: lymphocyte interactions and lymphocyte chemotaxis (West et al., 2018). Complement activation at the blood-CSF and CSF-brain barriers of the choroid epithelium, ependyma, pia mater and vascular endothelia are a feature of neuromyelitis optica, and complement activation is noted at the choroid plexus and in acute WM lesions in MS (Compston et al., 1989; Wayne Moore et al., 2016; Guo et al., 2017). It is not clear whether raised complement proteins in the CSF are accompanied by complement activation at CSF—blood brain barriers of the leptomeninges, pia and vasculature, or if complement activation at these brain barriers is associated with inflammatory changes in the underlying cortical GM.

Complement activation results in generation of anaphylatoxins C3a and C5a, which bind to G-protein-coupled anaphylatoxin receptors C3aR1 and C5aR1 (CD88) expressed by monocytes, macrophages, microglia, and some activated astrocytes (Müller-Ladner et al., 1996; Gasque et al., 1997, 1998; Ischenko et al., 1998). Complement anaphylatoxins are raised in MS CSF (Ingram et al., 2010; Håkansson et al., 2020) and CSF C5a levels and C5a inhibition in the CSF ameliorates blood-brain barrier disruption (Faustmann et al., 1995; Flierl et al., 2009). Activation of C3aR1 and C5aR1 on immune cells promote upregulation of functional pathways relevant to inflammation (including oxidative burst), the release of soluble chemoattractant and pro-inflammatory cytokines [including tumour necrosis factor α (TNFα) and interferon γ] and stimulates phagocytosis and metabolic dysfunction (Haas and van Strijp, 2007; Klos et al., 2009; Vandendriessche et al., 2021). The extent of experimentally induced demyelination and inflammation is enhanced in mice overexpressing C3a and C5a, and deletion of C5aR1 or the application of C5aR1 antagonists, reduces the severity of injury (Nataf et al., 1998, 1999; Ingersoll et al., 2010; Peterson et al., 2017). These findings indicate the potential value of targeting the C5a—C5aR1 axis to improve disease outcome.

To better understand the contribution of complement activation and anaphylatoxin receptor expressing cells to processes of compartmentalised inflammation and cortical pathology, our post-mortem study of MS investigated: (i) the presence of products of complement activation at the brain

surfaces (pia and around blood vessels of the cortex); (ii) the association between complement, microglial and astroglial activation and; (iii) differences in complement C3aR1 and C5aR1 positive cell numbers in areas of cortical demyelination in comparison to non-lesion and control GM samples. We found that complement at the brain surfaces associated with the extent of compartmentalised inflammation, cortical demyelination and complement anaphylatoxin receptor positive microglia at the expanding lesion edge. Collectively, our findings add to the weight of evidence implicating a key role for complement activation at the brain surface and complement-microglia interactions *via* C5aR1 to the pathological severity of MS.

Materials and methods

Post-mortem tissue

We used cryopreserved cortical tissue sections containing cortical GM and subcortical WM from regions of frontal, temporal and parietal lobes of the forebrain from post-mortem cases of progressive MS [n = 22; provided by the UK MS Tissue Bank (MSTB), Imperial College London], non-neurological disease controls (NNDC; n = 13), and inflammatory disease controls (n = 8; provided by the UK MSTB and Oxford tissue bank) with appropriate ethical approval (08/MRE09/31 + 5 and 13/WA/0292). Please see **Table 1** for further details and demographics.

Immunohistochemistry

Cryosections (8 μm thick) were incubated in hydrogen peroxide solution (Sigma-Aldrich), blocked with normal horse serum and incubated with the primary antibody overnight (**Table 2** contains details of primary antibodies used). Sections were then incubated with a biotinylated species-specific secondary antibody prior to the addition of a peroxidase-linked avidin-biotin complex (ABC Elite, Vector Laboratories Ltd.) and immunostaining visualised with diamino-benzidine (DAB; Immpact DAB, Vector Laboratories Ltd.) as the chromogen. If a second antigen was to be detected in a dual immunostaining experiment (e.g., C5aR1 and proteolipid protein; PLP), then sections were briefly heated in Tris-EDTA buffer (20 min in a bench top steamer following the completed detection and DAB chromogen development) to remove the first immune complexes, prior to the addition of the second primary antibody of interest in preparation for the biotinylated-secondary antibody and tertiary amplification using an alkaline-phosphatase linked reporter enzyme and Vector Blue as the chromogen (Bauer and Lassmann, 2014). Cells were counterstained with haematoxylin or cresyl violet. Dependent on the chromogen(s) used, sections were either rinsed in H_2O, dried, and mounted with VecaMount permanent mounting media (Vector labs.) or dehydrated through alcohol, cleared in xylene and depex mounted (Thermofisher Scientific). All sections from all cases were immunostained for a single or dual target as part of the same experiment and included primary antibody-negative controls and irrelevant species-specific antisera as positive controls. Images were taken with a Zeiss Axio Scope 1 at 100–630× magnification fitted with a Zeiss MRm 503 colour camera or with a Zeiss Axio Scanner 1 and handled in QuPath (Bankhead et al., 2017)[1] or FUJI.[2]

Neuropathological characterisation and quantitative analysis

For histological analysis, tissue was stained with luxol fast blue (LFB; ThermoFisher), and sequential sections immunohistochemically stained with anti- myelin oligodendrocyte protein (MOG) and anti- HLA-D. Cortical GM lesions were characterised based on their relative location (subpial, intracortical, leukocortical or cortex spanning—also termed type 4) and were further sub-categorised as chronic active or chronic inactive cortical GM lesions (no active lesions were noted) based on the presence of a visible rim of HLA-D and/or CD68+ microglia/macrophages (Peterson et al., 2001).

Areas of demyelination were measured from digitally scanned slides and lesions (GM or WM), total section and total GM and WM areas annotated and measured using QuPath. The percent area of demyelinated GM or WM was calculated relative to total grey or white matter in that sample and the mean percent lesion area per lesion type (subpial, cortex spanning—type 4 or leukocortical, WM lesion) calculated per case.

A manual quantification of GFAP and GFAP/C3b+ astrocytes was performed across the entire depth of the cortical GM, for each dual GFAP/C3b stained section. Six equal sized regions of interest (ROIs; total area 1.1 mm^2) were placed perpendicularly across the neocortex starting at the pial surface and extending to the grey/WM border, to capture a report of the density of cells at superficial, medial, and more distal points of the cortex. All measurements were acquired at the margins of the sulci to ensure consistency of data collection. The density of astrocytes was investigated in cortical samples from cases with subpial lesions, normal appearing GM and control cortex.

A rating of relative leptomeningeal and perivascular cellular infiltration was generated for each case which reflected the most significant cellular infiltrate in the leptomeninges and/or perivascular space from a minimum of eight separate cortical tissue blocks per case. The extent of leptomeningeal inflammation was scored semi-quantitatively as: absent = 0; mild (+); moderate (++) and substantial (+++, including aggregates resembling follicle-like structures) in accordance with (Choi et al., 2012; Bevan et al., 2018; see **Supplementary Figure 1**).

Microglia/macrophage quantification (HLA-D, CD68, C3aR, C5aR1) was performed within GM lesions, NAGM and control GM in anatomically matched regions of subpial and deep cortical GM. Four 200× (area 0.239 mm^2/field of view; Aperio, ImageScope) images were captured per lesion, anatomically matched NAGM and control GM. The number of immunopositive cells with an identifiable cell soma were quantified per ROI (average across the four fields of view) for comparison.

1 https://qupath.github.io/

2 https://imagej.nih.gov/ij/index.html

10.3389/fncel.2023.1094106

TABLE 1 Summary of MS, non-neurological disease controls, and inflammatory disease controls (Inflam) used in this study.

Case MS	Sex	Age of death	Cause of death	PMD (hours)	MS type	MS disease Duration (years)	MS inflam. (1–3)
MS402	M	46	MS	12	SPMS	20	+++
MS405	M	62	MS	12	SPMS	25	+
MS407	F	44	MS	22	SPMS	19	+++
MS408	M	39	MS	21	SPMS	10	++
MS422	M	58	MS	25	SPMS	13	++
MS423	F	54	MS	11	SPMS	30	++
MS425	F	46	MS	25	SPMS	21	+
MS438	F	53	MS	17	SPMS	18	+++
MS444	M	49	MS	18	SPMS	20	++
MS473	F	39	MS	9	PPMS	13	++
MS485	F	57	MS	24	PPMS	29	+
MS491	F	64	MS	9	SPMS	25	+
MS492	F	66	MS	15	PPMS	31	+
MS497	F	60	MS	26	SPMS	29	+++
MS510	F	38	MS	19	SPMS	22	+++
MS513	M	51	MS	17	SPMS	18	++
MS517	F	48	MS	12	PPMS	25	+
MS523	F	63	MS	20	SPMS	32	+
MS527	M	47	MS	10	SPMS	25	0
MS528	F	75	MS	17	SPMS	25	++
MS530	M	42	MS	15	SPMS	24	+++
MS538	F	61	MS	12	SPMS	39	++
***N* = 22 MS**	**8 M 14 F**	**53** years (38–75)		17 h (9–26)	4 PPMS 18 SPMS	23 years (10–39)	
Case Controls	**Sex**	**Age of death**	**Cause of death**	**PMD (hours)**			
CO25	M	35	Carcinoma of the Tongue	22			
12/023	M	69	Unknown	24			
12/046	M	72	Unknown	24			
12/048	F	65	Ovarian cancer	48			
12/052	F	42	Pancreatic cancer	48			
12/088	M	51	Cardiac arrest	24			
11/093	F	52	Chronic liver disease	48			
11/122	F	65	Unknown	24			
12/132	F	67	Unknown	48			
1231/93	M	58	Unknown	n/a			
***N* = 10 controls**	**5 M 5 F**	58 years (35–72)		34 h (22–48)			
Case Inflam	**Sex**	**Age of death**	**Cause of death**	**PMD (h)**			
B4938	M	18	HSV encephalopathy	n/a			
C2342	M	17	HIV encephalopathy	24			

(Continued)

TABLE 1 (Continued)

Case Inflam	Sex	Age of death	Cause of death	PMD (h)			
C3727	M	41	HIV encephalopathy	n/a			
C4178	M	59	CMV encephalopathy	n/a			
91/1343	M	32	Bronchopneumonia	48			
1140/95	F	65	Ischaemic encephalopathy	n/a			
1078/95	M	32	Ischaemic encephalopathy	24			
1062/00	F	49	Ischaemic encephalopathy	72			
***N* = 8 Inflam controls**	**6 M 2 F**	**40 years** (17–65)	**4 Viral encephalitis 4 Ischaemic stroke**	42 h (24–72)			

Sex, age at death, cause of death and post-mortem delay (PMD) are reported where available. In addition, for the MS cohort, disease subtype at death (either SP or PPMS), duration of disease from first symptom onset, and the relative extent of leptomeningeal and perivascular inflammation (MS inflam; graded 0–3, as described in the methods) are reported. Text in bold summarises the number of cases and column means (and range) for each cohort. CMV, cytomegalovirus; F, female; HIV, Human immunodeficiency virus; HSV, herpes simplex virus; M, male; PMD, post-mortem delay; PPMS, primary progressive MS; SPMS, secondary progressive MS.

TABLE 2 Primary antibodies used in this study.

Antigen	Host	Clone	Source
C1q	Rabbit	Polyclonal	Dako/agilent
C3b-iC3b	Mouse	C330	In-house (Cardiff University)
Fragment Bb	Mouse	Monoclonal IgG2	Pathway diagnostics
C4d	Mouse	Monoclonal IgG1	Pathway diagnostics
Myelin oligodendrocyte glycoprotein	Mouse	Y10	Imperial (Prof. Reynolds)
Proteolipid protein	Mouse	PLPC1	AbD Serotec/Merck
Human leukocyte antigens DP-DQ-DR	Mouse	Cr3/43	Dako/agilent
TMEM119	Rabbit	Polyclonal	Sigma
CD68	Mouse	KP1	Dako/agilent
Ionised calcium binding adapter molecule 1	Rabbit	Polyclonal	WAKO/Fujifilm
C5aR1/CD88	Rabbit	Polyclonal	BG Pharmingen
C3aR1	Mouse	hC3aRZ8	Hycult Biotech
Triggering receptor expressed on myeloid cells 2	Mouse	9D10	In-house (Cardiff University)
Microtubule associated protein 2	Mouse	Ap-20	Abcam
Neurofilament-H	Mouse	RT-97	Merck
Synaptophysin	Mouse	SY38	Merck
OLIG2	Rabbit	Polyclonal	Merck
Glial fibrillary acidic protein	Rabbit	Polyclonal	Dako/agilent
Tumour necrosis factor α	Goat	Polyclonal	R&D Systems
Inducible nitric oxide synthase	Mouse	2D2-B2	R&D Systems

Antibody name, target, clone, and source are listed.

Morphological analysis of complement receptor expressing microglia/macrophages was performed on cells from the same GML ROI used for quantitative analysis (above). A 4 × 4 grid was overlaid onto the images and the entire cell body of complement receptor immunopositive cells was encapsulated using the wand tool in FIJI,[3] whilst adjusting the threshold detection as necessary to

3 https://imagej.net/downloads

ensure best fit. Five immunopositive cells were selected at random from each of the four images per ROI, per case (20 cells per ROI, 6 separate ROIs per MS case). Captured cell morphology was measured using the shape descriptors: Area; perimeter and circularity [$4\pi \times (\text{Area})/(\text{perimeter})^2$]. All values per cell were plotted and compared by Kruskal–Wallis and Dunn's post-test.

Semi-quantitative scoring of complement immunostaining

Cases of progressive MS, neuroinflammatory disease controls and non-neurological disease controls were immunostained for complement component C1q and complement activation products C3b/iC3b (herein termed C3b), C4d and Bb. The extent of complement immunoreactivity for each individual complement marker was rated between 0 and 5, as assessed from 400× images captured in quadruplicate across each ROI per cortical block for each case for MS, non-neurological disease control and neuroinflammatory-disease control cases, respectively. An assessment of complement at the leptomeninges and subpial was determined by the relative extent of positive staining of the connective tissue, meningeal blood vessels, pia mater and the relative number of immunopositive cells in the underlying subpial. The rating of complement immunostaining of the blood vessels in the GM and WM included an assessment of vessel and perivascular staining and the maximum number of complement + cells immediately adjacent to the blood vessels (please see **Supplementary Table 1** for further details). Ratings were averaged per case for comparative analysis. Average case ratings were compared with the percent demyelination and connective tissue inflammation ratings for that case by non-parametric analysis as described in the results.

In situ hybridisation

To detect transcripts of complement C3 (NM_000064.4) we used a 50 fluorescein (FAM)-labelled 19mer antisense oligonucleotide containing locked nucleic acid (LNA) and 2'-O-methyl RNA moieties at a 1:2 ratio using a previously described approach (Budde et al., 2008; Watkins et al., 2016). Probes; antisense C3 (FAM-TaaTccAccAauCauTucT) and sense C3 (FAM-AgaAauGauUggUggAuuA; where capitals indicate LNA and lower case 2'-O-Methyl RNA in all instances; Eurogentec, Southampton, UK). Hybridisation and wash conditions were optimised so that all sense probes yielded essentially no signal; sense probe, and no probe controls, were included in each experiment. Probe detection was performed on 10 μm thick frozen sections prepared from two controls (13/011 and 13/073) and four MS cases (MS422, MS425, MS438, MS527). Hybridised probe was visualised with a peroxidase-conjugated goat anti-FAM (Vector Laboratories) and DAB prior to anti-TMEM119 immunostaining, with detection with an anti-rabbit biotinylated secondary and an ABC-alkaline phosphate tertiary complex with Vector Blue as the chromogen (Vector Labs.).

Generation of human monocyte-derived microglia-like cells

Peripheral blood mononuclear cells (PBMCs) were extracted from whole blood from healthy donors. Blood was layered onto an equal volume of lymphoprep (Stemcell Technologies) in 50 ml sterile falcon tubes, centrifuged at room temperature for 20 min at 2000 × *g*, and the buffy coat (layer containing PBMCs) was collected and gently transferred to a universal tube. The PBMCs were washed twice by centrifugation with pre-warmed media (RPMI-1640 with GlutaMax; Fisher Scientific), the pellet resuspended in 80 μl of ice-cold MACS buffer [phosphate buffered saline (PBS) containing 2% foetal bovine serum (FBS; Fisher Scientific)], and 20 μl CD14 magnetic microbeads (Miltenyi Biotec) added per 1×10^7 cells. Cells were sorted twice by positive selection using an autoMACS pro (Miltenyi Biotec), the resultant CD14+ monocytes resuspended in medium (RPMI-1640 with glutaMAX containing 10% FBS and 1% pen-strep; Fisher Scientific) and plated onto poly-L-lysine (100 μg/ml) coated 96-well plates, 100 μl/well, at a density of 1×10^5 cells/well and left to adhere for 24 h. Differentiation of CD14+ monocytes to microglia-like cells was achieved by incubation in the above medium containing 0.1 μg/ml IL-34 and 0.01 μg/ml granulocyte-macrophage colony-stimulating factor (Bio-Techne). Every other day, half the medium was aspirated and replaced with fresh cytokine containing medium. Cells were paraformaldehyde (PFA)-fixed for immunocytochemistry on day 10.

Generation of primary murine dissociated neural cultures

Dissociated cultures of primary murine CNS tissue were generated from whole brains of day seven postnatal C57BL/6 pups (Dittmer et al., 2018). All animal maintenance and experiments followed the UK home office and approved by the Universities ethics committee (Queen's University Belfast). Pups were sacrificed by decapitation, brain harvested, olfactory bulbs removed from the dissected whole brain tissue before cortical, cerebellar, and brain-stem tissue was minced, dissociated, washed and resuspended in mixed glial media (Dulbecco's modified essential media; 10% low endotoxin foetal calf serum; 1% pen-strep; 1% L-glutamine) at 6.67×10^5 cells/ml and seeded in 150 μl media per well (1×10^5 cells/well) onto poly-L-lysine coated (10 μg/ml; Sigma) black flat-bottom 96-well plates (Thermofisher). Once plated, cells were cultured at 37°C, 5% CO_2 for 5 days and medium was replenished on days 1, 3, and 5. Cell cultures were directly fixed with 4% PFA solution for 15 min after medium removal for immunocytochemistry as described (Dittmer et al., 2018).

Data handling and statistical analysis

Data was handled and visualised in GraphPad Prism (Version 9). D'Agostino-Pearson normality testing revealed the majority of the data to be non-parametric. Results were presented as box and whisker plots showing minimum to maximum values, interquartile range, and group medians. Two-group comparisons, for example, in comparing the extent of GM and WM demyelination,

were made using the non-parametric Mann–Whitney *t*-test. Three or more groups, for example, when comparing the semi-quantitative complement ratings from immunohistochemical analysis of leptomeningeal and pial/subpial tissue, perivascular sites of cortical GM and subcortical WM, relative to control and inflammatory disease controls, used the Kruskal–Wallis and Dunn's multiple adjusted post-tests. Associations between the extent of complement immunostaining and demyelination were investigated by Spearman's analysis. Statistical significance was set at $p < 0.05$ (*), $p < 0.01$ (**), $p < 0.001$ (***), and $p < 0.0001$ (****) .

Results

Complement is activated in brain connective tissue spaces and parenchyma and associates with the extent of compartmentalised inflammation and cortical demyelination

We sought to investigate the relationship between complement activation, compartmentalised inflammation, and demyelination in progressive MS. Our cohort of 22 progressive MS cases was representative of the inflammatory and actively worsening pathology of chronic disease. Cases harboured widespread microglia/macrophage activation, connective tissue infiltrates and displayed a variable abundance of cortical GM and subcortical WM demyelinating lesions (**Supplementary Figure 1** and **Table 1**). The median rating for connective tissue inflammation was ++ (range 0 to +++), with 6/22 (27.3%) cases rated +++ (substantial immune cell infiltration and/or tertiary lymphoid-like structures; **Supplementary Figures 1D, E**). The median percentage lesion area was 19.2% (range 0–88.3%) of total GM for GM lesions and 16.6% (0–77.4%) of total WM for WM lesions. There were 64 lesions in total, with 53 GM lesions and 11 WM lesions. Cortical GM lesions were predominantly characterised as chronic inactive (C/I), and 60.3% (32 of 53) GM lesions were subpial lesions (**Supplementary Figures 1F, G**).

Immunostaining revealed C1q and complement activation products in the choroid plexus, leptomeninges (including pia mater), and parenchyma of cortical GM and subcortical WM (**Figure 1**). Examples of complement recognition molecule C1q immunoreactivity decorating the choroid epithelium and vasculature, cells of the leptomeninges and parenchyma at subpial and perivascular sites of the underlying neocortex are shown (**Figures 1A–D**). Immunoreactivity for complement activation fragments Bb and C3b was variable, marking subpial and parenchymal sites near vessels of the GM (**Figures 1E"–H"**), in broad accordance with the pattern of demyelination (anti-MOG; **Figures 1E–H**) and the distribution and density of microglial/macrophages (anti- HLA-D; **Figures 1E'–H'**).

Microglial activation was associated with reactive morphological and phenotypic changes in astrocytes (**Figures 1I–K**). We observed GFAP/C3b+ astrocytes in close apposition with the glial limitans at subpial and perivascular sites of the progressive MS cortex (**Figures 1I, J**). C3b immunostaining was cytoplasmic, suggesting uptake of C3b-opsonised material, or the intracellular cleavage of C3 by astrocytes in the MS neocortex (**Figure 1K**). Quantification of GFAP and GFAP/C3b+ astrocytes in the normal appearing and demyelinated MS cortex revealed the loss of GFAP single positive astrocytes in areas of demyelination, whilst GFAP/C3b+ numbers were unchanged (**Supplementary Figure 2**) between control, non-lesioned, and lesioned GM.

Semi-quantitative rating of complement recognition molecule C1q and products of complement activation C4d (classical and lectin/mannose binding pathways to activation), Bb (alternative pathway) and C3b (all pathways; **Figure 2A**) revealed increased complement immunoreactivity in progressive MS cases in comparison to non-neurological disease controls and to inflammatory disease controls (which were selected based on the presence of an anatomically matched tissue block that in most cases, did not harbour sites of extensive inflammatory pathology; **Figures 2B–E** and **Supplementary Table 1**). The relative extent of C1q immunoreactivity was increased at perivascular sites in cortical and subcortical areas of MS brain (**Figure 2B**), whilst the extent of C4d, Bb, and C3b immunoreactivity was increased in comparison to control and inflammatory disease controls at leptomeningeal/pial sites, and at perivascular/parenchymal sites in the GM and WM (**Figures 2C–E**).

By comparing assessments of complement immunoreactivity to measures of leptomeningeal cellular infiltrates, and the relative area of cortical and subcortical demyelination, we show that the extent of C1q immunoreactivity of the meninges/subpial was correlated with connective tissue inflammation; C4d and Bb immunoreactivity at the meninges/subpial was correlated with cortical demyelination (% total GM), whilst increased Bb and C3b at perivascular sites in the cortical GM correlated with the extent of GM demyelination (Spearman $r \geq 0.43$, $p < 0.05$ in all instances; **Figure 2F**).

C3aR1 and C5aR1 expression was widespread and associated with complement activation in cortical grey matter lesions

We assessed C3aR1 and C5aR1 expression in samples of cortical GM (**Figure 3**). C5aR1+ amoeboid and ramified cells with a microglia/macrophage-like morphology of the cortical GM were associated with C3b immunoreactivity at the leptomeninges and perivascular spaces (**Figures 3A–C**). Resident (TMEM119+; blue reaction product) microglia were noted in close apposition to large cells expressing transcripts for C3 (brown reaction product), showing that some of this complement-specific signal is generated in the CNS (**Figure 3D**). Immunofluorescence revealed C5aR1+ cells near sites of C3b deposition (**Figures 3E–E"**). C3aR1 and C5aR1+ cells with a ramified, microglia-like morphology, were seen at variable densities across the demyelinated and normal- appearing cortical GM (**Figures 3F–I**).

Microglia/macrophages express complement anaphylatoxin C3a and C5a receptors

Frequently, cells with a microglia-like morphology, immunopositive for HLA-D and TMEM119, co-expressed

10.3389/fncel.2023.1094106

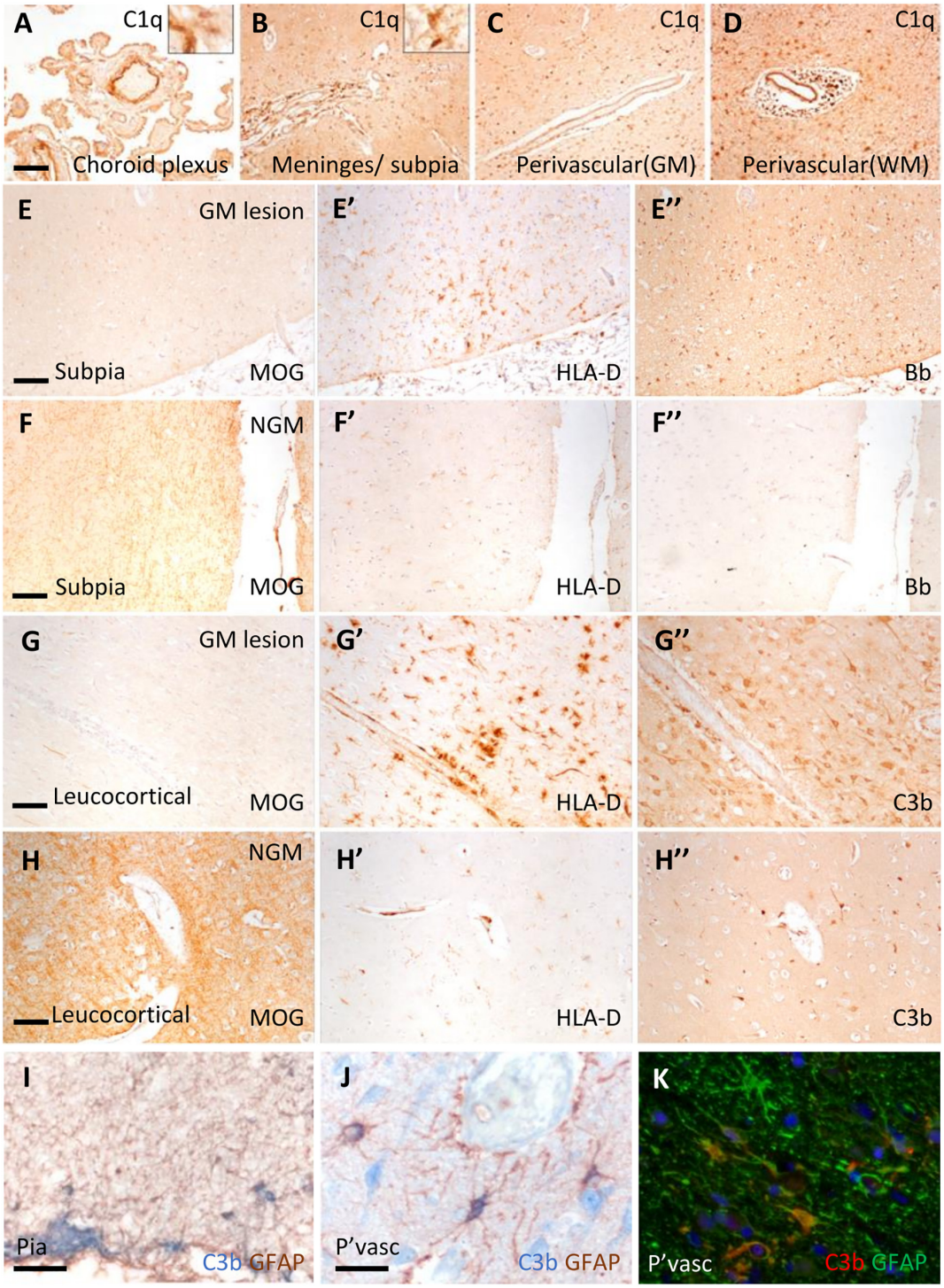

FIGURE 1
Complement recognition molecule C1q and activation products decorated brain barriers of the choroid plexus, leptomeninges, and perivascular spaces. Representative example of C1q immunostaining of the choroid plexus, leptomeninges, and perivascular cuffs and more diffusely in the tissue parenchyma of both the white (WM) and grey matter (GM; **A–D**). Complement Bb **(E–F")**, and C3b **(G–H")** immunoreactivity was elevated at sites of subpial and leukocortical GM lesions in comparison to normal appearing GM (NAGM; MOG and HLA-D immunostaining) from the same case **(E–E")**. Dual-immunostaining revealed C3b + subpial astrocytes (GFAP+) and neuron-like cells at the glial-limitans at vascular and subpial sites **(I,J)**. C3b + /GFAP + astrocytes in the deeper laminae of the cortical GM **(K)**. Scale bars panels **(A–D)** = 100 μm; panels **(E–I)** = 50 μm; panels **(J,K)** = 25 μm.

C3aR1 or C5aR1 (Figures 4A–C"). Some microglia-like cells were C3aR1+/C5aR1+ (Figures 4D–D"). Staining of human monocyte-derived microglia-like cells that express microglia/macrophage markers, such as TMEM119 and TREM2 (Figures 4E, F), showed a robust and near-ubiquitous co-expression of C3aR1 and C5aR1 (Figures 4G, H). We generated primary dissociated

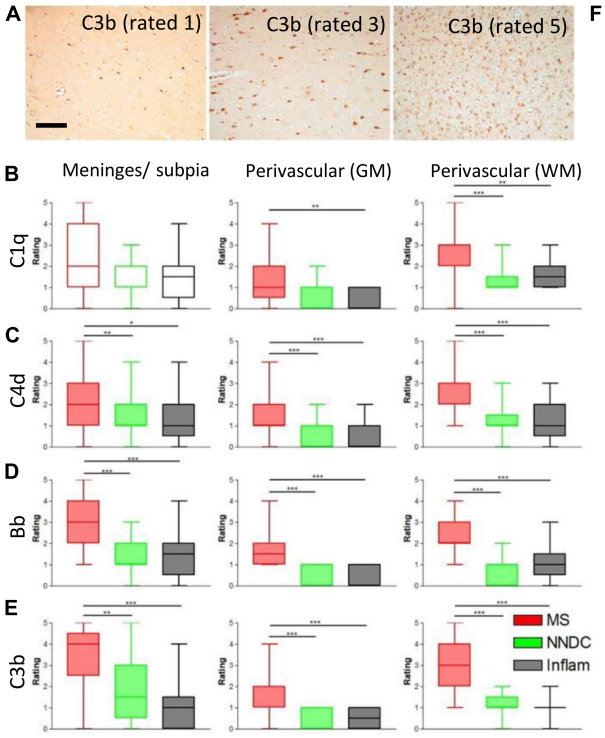

F

C1q	% Total DM	% Total GM DM	% Total WM DM	Inflammation (Meninges/ p'vasc)
Meninges/ subpia	r = 0.462 p = 0.034	r = 0.482 p = 0.027	r = 0.221 p = 0.335	r = 0.540 p = 0.014
P'vasc GM	r = 0.456 p = 0.037	r = 0.327 p = 0.147	r = 0.252 p = 0.27	
P'vasc WM	r = 0.149 p = 0.517	r = -0.069 p = 0.765	r = 0.249 p = 0.274	

C4d	% Total DM	% Total GM DM	% Total WM DM	
Meninges/ subpia	r = 0.699 p = 0.0004	r = 0.597 p = 0.004	r = 0.494 p = 0.022	r = 0.283 p = 0.222
P'vasc GM	r = 0.435 p = 0.048	r = 0.341 p = 0.129	r = 0.179 p = 0.436	
P'vasc WM	r = 0.182 p = 0.428	r = 0.226 p = 0.323	r = -0.066 p = 0.775	

Bb	% Total DM	% Total GM DM	% Total WM DM	
Meninges/ subpia	r = 0.632 p = 0.002	r = 0.539 p = 0.015	r = 0.612 p = 0.003	r = 0.034 p = 0.901
P'vasc GM	r = 0.596 p = 0.004	r = 0.535 p = 0.012	r = 0.415 p = 0.060	
P'vasc WM	r = 0.476 p = 0.028	r = 0.365 p = 0.103	r = 0.401 p = 0.070	

C3b	% Total DM	% Total GM DM	% Total WM DM	
Meninges/ subpia	r = 0.491 p = 0.023	r = 0.389 p = 0.081	r = 0.247 p = 0.278	r = 0.019 p = 0.847
P'vasc GM	r = -0.339 p = 0.132	r = 0.514 p = 0.017	r = -0.061 p = 0.789	
P'vasc WM	r = -0.171 p = 0.458	r = -0.392 p = 0.078	r = -0.057 p = 0.804	

FIGURE 2
Semi-quantitative assessment of complement immunoreactivity in the progressive MS neocortex. Examples of complement C3b immunostaining rated as mild (1/5), modest (3/5), and substantial (5/5; **A**). Region-matched cortical tissue blocks from 22 progressive MS, 10 non-neurological controls (green bars) and 6 inflammatory disease controls (grey bars) were assessed for complement C1q, C4d, Bb, and C3b immunoreactivity at the meninges/subpial (left column) and perivascular sites of the grey (GM, centre column) and white mater (WM, right column of graphs; **B–E**). The relative abundance of C1q in the meninges/subpial correlated with the extent of underlying cortical demyelination and leptomeningeal inflammation; **F**), whilst expression of complement activation products C4d and Bb associated with the extent of GM demyelination (% total GM DM), and Bb abd C3b at and adjacent to vessels of the GM (P'vasc GM) correlated with the extent of GM demyelination (**F**; Blue areas indicate correlations with significant results). Group medians were compared with Kruskal–Wallis and Dunn's multiple comparisons post-test and minimum and maximum values displayed. The extent of complement immunoreactivity was compared to GM pathology by Spearman correlation and *r*-values and *p*-values are shown for all comparisons. Pvasc, perivascular sites; % total DM, percent demyelination of the block, % total GM or WM, percent demyelination of the white or grey matter. Scale bar = 100 μm.

cultures from the neonatal mouse brain and confirmed a microglia/macrophage expression of C5aR1 (co-localised with IBA-1+ cells; Figures 4J', J"), whilst astrocytes (GFAP+), neurons (MAP2+), and oligodendrocyte-lineage cells (Olig2+) were negative for anti-C5aR1 immunoreactivity (Figures 4I–J"') in day 5 cultures. As anticipated, these cultures represented a reliable source of expanding numbers of glial and neuronal cell populations (Supplementary Figure 3; Dittmer et al., 2018).

The density of C5aR1 positive microglia/macrophages is increased at the expanding cortical grey matter lesion edge

We next sought to quantify the density of C3aR1 and C5aR1+ cells in subpial and leukocortical lesions (Figure 5). The density of HLA-D+ and CD68+ microglia/macrophages was increased at the lesion centre and edge of deep lying (leukocortical) GM lesions in comparison to anatomically matched control GM (Figures 5A, B), reflecting the chronic active inflammatory component of many of these lesions (Figures 5A–F). The density of HLA-D+ and CD68 microglia/macrophages was also increased at the edge of subpial lesions in comparison to control GM. The number of C3aR1+ microglia/macrophages per field of view were elevated at the GM lesion centre in comparison to control GM and normal appearing GM. There was no significant difference in the density of C3aR1+ microglia/macrophages between the different regions of interest in the subpial GM (Figures 5G, I, K).

The greatest increase in quantity of C5aR1+ microglia/macrophages was noted at the GM lesion edge of both leukocortical and subpial GM lesions, where additionally, the number of C5aR1+ cells also differed between the leukocortical GM lesion centre and control GM (Figures 5H, J, L).

Complement anaphylatoxin receptor positive microglia/macrophages are associated with myelin and neuronal damage

Microglia/macrophages undergo morphological and phenotypic alterations in disease settings. We investigated the morphology of C5aR1+ microglia/macrophages at the

10.3389/fncel.2023.1094106

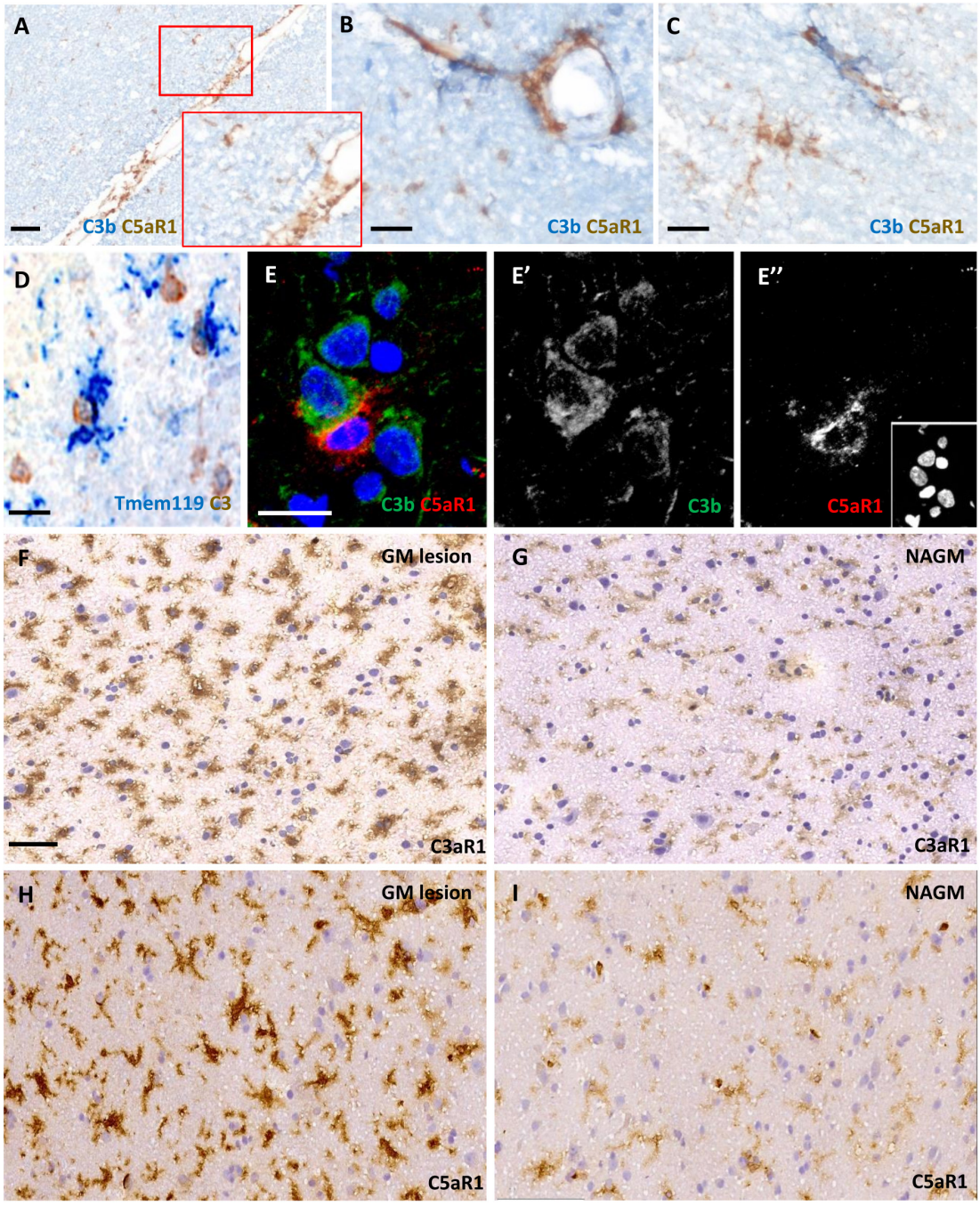

FIGURE 3
Anaphylatoxin receptor expression at sites of complement activation. Complement C3b (blue reaction product) and C5aR1 + cells (brown reaction product) and subpial and perivascular sites of the cortical GM **(A–C)**. TMEM119 + immunopositive microglia (blue) in close contact with large neuron-like cells expressing C3 transcript **(D)** and an example of a C5aR1 + cell contacting a C3b immunoreactive cortical neuron **(E–E")**. Immunostaining revealed an elevated number and more darkly stained C3aR1 and C5aR1 + cells with a microglia-like morphology in the demyelinated cortical GM (GM lesion; **F,H**) in comparison to adjacent normal appearing GM (NAGM; **G,I**). Scale bars; panels **(A,F–I)** = 50 μm and panels **(B–E")** = 20 μm.

cortical GM lesion edge and centre in comparison to the paired normal appearing GM from the same case (Figures 6A–C). C5aR1+ microglia/macrophages had an altered morphology; they were larger, with a greater perimeter and more rounded (more macrophage-like) in GM lesion edge and centre regions in comparison to anatomically matched normal appearing GM (Figures 6D–F). C5aR1+ microglia/macrophages were immunopositive for inducible nitic oxide synthase (iNOS; 6G and inset), TNFα (Figure 6H and inset), and those at or near inflammatory demyelinating lesions of the progressive MS cortex were associated with inclusions of debris-like material that stained immunopositive for PLP, non-phosphorylated neurofilament (heavy chain) and synaptophysin (Figure 6I).

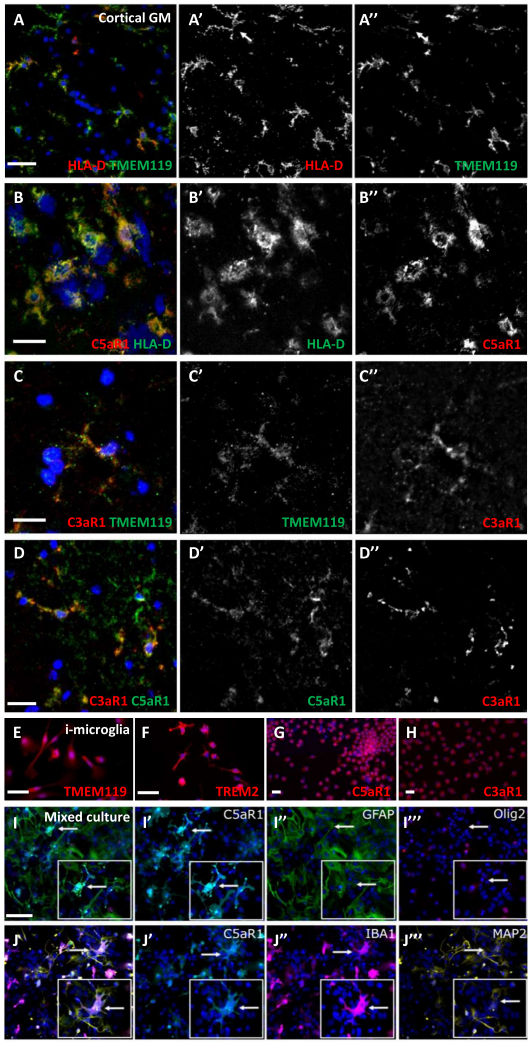

FIGURE 4
Microglia/macrophages express complement anaphylatoxin C3a and C5a receptors. C5aR1 microglia/macrophages were seen in the cortical GM in association with TMEM119 **(A–A")** and HLA-D **(B–B")**, and an example of C3aR1 + /TMEM119 + **(C–C")**. Dual C3a/C5aR1 immunostaining showing co-positive C3aR1/C5aR1 cells **(D–D")**. Human monocyte-derived microglia-like cells (i-microglia) were cultured for 10 days *in vitro* and expressed TMEM119 **(E)**, TREM2 **(F),** and C3aR1 and C5aR1 **(G,H)**. Multiplex immunocytochemistry of primary cultures from neonatal mouse brains revealed C5aR1 expression was associated with IBA-1 + microglia but not astrocytes, oligodendrocyte precursor cells (GFAP+, Olig2+, respectively, **I–J")** or neurons (MAP2 + ; **J"'**, arrows represent cells shown in inserts) in day 5 cultures. Scale bars = 20 μm.

Discussion

We describe the presence of products of complement activation in the leptomeninges, perivascular spaces and parenchyma of MS characterised by extensive cortical demyelination and compartmentalised inflammation. The presence of complement activation proteins from both classical and alternative pathways implies complement activation at the CSF-brain barriers is ongoing throughout the disease process, which was in excess of 30 years in some cases. The localisation of complement activation proteins on damaged neurons, myelin and synapses is well described in the MS literature, but the relationship between complement activation at the brain barriers and changes in parenchymal, resident cell populations, such as microglia/macrophages, and the severity of GM and WM pathology is not clearly defined. Complement anaphylatoxin receptor positive cells (C3aR1 and C5aR1) were increased in density at, or near, cortical demyelinating lesions. C5aR1+ microglia/macrophages associated with ongoing expansion of both subpial and leukocortical GM lesions, displayed an altered morphology, expressed TNFα, iNOS and contained puncta immunoreactive for PLP, neurofilament and synaptophysin antigens. The generation of anaphylatoxin peptides associated with activated, proinflammatory microglia/macrophages and ongoing phagocytosis of neural and oligodendrocyte membranes suggests the C5a/C5aR1 axis may represent a treatment target to abrogate compartmentalised inflammation and cortical pathology in progressive MS.

Compartmentalised inflammation drives disease worsening independently of acute clinical relapses and inflammatory lesions (Cree et al., 2019). The compartmentalised inflammatory response is composed of activated immune cells in the parenchyma, reactive microglia and astroglia, increased numbers of leptomeningeal and connective tissue T and B lymphocytes, long-lived plasma cells, and elevated levels of circulating cytokines in the CSF (Lassmann, 2019). An overtly inflammatory CSF cytokine profile is associated with a more severe MS at presentation and follow-up, and pathologically, is linked to subpial tissue damage in a gradient-like pattern, which can be replicated in experimental models by the induced expression of inflammatory cytokines in the leptomeninges (Magliozzi et al., 2010, 2018, 2020; Gardner et al., 2013; James Bates et al., 2022). The levels of complement proteins, including C1q, C2, C4, and C5 in MS CSF and serum are altered in comparison to healthy individuals and between different MS clinical subtypes (Sellebjerg et al., 1998; Jongen et al., 2000; Finehout et al., 2005; Stoop et al., 2008; Ingram et al., 2010; Aeinehband et al., 2015; Magliozzi et al., 2019a; Zelek et al., 2019). Complement, together with serum proteins, including fibrin, represent effector proinflammatory molecules with the potential to signal across the CSF- brain barriers to activate microglia and astrocytes (Faustmann et al., 1995; Davalos et al., 2012; Ryu et al., 2015; Lee et al., 2018). Only a small number of prior studies have investigated the presence of complement proteins and activation products at the key CSF- and blood- brain barrier sites of pathological samples of MS (Wayne Moore et al., 2016; Guo et al., 2017). We show the widespread localisation of C1q, C4d, Bb, and C3b at the choroid plexus, ventricular ependyma and a relative increase at leptomeningeal and parenchymal vessels, which associated with the extent of cortical GM pathology. Therefore, complement deposition and activation at the pia and perivascular sites represents a component of the compartmentalised inflammatory response in MS, which is positioned to stimulate inflammation, lead to disruption of essential brain barriers, and support the formation or expansion of GM lesions by triggering local microglia and astrocytes.

The relative extent of complement immunoreactivity correlated modestly with the degree of leptomeningeal cellular infiltration and the extent of cortical GM demyelination (**Figure 2**), whilst parenchymal C3b immunoreactivity has been associated with activated microglia in the medial thalamus, another structure which lies close to CSF-filled spaces in the brain (Cooze et al., 2022).

10.3389/fncel.2023.1094106

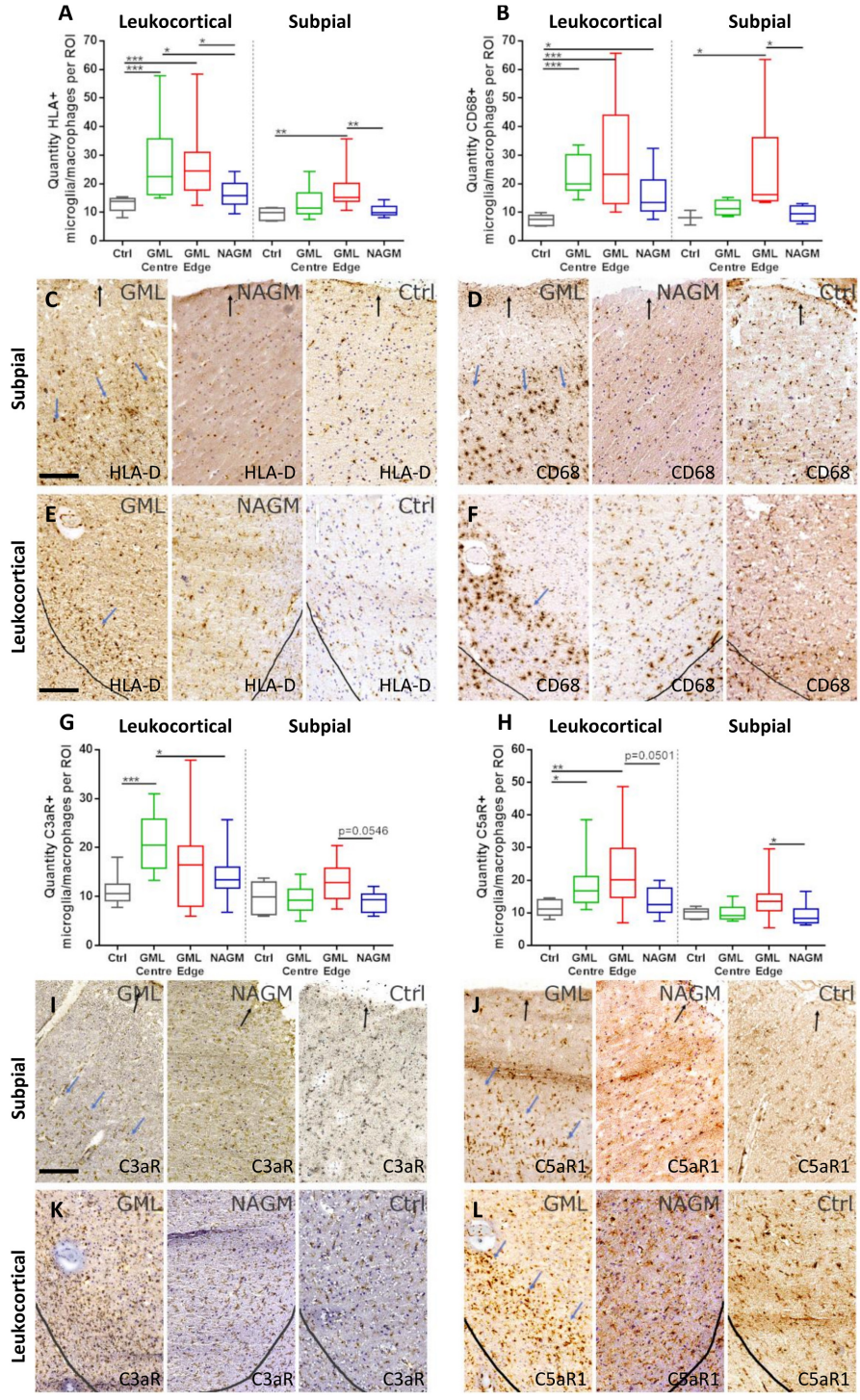

FIGURE 5

C5aR1 + microglia/macrophages are increased in density at the expanding grey matter lesion edge. Microglia/macrophages immunopositive for activation markers HLA-D and CD68 were quantified in leukocortical and subpial GM lesions **(A,B)**. The density of immunostained cells were significantly increased at the centre and edge, and at the edge of GM lesions, respectively, for both markers compared to non-neurological control GM at matched anatomical cortical level **(A,B)**. Examples of HLA-D **(C,E)** and CD68 **(D,F)** immunostaining in GM lesion (GML), normal appearing GM (NAGM), and control (ctrl). Quantification of C3aR1 + microglia/macrophages revealed a significant increase in quantity at the centre of deep cortical GM lesions compared to controls and NAGM and there were no significant changes in subpial GM lesions **(G,I,K)**.
C5aR1 + microglia/macrophages were significantly elevated at the GM lesion centre and edge of leukocortical GM lesions compared to control GM, and at the GM lesion edge of subpial lesions compared to NAGM **(H,J,L)**. Blue arrows represent the expanding lesion edge of leukocortical and subpial lesions. Black arrows show the pial surface and grey lines represent the grey/white matter border. Data compared by Kruskal–Wallis and Dunn's multiple comparison post-test. Scale bars = 100 μm.

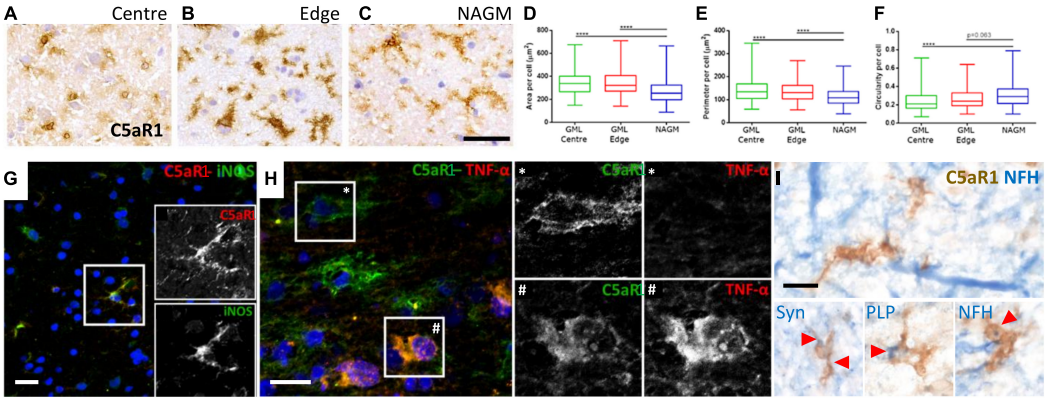

FIGURE 6
Activated C5aR1 + microglia/macrophages in cortical grey matter lesions. C5aR1 + microglia/macrophages in the centre or at the edge of subpial lesions display an altered morphology **(A–C)** and were quantifiably larger in area **(D)**, with a smaller perimeter **(E)**, and were more circular **(F)**, in comparison to C5aR1 + cells of the paired normal appearing GM (NAGM). C5aR1 + microglia/macrophages in a chronic active cortical GM lesion (case MS438) demonstrating dual-immunostaining for iNOS (**G** and inset), and TNFα (**H** and inset *, #). C5aR1 + microglia-like cells (brown immunostain) in close apposition to neurofilament-H + neurites (blue reaction product; **I**) or associated with inclusions of neuronal (synaptophysin, Syn +) and myelin (PLP +) products of degeneration. Scale bars, panels **(A–H)** = 25 μm; panel **(I)** = 10 μm.

Infiltrating lymphocytes are a source of complement proteins in the subarachnoid space (Stahel et al., 1997) and the density of leptomeningeal infiltrates correlates closely with the degree of inflammation, demyelination, and neuro-axonal loss in the MS neocortex, cerebellum, and spinal cord (Magliozzi et al., 2007; Howell et al., 2011, 2015; Reali et al., 2020). The intrathecal activation of the classical (C1q, C4d) and alternative (Bb) pathways generates C3- and C5-convertases essential for the synthesis of the potent soluble anaphylatoxin fragments, which are also elevated in MS CSF (Ingram et al., 2010; Håkansson et al., 2020). The soluble complement anaphylatoxins can activate chemotactic, protective and neuron damaging functional pathways in microglia/macrophages and other cells by engaging with C3aR1 and C5aR1 (Woodruff et al., 2006; Ingersoll et al., 2010; Pavlovski et al., 2012). In addition, C3b-iC3b on cell surfaces is the ligand for complement receptor 3 (CR3, CD11b, MAC-1)-mediated phagocytosis and is important in mediating processes of synapse removal during development and in disease (Salter and Stevens, 2017). The phagocytosis of neural membranes and synapses labelled with C1q-C3 by activated microglia is seen in MS and its models, where reducing complement activation or increasing its clearance, protects neurites and synapses and preserves neurological function (Hammond et al., 2020; Werneburg et al., 2020; Gharagozloo et al., 2021; Ramaglia et al., 2021). Therefore, complement activation in the vicinity of resident microglial could be an important component mediating the extensive damage and loss of synapses, neurites and neurons of the cortical GM, which is a key component to the irreversible clinical worsening of progressive MS (Peterson et al., 2001; Magliozzi et al., 2010; Jürgens et al., 2016).

Several studies have documented the increased number of C3aR1 and C5aR1 cells in MS lesions (Gasque et al., 1998; Ischenko et al., 1998; Ingram et al., 2014), including cortical GM lesions (Watkins et al., 2016; Loveless et al., 2018). However, the identity of the cells most widely expressing the anaphylatoxin receptors, or their relative contribution to the extent of inflammation and demyelination, has not been clarified. Alongside a robust expression on myeloid lineage cells (Klos et al., 2013), earlier reports demonstrated anaphylatoxin receptor expression (both C3aR1 and C5aR1) on neurons, astrocytes and endothelia (Gasque et al., 1997, 1998; Ischenko et al., 1998; Davoust et al., 1999; Stahel et al., 2000; Farkas et al., 2003; Brennan et al., 2015). In MS, the expression appears restricted to myeloid cells, including microglia, and activated astrocytes (Müller-Ladner et al., 1996; Ischenko et al., 1998). We confirmed C3aR1 and C5aR1 expression by HLA-D+ and TMEM119 microglia/macrophages. Note that TMEM119 expression is downregulated in activated, non-homeostatic microglia, such as those found at the chronic active lesion edge (Zrzavy et al., 2017; Vankriekelsvenne et al., 2022). We did not anaphylatoxin receptor expression on cortical astrocytes, cells that are phenotypically and morphologically diverse and distinct from astrocytes of the WM (Oberheim et al., 2009; Schirmer et al., 2019). We confirmed a specific microglia/macrophage pattern of C3aR1 and C5aR1 expression in primary mouse dissociated cultures and induced human microglia-like cells. Induced human microglia-like cells expressed TMEM119 and TREM2 and are a useful source of human-derived cells for the analysis of microglial/macrophage biology (Sellgren et al., 2019). Microglia expressing TREM2 are associated with phagocytosis of apoptotic neurons and the subsequent loss of homeostatic function and the adoption of a neurodegenerative phenotype, which associated with neuronal loss (Krasemann et al., 2017). Reducing TREM2 expression on microglia attenuates inflammation and is protective against neurodegenerative pathology (Leyns et al., 2017). Therefore, our demonstration of the expression of TREM2, TMEM119 together with C3aR/C5aR1, is consistent with a population of reactive microglia that have lost some homeostatic functions and acquired detrimental phenotypic features.

It is important to note that complement can elicit a range of protective as well as damaging responses in the CNS. For example, C3a/C3aR1 and C5a/C5aR1 axis activation is reported to protect cultured neurons from excitotoxic death (van Beek et al., 2001; Mukherjee et al., 2008) and is associated with the induced release of neurotrophins, cell survival and enhanced neurogenesis, in some settings (Jauneau et al., 2006; Haynes et al., 2013;

Westacott et al., 2021); whilst C3a and C5a overexpressing mice displayed similar rates of remyelination (Ingersoll et al., 2010), although presenting larger and more inflammatory demyelinating lesions. More work clearly needs to be done to fully understand the role of C3aR1 and C5aR1 activation at all stages of MS. A third receptor C5aR2 (C5L2 or GPR77), is less well characterised and regarded as a scavenger or default receptor competing with C5aR for C5a binding. The functional role for C5aR2 and its relationship to the intracellular signalling pathways regulating inflammation remains to be determined (Ward, 2009; Klos et al., 2013); expression of C5aR2 was not investigated in this study.

The borders of leukocortical and subpial GM lesions were demarcated by elevated numbers of HLA-D and CD68 + cells, which were mirrored by an increased number of C3aR1 and C5aR1+ microglia/macrophages. Previously, we have shown that the number of C1q and Bb immunopositive cells in MS leukocortical lesions correlated with the density of HLA-D+ and C5aR1+ microglia (Watkins et al., 2016). Our current findings implicate circulating as well as locally generated complement, to be playing a role in driving pathology in both subpial and deeper cortical laminae. C5aR1+ microglia within a chronic active GM lesion demonstrated subtle morphological alterations consistent with a transition of process bearing microglia to a more rounded and simpler morphological state (**Figure 5**), reminiscent of IBA-1+ microglia that associate with a more profound cortical pathology in progressive MS (van Olst et al., 2021). C5aR1+ microglia/macrophages in MS cortical GM co-stained for iNOS and TNFα and demonstrated cytoplasmic PLP, neurofilament + and synaptophysin + phagocytosed material and were in close proximity to C3b+ stressed/damaged cortical neurons (**Figure 3**; Watkins et al., 2016), suggesting that some of these cells contribute to worsening tissue damage.

C5aR1 activation, *via* the induced production of interferon γ and TNFα by macrophages and other monocytes (Pandey et al., 2017; Serfecz et al., 2021), may be one mechanism by which activated complement elicits damage. The induced expression of such cytokines can be blocked with the brain penetrant C5aR1 inhibitor PMX53 (Serfecz et al., 2021). Other small molecule antagonists of C5aR1 are effective in abrogating neuroinflammation, inflammasome activation and neurodegeneration *in vivo*, are brain penetrant and non-toxic. Eculizumab, a monoclonal antibody approved for use in paroxysmal nocturnal hemoglobinuria, prevents C5 convertase cleaving C5 into C5a. Trials of eculizumab in neuromyelitis optica have been encouraging (Pittock et al., 2019). Avdoralimab, a monoclonal antibody designed to block C5a binding to C5aR1, can prevent neutrophil migration into lungs and blocked inflammatory cytokine release in COVID-19 infection (Woodruff and Shukla, 2020). Therefore, these distinct pharmaceutical approaches to reduce C5aR1 activation may represent useful mechanisms to modulate resident microglia and other C5aR1 expressing cells in MS (Vergunst et al., 2007; Michailidou et al., 2018; Carpanini et al., 2019; Schartz and Tenner, 2020).

Cultured astrocytes and microglia can be induced to synthesise complement components, including C1q, C3, and factor B, when exposed to CSF from lymphotoxin-α treated rats. Lymphotoxin-α is elevated in concentration in the MS CSF and when over-expressed in the leptomeninges, recapitulates the pattern of subpial demyelination seen in disease (James Bates et al., 2022). Therefore, complement activation in the connective tissue spaces and parenchyma can stimulate the production of TNFα and other pleiotropic cytokines, which can be directly cytotoxic (and differentially expressed in cases characterised by leptomeningeal inflammation and more extensive cortical demyelination) (Magliozzi et al., 2019b; Picon et al., 2021), whilst cytokine release by activated glia can further drive the transcription of genes encoding early complement proteins. Future work, for example, could assess the effect of blocking C5aR1 activation in models of leptomeningeal inflammation and subpial cortical demyelination.

Microglia can induce a reactive astrocyte response *in vitro*, in part requiring IL-1β, TNFα and C1q, that is associated with a neuroinflammatory and non-homeostatic response and the elevated transcription of C3 and other signature genes (Liddelow et al., 2017). C3+ astrocytes are seen in actively demyelinating MS WM lesions and C3b+ astrocytes, some with a dysmorphic appearance, were frequently observed in subpial and peri-vascular sites in our MS GM (**Supplementary Figure 2**). The expression of C3 is not by itself an indicator of the neurotoxic potential of an astrocyte and such findings should be treated cautiously (Escartin et al., 2021). Indeed, we found the density of C3b+ astrocytes were unchanged between control and MS, whilst conversely, the density of C3b-/GFAP+ astrocytes were significantly reduced at subpial and perivascular GM lesions. These data demonstrate alterations in astrocytes occur in association with complement activation at or near the cortical GM.

Our current study is limited by the non-availability of neuroinflammatory disease control tissues harbouring frank inflammatory lesions in the selected blocks of interest, which were chosen as they anatomically matched the available MS blocks. A further limitation was that the assessment of complement immunostaining was performed semi-quantitatively and was not automated. The presence of staining artefacts of the delicate leptomeninges could be recognised by the investigator but was challenging to quantify digitally.

Conclusion

The presence of elevated levels of complement C1q, C3b, C4d, and Bb, and the release of anaphylatoxins that engage C3aR1 and C5aR1 expressed by microglia, may stimulate functional pathways leading to the induced expression of inflammatory cytokines and phagocytic processes in the MS grey matter. Therefore, complement activation of anaphylatoxin receptor bearing microglia/macrophages represents a modifiable pathway to abrogate the extent of compartmentalised inflammation and cortical grey matter pathology to improve the outcome for some people with progressive MS.

Data availability statement

The original contributions presented in this study are included in the article/**Supplementary material**, further inquiries can be directed to the corresponding author.

Ethics statement

The studies involving human participants were reviewed and approved by the South Wales Research Ethics Committee (study numbers 08/MRE09/31+5 and 13/WA/0292). The patients/participants provided their written informed consent to participate in this study.

Author contributions

RE, LW, BM, JN, and OH: methodology, investigation, writing – original draft, review and editing, and funding. KH, GS, CD, MN, and MD: methodology, investigation, and writing – review and editing. MR and DF: resources and writing – review and editing. All authors contributed to the article and approved the submitted version.

Funding

This work was supported by funds from the MacDaid Fellowship, Worshipful Livery Company of Wales, the Life Science Research Network Wales, the UK Multiple Sclerosis Society, and the Research Wales Innovation Fund and the *BRAIN* Unit Infrastructure Award (Grant no: UA05; funded by Welsh Government through Health and Care Research Wales).

Acknowledgments

We would like to thank Dr. Djordje Gveric and the team of the UK MS Society Tissue Bank [The Multiple Sclerosis Society Tissue Bank is funded by the Multiple Sclerosis Society of Great Britain and Northern Ireland (registered charity 207495)], and Drs. Carolyn Sloan and Marie Hamard at the Oxford Brain Bank (supported by the Medical Research Council, Brains for Dementia Research, Alzheimer's Society and Alzheimer's Research UK, Autistica UK and the NIHR Oxford Biomedical Research Centre).

Conflict of interest

The authors declare that the research was conducted in the absence of any commercial or financial relationships that could be construed as a potential conflict of interest.

The handling editor declared a past co-authorship/collaboration (DOI: 10.1159/000524587) with the author BM.

Publisher's note

All claims expressed in this article are solely those of the authors and do not necessarily represent those of their affiliated organizations, or those of the publisher, the editors and the reviewers. Any product that may be evaluated in this article, or claim that may be made by its manufacturer, is not guaranteed or endorsed by the publisher.

Supplementary material

The Supplementary Material for this article can be found online at: https://www.frontiersin.org/articles/10.3389/fncel.2023.1094106/full#supplementary-material

References

Absinta, M., Lassmann, H., and Trapp, B. (2020). Mechanisms underlying progression in multiple sclerosis. *Curr. Opin. Neurol.* 33, 277–285.

Aeinehband, S., Lindblom, R., Al Nimer, F., Vijayaraghavan, S., Sandholm, K., and Khademi, M. (2015). Complement component C3 and butyrylcholinesterase activity are associated with neurodegeneration and clinical disability in multiple sclerosis. *PLoS One* 10:e0122048. doi: 10.1371/journal.pone.0122048

Bankhead, P., Loughrey, M., Fernández, J., Dombrowski, Y., McArt, D., Dunne, P., et al. (2017). QuPath: open source software for digital pathology image analysis. *Sci. Rep.* 7:16878.

Barnett, M., Parratt, J., Cho, E., and Prineas, J. (2009). Immunoglobulins and complement in postmortem multiple sclerosis tissue. *Ann. Neurol.* 65, 32–46.

Bauer, J., and Lassmann, H. (2014). Neuropathological techniques to investigate central nervous system sections in multiple sclerosis. *Methods Mol. Biol.* 1304, 211–229.

Bevan, R., Evans, R., Griffiths, L., Watkins, L., Rees, M., Magliozzi, R., et al. (2018). Meningeal inflammation and cortical demyelination in acute multiple sclerosis. *Ann. Neurol.* 84, 829–842.

Breij, E., Brink, B., Veerhuis, R., van den Berg, C., Vloet, R., Yan, R., et al. (2008). Homogeneity of active demyelinating lesions in established multiple sclerosis. *Ann. Neurol.* 63, 16–25.

Brennan, F., Gordon, R., Lao, H., Biggins, P., Taylor, S., Franklin, R., et al. (2015). The complement receptor C5aR controls acute inflammation and astrogliosis following spinal cord injury. *J. Neurosci.* 35, 6517–6531. doi: 10.1523/JNEUROSCI.5218-14.2015

Budde, B., Namavar, Y., Barth, P., Poll-The, B., Nürnberg, G., Becker, C., et al. (2008). tRNA splicing endonuclease mutations cause pontocerebellar hypoplasia. *Nat. Genet.* 40, 1113–1118.

Calabrese, M., Magliozzi, R., Ciccarelli, O., Geurts, J., Reynolds, R., and Martin, R. (2015). Exploring the origins of grey matter damage in multiple sclerosis. *Nat. Rev. Neurosci.* 16, 147–158. doi: 10.1038/nrn3900

Carpanini, S., Torvell, M., and Morgan, B. (2019). Therapeutic inhibition of the complement system in diseases of the central nervous system. *Front. Immunol.* 10:362. doi: 10.3389/fimmu.2019.00362

Choi, S., Howell, O., Carassiti, D., Magliozzi, R., Gveric, D., Muraro, P., et al. (2012). Meningeal inflammation plays a role in the pathology of primary progressive multiple sclerosis. *Brain* 135(Pt 10), 2925–2937. doi: 10.1093/brain/aws189

Compston, D., Morgan, B., Cambell, A., Wilkins, P., Cole, G., Thomas, N., et al. (1989). Immunocytochemical localization of the terminal complement complex in multiple sclerosis. *Neuropathol. Appl. Neurobiol.* 15, 307–316. doi: 10.1111/j.1365-2990.1989.tb01231.x

Cooze, B., Dickerson, M., Loganathan, R., Watkins, L., Grounds, E., Pearson, B., et al. (2022). The association between neurodegeneration and local complement activation in the thalamus to progressive multiple sclerosis outcome. *Brain Pathol.* 32:e13054. doi: 10.1111/bpa.13054

Cree, B., Hollenbach, J., Bove, R., Kirkish, G., Sacco, S., Caverzasi, E., et al. (2019). Silent progression in disease activity–free relapsing multiple sclerosis. *Ann. Neurol.* 85, 653–666. doi: 10.1002/ana.25463

Davalos, D., Ryu, J., Merlini, M., Baeten, K., Le Moan, N., Petersen, M. A., et al. (2012). Fibrinogen-induced perivascular microglial clustering is required for the

development of axonal damage in neuroinflammation. *Nat. Commun.* 3:1227. doi: 10.1038/ncomms2230

Davoust, N., Jones, J., Stahel, P., Ames, R., and Barnum, S. (1999). Receptor for the C3a anaphylatoxin is expressed by neurons and glial cells. *Glia* 26, 201–211.

Dittmer, M., Young, A., O'Hagan, T., Eleftheriadis, G., Bankhead, P., Dombrowski, Y., et al. (2018). Characterization of a murine mixed neuron-glia model and cellular responses to regulatory T cell-derived factors. *Mol. Brain* 11:25. doi: 10.1186/s13041-018-0367-6

Escartin, C., Galea, E., Lakatos, A., O'Callaghan, J., Petzold, G., Serrano-Pozo, A., et al. (2021). Reactive astrocyte nomenclature, definitions, and future directions. *Nat. Neurosci.* 24, 312–325. doi: 10.1038/s41593-020-00783-4

Farkas, I., Takahashi, M., Fukuda, A., Yamamoto, N., Akatsu, H., Baranyi, L., et al. (2003). Complement C5a receptor-mediated signaling may be involved in neurodegeneration in Alzheimer's disease. *J. Immunol.* 170, 5764–5771. doi: 10.4049/jimmunol.170.11.5764

Faustmann, P., Dux, R., Krause, D., and Dermietzel, R. (1995). Morphological study in the early stages of complement C5a fragment-induced experimental meningitis: activation of macrophages and astrocytes. *Acta Neuropathol.* 89, 239–247. doi: 10.1007/BF00309339

Finehout, E., Franck, Z., and Lee, K. (2005). Complement protein isoforms in CSF as possible biomarkers for neurodegenerative disease. *Dis. Markers* 21, 93–101. doi: 10.1155/2005/806573

Flierl, M., Stahel, P., Rittirsch, D., Huber-Lang, M., Niederbichler, A., Marco, L., et al. (2009). Inhibition of complement C5a prevents breakdown of the blood-brain barrier and pituitary dysfunction in experimental sepsis. *Crit. Care.* 13:R12. doi: 10.1186/cc7710

Gardner, C., Magliozzi, R., Durrenberger, P., Howell, O., Rundle, J., and Reynolds, R. (2013). Cortical grey matter demyelination can be induced by elevated pro-inflammatory cytokines in the subarachnoid space of MOG-immunized rats. *Brain* 136, 3596–3608. doi: 10.1093/brain/awt279

Gasque, P., Singhrao, S., Neal, J., Götze, O., and Morgan, B. (1997). Expression of the receptor for complement C5a (CD88) is up-regulated on reactive astrocytes, microglia, and endothelial cells in the inflamed human central nervous system. *Am. J. Pathol.* 150, 31–41.

Gasque, P., Singhrao, S., Neal, J., Wang, P., Sayah, S., Fontaine, M., et al. (1998). The receptor for complement anaphylatoxin C3a is expressed by myeloid cells and nonmyeloid cells in inflamed human central nervous system: analysis in multiple sclerosis and bacterial meningitis. *J Immunol.* 160, 3543–3554.

Gharagozloo, M., Smith, M., Jin, J., Garton, T., Taylor, M., Chao, A., et al. (2021). Complement component 3 from astrocytes mediates retinal ganglion cell loss during neuroinflammation. *Acta Neuropathol.* 142, 899–915. doi: 10.1007/s00401-021-02366-4

Griffiths, L., Reynolds, R., Evans, R., Bevan, R., Rees, M., Gveric, D., et al. (2020). Substantial subpial cortical demyelination in progressive multiple sclerosis: have we underestimated the extent of cortical pathology? *Neuroimmunol. Neuroinflamm.* 7, 51–67.

Guo, Y., Weigand, S., Popescu, B., Lennon, V., Parisi, J., Pittock, S., et al. (2017). Pathogenic implications of cerebrospinal fluid barrier pathology in neuromyelitis optica. *Acta Neuropathol.* 133, 597–612. doi: 10.1007/s00401-017-1682-1

Haas, P., and van Strijp, J. (2007). Anaphylatoxins: their role in bacterial infection and inflammation. *Immunol. Res.* 37, 161–175.

Håkansson, I., Ernerudh, J., Vrethem, M., Dahle, C., and Ekdahl, K. (2020). Complement activation in cerebrospinal fluid in clinically isolated syndrome and early stages of relapsing remitting multiple sclerosis. *J. Neuroimmunol.* 340:577147. doi: 10.1016/j.jneuroim.2020.577147

Hammond, J., Bellizzi, M., Ware, C., Qiu, W., Saminathan, P., Li, H., et al. (2020). Complement-dependent synapse loss and microgliosis in a mouse model of multiple sclerosis. *Brain Behav. Immun.* 87, 739–750. doi: 10.1016/j.bbi.2020.03.004

Haynes, T., Luz-Madrigal, A., Reis, E., Echeverri Ruiz, N., Grajales-Esquivel, E., Tzekou, A., et al. (2013). Complement anaphylatoxin C3a is a potent inducer of embryonic chick retina regeneration. *Nat. Commun.* 4:2312. doi: 10.1038/ncomms3312

Howell, O., Reeves, C., Nicholas, R., Carassiti, D., Radotra, B., Gentleman, S., et al. (2011). Meningeal inflammation is widespread and linked to cortical pathology in multiple sclerosis. *Brain* 134, 2755–2771.

Howell, O., Schulz-Trieglaff, E., Carassiti, D., Gentleman, S., Nicholas, R., Roncaroli, F., et al. (2015). Extensive grey matter pathology in the cerebellum in multiple sclerosis is linked to inflammation in the subarachnoid space. *Neuropathol. Appl. Neurobiol.* 41, 798–813. doi: 10.1111/nan.12199

Ingersoll, S., Martin, C., Barnum, S., and Martin, B. K. (2010). CNS-specific expression of C3a and C5a exacerbate demyelination severity in the cuprizone model. *Mol. Immunol.* 48, 219–230. doi: 10.1016/j.molimm.2010.08.007

Ingram, G., Hakobyan, S., Robertson, N., and Morgan, B. (2010). Elevated plasma C4a levels in multiple sclerosis correlate with disease activity. *J. Neuroimmunol.* 223, 124–127.

Ingram, G., Loveless, S., Howell, O., Hakobyan, S., Dancey, B., Harris, C., et al. (2014). Complement activation in multiple sclerosis plaques: an immunohistochemical analysis. *Acta Neuropathol. Commun.* 2:53.

Ischenko, A., Sayah, S., Patte, C., Andreev, S., Gasque, P., Schouft, M. T., et al. (1998). Expression of a functional anaphylatoxin C3a receptor by astrocytes. *J. Neurochem.* 71, 2487–2496.

James Bates, R., Browne, E., Schalks, R., Jacobs, H., Tan, L., Parekh, P., et al. (2022). Lymphotoxin-alpha expression in the meninges causes lymphoid tissue formation and neurodegeneration. *Brain* 145, 4287–4307. doi: 10.1093/brain/awac232

Jauneau, A. C., Ischenko, A., Chatagner, A., Benard, M., Chan, P., Schouft, M. T., et al. (2006). Interleukin-1beta and anaphylatoxins exert a synergistic effect on NGF expression by astrocytes. *J. Neuroinflamm.* 3:8. doi: 10.1186/1742-2094-3-8

Jongen, P., Doesburg, W., Ibrahim-Stappers, J., Lemmens, W., Hommes, O., and Lamers, K. (2000). Cerebrospinal fluid C3 and C4 indexes in immunological disorders of the central nervous system. *Acta Neurol. Scand.* 101, 116–121. doi: 10.1034/j.1600-0404.2000.101002116.x

Junker, A., Wozniak, J., Voigt, D., Scheidt, U., Antel, J., Wegner, C., et al. (2020). Extensive subpial cortical demyelination is specific to multiple sclerosis. *Brain Pathol.* 30, 641–652.

Jürgens, T., Jafari, M., Kreutzfeldt, M., Bahn, E., Brück, W., Kerschensteiner, M., et al. (2016). Reconstruction of single cortical projection neurons reveals primary spine loss in multiple sclerosis. *Brain* 139, 39–46. doi: 10.1093/brain/awv353

Kee, R., Naughton, M., McDonnell, G. V., Howell, O. W., and Fitzgerald, D. C. (2022). A review of compartmentalised inflammation and tertiary lymphoid structures in the pathophysiology of multiple sclerosis. *Biomedicines* 10:2604. doi: 10.3390/biomedicines10102604

Klos, A., Tenner, A., Johswich, K., Ager, R., Reis, E., and Köhl, J. (2009). The role of the anaphylatoxins in health and disease. *Mol. Immunol.* 46:2753.

Klos, A., Wende, E., Wareham, K., and Monk, P. (2013). International union of basic and clinical pharmacology. LXXXVII. complement peptide C5a, C4a, and C3a receptors. *Pharmacol. Rev.* 65, 500–543. doi: 10.1124/pr.111.005223

Krasemann, S., Madore, C., Cialic, R., Baufeld, C., Calcagno, N., El Fatimy, R., et al. (2017). The TREM2-APOE pathway drives the transcriptional phenotype of dysfunctional microglia in neurodegenerative diseases. *Immunity* 47, 566–581.e9. doi: 10.1016/j.immuni.2017.08.008

Lassmann, H. (2019). Pathogenic mechanisms associated with different clinical courses of multiple sclerosis. *Front. Immunol.* 10:3116. doi: 10.3389/fimmu.2018.03116

Lee, N., Ha, S., Sati, P., Absinta, M., Luciano, N., Lefeuvre, J., et al. (2018). Spatiotemporal distribution of fibrinogen in marmoset and human inflammatory demyelination. *Brain* 141, 1637–1649. doi: 10.1093/brain/awy082

Leyns, C., Ulrich, J., Finn, M., Stewart, F., Koscal, L., Serrano, J., et al. (2017). TREM2 deficiency attenuates neuroinflammation and protects against neurodegeneration in a mouse model of tauopathy. *Proc. Natl. Acad. Sci. USA.* 114, 11524–11529. doi: 10.1073/pnas.1710311114

Liddelow Sa, Guttenplan, K., Clarke, L., Bennett, F., Bohlen, C., Schirmer, L., et al. (2017). Neurotoxic reactive astrocytes are induced by activated microglia. *Nature* 541, 481–487.

Loveless, S., Neal, J., Howell, O., Harding, K., Sarkies, P., Evans, R., et al. (2018). Tissue microarray methodology identifies complement pathway activation and dysregulation in progressive multiple sclerosis. *Brain Pathol.* 28, 507–520. doi: 10.1111/bpa.12546

Magliozzi, R., Hametner, S., Facchiano, F., Marastoni, D., Rossi, S., Castellaro, M., et al. (2019a). Iron homeostasis, complement, and coagulation cascade as CSF signature of cortical lesions in early multiple sclerosis. *Ann. Clin. Transl. Neurol.* 6, 2150–2163. doi: 10.1002/acn3.50893

Magliozzi, R., Howell, O., Durrenberger, P., Aricò, E., James, R., Cruciani, C., et al. (2019b). Meningeal inflammation changes the balance of TNF signalling in cortical grey matter in multiple sclerosis. *J. Neuroinflamm.* 16:259. doi: 10.1186/s12974-019-1650-x

Magliozzi, R., Howell, O., Nicholas, R., Cruciani, C., Castellaro, M., Romualdi, C., et al. (2018). Inflammatory intrathecal profiles and cortical damage in multiple sclerosis. *Ann. Neurol.* 83, 739–755.

Magliozzi, R., Howell, O., Reeves, C., Roncaroli, F., Nicholas, R., Serafini, B., et al. (2010). A gradient of neuronal loss and meningeal inflammation in multiple sclerosis. *Ann. Neurol.* 68, 477–493.

Magliozzi, R., Howell, O., Vora, A., Serafini, B., Nicholas, R., Puopolo, M., et al. (2007). Meningeal B-cell follicles in secondary progressive multiple sclerosis associate with early onset of disease and severe cortical pathology. *Brain* 130(Pt 4), 1089–1104. doi: 10.1093/brain/awm038

Magliozzi, R., Scalfari, A., Pisani, A., Ziccardi, S., Marastoni, D., Pizzini, F., et al. (2020). The CSF profile linked to cortical damage predicts multiple sclerosis activity. *Ann. Neurol.* 88, 562–573. doi: 10.1002/ana.25786

Mainero, C., Louapre, C., Govindarajan, S., Gianni, C., Nielsen, A., Cohen-Adad, J., et al. (2015). A gradient in cortical pathology in multiple sclerosis by in vivo quantitative 7 T imaging. *Brain* 138, 932–945.

Michailidou, I., Jongejan, A., Vreijling, J., Georgakopoulou, T., de Wissel, M., Wolterman, R., et al. (2018). Systemic inhibition of the membrane attack complex impedes neuroinflammation in chronic relapsing experimental autoimmune encephalomyelitis. *Acta Neuropathol. Commun.* 6:36. doi: 10.1186/s40478-018-0536-y

Michailidou, I., Naessens, D., Hametner, S., Guldenaar, W., Kooi, E., Geurts, J., et al. (2017). Complement C3 on microglial clusters in multiple sclerosis occur in chronic but not acute disease: implication for disease pathogenesis. *Glia* 65, 264–277. doi: 10.1002/glia.23090

Michailidou, I., Willems, J., Kooi, E., van Eden, C., Gold, S., Geurts, J., et al. (2015). Complement C1q-C3-associated synaptic changes in multiple sclerosis hippocampus. *Ann. Neurol.* 77, 1007–1026. doi: 10.1002/ana.24398

Mukherjee, P., Thomas, S., and Pasinetti, G. (2008). Complement anaphylatoxin C5a neuroprotects through regulation of glutamate receptor subunit 2 in vitro and in vivo. *J. Neuroinflamm.* 5:5. doi: 10.1186/1742-2094-5-5

Müller-Ladner, U., Jones, J., Wetsel, R., Gay, S., Raine, C., and Barnum, S. (1996). Enhanced expression of chemotactic receptors in multiple sclerosis lesions. *J. Neurol. Sci.* 144, 135–141.

Nataf, S., Davoust, N., and Barnum, S. (1998). Kinetics of anaphylatoxin C5a receptor expression during experimental allergic encephalomyelitis. *J. Neuroimmunol.* 91, 147–155. doi: 10.1016/s0165-5728(98)00169-6

Nataf, S., Stahel, P., Davoust, N., and Barnum, S. (1999). Complement anaphylatoxin receptors on neurons: new tricks for old receptors? *Trends Neurosci.* 22, 397–402. doi: 10.1016/s0166-2236(98)01390-3

Oberheim, N., Takano, T., Han, X., He, W., Lin, J., Wang, F., et al. (2009). Uniquely hominid features of adult human astrocytes. *J. Neurosci.* 29, 3276–3287.

Pandey, M., Burrow, T., Rani, R., Martin, L., Witte, D., Setchell, K., et al. (2017). Complement drives glucosylceramide accumulation and tissue inflammation in Gaucher disease. *Nature* 543, 108–112.

Pavlovski, D., Thundyil, J., Monk, P., Wetsel, R., Taylor, S., and Woodruff, T. (2012). Generation of complement component C5a by ischemic neurons promotes neuronal apoptosis. *FASEB J.* 26, 3680–3690. doi: 10.1096/fj.11-202382

Peterson, J., Bö, L., Mörk, S., Chang, A., and Trapp, B. (2001). Transected neurites, apoptotic neurons, and reduced inflammation in cortical multiple sclerosis lesions. *Ann. Neurol.* 50, 389–400. doi: 10.1002/ana.1123

Peterson, S., Nguyen, H., Mendez, O., and Anderson, A. (2017). Complement protein C3 suppresses axon growth and promotes neuron loss. *Sci. Rep.* 7:12904. doi: 10.1038/s41598-017-11410-x

Picon C, Jayaraman, A., James, R., Beck, C., Gallego, P., Witte, M., et al. (2021). Neuron-specific activation of necroptosis signaling in multiple sclerosis cortical grey matter. *Acta Neuropathol.* 141, 585–604. doi: 10.1007/s00401-021-02274-7

Pittock, S., Berthele, A., Fujihara, K., Kim, H., Levy, M., Palace, J., et al. (2019). Eculizumab in Aquaporin-4–Positive neuromyelitis optica spectrum disorder. *New Engl. J. Med.* 381, 614–625.

Ramaglia, V., Dubey, M., Malpede, M., Petersen, N., de Vries, S., Ahmed, S., et al. (2021). Complement-associated loss of CA2 inhibitory synapses in the demyelinated hippocampus impairs memory. *Acta Neuropathol.* 142, 643–667. doi: 10.1007/s00401-021-02338-8

Reali, C., Magliozzi, R., Roncaroli, F., Nicholas, R., Howell, O., and Reynolds, R. B. (2020). cell rich meningeal inflammation associates with increased spinal cord pathology in multiple sclerosis. *Brain Pathol.* 30, 779–793. doi: 10.1111/bpa.12841

Reynolds, R., Roncaroli, F., Nicholas, R., Radotra, B., Gveric, D., and Howell, O. (2011). The neuropathological basis of clinical progression in multiple sclerosis. *Acta Neuropathol.* 122, 155–170.

Ryu, J., Petersen, M., Murray, S., Baeten, K., Meyer-Franke, A., Chan, J., et al. (2015). Blood coagulation protein fibrinogen promotes autoimmunity and demyelination via chemokine release and antigen presentation. *Nat. Commun.* 6:8164. doi: 10.1038/ncomms9164

Salter, M., and Stevens, B. (2017). Microglia emerge as central players in brain disease. *Nat. Med.* 23, 1018–1027.

Schartz, N., and Tenner, A. (2020). The good, the bad, and the opportunities of the complement system in neurodegenerative disease. *J. Neuroinflamm.* 17:354. doi: 10.1186/s12974-020-02024-8

Schirmer, L., Velmeshev, D., Holmqvist, S., Kaufmann, M., Werneburg, S., Jung, D., et al. (2019). Neuronal vulnerability and multilineage diversity in multiple sclerosis. *Nature* 573, 75–82. doi: 10.1038/s41586-019-1404-z

Sellebjerg, F., Jaliashvili, I., Christiansen, M., and Garred, P. (1998). Intrathecal activation of the complement system and disability in multiple sclerosis. *J. Neurol. Sci.* 157, 168–174.

Sellgren, C., Gracias, J., Watmuff, B., Biag, J., Thanos, J., Whittredge, P., et al. (2019). Increased synapse elimination by microglia in schizophrenia patient-derived models of synaptic pruning. *Nat. Neurosci.* 22, 374–385. doi: 10.1038/s41593-018-0334-7

Serfecz, J., Saadin, A., Santiago, C., Zhang, Y., Bentzen, S., Vogel, S., et al. (2021). C5a activates a pro-inflammatory gene expression profile in human gaucher iPSC-Derived macrophages. *Int. J. Mol. Sci.* 22:9912. doi: 10.3390/ijms22189912

Stahel, P., Frei, K., Fontana, A., Eugster, H. P., Ault, B. H., and Barnum, S. R. (1997). Evidence for intrathecal synthesis of alternative pathway complement activation proteins in experimental meningitis. *Am. J. Pathol.* 151, 897–904.

Stahel, P., Kariya, K., Shohami, E., Barnum, S., Eugster, H., Trentz, O., et al. (2000). Intracerebral complement C5a receptor (CD88) expression is regulated by TNF and lymphotoxin-alpha following closed head injury in mice. *J. Neuroimmunol.* 109, 164–172. doi: 10.1016/s0165-5728(00)00304-0

Stoop, M., Dekker, L., Titulaer, M., Burgers, P., Sillevis Smitt, P. A. E., Luider, T. M., et al. (2008). Multiple sclerosis-related proteins identified in cerebrospinal fluid by advanced mass spectrometry. *Proteomics* 8, 1576–1585. doi: 10.1002/pmic.200700446

van Beek, J., Nicole, O., Ali, C., Ischenko, A., MacKenzie, E., Buisson, A., et al. (2001). Complement anaphylatoxin C3a is selectively protective against NMDA-induced neuronal cell death. *Neuroreport* 12, 289–293. doi: 10.1097/00001756-200102120-00022

van Olst, L., Rodriguez-Mogeda, C., Picon, C., Kiljan, S., James, R., Kamermans, A., et al. (2021). Meningeal inflammation in multiple sclerosis induces phenotypic changes in cortical microglia that differentially associate with neurodegeneration. *Acta Neuropathol.* 141, 881–899. doi: 10.1007/s00401-021-02293-4

Vandendriessche, S., Cambier, S., Proost, P., and Marques, P. (2021). Complement receptors and their role in leukocyte recruitment and phagocytosis. *Front. Cell Dev. Biol.* 9:624025. doi: 10.3389/fcell.2021.624025

Vankriekelsvenne, E., Chrzanowski, U., Manzhula, K., Greiner, T., Wree, A., Hawlitschka, A., et al. (2022). Transmembrane protein 119 is neither a specific nor a reliable marker for microglia. *Glia* 70, 1170–1190.

Vergunst, CE., Gerlag, D., Dinant, H., Schulz, L., Vinkenoog, M., Smeets, T., et al. (2007). Blocking the receptor for C5a in patients with rheumatoid arthritis does not reduce synovial inflammation. *Rheumatology* 46, 1773–1778.

Ward, P. (2009). Functions of C5a receptors. *J. Mol. Med.* 87, 375–378.

Watkins, L., Neal, J., Loveless, S., Michailidou, I., Ramaglia, V., Rees, M., et al. (2016). Complement is activated in progressive multiple sclerosis cortical grey matter lesions. *J. Neuroinflamm.* 13:161.

Wayne Moore, G., Laule, C., Leung, E., Pavlova, V., Paul Morgan, B., and Esiri, M. (2016). Complement and humoral adaptive immunity in the human choroid plexus: roles for stromal concretions, basement membranes, and epithelium. *J. Neuropathol. Exp. Neurol.* 75, 415–428. doi: 10.1093/jnen/nlw017

Werneburg, S., Jung, J., Kunjamma, R., Ha, S., Luciano, N., Willis, C., et al. (2020). Targeted complement inhibition at synapses prevents microglial synaptic engulfment and synapse loss in demyelinating disease. *Immunity* 52, 167–182.e7. doi: 10.1016/j.immuni.2019.12.004

West, E., Kolev, M., and Kemper, C. (2018). Complement and the regulation of T cell responses. *Annu. Rev. Immunol.* 36:309.

Westacott, L., Haan, N., Evison, C., Marei, O., Hall, J., Hughes, T., et al. (2021). Dissociable effects of complement C3 and C3aR on survival and morphology of adult born hippocampal neurons, pattern separation, and cognitive flexibility in male mice. *Brain Behav. Immun.* 98, 136–150. doi: 10.1016/j.bbi.2021.08.215

Woodruff, T., and Shukla, A. (2020). The Complement C5a-C5aR1 GPCR Axis in COVID-19 therapeutics. *Trends Immunol.* 41:965. doi: 10.1016/j.it.2020.09.008

Woodruff, T., Crane, J., Proctor, L., Buller, K., Shek, A., de Vos, K., et al. (2006). Therapeutic activity of C5a receptor antagonists in a rat model of neurodegeneration. *FASEB J.* 20, 1407–1417. doi: 10.1096/fj.05-5814com

Zelek, W., Watkins, L., Howell, O., Evans, R., Loveless, S., Robertson, N., et al. (2019). Measurement of soluble CD59 in CSF in demyelinating disease: evidence for an intrathecal source of soluble CD59. *Multiple Sclerosis* 25, 523–531. doi: 10.1177/1352458518758927

Zrzavy, T., Hametner, S., Wimmer, I., Butovsky, O., Weiner, H., and Lassmann, H. (2017). Loss of 'homeostatic' microglia and patterns of their activation in active multiple sclerosis. *Brain* 140, 1900–1913.

frontiers | Frontiers in Cellular Neuroscience

TYPE Original Research
PUBLISHED 10 May 2023
DOI 10.3389/fncel.2023.1170031

OPEN ACCESS

EDITED BY
Marina Boziki,
Aristotle University of Thessaloniki, Greece

REVIEWED BY
Nirmal Banda,
University of Colorado Hospital, United States
Iliana Michailidou,
Leiden University Medical Center (LUMC), Netherlands

*CORRESPONDENCE
Eugene D. Ponomarev
✉ eugene.ponomarev@cityu.edu.hk;
✉ eugene.ponomarev@nu.edu.kz

RECEIVED 20 February 2023
ACCEPTED 26 April 2023
PUBLISHED 10 May 2023

CITATION
Veremeyko T, Jiang R, He M and Ponomarev ED (2023) Complement C4-deficient mice have a high mortality rate during PTZ-induced epileptic seizures, which correlates with cognitive problems and the deficiency in the expression of Egr1 and other immediate early genes. *Front. Cell. Neurosci.* 17:1170031. doi: 10.3389/fncel.2023.1170031

Complement C4-deficient mice have a high mortality rate during PTZ-induced epileptic seizures, which correlates with cognitive problems and the deficiency in the expression of Egr1 and other immediate early genes

Tatyana Veremeyko[1,2,3], Rongcai Jiang[4,5], Mingliang He[1] and Eugene D. Ponomarev[1,2,3]*

[1]Department of Biomedical Sciences, Jockey Club College of Veterinary Medicine and Life Sciences, City University of Hong Kong, Hong Kong, Hong Kong SAR, China, [2]Department of Biology, School of Sciences and Humanities, Nazarbayev University, Astana, Kazakhstan, [3]Chinese University of Hong Kong Joint Laboratory of Bioresources and Molecular Research of Common Diseases, Kunming Institute of Zoology, Chinese Academy of Sciences, Kunming, China, [4]Department of Neurosurgery, Tianjin Medical University General Hospital, Tianjin, China, [5]Tianjin Neurological Institute, Key Laboratory of Post Neuro-Injury Neuro-Repair and Regeneration in Central Nervous System, Ministry of Education and Tianjin City, Tianjin, China

Complement system plays an important role in the immune defense against pathogens; however, recent studies demonstrated an important role of complement subunits C1q, C4, and C3 in normal functions of the central nervous system (CNS) such as non-functional synapse elimination (synapse pruning), and during various neurologic pathologies. Humans have two forms of C4 protein encoded by C4A and C4B genes that share 99.5% homology, while mice have only one C4B gene that is functionally active in the complement cascade. Overexpression of the human C4A gene was shown to contribute to the development of schizophrenia by mediating extensive synapse pruning through the activation C1q-C4-C3 pathway, while C4B deficiency or low levels of C4B expression were shown to relate to the development of schizophrenia and autism spectrum disorders possibly via other mechanisms not related to synapse elimination. To investigate the potential role of C4B in neuronal functions not related to synapse pruning, we compared wildtype (WT) mice with C3- and C4B-deficient animals for their susceptibility to pentylenetetrazole (PTZ)- induced epileptic seizures. We found that C4B (but not C3)–deficient mice were highly susceptible to convulsant and subconvulsant doses of PTZ when compared to WT controls. Further gene expression analysis revealed that in contrast to WT or C3-deficient animals, C4B-deficient mice failed to upregulate expressions of multiple immediate early genes (IEGs) Egrs1-4, c-Fos, c-Jus, FosB, Npas4, and Nur77 during epileptic seizures. Moreover, C4B-deficient mice had low levels of baseline expression of Egr1 on mRNA and protein levels, which was correlated with the cognitive problems of these animals. C4-deficient animals also failed to upregulate several genes downstream of IEGs such as BDNF

and pro-inflammatory cytokines IL-1β, IL-6, and TNF. Taken together, our study demonstrates a new role of C4B in the regulation of expression of IEGs and their downstream targets during CNS insults such as epileptic seizures.

KEYWORDS

complement, C4, epilepsy, Egr1, cognitive functions, BDNF, neuroinflammation, immediate early gene (IEG)

1. Introduction

The complement system consists of more than 30 proteins forming an enzymatic activating cascade that is initiated by various "danger signals" such as pathogens, cellular debris, apoptotic bodies, and blood coagulation processes (Foley and Conway, 2016; Reis et al., 2019). Specifically, complement may be activated via the classical, lectin, and alternative pathways, or an extrinsic blood coagulation cascade (Foley and Conway, 2016; Chen et al., 2022). The classical pathway is initiated by antigen–antibody complexes that bind C1q, leading to the proteolytic cleavage of C2 into C2a and C2b fragments, and then cleavage of C4 into C4a and C4b fragments. Fragments C4b and C2a bind to each other to form the C4bC2a dimer complex (also referred to as C3-convertase), which then cleaves C3 into C3a and C3b fragments. Subsequently, fragment C3b and C4bC2a dimer form C5-convertase (C3bC4bC2a trimer) that further cleaves C5 leading to the formation of membrane attack complex. In the lectin pathway, C4 is cleaved by the MASP-2 enzyme into C4a and C4b (Wallis et al., 2007). Thus, both classical and lectin pathways lead to C4 activation, and C4b could further activate downstream C3, or C4b could just act as an opsonin. The liver is the dominant source of most complement proteins in the plasma or serum, except for C1q, which is mainly synthesized by immune cells. In the central nervous system (CNS), several complement components, including C1q, C4, and C3 are synthesized by astrocytes, oligodendrocytes, neurons, and microglia (Cho, 2019; Schartz and Tenner, 2020; Peoples and Strang, 2021; Chen et al., 2022). In the normal CNS, microglia produce C1q, which then recruits C3 to axons via activation of C4 in the classical pathway and thus marks unfunctional synapses for elimination by microglia via microglial complement receptor 3 (CR3) that specifically binds to C3b (Stevens et al., 2007; Paolicelli et al., 2011; Cho, 2019; Gomez-Arboledas et al., 2021). It was recently demonstrated that the complement system is involved in the pathogenesis of many types of neurologic diseases including traumatic brain injury, Alzheimer's disease, amyotrophic lateral sclerosis, Parkinson's disease, and multiple sclerosis (Schartz and Tenner, 2020; Gomez-Arboledas et al., 2021; Chen et al., 2022). Genome-wide association studies demonstrated a strong association between human *C4* gene polymorphisms and schizophrenia (SZ) (Sekar et al., 2016).

Complement C4 protein is a non-enzymatic, but essential component of C3 and C5 convertases that plays a key role in the propagation of classical and lectin complement activation pathways (Blanchong et al., 2001; Peoples and Strang, 2021). Human *C4* genes are located in MHC (HLA) class III locus on chromosome 6 and, similar to other MHC genes, *C4* genes have a high level of polymorphism. Human C4 protein has two isoforms encoded by *C4A* and *C4B* genes, which share 99.5% homology, but have distinct affinities to their carbohydrate targets on cell/pathogen surface and their patterns of expression (Blanchong et al., 2001). More specifically, *C4A* is induced or enhanced by IFNγ during inflammation, while *C4B* is constitutively present in high concentrations in plasma or serum (Kulics et al., 1990; Blanchong et al., 2001). Mice have *Slp* and *C4B* homologs for human *C4A* and *C4B* genes, respectively. Unlike human C4 genes, *Slp* and *C4B* share only 95% homology and the *Slp* gene is not functionally active in complement enzymatic cascade having *C4B* as the single functional gene for complement C4 component in mice (Blanchong et al., 2001).

The elevated level of *C4A* and, to lesser extent, *C4B* were associated with SZ (Sekar et al., 2016), which was also investigated in mouse models with overexpression of human *C4A* or mouse *C4B* genes that mediated excessive synapse elimination and behavior changes (Comer et al., 2020; Druart et al., 2021; Yilmaz et al., 2021). On the other hand, in humans, low levels, or deficiency in *C4B* expression were associated with a high risk of SZ, autism spectrum disorders (ASD), and certain autoimmune diseases (Mayilyan et al., 2008; Mostafa and Shehab, 2010; Zhou et al., 2021). It was demonstrated that *C1q*-, *C4B*-, and *C3*- deficient mice have a higher density of synapses and these elevated densities of synapses were comparable for these three groups of animals (Stevens et al., 2007; Sekar et al., 2016; Cho, 2019; Yilmaz et al., 2021). Given the fact that C1q and C4 are upstream of C3 activation in the classical complement activation pathway (Peoples and Strang, 2021; Chen et al., 2022), these results are not surprising in terms of insufficient synapse pruning in these animals when compared to wild-type (WT) controls. However, it is not clear why C4-, but not C3-, deficiency and/or polymorphism is associated with neurological disorders such as SZ and ASD in humans.

The role of complement in the development of epilepsy appeared to be even more complex and controversial. It was demonstrated that *C1q*-deficient mice are prone to behavior seizures and have a higher baseline level of neuronal electric activity, which was due to the elevated density of neuronal processes as a consequence of insufficient synaptic pruning via C1q-C3-CR3 mechanism (Chu et al., 2010). Above mentioned study showed the anti-epileptic role of C1q. On the other hand, it was demonstrated that C1q and C3 contributed to epilepsy in several mouse models (Holden et al., 2021; Jiang et al., 2021), while elevated plasma level of C4 was found to be a marker of uncontrolled seizures in humans (Kopczynska et al., 2018). Finally, the classical C1q-C4-C3 pathway of complement activation was demonstrated to occur during epileptic seizures (Chu et al., 2010). Thus, the differential

role of C4 vs. C3 in the development of seizures or other pathologies such as SZ and ASD were not extensively studied so far in terms of the basic functions of C4 in the CNS.

In this study, we hypothesize that C4 plays an additional role in neuronal cell functions besides its established role as an upstream activator of C3 in the classical pathway that is required for synapse pruning. To test our hypothesis, we induced epileptic seizures in WT, C4B-, and C3- deficient mice using pentylenetetrazole (PTZ), a $GABA_A$ receptor antagonist (MacDonald and Barker, 1977), a well-known convulsant that induces seizures in various species from humans to mice. We found that C4B-, but not C3-, deficient mice were highly sensitive to the standard convulsant dose of PTZ (80 mg/kg) with very severe seizures leading to a 100% mortality rate when compared to WT controls. Moreover, a subconvulsant dose of PTZ (50 mg/kg) induced severe seizures with a 60% mortality rate in C4B-deficient mice but failed to do so in C3-deficient and WT mice. Further gene expression analysis revealed that in contrast to WT or C3-deficient groups, C4B-deficient mice were unable to upregulate mRNA for several immediate early genes (IEGs): *Egr1*, *Egr2*, *Egr3*, *Egr4*, *c-Fos*, *c-Jun*, *FosB*, *Npas4*, *Nur77*, as well as neurotrophic factor *BDNF* and major pro-inflammatory cytokines *IL-1β*, *IL-6*, and *TNF*, which are downstream of IEGs. Our data indicate that in contrast to WT or C3-deficient mice, C4B-deficient animals could not adequately respond to CNS insults or stress conditions such as epileptic seizures, which likely lead to extensive dysregulation of neuronal functions and a high mortality rate.

2. Materials and methods

2.1. Mice

C57BL/6 (B6; WT), *C3*-deficient *B6.129S4-C3tm1Crr/J* ($C3^{-/-}$), and *C4B*-deficient *B6.129S4-C4btm1Crr/J* ($C4B^{-/-}$) mice were purchased from Jackson Laboratories (Bar Harbour, ME, USA), and then maintained and experimentally manipulated at the Laboratory Animal Service Centre at the Chinese University of Hong Kong (Shatin, Hong Kong). The study was performed following the recommendations of the ARRIVE guidelines[1] and all experimental procedures were approved by a health and food department of the government of Hong Kong, the Chinese University of Hong Kong, and the City University of Hong Kong Animal Experimentation Ethics Committees. All mice were housed in a temperature-controlled environment with an automatic 12 h light/dark cycle and were fed *ad libitum*. Genotyping of $C3^{-/-}$ and $C4B^{-/-}$ animals was performed in comparison with WT controls by standard PCR using primer sets and the protocols provided by Jackson Laboratory. In addition to genotyping, the phenotype of C3- and C4B- deficient mice was further confirmed by examining the levels of C3 and C4B in mouse serum using western blotting as shown in **Supplementary Figures 1**, **2**, respectively. The blood samples were collected from retro-orbital sinuses of anesthetized animals using glass capillaries as we did in our earlier studies (Starossom et al., 2014) and allowed to be coagulated for 1 h at 37°C. The serum samples were obtained by centrifugation of coagulated blood samples according to standard protocol (Starossom et al., 2015).

2.2. PTZ-induced seizures

Pentylenetetrazole (PTZ; also known as pentylenetetrazole, leptazol, metrazol, pentetrazol, pentamethylenetetrazol, corazol, cardiazol, and deumacard) was purchased from Sigma (Cat. No. P6500, Sigma, St. Louis, MO, USA), dissolved in PBS, and was injected intraperitoneally (i.p.) in 8–12-week-old WT, $C3^{-/-}$ or $C4B^{-/-}$ female mice at a dose of 80 mg/kg (convulsant dose) or 50 mg/kg (subconvulsant dose) as we did earlier in our previous study (Kopeikina et al., 2020). We used only female animals in our studies since it was shown that WT females are more susceptible to seizures than males in case of subconvulsant (50–60 mg/kg) dosage of PTZ (Medina et al., 2001). At the same time, there was no sex-specific difference for seizure susceptibility for convulsant dosage of PTZ [70–80 mg/kg; (Medina et al., 2001) and unpublished observation]. The mice were video-recorded for 10 min post-PTZ administration to analyze the latency of severe seizure development, and to determine the maximal clinical epileptic scores developed over the 10-min period. Clinical epileptic scores were assigned as we previously described in our study: (0) normal behavior, no abnormality; (1) facial twitching, restless behavior; (2) myoclonic body jerks; (3) fore limb clonus; (4) rearing, tonic seizure, falling on their side; (5) tonic-clonic seizure, falling on their backs, wild rushing, jumping; and (6) death. The seizure latency was measured as the delay time until the start of tonic-clonic seizures of epileptic score 3 or above during the 10-min period post-PTZ administration. If tonic-clonic seizure did not appear within the 10-min period, we followed the mice for 4h to monitor recovery and recorded the latency time as 10 min.

2.3. Gene expression analysis by real-time RT PCR

For RNA isolation from brain tissues, unmanipulated WT, $C3^{-/-}$ or $C4B^{-/-}$ mice, or alive WT, $C3^{-/-}$ or $C4B^{-/-}$ animals 9 ± 1 min post-PTZ injection were euthanized by swift decapitation. Brain frontal cortexes were dissected as we did earlier in our studies (Kopeikina et al., 2020; Strekalova et al., 2021a,b), washed with PBS, frozen in dry ice, stored for 1–2 weeks at −80°C till further processing, and then transferred to the laboratory in dry ice. Subsequently the samples were unfrozen, homogenized using a 10 ml glass/Teflon Wheaton tissue grinder (Cat. No. 358039, DWK Life Sciences LLC, Millville, NJ, USA), and lysed using QIAzol Lysis Reagent (Cat. No. 79306, Qiagen, Hilden, Germany) as described in our previous studies (Dukhinova et al., 2019; Veremeyko et al., 2019b; Kopeikina et al., 2020). Further RNA purification was performed using DNase digestion and miRNeasy Mini Kit from Qiagen (Cat. No. 217004). Real-time RT PCR was performed using ABI ViiA 7 and ABI QuantStudio 7 (QS7) Flex Systems. The primer sets are summarized in **Table 1**. Relative expression levels were calculated using the $\Delta\Delta C_T$ method and normalized to the expression of

1 http://www.nc3rs.org.uk/arrive-guidelines

TABLE 1 Primer sequence for gene expression analysis.

Gene	Primer	Sequence
GADPH	Forward	5′-ATGACCACAGTCCATGCCATC -3′
	Reverse	5′-GAGCTTCCCGTTCAGCTCTG -3′
Egr1	Forward	5′-GCAGCGCCTTCAATCCTCAAG-3′
	Reverse	5′-GCTCACGAGGCCACTGACTAG-3′
Egr2	Forward	5′- CCCTTTGACCAGATGAACGGAG-3′
	Reverse	5′-AAGCTACTCGGATACGGGAGATC-3′
Egr3	Forward	5′- CGACTCGGTAGCCCATTACAATC -3′
	Reverse	5′-GGGCTTCTCGTTGGTCAGAC-3′
Egr4	Forward	5′-GCTTCTTCATCCAGGCGGTTC-3′
	Reverse	5′-GCCCAAGATGCCAGACATGAG-3′
c-Fos	Forward	5′-ATCGGCAGAAGGGGCAAAGTAG-3′
	Reverse	5′-GCAAGGGTAACAGCGGTGAA-3′
c-Jun	Forward	5′-GTTGCG GCCGCGAAACTT-3′
	Reverse	5′-CATTGCCCTCGAGCCCTG-3′
FosB	Forward	5′-GGGAGCTGACAGATCGACTTC-3′
	Reverse	5′-CAAACTCCAGGCGTTCCTTCTC-3′
Nur77	Forward	5′-GCTAGAGTCTGCCTTCCTGGAAC-3′
	Reverse	5′-GCACACTGCAGCTGGTGTAG-3′
Npas4	Forward	5′-GGAGGCTGGACATGGATTTACTG-3′
	Reverse	5′-CTGCCTGGGTGTCTTCAGAG-3′
Arc	Forward	5′- GTGATCCTGCAGATTGGTAAGTGC -3′
	Reverse	5′- ACGTGCATCTCACGCTTGAC -3′
BDNF	Forward	5′-GTCATCGAAGAGCTGCTGGATG -3′
	Reverse	5′-CTCCAAAGGCACTTGACTGCTG -3′
GABRQ	Forward	5′-CACGGTCCTCACCACCATTC -3′
	Reverse	5′-CCGCATATGTGAGTCGATGGTAG -3′
GABRA2	Forward	5′-CTTCTGACTCCGTTCAGGTTGC -3′
	Reverse	5′-GCAAGGCAGATAGGTCTGAATCAC -3′
IL-1B	Forward	5′- CTTCCAGGATGAGGACATGAGCAC -3′
	Reverse	5′-TCATCATCCCATGAGTCACAGAGG -3′
IL-6	Forward	5′-CCTTCTTGGGACTGATGCTGGTG-3′
	Reverse	5′- AGGTCTGTTGGGAGTGGTATCCTC-3′
TNF	Forward	5′-AGCCGATGGGTTGTACCTTG- 3′
	Reverse	5′- GTGGGTGAGGAGCACGTAGTC -3′
PSD95	Forward	5′-TCTGTGCGAGAGGTAGCAGA-3′
	Reverse	5′-AAGCACTCCGTGAACTCCTG-3′
Syn1	Forward	5′-CCGCCAGCTGCCTTC-3′
	Reverse	5′-TGCAGCCCAATGACCAAA-3′
Mecp2	Forward	5′-GCCGATCTGCTGGAAAGTATGATG-3′
	Reverse	5′-CCTCTCCCAGTTACCGTGAAGTC-3′

the GADPH housekeeping gene and then to the expression of a control sample, which was defined as 1 as we did in our previous studies (Gorlova et al., 2019; Pavlov et al., 2019; Veremeyko et al., 2019a).

2.4. Western blotting

Western blot analysis was performed according to a standard protocol as previously reported in our earlier studies (Veremeyko et al., 2018, 2019a; Dukhinova et al., 2019). The following antibodies were used for β-Actin (Cell Signalling, Gene Company Limited, Chai Wan, Hong Kong, Cat. No. 4967, dilution 1:10000), Egr1 (Cell Signalling, Cat. No. 4154, dilution 1:1000), C3 (Invitrogen, Waltham, MA, USA, Cat. No. PA1-29715, dilution 1:1000), C4 (Abbexa, Cambridge, U.K., Cat. No. abx129540, dilution 1:1000), and PSD95 (Cell Signalling, Cat. No. 3450, dilution 1:1000). As a secondary antibody, we used various anti-rabbit or anti-goat antibodies conjugated with alkaline phosphatase (purchased from Abcam, Cambridge, U.K.). For quantitative EGR1 and PSD95 protein level analysis, β-Actin was used as a loading control. For analysis of plasma levels of α- and β-chains of C3 (**Supplementary Figure 1**) and γ-chain of C4 (**Supplementary Figure 2**), the total protein concentration in serum samples was measured by Bradford assay (Sigma, Cat. No. B6916), equal quantities of serum proteins were loaded on polyacrylamide gels (ThermoFisher Inc., Life Technologies, Carlsbad, CA, USA), and Ponceau S (Abcam, Cat. No. ab270042) staining was used as a loading control (**Supplementary Figures 1**, **2**).

2.5. Behavior tests

To test motor functions, we utilized a standard five-lane mouse Rotarod set-up (Med Associates Inc., Fairfax, VT, USA) with programmed accelerated rotation (4–40 rpm). For testing, the animals were first trained to stay on the rotating rod at a low speed of 4 rpm on day 1 for 10–15 min, and then the total time that an animal can stay on the accelerated rod before falling was used to measure the motor functions (coordination and balance) on days 1–5 as similar as it was described earlier in our previous study (Kopeikina et al., 2020).

To test cognitive functions in mice, we used a custom-made Barns maze set-up. Particularly, we used a white-color circular platform (92 cm in diameter) with 20 equally spaced holes (5 cm in diameter; the distance is 7.5 cm between holes) as described in our earlier studies (Dukhinova et al., 2018, 2019). The bright lighting and fan were turned on during testing to stimulate mice to locate one hole with the escape box attached to it. Mice were trained to locate a hole where they can escape from the platform into the escape box during three daily training sessions. The platform was randomly rotated and washed with 70% ethanol before each training session for each mouse. Latency to escape was scored manually on days 1–4 during the training sessions (three training sessions per day for each mouse). On day 5, the final trial was performed, where animals could not escape the platform with the escape hole closed and their time to reach the area of the closed hole was evaluated using Noldus EthoVision XT (v. 11) software (Wageningen, the Netherlands).

2.6. Statistics

The results are presented as box and whisker plots or mean ± standard error (SE) with overlayed dot plots. One-way

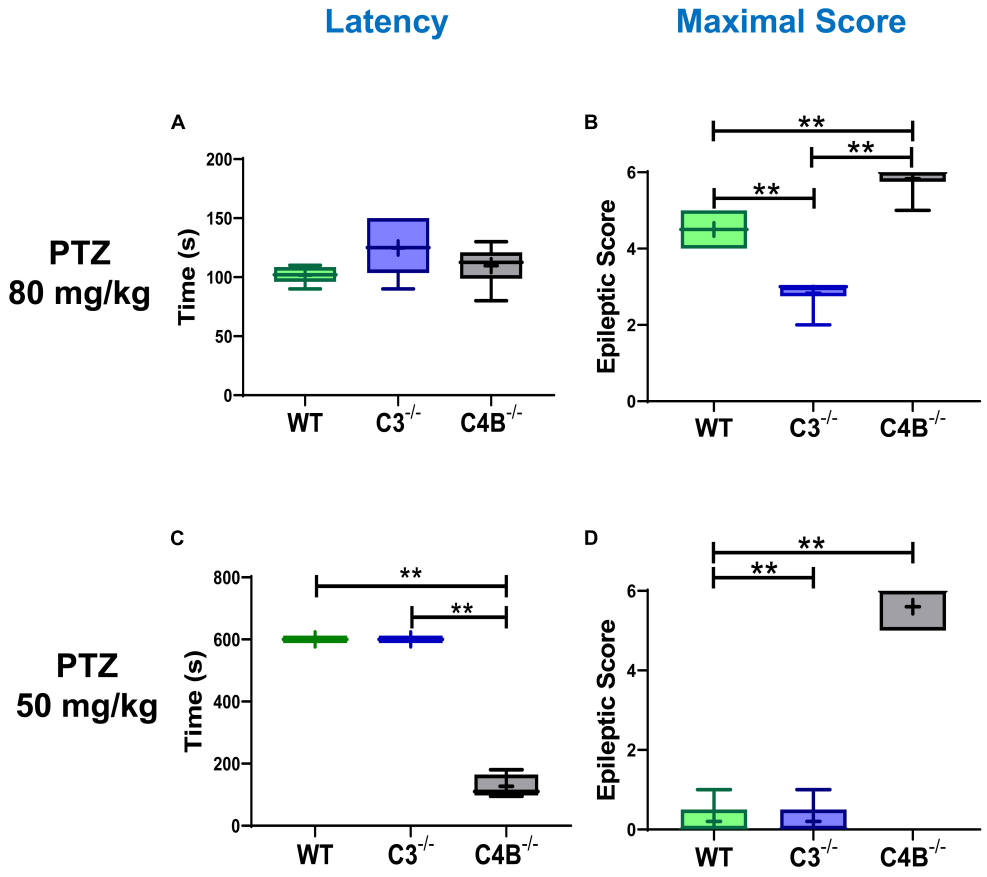

FIGURE 1
Comparison of seizure latency and severity in WT, C3- and C4B-deficient mice. Groups of WT, or $C3^{-/-}$, or $C4B^{-/-}$ mice were injected i.p. with convulsant (80 mg/kg) **(A,B)** or subconvulsant (50 mg/kg) **(C,D)** doses of PTZ, and the seizure latency **(A,C)**, and maximal epileptic scores **(B,D)** were measured as described in Section "2. Materials and methods". The median with 10%/90% percentiles of individual mice is shown in a box and whisker plot with the mean value indicated by "+". The indicated differences were statistically significant, as determined by one-way ANOVA followed by Tukey *post-hoc* tests [**$p < 0.01$ for comparisons between two groups; **(A,B)** $n = 6$ mice; **(B)** $p < 0.0001$, $F(2,15) = 64.21$; **(C,D)** $n = 5$; **(C)** $p < 0.0001$, $F(2,12) = 831.7$; **(D)** $p < 0.0001$, $F(2,12) = 208.3$].

or two-way ANOVA with or without the Tukey *post-hoc* tests were used to determine statistical significance for experiments with three or more experimental groups. *P*-values of less than 0.05 were considered significant. GraphPad Prism software (Boston MA, USA) was used for the creation of the graphs and further statistical analysis.

3. Results

3.1. CB4-, but not C3-, deficient mice develop very severe seizures with a 100% mortality rate

To determine the differential role of C4 vs. C3 proteins during epileptic insult, we induced seizures in WT, $C3^{-/-}$, and $C4B^{-/-}$ mice using the standard convulsant dose of PTZ of 80 mg/kg (Kopeikina et al., 2020). All three experimental groups developed seizures, with a comparable mean latency time of 102 s for WT and 110 s for $C4B^{-/-}$ mice (Figure 1A). There was a trend of a slight increase in mean latency for C3-deficient mice (125 s), but it was not statistically significant (Figure 1A). However, when we analyzed the severity of seizures using epileptic scores, we found that C4B-deficient mice had very severe seizures with maximal epileptic scores of 5–6 developed within 10 min period post-PTZ administration (Figure 1B), and 100% mortality rate within 6–12 min period post-PTZ-administration (Table 2). At the same time, WT mice had maximal epileptic scores of 4–5 (Figure 1B) with a mortality rate of 0% (Table 2). Quite surprisingly in contrast to C4B-deficient mice, $C3^{-/-}$ mice had lower maximal epileptic scores of 2–3 when compared to WT mice; however, one C3-deficient mouse out of six died 28 min post-PTZ injection comprising a 16% mortality rate (Table 2). When we injected a subconvulsant dose of PTZ [50 mg/kg (Kopeikina et al., 2020)], we found, as it was expected, that WT mice did not develop tonic-clonic seizures with scores 3 or above over 10 min period with maximal epileptic scores 0–1 (no symptoms or facial twitching) and 0% mortality (Figures 1C, D; Table 2). Interestingly C3-deficient mice showed the same results as the WT group with a maximal score of 0–1 and 0% mortality rate (Figures 1C, D; Table 2). However, C4B-deficient mice developed severe seizures with ~100 s latency to score 3 or above (Figure 1C), maximal epileptic scores 5–6 (Figure 1D), and a 60% mortality

rate (Table 2). Thus, these data indicate that C4B-, but not C3-, deficient animals were very susceptible to seizure development with convulsant and subconvulsant doses of PTZ.

3.2. C4-deficient mice fail to upregulate immediate early genes during epileptic seizures

It is well known that during epileptic seizures neuronal cells upregulate IEGs within minutes (Kalinina et al., 2022). IEGs are responsible for many neuronal functions including their activation, long-term potentiation (LTP), memory, and CNS repair (Kiessling and Gass, 1993; Dragunow, 1996; Gallo et al., 2018). We hypothesized that C4-deficient mice abnormally respond to stress conditions such as seizures, which is reflected in the abnormal pattern of IEG expression in the CNS. To test our hypothesis, we performed selective profiling of ten IEGs at a baseline level in unmanipulated mice and 9 ± 1 min post-PTZ injection in the brain of WT, C3- and C4B-deficient mice. Time-point of 9 ± 1 min was selected to ensure that all tested animals including C4B$^{-/-}$ are alive. We found that out of 10 tested IEGs, nine were expressed in the brain of WT, C3-, and C4B-deficient mice at comparable baseline levels (Figures 2, 3; WT, C3$^{-/-}$, C4$^{-/-}$), except for Egr1 that was significantly reduced in the brain of C4B-deficient mice when compared to C3$^{-/-}$ and WT groups (Figure 2A; WT, C3$^{-/-}$, C4$^{-/-}$). Nine minutes post-PTZ injection, WT and C3$^{-/-}$ mice substantially upregulated (from ∼2 to 40-fold changes) all ten tested IEGs: *Egrs1-4*, *c-Fos*, *c-Jun* (Figure 2), *FosB*, *Nur77, Npas 4* and *Arc* (Figures 3A-D); however, C4B$^{-/-}$ mice could not upregulate expression of nine of ten tested IEGs to the level of WT or C3$^{-/-}$ animals except for *Arc,* which was upregulated in C4B$^{-/-}$ mice to the level comparable to WT and C3$^{-/-}$ mice (Figure 3D). Thus, these data indicate that after PTZ administration C4B$^{-/-}$, but not WT or C3$^{-/-}$, mice could not substantially upregulate nine out of ten tested IEGs: *Egrs1-4*, *c-Fos*, *c-Jun*, *ForB*, *Naps4*, and *Nur77*.

3.3. C4-deficient mice fail to upregulate CNS repair and pro-inflammatory genes

In the next series of experiments, we investigated the expression of other genes in the CNS, which are downstream of IEGs. It was demonstrated that *Npas4* directly regulates *BDNF*, an important neurotrophic factor involved in neuronal protection and CNS repair (Fu et al., 2020). Indeed, we found that C4B-deficient mice could not upregulate *BDNF* in the brain after PTZ injection when compared to WT and C3-deficient mice (Figure 4A). It was also demonstrated that *Egr1* directly regulate expression of *GABRA2* and *GABRQ* genes that are involved in inhibitory synapse activity by forming subunits for $GABA_A$ receptors in post-synaptic membranes (Mo et al., 2015). Since C4B-deficient mice had a lower level of *Egr1* at baseline level in the CNS and it was not substantially upregulated in the brain after PTZ injection when compared to WT and C3$^{-/-}$ controls (Figure 2A), we investigated the level of *GABRA2* and *GABRQ* genes in WT vs. C3$^{-/-}$ vs. C4B$^{-/-}$ mice. We did not find differences in *GABRQ* expression levels (not shown), but C3$^{-/-}$ mice had a 2.8-fold higher level of *GABRA2* at the baseline level in the brain, which was not altered after PTZ injection (Figure 4B), when compared to WT and C4B$^{-/-}$ mice. An elevated level of *GABRA2* in the brain of C3-deficient mice might explain lower maximal epileptic scores in these mice after injection of PTZ (Figure 1B), which is a $GABA_A$ receptor antagonist. Finally, we investigated the expression of three major pro-inflammatory cytokines IL-1β, IL-6, and TNF in the CNS at the baseline level and post-PTZ injection in three experimental groups. Two IEGs c-Fos and c-Jun form dimers comprising transcription factor AP-1, which is known to induce the expression of pro-inflammatory cytokines in innate immune cells (Guha and Mackman, 2001; Veremeyko et al., 2019b). Since C4B-deficient mice failed to upregulate both c-Fos (Figure 2E) and c-Jun (Figure 2F) in the brain, we expected to find lower levels of major innate pro-inflammatory cytokines in the CNS after PTZ injection. Indeed, C4B-deficient mice could not efficiently upregulate these three cytokines in the brain when compared to WT or C3$^{-/-}$ mice (Figures 4C-E). At the same time, both C3- and C4B-deficient mice had ∼3-fold higher baseline levels of IL-6 in the CNS (Figure 4D). Thus, our data indicate that C4B-deficient mice could not efficiently upregulate genes downstream of IEGs such as neurotrophic factor BDNF and major pro-inflammatory cytokines IL-1β, IL-6, and TNF.

TABLE 2 The mortality rate in wild-type (WT), C3-, and C4-deficient mice with epileptic seizures induced by convulsant (80 mg/kg) and sub-convulsant (50 mg/kg) dosages of PTZ[1].

PTZ dosage	80 mg/kg			50 mg/kg		
Mouse genotype	WT	C3$^{-/-}$	C4$^{-/-}$	WT	C3$^{-/-}$	C4$^{-/-}$
Mortality rate, % (m/n)	0% (0/6)	16%[2] (1/6)	100%[3] (6/6)	0% (0/5)	0% (0/5)	60%[3] (3/5)

[1]Epileptic seizures were induced by i.p. injection of PTZ in WT, C3$^{-/-}$, and C4$^{-/-}$ mice at the dosage of 80 mg/kg or 50 mg/kg, and mice were monitored for 4h for their survival as described in Section "2. Materials and methods".
[2]Died 28 min post-PTZ injection.
[3]Died 6–12 min post-PTZ injection.

3.4. C3- and C4-deficient animals have elevated baseline levels of synaptic marker PSD95

It was established that C4B- and C3-deficient mice had a higher density of axons and a higher number of synapses (Chu et al., 2010; Yilmaz et al., 2021). However, the axonal density and number of synapses (and PSD95-positive post-synaptic densities) were shown to be comparable in the CNS of C3 vs. C4 deficient mice (Gomez-Arboledas et al., 2021; Yilmaz et al., 2021). To confirm this, we compared the number of synaptic and neuronal genes in the brain of WT, C3, and C4B-deficient animals at baseline level and after PTZ injection. We found that both C3- and C4B-deficient mice had ∼1.5-fold higher baseline mRNA level of expression of *PSD95* in the brain (Figure 4F), which was confirmed on a protein level (Supplementary Figure 3). After PTZ injection, mRNA expression of PSD95 was decreased in the brain compared to unmanipulated animals and was not statistically different among WT, C3$^{-/-}$, and C4B$^{-/-}$ experimental groups (Figure 4F). We did not find

10.3389/fncel.2023.1170031

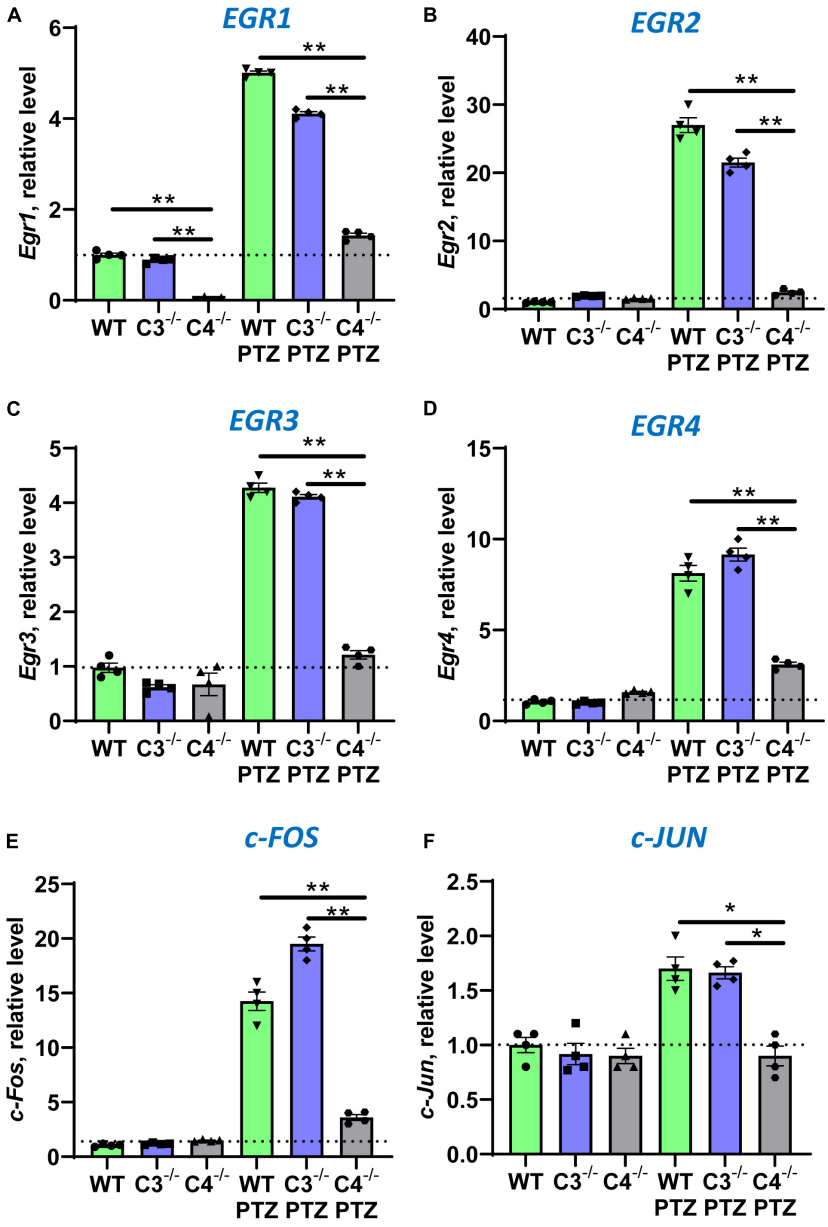

FIGURE 2
Analysis of the expression of *Egr1*, *Egr2*, *Egr3*, *Egr4*, *c-Fos*, and *c-Jun* immediate early genes in the brain cortex of unmanipulated mice or mice with PTZ-induced seizures in groups of WT, or $C3^{-/-}$, or $C4B^{-/-}$ animals. RNA was isolated from brain cortexes of unmanipulated WT, or $C3^{-/-}$, or $C4B^{-/-}$ mice (left three bars in each panel) vs. WT, or $C3^{-/-}$, or $C4B^{-/-}$ mice 9 ± 1 min post-PTZ administration (right three bars in each panel), and the expressions of *Egr1* **(A)**, *Egr2* **(B)**, *Egr3* **(C)**, *Egr4* **(D)**, *c-Fos* **(E)**, and *c-Jun* **(F)** were analyzed by real-time RT PCR as described in the Section "2. Materials and methods". Mean ± standard error (SE) with overlayed dot plots is shown. The indicated differences were statistically significant, as determined by one-way ANOVA followed by Tukey *post-hoc* test (*$p < 0.05$, **$p < 0.01$ for comparisons between two indicated groups; $n = 4$ mice).

statistically significant differences for baseline and post-PTZ levels for other tested neuronal genes *Syn1* and *Mecp2* in the brain (not shown). Thus, we found elevated baseline levels of synaptic marker PSD95 on mRNA and protein levels for both C3- and C4B-deficient mice when compared to WT mice, which is likely connected with the higher number of synapses in these animals. In support of our conclusion, it was shown that C3b deposits required for synapse elimination were found to be co-localized with PSD95 (Gomez-Arboledas et al., 2021), while the level of C3 is also reduced in CNS of C4B-deficient mice (Yilmaz et al., 2021).

3.5. C4B-, but not C3-, deficient mice have low baseline level of EGR1 protein

Following our experiment that demonstrated a very low baseline mRNA level of Egr1 in the CNS of unmanipulated $C4B^{-/-}$ mice (**Figure 2A**), we investigated the baseline level of expression of EGR1 in the brain on a protein level in these animals by western blotting. Quantitative analysis revealed ~5-fold lower level of ERG1 in the CNS of unmanipulated C4B-deficient mice when compared to WT and C3-deficient animals (**Figure 5**). Thus, C4B-deficient

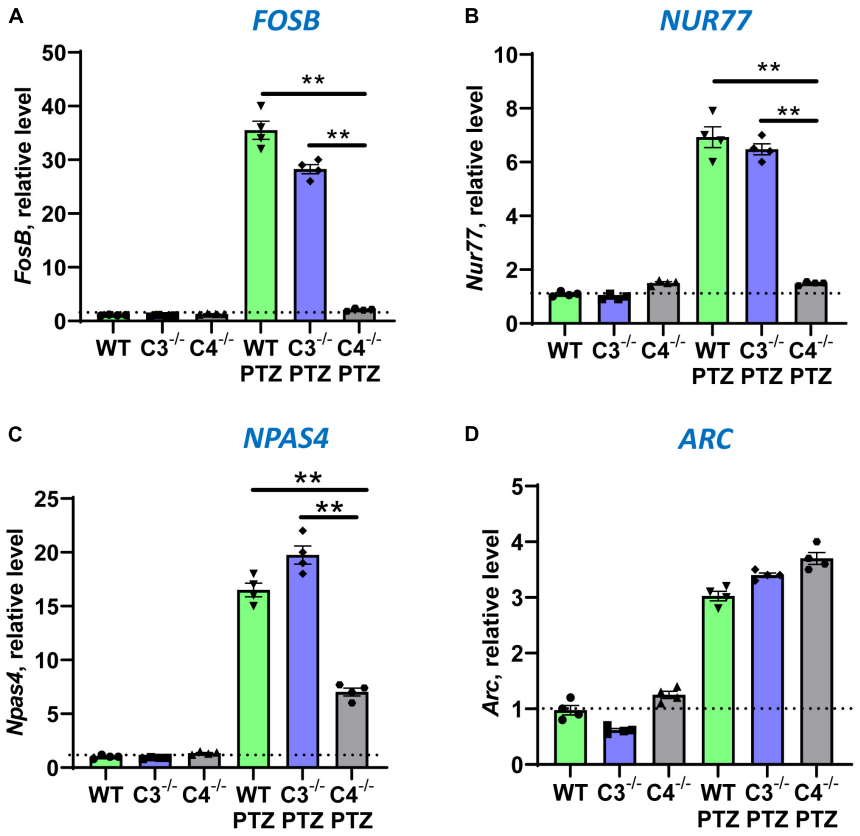

FIGURE 3
Analysis of the expression of *FosB*, *Nur77*, *Npas4*, and *Arc* immediate early genes in brain cortexes of unmanipulated mice or mice with PTZ-induced seizures in groups of WT, or $C3^{-/-}$, or $C4B^{-/-}$ animals. RNA was isolated from brain cortexes of unmanipulated WT, or $C3^{-/-}$, or $C4B^{-/-}$ mice (left three bars in each panel) vs. WT, or $C3^{-/-}$, or $C4B^{-/-}$ mice 9 ± 1 min post-PTZ administration (right three bars in each panel), and the expressions of *FosB* **(A)**, *Nur77* **(B)**, *Npas4* **(C)**, and *Arc* **(D)** were analyzed by real-time RT PCR as described in Section "2. Materials and methods". Mean ± standard error (SE) with overlayed dot plots is shown. The indicated differences were statistically significant, as determined by one-way ANOVA followed by Tukey *post-hoc* test (**$p < 0.01$ for comparisons between two indicated groups; $n = 4$ mice).

mice have a low baseline level of Egr1 in the CNS on mRNA and protein levels.

3.6. C3-/- and $C4B^{-/-}$ animals have motor function deficiency

We hypothesized that a low baseline level of Egr1 in C4B-deficient mice could be associated with behavior changes, which is reflected in the performance in motor and cognitive function tests. We found that both C3- and C4B-deficient mice had significantly worse performance in the Rotarod test during a 5-day training course when compared to WT mice (Figure 6A). Thus, we found that both C3- and C4B-deficient mice had deficiency in their motor functions, which is likely linked to the deficiency in synapse pruning in these animals.

3.7. C4B-, but not C3-, deficient mice have cognitive dysfunctions

We further investigated whether a low baseline level of Egr1 in C4B-deficient mice could be associated with worse performance in cognitive function test. When we compared cognitive (memory) functions in the Barns maze test, we found for both the training session on day 4 (Figure 6B) and the final trial on day 5 (Figure 6C) the performance results were statistically significantly worse for $C4B^{-/-}$, but not $C3^{-/-}$ mice when compared to WT animals (Figures 6B, C). Thus, these data indicate that the deficiency in Egr1 expression at the baseline level is associated with cognitive problems in $C4B^{-/-}$ animals.

4. Discussion

In this study, we compared the outcome of PTZ-induced epileptic seizures and behavior deviations in $C3^{-/-}$ vs. $C4B^{-/-}$ mutant mice in comparison with non-mutant WT animals. The rationale for this study was to identify a new role of C4 beyond its upstream activator of C3. We found that *C3*- and *C4B*-deficient mice shared several phenotypical features: both mutants have elevated levels of synaptic marker PSD95 (Figure 4F, Supplementary Figure 3), an elevated baseline level of pro-inflammatory cytokine IL-6 (Figure 4D), and problems in motor functions (Figure 6A). These data support the currently dominating paradigm that C4 acts as an upstream activator of C3

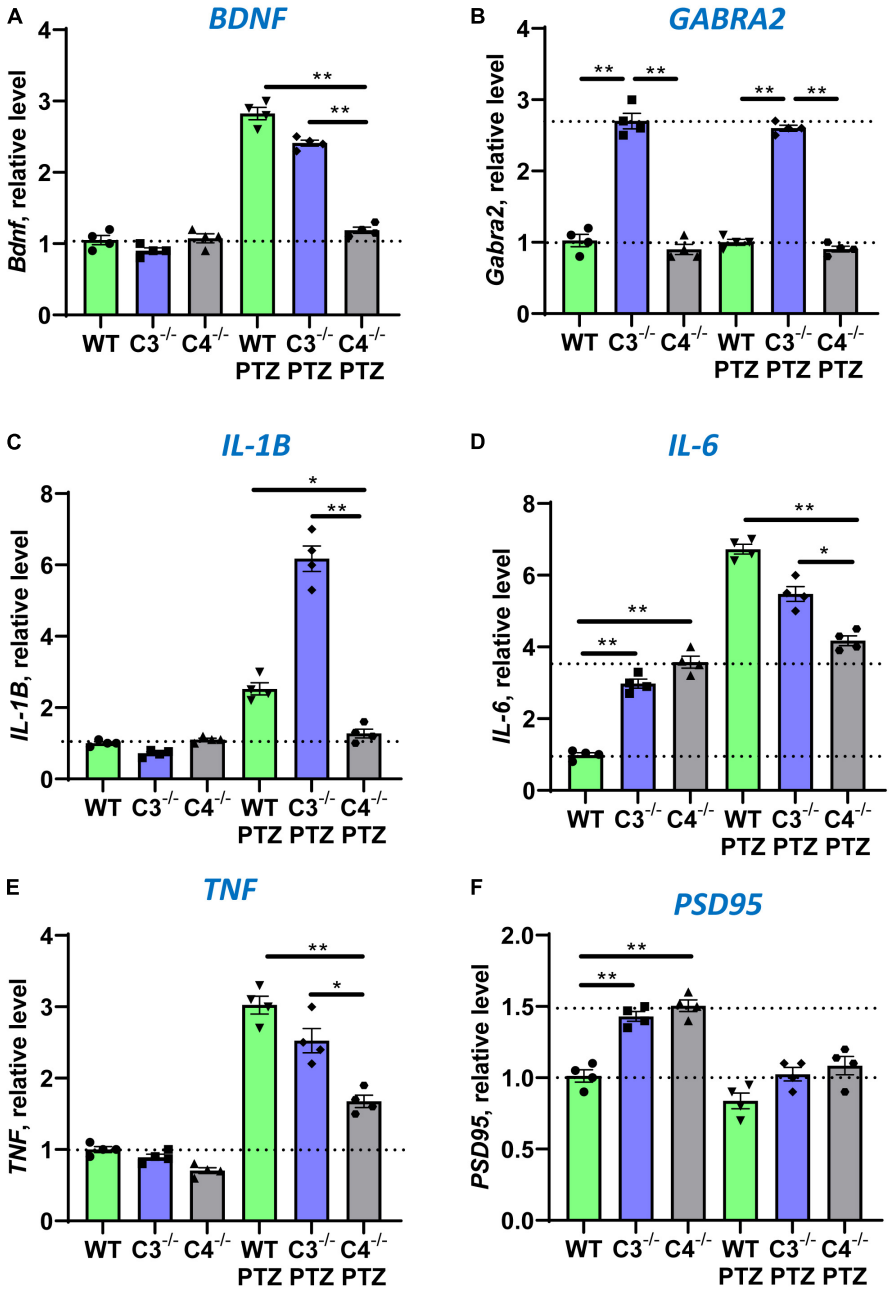

FIGURE 4
Analysis of the expression of *BDNF*, *GABRA2*, *IL-1β*, *IL-6*, *TNF*, and *PSD95* in the brain cortex of unmanipulated mice or mice with PTZ-induced seizures in groups of WT, or $C3^{-/-}$, or $C4B^{-/-}$ animals. RNA was isolated from brain cortexes of unmanipulated WT, or $C3^{-/-}$, or $C4B^{-/-}$ mice (left three bars in each panel) vs. WT, or $C3^{-/-}$, or $C4B^{-/-}$ mice 9 ± 1 min post-PTZ administration (right three bars in each panel), and the expressions of *BDNF* **(A)**, *GABRA2* **(B)**, *IL-1β* **(C)**, *IL-6* **(D)**, *TNF* **(E)**, and PSD95 **(F)** were analyzed by real-time RT PCR as described in Section "2. Materials and methods". Mean ± standard error (SE) with overlayed dot plots is shown. The indicated differences were statistically significant, as determined by one-way ANOVA followed by Tukey *post-hoc* test (*$p < 0.05$, **$p < 0.01$ for comparisons between two groups; $n = 4$ mice).

in classical pathway that are involved in CNS functions such as synapse pruning. In the frame of this paradigm, the phenotype of C4- and C3-deficient animals is identical or at least very similar. However, we also found that $C4B^{-/-}$ has many phenotypical features very different from $C3^{-/-}$ animals. Specifically, $C4B^{-/-}$, but not $C3^{-/-}$ mutants, were highly sensitive to PTZ-induced epileptic seizures leading to very severe seizures with 100% mortality rate in a convulsant dose of PTZ (80 mg/kg) and a 60% mortality even in case of subconvulsant dose of PTZ (50 mg/kg) (Figure 1; Table 2). The high susceptibility of C4B-deficient animals to PTZ was associated with the inability of these mutants to upregulate multiple IEGs (Egrs1-4, c-Fos, c-Jun, FosB, Nur77, and Npas4) and their downstream targets such as neurotrophic factor BDNF and cytokines IL-1β, IL-6 and TNF (Figures 2–4). In addition, $C4B^{-/-}$ mice had a low baseline level of Egr1 in the CNS on mRNA and protein levels (Figures 2, 5), which is related

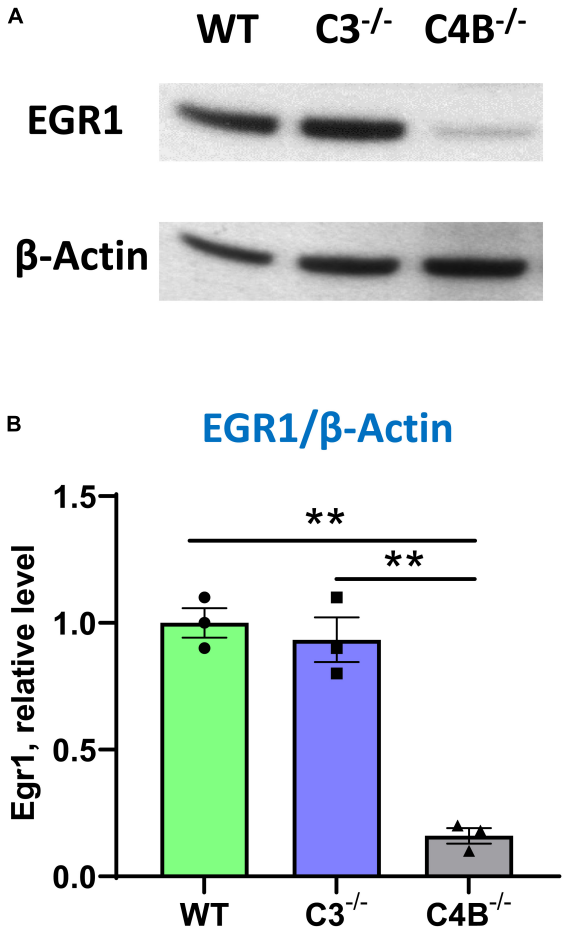

FIGURE 5
Analysis of the expression of Egr1 on a protein level in the brain cortex of unmanipulated WT, or C3$^{-/-}$, or C4B$^{-/-}$ mice. Expressions of Egr1 and β-Actin were analyzed by western blot as described in Section "2. Materials and methods". A representative blot for Egr1 [**(A)**, upper image], β-Actin [**(A)**, bottom image], and quantitative analysis of Erg1/βActin ratio **(B)** are shown. In panel **(B)**, mean ± standard error (SE) with overlayed dot plots is shown. The indicated differences were statistically significant, as determined by one-way ANOVA followed by Tukey *post-hoc* test (**$p < 0.01$ for comparisons between two groups; $n = 3$ mice).

to cognitive problems in these animals (Figures 6B, C). We believe that the inability to upregulate IEGs and their downstream targets leads to the poor outcome of epileptic seizures and possibly other conditions such as stress or neuronal injury as summarized in Figure 7A.

Thus, our data indicate that C4B, but not C3, play an important role in the CNS to facilitate upregulation of IEG expression during CNS insults such as seizures (and likely other stress conditions), and the expression of these IEGs and their downstream targets (e.g., BDNF) is very important to cope with neuropathological conditions. The results from our study make us believe that poor ability to deal with stresses, injuries, or CNS insults (e.g., failure upregulate multiple IEGs or maintain Egr1 at baseline level) in case of C4B functional deficiency could potentially predispose to the development of certain neurologic conditions such as SZ and ASD, where stress was shown to be an aggravating factor (Walker et al., 2008; Theoharides and Kavalioti, 2019). In the case of epilepsy, a traumatic brain injury could be a such factor that predisposes to the development of seizures (Englander et al., 2014). Moreover, the baseline level of certain IEGs such as Egr1 in the CNS of C4B-deficient individuals could lead to insufficient axonal growth and synapse formation during CNS development in humans and subsequent cognitive problems and behavior deviations. Recently it was demonstrated that iPSC-derived astrocytes of patients with ASD express low levels of C4 (the study did not discriminate C4A and C4B isoforms) on both mRNA and protein levels (Mansur et al., 2021). These low baseline levels of C4 in the CNS of these subjects could potentially lead to low Egr1 levels in ASD subjects, as we observed in C4B-deficient mice. Studies in mouse and zebrafish models demonstrated an important role for Egr1 in social behavior and the formation of proper neuronal circuits (Tallafuss et al., 2022), while in humans Egr1 was shown to be connected with stress-related mood disorders, schizophrenia, and depression (Duclot and Kabbaj, 2017). Patients with certain systemic autoimmune diseases such as systemic lupus erythematosus (SLE) exhibit neuropsychiatric symptoms and cognitive problems known as "lupus fog" (Monahan et al., 2021). At the same time SLE patients have low level of C4 (Wang and Liu, 2021), which might be connected with these neurologic symptoms. It was also found recently that Egr1 gene is related to SLE pathology (Udhaya Kumar et al., 2020). Thus, our study provides the missing link between C4 and Erg1 in the pathogenesis of aforementioned disorders.

Egr1 belongs to the family of IEGs, which is the family of genes that can become transcribed immediately using an existing pool of kinases or other secondary messengers within minutes after stimulation without the need of the synthesis of new proteins (Pérez-Cadahía et al., 2011). Multiple stimuli induce expression of IEGs that include trophic factors downstream of receptor tyrosine kinases (RTKs, e.g., EGFR, TrkA, TrkB), calcium channels (e.g., NMDAR), neurotransmitters (glutamine, dopamine), and viral infection (Bahrami and Drabløs, 2016; Minatohara et al., 2016; Gallo et al., 2018). In the CNS, c-Fos, Egr1, and Arc are used as a markers of neuronal activity in the context of memory formation and development of multiple psychiatric disorders such as SZ and ASD (Minatohara et al., 2016; Gallo et al., 2018). It was previously shown that multiple IEGs, including Egr1, Egr4, c-Fos, c-Jun, Naps4, Nur77, and Arc were upregulated in *in vivo* animal (from rodents to primates) and in *in vitro* models of epilepsy, as was confirmed in our study (Kiessling and Gass, 1993; Barros et al., 2015; Kalinina et al., 2022; Rienecker et al., 2022). However, in contrast to earlier studies that used *in situ* hybridization, repetitive stimulations with PTZ, or using the earliest time-point at 30 min, we used more sensitive quantitative real-time PCR, which allowed us to detect upregulation of ten IEGs within a 9 ± 1 min period post-PTZ injections to ensure that all tested animals are alive. We were very strict in our kinetic time-point since C4B$^{-/-}$ mice died 8–12 post PTZ and we had to select only alive animals for gene expression analysis. Using this technique, we also showed defective upregulation of cytokines (IL-1β, IL-6, TNF) and tissue repair factors (BDNF) in C4B-deficient mice, but not $GABA_A$ receptor subunits, which probably require more time for upregulation within a 9-min period. Neuronal c-Fos, Egr1, and Arc have been also implicated in learning, memory, and long-term potentiation (LTP) (Gallo et al., 2018), and we found a significant reduction of Egr1 in normal CNS and during seizures

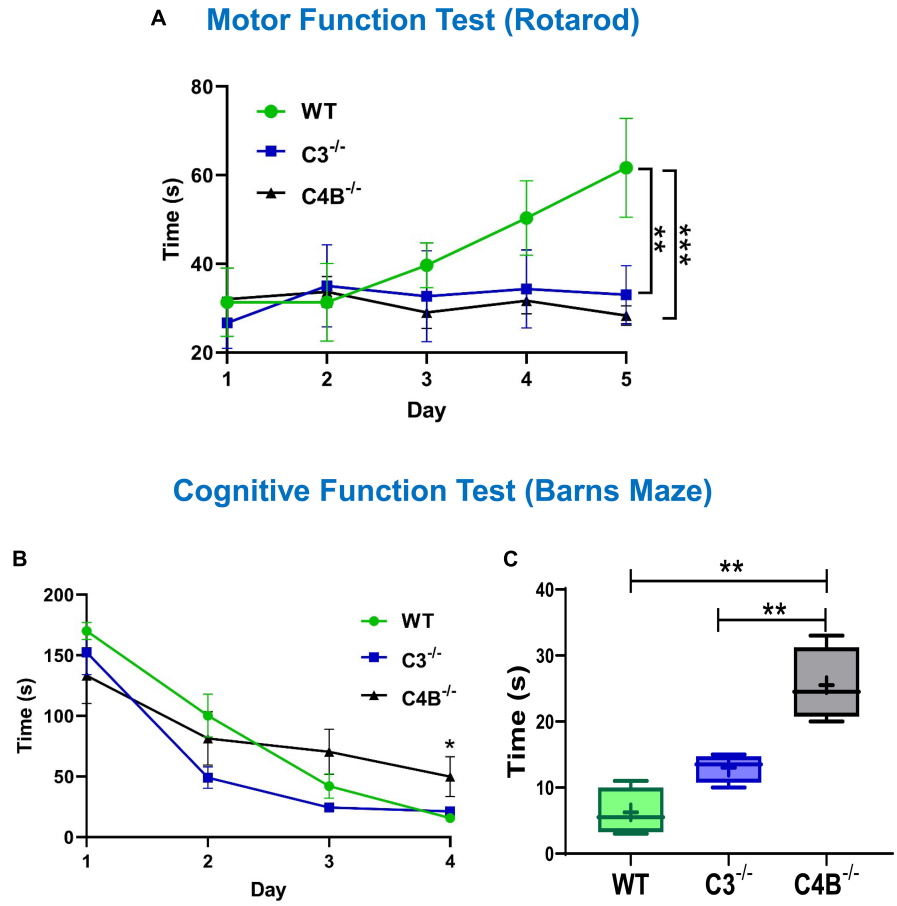

FIGURE 6
Comparison of motor and cognitive functions of unmanipulated WT, C3-, and C4B-deficient mice. Unmanipulated WT, or C3$^{-/-}$, or C4B$^{-/-}$ mice were assessed for their performance in Rotarod **(A)** and Barns maze **(B,C)** tests as described in Section "2. Materials and methods". In panel **(A)**, the time to fall from the rotating rod is shown for WT, or C3$^{-/-}$, or C4B$^{-/-}$ mice in the Rotarod test on day 1, day 2, day 3, day 4, and day 5. The mean ± standard error (SE) of time to fall (y-axis) vs. day of training (x-axis) is shown [C3$^{-/-}$ vs. WT: $^{**}p < 0.01$, C4$^{-/-}$ vs. WT: $^{***}p < 0.001$; two-way ANOVA, C4$^{-/-}$ vs. WT: $F(4,16) = 13.90$; C3$^{-/-}$ vs. WT: $F(4,16) = 6.439$; C4$^{-/-}$ vs. C3$^{-/-}$: not significant; $n = 3$ mice]. In panels **(B,C)**, the latency time is shown for WT, or C3$^{-/-}$, or C4B$^{-/-}$ mice in the Barns maze test during the training period on day 1, day 2, day 3, and day 4 **(B)**, and the final trial on day 5 **(C)**. In panel **(B)**, the mean ± standard error (SE) of latency time (y-axis) vs. day of training (x-axis) is shown. The indicated difference on day 4 was statistically significant, as determined by one-way ANOVA followed by Tukey *post-hoc* tests [$^{*}p < 0.05$ for comparisons C4$^{-/-}$ vs. WT and C4$^{-/-}$ vs. C3$^{-/-}$ on day 4; n = (4 mice × 3 trails) = 12]. In panel **(C)**, the median with 10%/90% percentiles of individual mice are shown in a box and whisker plot with the mean value indicated by "+". The indicated differences were statistically significant for the final trial on day 5, as determined by one-way ANOVA followed by Tukey *post-hoc* tests [$^{**}p < 0.01$ for comparisons between two groups; $F(2,9) = 23.56$; $n = 4$ mice].

in C4B-deficient mice. Thus, there is a possible link between memory function and expression of Egr1, as we also found in our study, which demonstrates the correlation between a low level of baseline Egr1 expression and performance in the Barns maze test. However, our study shows only association of behavior problems in C4-deficient mice with low level of Erg1 expression in the CNS.

The exact mechanism of connection of IEG expression and C4 activation in the CNS is currently not clear. Among known classical complement receptors (CR), only type 1 complement receptor (CR1/CD35) was shown to bind both C4b and C3b fragments of cleaved C4 and C3 using two different domains for C4b and C3b, and this receptor is associated with the pathogenesis of certain autoimmune diseases (Khera and Das, 2009). Thus, CR1 was the only documented receptor for C4. Despite CR1 being mainly expressed in erythrocytes, B cells, macrophages, and granulocytes (Khera and Das, 2009), the new type 1 complement receptor CSMD1 was found to be highly expressed in the CNS and epithelial cells (Kraus et al., 2006). CSMD family consists of CSMD1, CSMD2, and CSMD3 members, and CSMD1 is the most well-studied member (Ermis Akyuz and Bell, 2022). Similar to CR1, CSMD1 was shown to bind C4b and C3b to promote their degradation by Factor I (Escudero-Esparza et al., 2013), and it is highly expressed in the CNS in 80% of GABAR-positive synapses and 40% of NMDAR-positive synapses (Baum et al., 2020). CSMD1 and CSMD2 polymorphisms were associated with SZ (Håvik et al., 2011; Rose et al., 2013), while CSMD3 was associated with both SZ and ASD (Mizukami et al., 2016). It was shown that CSMD1 could bind and inhibit RTKs such as EGFR (potent inducer of IEGs) and CSMD1 can also modulate TGFβ receptor signaling (Gialeli et al., 2021; Ermis Akyuz and Bell, 2022). Although both EGFR and TGFβRs are expressed in the CNS (Dobolyi et al., 2012; Romano and Bucci, 2020), neuronal cells have other important RTKs such as TrkA and TrkB neurotrophic

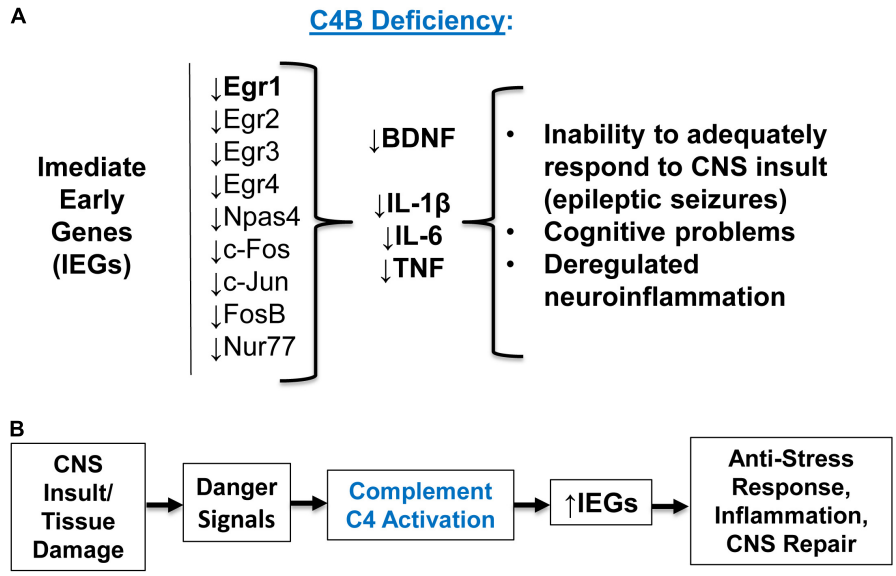

FIGURE 7
The summary of experimental results and concluding model. **(A)** Summary of the experimental results. C4B deficiency results in a low level of Egr1 in the CNS at the baseline level, and these animals are unable to upregulate Egr1-4, c-Fos, c-Jun, Npas4, and other immediate early genes (IEGs) during epileptic seizures. Inability to upregulate IEGs results in the inability to upregulate downstream target genes BDNF and pro-inflammatory cytokines IL-1β, IL-6, and TNF. Deficiency in IEGs and their downstream targets result in inappropriate responses to CNS insult, injury, or stress conditions. **(B)** Concluding model. Complement C4 activation requirement for IEG upregulation. CNS (or other tissue) insult or infection results in initial tissue damage and release of proper "danger signals", which lead to activation of complement C4. Activated C4 induces expression of IEGs and their downstream genes required for anti-stress, inflammatory, and tissue repair responses.

receptors, that bind BDNF and NGF, respectively (Haddad et al., 2017). There is the possibility that CSMD1 or other members of this family could bind to certain neuronal RTKs and inhibit them in normal CNS. Upon C4 cleavage into the C4b fragment during epileptic seizures or other stress conditions CSMD1 could bind to C4b and no longer inactivate RTKs and the level of IEGs is elevated. Alternatively, CSMDs could also send intracellular signals to induce IEG expression. Further studies will allow us to further elucidate the exact mechanisms of induction of neuronal IEGs by C4. In support of our hypotheses and assumptions stated above, we have previously found that the blood-brain barrier becomes compromised during PTZ-induced seizures, which is accompanied by rapid activation of platelets and blood coagulation cascade leading to activation of complement as well (Dukhinova et al., 2018; Kopeikina et al., 2020; Kopeikina and Ponomarev, 2021).

It is also not clear why C4 plays a more important role in the process of IEG induction when compared to C3. We believe this happens because, in the case of C4 deficiency, the activation of both C4 and C3 is affected (both C4b and C3b fragments are missing), while in the case of C3 deficiency, activation of C4 is still intact (C4b fragments are still present). This is especially important if we remember the fact that CR1 receptors (CR1/CD35 and CSMDs) bind both C4b and C3b (Khera and Das, 2009; Ermis Akyuz and Bell, 2022). In support of this assumption, it was found that the level of C4 remains high in the CNS of C3-deficient mice, while $C4B^{-/-}$ mice have a decrease in both C3 and C4 in the CNS (Yilmaz et al., 2021). In the periphery, we also found in our study that the level of C4 was normal in the serum of C3-deficient mice (**Supplementary Figure 2**), while $C4B^{-/-}$ had a lower level of C3 activation when compared to WT mice as determined by the intensity of small C3α fragments (within 37–50 kDa range) in western blot analysis of mouse serum (**Supplementary Figure 1**). We assume that during blood coagulation C4 also play an important role and we see lower level of C3 cleavage in serum samples of C4B-deficient mice (**Supplementary Figure 1A**). Giving the fact that C4 and C3 have structural similarity (C4 is a paralog for C3 sharing ∼30% of sequence homology) (Blanchong et al., 2001; Mortensen et al., 2015), and both bind to CRs of type 1, it is not very surprising that C4 genetic deficiency in mice has a stronger influence on phenotype when compared to C3 deficiency. In our study we did not analyze the presence of activated C4 in the brain of mice after PTZ administration. Most likely C4 is cleaved in the CNS during seizures by Factor I into iC4b, then into C4d and C4c (Wang and Liu, 2021), and C4d could be deposited on injured neuronal cells. Future studies will investigate C4 depositions in the CNS after seizures.

We believe that initiation/enhancement of IEGs by C4 is a general mechanism of the response of many cell types to pathogen invasion and/or tissue injury where C4 play a key role as a main opsonin of damaged or infected cells (Mortensen et al., 2015). A recent study indicates that a low level of C4B is associated with a high level of mortality after acute myocardial infarction (Blaskó et al., 2008). Given the important role of Egr1 in the regulation of myocardial cell injury (Khachigian, 2016), it is highly likely that expression of Egr1 and other IEGs is enhanced by C4 complement activation during cardiovascular pathological conditions. During viral infection, many viruses specifically inactivate C4, most likely avoiding the upregulation of IEGs in infected cells

(Wang and Liu, 2021). Finally, in certain autoimmune diseases such as SLE, C4, and CR1 were shown to play an important role (Blanchong et al., 2001; Zhou et al., 2021).

Our concluding model is shown in **Figure 7B**. According to this model, CNS (or other tissues) insults result in initial tissue injury when complement activation occurs in response to "danger signals" as was proposed recently (Reis et al., 2019). Activation of complement C4 results in the upregulation of IEGs and proper downstream anti-stress, inflammatory, and tissue repair genes (**Figure 7B**). Thus, we believe that the connection between C4 and IEG expression could be a new and universal mechanism of cell activation during pathogen invasion and/or tissue injury in the CNS and the periphery.

Data availability statement

The original contributions presented in this study are included in the article/**Supplementary material**, further inquiries can be directed to the corresponding author.

Ethics statement

This animal study was reviewed and approved by the Food Department of the Government of Hong Kong, the Chinese University of Hong Kong, and the City University of Hong Kong Animal Experimentation Ethics Committee.

Author contributions

TV and EP conceived the study and performed the experiments. TV, RJ, MH, and EP analyzed the data and prepared the manuscript. All authors contributed to the article and approved the submitted version.

Funding

This work was supported by the Research Grant Council–Areas of Excellence Fund grant (Hong Kong Government, Hong Kong), reference no. AoE/M-604/16 and the Social Policy Research Grant (SPG) from Nazarbayev University (Nazarbayev Fund, Kazakhstan).

Conflict of interest

The authors declare that the research was conducted in the absence of any commercial or financial relationships that could be construed as a potential conflict of interest.

Publisher's note

All claims expressed in this article are solely those of the authors and do not necessarily represent those of their affiliated organizations, or those of the publisher, the editors and the reviewers. Any product that may be evaluated in this article, or claim that may be made by its manufacturer, is not guaranteed or endorsed by the publisher.

Supplementary material

The Supplementary Material for this article can be found online at: https://www.frontiersin.org/articles/10.3389/fncel.2023.1170031/full#supplementary-material

References

Bahrami, S., and Drabløs, F. (2016). Gene regulation in the immediate-early response process. *Adv. Biol. Regul.* 62, 37–49. doi: 10.1016/j.jbior.2016.05.001

Barros, V., Mundim, M., Galindo, L., Bittencourt, S., Porcionatto, M., and Mello, L. (2015). The pattern of c-Fos expression and its refractory period in the brain of rats and monkeys. *Front. Cell Neurosci.* 9:72. doi: 10.3389/fncel.2015.00072

Baum, M., Wilton, D., Muthukumar, A., Fox, R., Carey, A., Crotty, W., et al. (2020). CUB and sushi multiple domains 1 (CSMD1) opposes the complement cascade in neural tissues. *bioRxiv* [Preprint] doi: 10.1101/2020.09.11.291427

Blanchong, C., Chung, E., Rupert, K., Yang, Y., Yang, Z., Zhou, B., et al. (2001). Genetic, structural and functional diversities of human complement components C4A and C4B and their mouse homologues, Slp and C4. *Int. Immunopharmacol.* 1, 365–392. doi: 10.1016/S1567-5769(01)00019-4

Blaskó, B., Kolka, R., Thorbjornsdottir, P., Sigurdarson, S., Sigurdsson, G., Rónai, Z., et al. (2008). Low complement C4B gene copy number predicts short-term mortality after acute myocardial infarction. *Int. Immunol.* 20, 31–37. doi: 10.1093/intimm/dxm117

Chen, Y., Chu, J., Chang, R., and Wong, G. (2022). The complement system in the central nervous system: from neurodevelopment to neurodegeneration. *Biomolecules* 12:337. doi: 10.3390/biom12020337

Cho, K. (2019). Emerging roles of complement protein C1q in neurodegeneration. *Aging Dis.* 10, 652–663. doi: 10.14336/AD.2019.0118

Chu, Y., Jin, X., Parada, I., Pesic, A., Stevens, B., Barres, B., et al. (2010). Enhanced synaptic connectivity and epilepsy in C1q knockout mice. *Proc. Natl. Acad. Sci. U.S.A.* 107, 7975–7980. doi: 10.1073/pnas.0913449107

Comer, A., Jinadasa, T., Sriram, B., Phadke, R., Kretsge, L., Nguyen, T., et al. (2020). Increased expression of schizophrenia-associated gene C4 leads to hypoconnectivity of prefrontal cortex and reduced social interaction. *PLoS Biol.* 18:e3000604. doi: 10.1371/journal.pbio.3000604

Dobolyi, A., Vincze, C., Pál, G., and Lovas, G. (2012). The neuroprotective functions of transforming growth factor beta proteins. *Int. J. Mol. Sci.* 13, 8219–8258. doi: 10.3390/ijms13078219

Dragunow, M. (1996). A role for immediate-early transcription factors in learning and memory. *Behav. Genet.* 26, 293–299. doi: 10.1007/BF02359385

Druart, M., Nosten-Bertrand, M., Poll, S., Crux, S., Nebeling, F., Delhaye, C., et al. (2021). Elevated expression of complement C4 in the mouse prefrontal cortex causes schizophrenia-associated phenotypes. *Mol. Psychiatry* 26, 3489–3501. doi: 10.1038/s41380-021-01081-6

Duclot, F., and Kabbaj, M. (2017). The role of early growth response 1 (EGR1) in brain plasticity and neuropsychiatric disorders. *Front. Behav. Neurosci.* 11:35. doi: 10.3389/fnbeh.2017.00035

Dukhinova, M., Kuznetsova, I., Kopeikina, E., Veniaminova, E., Yung, A., Veremeyko, T., et al. (2018). Platelets mediate protective neuroinflammation and

promote neuronal plasticity at the site of neuronal injury. *Brain Behav. Immun.* 74, 7–27. doi: 10.1016/j.bbi.2018.09.009

Dukhinova, M., Veremeyko, T., Yung, A., Kuznetsova, I., Lau, T., Kopeikina, E., et al. (2019). Fresh evidence for major brain gangliosides as a target for the treatment of Alzheimer's disease. *Neurobiol. Aging* 77, 128–143. doi: 10.1016/j.neurobiolaging.2019.01.020

Englander, J., Cifu, D., Diaz-Arrastia, R., and Center, M. (2014). Seizures and traumatic brain injury. *Arch. Phys. Med. Rehabil.* 95, 1–2. doi: 10.1016/j.apmr.2013.06.002

Ermis Akyuz, E., and Bell, S. (2022). The diverse role of CUB and sushi multiple domains 1 (CSMD1) in human diseases. *Genes* 13:2332. doi: 10.3390/genes13122332

Escudero-Esparza, A., Kalchishkova, N., Kurbasic, E., Jiang, W., and Blom, A. (2013). The novel complement inhibitor human CUB and Sushi multiple domains 1 (CSMD1) protein promotes factor I-mediated degradation of C4b and C3b and inhibits the membrane attack complex assembly. *FASEB J.* 27, 5083–5093. doi: 10.1096/fj.13-230706

Foley, J., and Conway, E. (2016). Cross talk pathways between coagulation and inflammation. *Circ. Res.* 118, 1392–1408. doi: 10.1161/CIRCRESAHA.116.306853

Fu, J., Guo, O., Zhen, Z., and Zhen, J. (2020). Essential functions of the transcription factor Npas4 in neural circuit development, plasticity, and diseases. *Front. Neurosci.* 14:1262. doi: 10.3389/fnins.2020.603373

Gallo, F., Katche, C., Morici, J., Medina, J., and Weisstaub, N. V. (2018). Immediate early genes, memory and psychiatric disorders: focus on c-Fos, Egr1 and Arc. *Front. Behav. Neurosci.* 12:79. doi: 10.3389/fnbeh.2018.00079

Gialeli, C., Tuysuz, E., Staaf, J., Guleed, S., Paciorek, V., Mörgelin, M., et al. (2021). Complement inhibitor CSMD1 modulates epidermal growth factor receptor oncogenic signaling and sensitizes breast cancer cells to chemotherapy. *J. Exp. Clin. Cancer Res.* 40:258. doi: 10.1186/s13046-021-02042-1

Gomez-Arboledas, A., Acharya, M., and Tenner, A. (2021). The role of complement in synaptic pruning and neurodegeneration. *Immunol. Targets Ther.* 10, 373–386. doi: 10.2147/itt.s305420

Gorlova, A., Pavlov, D., Anthony, D., Ponomarev, E., Sambon, M., Proshin, A., et al. (2019). Thiamine and benfotiamine counteract ultrasound-induced aggression, normalize AMPA receptor expression and plasticity markers, and reduce oxidative stress in mice. *Neuropharmacology* 156:107543. doi: 10.1016/j.neuropharm.2019.02.025

Guha, M., and Mackman, N. (2001). LPS induction of gene expression in human monocytes. *Cell Signal.* 13, 85–94. doi: 10.1016/S0898-6568(00)00149-2

Haddad, Y., Adam, V., and Heger, Z. (2017). Trk receptors and neurotrophin cross-interactions: new perspectives toward manipulating therapeutic side-effects. *Front. Mol. Neurosci.* 10:130. doi: 10.3389/fnmol.2017.00130

Håvik, B., Le Hellard, S., Rietschel, M., Lybæk, H., Djurovic, S., Mattheisen, M., et al. (2011). The complement control-related genes CSMD1 and CSMD2 associate to schizophrenia. *Biol. Psychiatry* 70, 35–42. doi: 10.1016/j.biopsych.2011.01.030

Holden, S., Grandi, F., Aboubakr, O., Higashikubo, B., Cho, F., Chang, A., et al. (2021). Complement factor C1q mediates sleep spindle loss and epileptic spikes after mild brain injury. *Science* 373:eabj2685. doi: 10.1126/science.abj2685

Jiang, G., Shao, L., Kong, S., Zeng, M., Cheng, J., Chen, T., et al. (2021). Complement C3 aggravates post-epileptic neuronal injury via activation of TRPV1. *Neurosci. Bull.* 37, 1427–1440. doi: 10.1007/s12264-021-00750-4

Kalinina, A., Krekhno, Z., Yee, J., Lehmann, H., and Fournier, N. (2022). Effect of repeated seizures on spatial exploration and immediate early gene expression in the hippocampus and dentate gyrus. *IBRO Neurosci. Rep.* 12, 73–80. doi: 10.1016/j.ibneur.2021.12.008

Khachigian, L. (2016). Early growth response-1 in the pathogenesis of cardiovascular disease. *J. Mol. Med.* 94, 747–753. doi: 10.1007/s00109-016-1428-x

Khera, R., and Das, N. (2009). Complement receptor 1: disease associations and therapeutic implications. *Mol. Immunol.* 46, 761–772. doi: 10.1016/j.molimm.2008.09.026

Kiessling, M., and Gass, P. (1993). Immediate early gene expression in experimental epilepsy. *Brain Pathol.* 3, 381–393. doi: 10.1111/j.1750-3639.1993.tb00766.x

Kopczynska, M., Zelek, W., Vespa, S., Touchard, S., Wardle, M., Loveless, S., et al. (2018). Complement system biomarkers in epilepsy. *Seizure* 60, 1–7. doi: 10.1016/j.seizure.2018.05.016

Kopeikina, E., and Ponomarev, E. (2021). The role of platelets in the stimulation of neuronal synaptic plasticity, electric activity, and oxidative phosphorylation: possibilities for new therapy of neurodegenerative diseases. *Front. Cell Neurosci.* 15:269. doi: 10.3389/fncel.2021.680126

Kopeikina, E., Dukhinova, M., Yung, A., Veremeyko, T., Kuznetsova, I., Lau, T., et al. (2020). Platelets promote epileptic seizures by modulating brain serotonin level, enhancing neuronal electric activity, and contributing to neuroinflammation and oxidative stress. *Prog. Neurobiol.* 188, 101783. doi: 10.1016/j.pneurobio.2020.101783

Kraus, D., Elliott, G., Chute, H., Horan, T., Pfenninger, K., Sanford, S., et al. (2006). CSMD1 is a novel multiple domain complement-regulatory protein highly expressed in the central nervous system and epithelial tissues. *J. Immunol.* 176, 4419–4430. doi: 10.4049/jimmunol.176.7.4419

Kulics, J., Colten, H., and Perlmutter, D. (1990). Counterregulatory effects of interferon-γ and endotoxin on expression of the human C4 genes. *J. Clin. Invest.* 85, 943–949. doi: 10.1172/JCI114523

MacDonald, R., and Barker, J. (1977). Pentylenetetrazol and penicillin are selective antagonists of GABA-mediated post-synaptic inhibition in cultured mammalian neurones. *Nature* 267, 720–721. doi: 10.1038/267720a0

Mansur, F., Teles E Silva, A., Gomes, A., Magdalon, J., de Souza, J., Griesi-Oliveira, K., et al. (2021). Complement c4 is reduced in ipsc-derived astrocytes of autism spectrum disorder subjects. *Int. J. Mol. Sci.* 22:7579. doi: 10.3390/ijms22147579

Mayilyan, K., Dodds, A., Boyajyan, A., Soghoyan, A., and Sim, R. (2008). Complement C4B protein in schizophrenia. *World J. Biol. Psychiatry* 9, 225–230. doi: 10.1080/15622970701227803

Medina, A., Manhães, A., and Schmidt, S. (2001). Sex differences in sensitivity to seizures elicited by pentylenetetrazol in mice. *Pharmacol. Biochem. Behav.* 68, 591–596. doi: 10.1016/S0091-3057(01)00466-X

Minatohara, K., Akiyoshi, M., and Okuno, H. (2016). Role of immediate-early genes in synaptic plasticity and neuronal ensembles underlying the memory trace. *Front. Mol. Neurosci.* 8:78. doi: 10.3389/fnmol.2015.00078

Mizukami, T., Kohno, T., and Hattori, M. (2016). CUB and Sushi multiple domains 3 regulates dendrite development. *Neurosci. Res.* 110, 11–17. doi: 10.1016/j.neures.2016.03.003

Mo, J., Kim, C., Lee, D., Sun, W., Lee, H., and Kim, H. (2015). Early growth response 1 (Egr-1) directly regulates GABAA receptor α2, α4, and θ subunits in the hippocampus. *J. Neurochem.* 133, 489–500. doi: 10.1111/jnc.13077

Monahan, R., Blonk, A., Baptist, E., Middelkoop, H., Kloppenburg, M., Huizinga, T., et al. (2021). Dissociation in SLE: a part of lupus fog? *Lupus* 30, 2151–2156. doi: 10.1177/09612033211050347

Mortensen, S., Kidmose, R., Petersen, S. V., Szilágyi, Á, Prohászka, Z., and Andersen, G. (2015). Structural basis for the function of complement component C4 within the classical and lectin pathways of complement. *J. Immunol.* 194, 5488–5496. doi: 10.4049/jimmunol.1500087

Mostafa, G., and Shehab, A. (2010). The link of C4B null allele to autism and to a family history of autoimmunity in Egyptian autistic children. *J. Neuroimmunol.* 223, 115–119. doi: 10.1016/j.jneuroim.2010.03.025

Paolicelli, R., Bolasco, G., Pagani, F., Maggi, L., Scianni, M., Panzanelli, P., et al. (2011). Synaptic pruning by microglia is necessary for normal brain development. *Science* 333, 1456–1458. doi: 10.1126/science.1202529

Pavlov, D., Bettendorff, L., Gorlova, A., Olkhovik, A., Kalueff, A. V., Ponomarev, E., et al. (2019). Neuroinflammation and aberrant hippocampal plasticity in a mouse model of emotional stress evoked by exposure to ultrasound of alternating frequencies. *Prog. NeuroPsychopharmacol. Biol. Psychiatry* 90, 104–116. doi: 10.1016/j.pnpbp.2018.11.014

Peoples, N., and Strang, C. (2021). Complement activation in the central nervous system: a biophysical model for immune dysregulation in the disease state. *Front. Mol. Neurosci.* 14:620090. doi: 10.3389/fnmol.2021.620090

Pérez-Cadahía, B., Drobic, B., and Davie, J. (2011). Activation and function of immediate-early genes in the nervous system. *Biochem. Cell Biol.* 89, 61–73. doi: 10.1139/O10-138

Reis, E., Mastellos, D., Hajishengallis, G., and Lambris, J. (2019). New insights into the immune functions of complement. *Nat. Rev. Immunol.* 19, 503–516. doi: 10.1038/s41577-019-0168-x

Rienecker, K., Poston, R., Segales, J., Finholm, I., Sono, M., Munteanu, S., et al. (2022). Mild membrane depolarization in neurons induces immediate early gene transcription and acutely subdues responses to a successive stimulus. *J. Biol. Chem.* 298:102278. doi: 10.1016/j.jbc.2022.102278

Romano, R., and Bucci, C. (2020). Role of EGFR in the nervous system. *Cells* 9:1887. doi: 10.3390/cells9081887

Rose, E., Morris, D., Hargreaves, A., Fahey, C., Greene, C., Garavan, H., et al. (2013). Neural effects of the CSMD1 genome-wide associated schizophrenia risk variant rs10503253. *Am. J. Med. Genet. B Neuropsychiatr. Genet.* 162, 530–537. doi: 10.1002/ajmg.b.32182

Schartz, N., and Tenner, A. (2020). The good, the bad, and the opportunities of the complement system in neurodegenerative disease. *J. Neuroinflamm.* 17, 1–25. doi: 10.1186/s12974-020-02024-8

Sekar, A., Bialas, A., De Rivera, H., Davis, A., Hammond, T., Kamitaki, N., et al. (2016). Schizophrenia risk from complex variation of complement component 4. *Nature* 530, 177–183. doi: 10.1038/nature16549

Starossom, S., Veremeyko, T., Dukhinova, M., Yung, A., and Ponomarev, E. (2014). Glatiramer acetate (Copaxone) modulates platelet activation and inhibits thrombin-induced calcium influx: possible role of copaxone in targeting platelets during autoimmune neuroinflammation. *PLoS One* 9:e96256. doi: 10.1371/journal.pone.0096256

Starossom, S., Veremeyko, T., Yung, A., Dukhinova, M., Au, C., Lau, A., et al. (2015). Platelets play differential role during the initiation and progression of autoimmune neuroinflammation. *Circ. Res.* 117, 779–792. doi: 10.1161/CIRCRESAHA.115.306847

Stevens, B., Allen, N., Vazquez, L., Howell, G., Christopherson, K., Nouri, N., et al. (2007). The classical complement cascade mediates CNS synapse elimination. *Cell* 131, 1164–1178. doi: 10.1016/j.cell.2007.10.036

Strekalova, T., Svirin, E., Veniaminova, E., Kopeikina, E., Veremeyko, T., Yung, A., et al. (2021a). ASD-like behaviors, a dysregulated inflammatory response and decreased expression of PLP1 characterize mice deficient for sialyltransferase ST3GAL5. *Brain Behav. Immun. Health* 16:100306. doi: 10.1016/j.bbih.2021.100306

Strekalova, T., Veniaminova, E., Svirin, E., Kopeikina, E., Veremeyko, T., Yung, A., et al. (2021b). Sex-specific adhd-like behaviour, altered metabolic functions and altered eeg activity in sialyltransferase st3gal5-deficient mice. *Biomolecules* 11:1759. doi: 10.3390/biom11121759

Tallafuss, A., Stednitz, S., Voeun, M., Levichev, A., Larsch, J., Eisen, J., et al. (2022). Egr1 Is necessary for forebrain dopaminergic signaling during social behavior. *eNeuro* 9:ENEURO.35–ENEURO.22. doi: 10.1523/ENEURO.0035-22.2022

Theoharides, T., and Kavalioti, M. (2019). Effect of stress on learning and motivation-relevance to autism spectrum disorder. *Int. J. Immunopathol. Pharmacol.* 33:2058738419856760. doi: 10.1177/2058738419856760

Udhaya Kumar, S., Thirumal Kumar, D., Siva, R., George Priya Doss, C., Younes, S., Younes, N., et al. (2020). Dysregulation of signaling pathways due to differentially expressed genes from the B-cell transcriptomes of systemic lupus erythematosus patients – A bioinformatics approach. *Front. Bioeng. Biotechnol.* 8:276. doi: 10.3389/fbioe.2020.00276

Veremeyko, T., Kuznetsova, I., Dukhinova, M., W Y Yung, A., Kopeikina, E., Barteneva, N., et al. (2019a). Neuronal extracellular microRNAs miR-124 and miR-9 mediate cell–cell communication between neurons and microglia. *J. Neurosci. Res.* 97, 162–184. doi: 10.1002/jnr.24344

Veremeyko, T., Yung, A., Anthony, D., Strekalova, T., and Ponomarev, E. (2018). Early growth response gene-2 is essential for M1 and M2 macrophage activation and plasticity by modulation of the transcription factor CEBPβ. *Front. Immunol.* 9:2515. doi: 10.3389/fimmu.2018.02515

Veremeyko, T., Yung, A., Dukhinova, M., Strekalova, T., and Ponomarev, E. (2019b). The role of neuronal factors in the epigenetic reprogramming of microglia in the normal and diseased central nervous system. *Front. Cell Neurosci.* 13:453. doi: 10.3389/fncel.2019.00453

Walker, E., Mittal, V., and Tessner, K. (2008). Stress and the hypothalamic pituitary adrenal axis in the developmental course of schizophrenia. *Annu. Rev. Clin. Psychol.* 4, 189–216. doi: 10.1146/annurev.clinpsy.4.022007.141248

Wallis, R., Dodds, A., Mitchell, D., Sim, R., Reid, K., and Schwaeble, W. (2007). Molecular interactions between MASP-2, C4, and C2 and their activation fragments leading to complement activation via the lectin pathway. *J. Biol. Chem.* 282, 7844–7851. doi: 10.1074/jbc.M606326200

Wang, H., and Liu, M. (2021). Complement C4, infections, and autoimmune diseases. *Front. Immunol.* 12:2682. doi: 10.3389/fimmu.2021.694928

Yilmaz, M., Yalcin, E., Presumey, J., Aw, E., Ma, M., Whelan, C., et al. (2021). Overexpression of schizophrenia susceptibility factor human complement C4A promotes excessive synaptic loss and behavioral changes in mice. *Nat. Neurosci.* 24, 214–224. doi: 10.1038/s41593-020-00763-8

Zhou, D., Rudnicki, M., Chua, G., Lawrance, S., Zhou, B., Drew, J., et al. (2021). Human complement C4B allotypes and deficiencies in selected cases with autoimmune diseases. *Front. Immunol.* 12:4254. doi: 10.3389/fimmu.2021.739430

frontiers | Frontiers in Cellular Neuroscience

TYPE Original Research
PUBLISHED 28 June 2023
DOI 10.3389/fncel.2023.1187400

OPEN ACCESS

EDITED BY
Kees Fluiter,
Leiden University Medical Center (LUMC), Netherlands

REVIEWED BY
Jesse Smith,
University of Colorado - Anschutz Medical Campus, United States
Lian Zhao,
National Eye Institute (NIH), United States

*CORRESPONDENCE
Heping Xu
✉ heping.xu@qub.ac.uk
Zhikuan Yang
✉ yangzhikuan@aierchina.com

RECEIVED 16 March 2023
ACCEPTED 12 June 2023
PUBLISHED 28 June 2023

CITATION
Zeng L, Li X, Pan W, Tang Y, Lin D, Wang M, Cai W, Zhu R, Wan J, Huang L, Xu H and Yang Z (2023) Intraocular complement activation is related to retinal vascular and neuronal degeneration in myopic retinopathy.
Front. Cell. Neurosci. 17:1187400.
doi: 10.3389/fncel.2023.1187400

Intraocular complement activation is related to retinal vascular and neuronal degeneration in myopic retinopathy

Ling Zeng[1,2,3], Xiaoning Li[2,4], Wei Pan[3], Yao Tang[2,3], Ding Lin[2], Min Wang[5], Wang Cai[2], Ruiling Zhu[2], Jianbo Wan[2], Linghua Huang[2], Heping Xu[1,3,6]* and Zhikuan Yang[1,2,3]*

[1]Aier School of Ophthalmology, Central South University, Changsha, China, [2]Changsha Aier Eye Hospital, Changsha, Hunan, China, [3]Aier Institute of Optometry and Vision Science, Aier Eye Hospital Group, Changsha, China, [4]Aier School of Optometry and Vision Science, Hubei University of Science and Technology, Xianning, Hubei, China, [5]Shanghai Aier Eye Hospital, Shanghai, China, [6]The Wellcome-Wolfson Institute for Experimental Medicine, School of Medicine, Dentistry and Biomedical Sciences, Queen's University Belfast, Belfast, United Kingdom

Purpose: To investigate the relationship between the intraocular levels of complement proteins and myopia-related retinal neuronal and vascular degeneration.

Methods: Aqueous humour from 147 myopic patients, including 60 low-myopia and 87 high-myopia were collected during Implantable Collamer Lens implantation surgery. All participants received comprehensive ophthalmic examinations, including logMAR best corrected visual acuity, axial length measurement, fundus photography and ocular B-scan ultrasonography. The myopic eyes were further classified into simple myopia (SM, n = 78), myopic posterior staphyloma (PS, n = 39) and PS with myopic chorioretinal atrophy (PS + CA, n = 30). Retinal thickness and vascular density in the macula (6 mm × 6 mm) and optic nerve head (4.5 mm × 4.5 mm) were measured using Optical Coherence Tomography (OCT) and OCT angiography (OCTA). The levels of complement proteins including C1q, C3, C3b/iC3b, C4, CFB, CFH, C2, C4b, C5, C5a, CFD, MBL and CFI in the aqueous humour were measured using the Luminex Multiplexing system. The real-time RT-PCR was conducted to examine the expression of complement genes (*C1q, C2, C3, C4, CFI* and *CFD)* in the guinea pig model of long-term form deprivation-induced myopic retinal degeneration.

Results: OCTA showed that retinal neuronal thickness and vascular density in superficial and deep layers of the macular zone as well as vascular density in the optic nerve head were progressively decreased from SM to PS and PS + CA ($p < 0.05$). The aqueous humour levels of C1q, C3, C3b/iC3b, C4, CFB, CFH, C2, C4b, C5 and CFI were significantly higher in high-myopic eyes compared to those in low-myopic eyes. Further subgroup analysis revealed the highest levels of complement components/fragments in the PS + CA group. The intraocular levels of complement factors particularly C3b/iC3b and C4 were negatively correlated with macular zone deep layer retinal thickness and vascular density

and optic nerve head vascular density. The expression of *C2, C3* and *C4* genes was significantly higher in guinea pig eyes with myopic retinal degeneration compared to control eyes.

Conclusions: The intraocular classical pathway and alternative pathway of the complement system are partially activated in pathological myopia. Their activation is related to the degeneration of retinal neurons and the vasculature in the macula and the vasculature in the optic nerve head.

KEYWORDS

aqueous humour, inflammation, myopic retinal degeneration, posterior staphyloma, myopic chorioretinal atrophy

1. Introduction

Myopia is an important public health problem around the world (Pascolini and Mariotti, 2012). It is estimated that approximately half of the world's population will have myopia, of whom 10% will suffer from high myopia by 2050, especially in the east and southeast of Asia (Holden et al., 2016). The incidence of myopia to high myopia progression increased with age, especially after grade three and those with high myopia had a significantly increased lifetime risk of visual impairment compared with those with emmetropia (Tideman et al., 2016; Li et al., 2022). Myopia-mediated visual impairment was associated with axial length and the spherical equivalent (Jonas et al., 2021). Pathological myopia refers to a type of myopia accompanied by retinal/choroidal degenerative changes including posterior staphyloma, lacquer cracks, optic disc abnormalities, chorioretinal atrophy, choroidal neovascularisation and myopic maculopathy (Ohno-Matsui et al., 2016, 2021). Although pathological myopia often occurs in high myopia, it can also develop in low-to-moderate myopia (Ohno-Matsui et al., 2021). Currently, there is no medication to prevent or treat myopic retinal degeneration due to poor knowledge of the pathogenesis of the condition.

The neural retina is an extension of the brain and is connected to the brain via the optic nerve (Neuringer et al., 1988). Thus, the retina has many functional and anatomical features similar to those of the brain. Several degenerative diseases like Alzheimer's disease and dementia have been reported to be attributable to chronic inflammation (Heneka et al., 2015; Pasqualetti et al., 2015). In retinal diseases, it is also reported that inflammation plays an important role in retinal neuronal degeneration with different causes, such as age-related macular degeneration (Kauppinen et al., 2016; Xu and Chen, 2022) diabetic retinopathy (Tang and Kern, 2011), and glaucomatous retinopathy (Baudouin et al., 2021). Microglia, the complement system and inflammasome activation are three key inflammatory pathways critically involved in retinal degeneration and have been targeted for therapy (Xu and Chen, 2016; Akhtar-Schäfer et al., 2018; Kaarniranta et al., 2018). Recent studies have uncovered strong links between altered immune response and myopia (Xue et al., 2021; Zeng et al., 2021). It has been shown that patients with inflammatory or autoimmune diseases have a higher incidence of myopia compared to those without (Herbort et al., 2011). Allergic conjunctivitis can promote myopic progression (Wei et al., 2018), and high-myopic eyes contain higher levels of inflammatory cytokines and complement proteins (Gao et al., 2015; Yuan et al., 2019; García-Gen et al., 2021). In addition, myopic refractive shifts were present in many ocular diseases such as multifocal chorioretinitis, punctate inner chorioretinopathy and diffuse subretinal fibrosis syndrome (Gross et al., 1993; Jampol, 1996; Nguyen and Foster, 1998). The results suggest that inflammation may play an important role in the development and progression of myopia and myopic retinopathy.

Among the three common retinal degeneration-related inflammatory pathways, complement system has been reported to be closely associated with myopia. Several altered systemic and local complement proteins or pathways were detected in chick and guinea pig models of myopia (Gao et al., 2015; Giummarra et al., 2018; Zeng et al., 2021). Patients with pathological myopia had higher intraocular levels of complement proteins (Xue et al., 2021). However, which complement pathways are activated in the progression of myopic retinopathy and exactly how complement activation promotes myopic progression remains unknown. In this clinical study, we investigated the levels of complement proteins involved in multiple complement pathways in the aqueous humour from myopic patients without and with different degrees of pathological myopia. We further investigated the relationship between intraocular complement proteins levels and myopia-related retinal neuronal and vascular degeneration. The upregulation of complement genes was further confirmed in the guinea pig model of myopia-induced retinal degeneration.

Abbreviations: AP, alternative pathway; Average RNFL, average thickness of retinal nerve fiber layers; BCVA, best corrected visual acuity; CA, myopic chorioretinal atrophy; CP, classical pathway; DRVD, deep layer retinal vessel density; DRT, deep layer retinal thickness; FAZ, Foveal avascular zone; FD, Foveal density; FDM, form-deprivation-induced myopia; GCC, ganglion cell complex; ICL, implantable collamer lens; IDVD-all vessels, inside disc all vessel density; IDVD- small vessels, inside disc small vessel density; OCT, optical coherence tomography; OCTA, OCT angiography; ONHVD-all vessels, optic nerve head all vessel density; ONHVD-small vessels, optic nerve head small vessel density; PERIM, FAZ perimeter; PS, posterior staphyloma; PS + CA, posterior staphyloma with myopic chorioretinal atrophy; SLO, scanning laser ophthalmoscope; SM, simple myopia; SRT, superficial retinal thickness; SRVD, superficial retinal vessels density; Peripapillary VD-all vessels, peripapillary all vessel density; Peripapillary VD-small vessels, peripapillary small vessel density.

2. Materials and methods

2.1. Clinical samples

2.1.1. Subjects

The clinical study was performed following the principles of the Declaration of Helsinki. Informed consent was obtained from all participants and the Institutional Review Board (IRB) at the Aier Eye Hospital Group approved the study (IRB number: AIER 2019IRB03). 147 myopic patients attending the Changsha Aier Eye Hospital, Hunan, China between November 2019 to October 2020 for Implantable Collamer Lens (ICLs) implantation were recruited for this study. The inclusion criteria were: (1) myopia; (2) receiving ICL surgery; (3) willing to participate in the study. Exclusion criteria were: (1) history of ocular trauma and ophthalmic surgery within 6 months; (2) history of retinal laser photocoagulation within 6 months; (3) use of antimetabolites, immunosuppressants or corticosteroids; (4) systemic inflammatory or autoimmune diseases; (5) pre-existing ocular inflammatory-related diseases. During data analysis, the participants were grouped into either high myopia (axial length $\geqq$26.5 mm or spherical equivalent $\leqq$-8.00D) and low myopia(axial length $<$ 26.5 mm and spherical equivalent $>$ $-$8.00D) (Tokoro, 1998), or with and without different degrees of pathological myopia (i.e., posterior staphyloma (PS) or with myopic chorioretinal atrophy (PS + CA).

Posterior staphyloma was diagnosed based on ocular B-scan ultrasonography. The diagnostic criteria were according to the definition of posterior staphyloma that an outpouching of a circumscribed posterior fundus region and had a curvature radius that was smaller than the curvature radius of the fellow eye (Spaide, 2014). Pathological myopia-related retinopathy was diagnosed using colour fundus images and scanning laser ophthalmoscope (SLO) examination. The diagnostic criteria were based on the META-PM classification and the definition of pathological myopia, including diffuse chorioretinal atrophy (myopic maculopathy category 2), patchy chorioretinal atrophy (myopic maculopathy category 3), macular atrophy (myopic maculopathy category 4), or presence of plus lesion, including neovascularization, Fuchs and lacquer cracks (Ohno-Matsui et al., 2015).

2.1.2. Clinical examination

All subjects received comprehensive ophthalmic examinations including logMAR best corrected visual acuity (BCVA), slit lamp examination, intraocular pressure measurement (with a non-contact tonometer), axial length measurement (with an optical biometric device, IOL-Master700, Carl Zeiss, Meditec, Dublin, California), spherical equivalent (defined as a sphere plus a half negative cylinder measured by phoropter, NIDEK, ARK-1), ocular B-scan ultrasonography (Aviso, Quantel Medical, France), and fundus examination. Fundus examinations were recorded using RTVue XR Avanti Angio-OCT (OCTA, Optovue, Fremont, CA, USA) scanned in 6 mm $\times$ 6 mm in the macular zone (**Supplementary Figures 1A–D**) and 4.5 mm $\times$ 4.5 mm in the optic nerve head (**Supplementary Figures 1E–G**) and SLO (Optos, Daytona, Dunfermline, United Kingdom).

The below measurements were conducted in OCTA images using the AngioVue Software (Version 2018.1.1.63, Optovue, Inc.). Macular zone: (1) superficial retinal vessel density (SRVD); (2) deep layer retinal vessel density (DRVD); (3) superficial retinal thickness (SRT); (4) deep layer retinal thickness (DRT); (5) foveal vessel density (FD); (6) foveal avascular zone (FAZ); (7) FAZ perimeter (PERIM); (8) average thickness of ganglion cell complex (GCC) (**Supplementary Figures 1A–D**). Optic nerve head: (1) average thickness of retinal nerve fiber layers (average RNFL); (2) optic nerve head all vessel density (ONHVD-all vessels); (3) optic nerve head small vessel density (ONHVD -small vessels); (4) inside disc all vessel density (IDVD-all vessels); (5) inside disc small vessel density (IDVD - small vessels); (6) Peripapillary all vessel density (Peripapillary VD- all vessels); (7) Peripapillary small vessel density (Peripapillary VD - small vessels) (**Supplementary Figures 1E–G**).

2.1.3. Aqueous sample collection

Aqueous humour was obtained immediately before ICL implantation. Approximately 100$\sim$150 μL of aqueous humour was drawn from the anterior chamber through the limbus using a disposable sterile syringe. The sample was transferred into a sterile Eppendorf and stored at $-$80°C until measurement.

2.1.4. Measurement of complement proteins

The levels of complement proteins in aqueous humour, including C1q, C3, C3b/iC3b, C4, CFB, CFH, C2, C4b, C5, C5a, CFD, MBL and CFI were assayed with the xMAP kits (No. HCMP1MAG-19K and HCMP2MAG-19K, Millipore, USA) using the Luminex XMAP system following manufacturer's instructions (Luminex Technology, Austin, USA). 25 μL of aqueous humour from each sample (original fluid) was used in the measurement of C1q, C3, C3b/iC3b, C4, CFB and CFH. 12.5 μL of aqueous humour from each sample diluted with RD6-52 (1:1 dilution) was used to measure C2, C4b, C5, C5a, CFD, MBL and CFI.

2.2. Quantitative real-time PCR analysis of complement expression in form deprivation-induced myopic retinal degeneration

We previously developed a form deprivation-induced high myopia (FDM) in pigmented guinea pigs and the animals presented early signs of retinal neuronal degeneration after 15 weeks of form deprivation (Zeng et al., 2021). The study protocols were approved by the Animal Care and Ethics Committee of the Central South University (Ref: 2021SYDW0026) and all procedures were performed according to the Association for Research in Vision and Ophthalmology (ARVO) statement for the Use of Animals in Ophthalmic and Vision Research.

Using mRNA samples from this study (Zeng et al., 2021), we conducted qRT-PCR analysis on complement related genes, including *C1q, C2, C3, C4(C4a), CFD*, and *CFI*. The mRNA from three groups of retinae was used in this study: FDM retinae, self-control retinae, and retinae from animals without form deprivation. Seven retinas were included in each group. 400 ng RNA from each retina sample was used to synthesize cDNA using a Reverse Transcription kit (Vazyme, Nanjing, China). The cDNA was diluted to 1.25 ng/μl for the subsequent qRT-PCR. qTR-PCR was conducted in 96-well plates using a lightcycle96@Real-Time PCR System (Roche, Germany) and each sample was triplicated.

The primers were purchased from Tsingke Biotechnology (Beijing, China) and detailed in Supplementary Table 8. *Actb* was used as a house-keeping gene. Each reaction (10 μL of volume) contained 1 μL of primer (10 μM), 2 μL cDNA, 5 μL Maxima SYBR Green Master Mix (2X) (Cat. K0252, Thermo Fisher Scientific, MA, USA) and 2 μL ddH2O. The reaction was conducted by 45 cycles of 95°C for 10 s, 60°C for 15 s and 72°C for 10 s (single acquire). The relative expression of candidate genes was obtained using the comparative threshold cycle ($2^{-\Delta\Delta Ct}$) method (Livak and Schmittgen, 2001).

3. Statistics

Data analyses were performed using the Statistical Package for Social Sciences software (SPSS, V. 21.0, IBM Corp., USA). The Kolmogorov-Smirnov test was used to determine the clinical study data normality. The continuous variables with homogeneity were compared by one-way Analysis of Variance (ANOVA), followed by the Bonferroni' *post hoc* analysis. For those variables that did not present homogeneity of variances, the Kruskal-Wallis test was used. Unadjusted linear regression was employed to examine the coefficients of two dependent variables. Chi-square analysis was used to analyze categorical variables such as gender, family history of myopia and history of photocoagulation etc. All continuous values were expressed as mean ± SD or mean ± SEM, and the categorical values were expressed as *N* (%). $P < 0.05$ was considered statically significant.

4. Results

4.1. Clinical study

4.1.1. Clinical characteristics of the participants

Of the 147 participants, 60 had low-myopia, 87 had high-myopia. There was no significant difference in age, gender, BCVA and family history of myopia between the two groups. As expected, the spherical equivalent and axial length were significantly different between the two groups (Supplementary Table 1).

4.1.2. Complement proteins levels in the aqueous humour in eyes with different degrees of myopia

We measured 13 complement components/fragments, four (C1q, C2, C4, and C4b) in the classical pathway (CP), four (CFB, CFH, CFI, and CFD) in the alternative pathway (AP), one (MBL) in the lectin pathway and four (C3, C3b/iC3b, C5 and C5a) in the common pathway. C5a was detected only in 4 out of 147 samples (ranging from 1.59∼12.44 pg/mL, sensitivity level: 1.14 pg/mL). Therefore, we did not conduct any further analysis on C5a. C5 was below the detectable limit (0.68 ng/mL) in 26 out of 147 samples, and 20 out of the 26 undetectable samples were in the low myopia group. In addition, the level of C2 was below the detectable threshold (0.25 ng/mL) in six samples of the low myopia group. Other complement components and complement fragments were detected in all samples.

When comparing the aqueous humour complement levels between the two groups, all components of the CP (C1q, C2, C4 and C4b) and the common pathway (C3, C3b/iC3b and C5) were significantly higher in the high-myopia group. In the AP, the aqueous levels of CFB and CFI were significantly higher in high myopic eyes. The levels of CFH, CFD and MBL did not differ between the two groups (Table 1).

TABLE 1 Complement proteins levels in the aqueous humor of patients with high myopia and low myopia (ng/ml).

	Low myopia	High myopia	*P*-values*
	(*n* = 60)	(*n* = 87)	
Complement components/fragments of the CP			
C1q	6.21 ± 3.32	9.31 ± 6.58	<0.001
C2	0.93 ± 0.52	2.15 ± 1.65	<0.001
C4	151.60 ± 55.00	197.67 ± 78.52	<0.001
C4b	18.59 ± 13.26	33.01 ± 27.21	<0.001
Complement components/fragments of the AP			
CFB	126.28 ± 35.65	142.57 ± 38.54	0.01
CFH	39.40 ± 17.53	42.11 ± 21.92	0.43
CFI	63.38 ± 20.84	76.12 ± 35.13	0.007
CFD	33.03 ± 9.77	32.39 ± 10.55	0.71
Lectin pathway			
MBL	0.18 ± 0.14	0.19 ± 0.14	0.47
Complement components/fragments of the shared pathway			
C3	112.02 ± 30.46	139.48 ± 49.28	<0.001
C3b/iC3b	73.44 ± 39.64	110.74 ± 85.33	<0.001
C5	1.77 ± 1.53	3.85 ± 2.81	<0.001

*Student's t-test.

4.1.3. Complement proteins levels in the aqueous humour in eyes with different degrees of pathological myopia

To understand if the complement system is involved in pathological myopia, we classified the subjects into three groups based on the severity of retinal degeneration: simple myopia (SM, without pathological myopia, *n* = 78), posterior staphyloma (PS, *n* = 39) and posterior staphyloma with myopic chororetinal atrophy (PS + CA, *n* = 30), including 27 diffuse chorioretinal atrophy, 3 patchy chorioretinal atrophy (Supplementary Figure 2). Apart from the spherical equivalent and axial length, there was no difference in age, gender, and history of myopia between the three groups (Supplementary Table 2).

One-way ANOVA analysis showed that the aqueous levels of the complement components and fragments in the CP (C1q, C4 and C4b), AP (CFB, CFH and CFI) and the common pathway (C3, C3b/iC3b, and C5) significantly differed among the three groups (Table 2). Further *post hoc* analysis uncovered the largest difference lies in SM vs PS + CA. The aqueous levels of these complement proteins progressively increase from SM to PS, with the highest values in the PS + CA group (Table 2). We did not detect any statistical difference in the aqueous levels of CFD and MBL among the three groups (Table 2).

TABLE 2 Complement proteins levels in the aqueous humor from different degrees of pathological myopia patients (ng/ml).

	SM (n = 78)	PS (n = 39)	PS + CA (n = 30)	P-value (all)[a]	P-value[b] SM vs PS	P-values[b] SM vs PS + CA	P-values[b] PS vs PS + CA
Complement components/fragments of the CP							
C1q	6.44 ± 3.37	7.92 ± 3.85	12.37 ± 9.31	<0.001	0.04	0.002	0.02
C2	1.22 ± 0.79	1.52 ± 1.04	2.93 ± 2.29	<0.001	0.12	<0.001	0.003
C4	157.10 ± 60.04	186.64 ± 76.09	225.33 ± 79.32	<0.001	0.02	<0.001	0.04
C4b	22.17 ± 18.40	24.83 ± 22.29	42.99 ± 30.41	<0.001	0.49	0.001	0.006
Complement components/fragments of the AP							
CFB	124.79 ± 35.27	140.60 ± 33.77	158.80 ± 40.18	<0.001	0.02	<0.001	0.04
CFH	36.96 ± 14.41	40.38 ± 17.80	52.32 ± 30.24	0.002	0.27	0.01	0.06
CFI	66.62 ± 25.54	63.14 ± 24.53	92.23 ± 40.26	<0.001	0.48	0.002	0.001
CFD	31.83 ± 9.73	31.92 ± 10.04	35.72 ± 11.36	0.18	0.97	0.08	0.15
Lectin pathway							
MBL	0.17 ± 0.13	0.19 ± 0.12	0.23 ± 0.18	0.14	0.31	0.11	0.38
Complement components/fragments of the shared pathway							
C3	121.65 ± 40.59	131.16 ± 49.44	141.75 ± 46.03	0.1	0.27	0.03	0.37
C3b/iC3b	75.67 ± 44.19	89.62 ± 51.88	154.77 ± 114.20	<0.001	0.13	<0.001	0.006
C5	2.15 ± 1.80	3.03 ± 2.08	5.18 ± 3.52	<0.001	0.02	<0.001	0.005

SM, simple myopia; PS, posterior staphyloma; CA, myopic chorioretinal atrophy; PS, posterior staphyloma; PS + CA, posterior staphyloma with myopic chorioretinal atrophy.
[a]ANOVA.
[b]Bonferroni'post hoc analysis.

4.1.4. Retinal neuronal and vascular degeneration in different groups of pathological myopia

The pathological myopic-related changes in retinal neurons and the vasculature around the optic nerve head and the macular zone were examined by angio-OCT (OCTA) (Supplementary Figure 1). In the macular zone, there was a significant difference among the three groups in SRVD, DRVD, SRT, DRT, and FD, but not FAZ, PERIM and average GCC. Further analysis of the subgroups showed that retinal vascular densities (SRVD, DRVD and FD) and neuronal thickness (SRT and DRT) were significantly reduced in the PS + CA group compared to SM and PS groups. A trend of reduction in DRVD, SRT, and DRT was also observed in the PS group compared to SM (Supplementary Table 3). These results suggest a progressive loss of macular zone blood vessels and neurons from SM to PS and PS + CA.

In the optic nerve head, the average RNFL showed no significant difference between the groups. The vessel densities, including all vessels and small vessels, were progressively reduced from PS to PS + CA, particularly the peripapillary vessel densities. Interestingly, the small vessel density inside the disc (IDVD-small vessels) was higher in PS than in SM (Supplementary Table 3). Our results suggest peripapillary vascular degeneration in myopic retinopathy.

4.1.5. The relationship between intraocular complement components/fragments and retinal neuronal and vascular degeneration

To understand if intraocular complement levels are related to retinal neuronal and vascular degeneration, we further analyzed the correlation between the laboratory and clinical parameters. Weak, but statistically significant negative correlations were observed between intraocular complement proteins (C4 and C3b/iC3b) and superficial retinal thickness and superficial vascular density (Supplementary Tables 4, 5). Whereas strong negative correlations were observed between intraocular complement proteins and the macular zone DRT and DRVD (Tables 3, 4; Supplementary Figure 3).

When all participants were analyzed together, apart from CFD and MBL, all other complement components/fragments showed a strong inverse correlation with macular zone DRT (Table 3); whereas except for C3, CFD and MBL, other components/fragments showed a strong correlation with macular zone DRVD (Table 4) with the highest being C3b/iC3b followed by C4 ($\beta = -1.95$ and -1.60 for DRT and -4.89 and -4.73 for DRVD respectively, $P < 0.001$, Tables 3, 4; Supplementary Figure 3). Further subgroup analysis revealed that most of the DRT-related correlations were in the PS + CA group (Table 3), whereas the DRVD-related correlations were more often in the PS group than the PS + CA group (Table 4).

In the optic nerve head, weak correlations were observed between RNFL and complement parameters such as C1q, CFB, CFH, C3, C3b/iC3b and MBL (with low values of regression coefficient) (Supplementary Table 6). Regarding the parameter of peripapillary VD-all vessels, significant reverse correlations with C1q, C2, C4, CFB, CFI, C3b/iC3b and C5 were detected with the highest correlation in C3b/iC3b, followed by C4 and CFB ($\beta = -5.72$, -3.37 and -2.90 for C3b/iC3b, C4 and CFB respectively, $P < 0.001$, Supplementary Table 7 and Supplementary Figure 4). Subgroup analysis showed that the negative correlations between peripapillary VD-all vessels and complement proteins were predominately in the PS + CA group.

TABLE 3 The correlations between intraocular complement levels and DRT in the macular zone.

	All group (*n* = 147)		SM (*n* = 78)		PS (*n* = 39)		PS + CA (*n* = 30)	
	β (SE)	*P*-values†	β (SE)	*P*-values†	β (SE)	*P*-values†	β (SE)	*P*-values†
Complement components/fragments of the CP								
C1q	−0.17 (0.03)	<0.001	−0.03 (0.04)	0.46	−0.09 (0.04)	0.02	−0.56 (0.14)	<0.001
C2	−0.04 (0.01)	<0.001	−0.00 (0.01)	0.74	−0.01 (0.01)	0.28	−0.09 (0.04)	0.06
C4	−1.60 (0.45)	<0.001	0.11 (0.67)	0.87	−1.23 (0.79)	0.13	−3.58 (1.43)	0.02
C4b	−0.51 (0.15)	0.001	−0.06 (0.21)	0.76	−0.35 (0.24)	0.16	−0.90 (0.60)	0.14
Complement components/fragments of the AP								
CFB	−0.60 (0.23)	0.01	0.76 (0.36)	0.04	−0.35 (0.34)	0.32	−2.81 (0.54)	<0.001
CFH	−0.34 (0.11)	0.002	0.18 (0.16)	0.27	−0.38 (0.19)	0.052	−1.18 (0.33)	0.002
CFI	−0.54 (0.19)	0.007	0.28 (0.27)	0.31	−0.14 (0.28)	0.61	−2.38 (0.70)	0.003
CFD	−0.07 (0.06)	0.25	0.14 (0.11)	0.2	−0.04 (0.11)	0.74	−0.58 (0.16)	0.001
Lectin Pathway								
MBL	0.00 (0.00)	0.77	0.00 (0.00)	0.28	0.00 (0.00)	0.46	−0.00 (0.00)	0.11
Complement components/fragments of the shared pathway								
C3	−0.80 (0.27)	0.003	0.09 (0.44)	0.84	−1.28 (0.47)	0.01	−2.17 (0.69)	0.005
C3b/iC3b	−1.95 (0.42)	<0.001	0.45 (0.46)	0.33	−1.16 (0.55)	0.04	−6.78 (1.69)	<0.001
C5	−0.04 (0.01)	0.003	−0.03 (0.02)	0.13	0.00 (0.02)	0.85	−0.04 (0.05)	0.48

β, regression coefficient; SE, standard error; SM, simple myopia; PS, posterior staphyloma; CA, myopic chorioretinal atrophy; PS, posterior staphyloma; PS + CA, posterior staphyloma with myopic chorioretinal atrophy; DRT, deep retinal layer thickness.
†Unadjusted Linear Regression.

TABLE 4 The correlation between intraocular complement levels and DRVD in the macular zone.

	Group (*n* = 147)		SM (*n* = 78)		PS (*n* = 39)		PS + CA (*n* = 30)	
	β (SE)	*P*-values	β (SE)	*P*-values†	β (SE)	*P*-values†	β (SE)	*P*-values†
Complement components/fragments of the CP								
C1q	−0.46 (0.08)	<0.001	−0.03 (0.09)	0.77	−0.44 (0.11)	<0.001	−0.72 (0.26)	0.01
C2	−0.11 (0.02)	<0.001	0.02 (0.02)	0.33	−0.09 (0.03)	0.01	−0.16 (0.07)	0.04
C4	−4.73 (1.11)	<0.001	−1.68 (1.64)	0.31	−3.96 (2.49)	0.12	−4.88 (2.37)	0.052
C4b	−1.08 (0.38)	0.005	−0.03 (0.53)	0.95	−0.95 (0.77)	0.23	−1.00 (0.98)	0.32
Complement components/fragments of the AP								
CFB	−2.20 (0.57)	<0.001	−0.32 (0.92)	0.73	−2.53 (1.00)	0.02	−1.89 (1.24)	0.14
CFH	−0.83 (0.27)	0.003	0.13 (0.39)	0.75	−1.23 (0.58)	0.04	−1.05 (0.63)	0.11
CFI	−1.56 (0.48)	0.002	0.08 (0.67)	0.9	−1.78 (0.81)	0.04	−1.94 (1.32)	0.16
CFD	−0.27 (0.16)	0.1	0.25 (0.27)	0.35	−0.38 (0.35)	0.29	−0.63 (0.30)	0.045
Lectin Pathway								
MBL	−0.00 (0.00)	0.21	−0.00 (0.00)	0.92	−0.00 (0.00)	0.43	−0.00 (0.00)	0.37
Complement components/fragments of the shared pathway								
C3	−0.88 (0.69)	0.21	0.97 (1.10)	0.38	−2.97 (1.56)	0.07	−0.52 (1.33)	0.7
C3b/iC3b	−4.89 (1.06)	<0.001	0.63 (1.14)	0.58	−4.17 (1.68)	0.02	−7.54 (3.19)	0.03
C5	−0.14 (0.03)	<0.001	−0.04 (0.04)	0.38	−0.10 (0.07)	0.19	−0.12 (0.08)	0.14

β, regression coefficient; SE, standard error; SM, simple myopia; PS, posterior staphyloma; CA, myopic chorioretinal atrophy; PS, posterior staphyloma; PS + CA, posterior staphyloma with myopic chorioretinal atrophy; DRVD, deep layer retinal vessel density.
†Unadjusted Linear Regression.

Taken together, our results suggest that intraocular activation of the CP and AP of the complement system is related to macular zone deep layer retinal neuronal and vascular degeneration as well as the peripapillary vascular degeneration in pathological myopia.

4.1.6. Complement gene expression in myopic retinal degeneration of guinea pigs

Real-time RT-PCR showed that the expression of *C2, C3* and *C4(C4a)* in the FDM retina was significantly higher compared

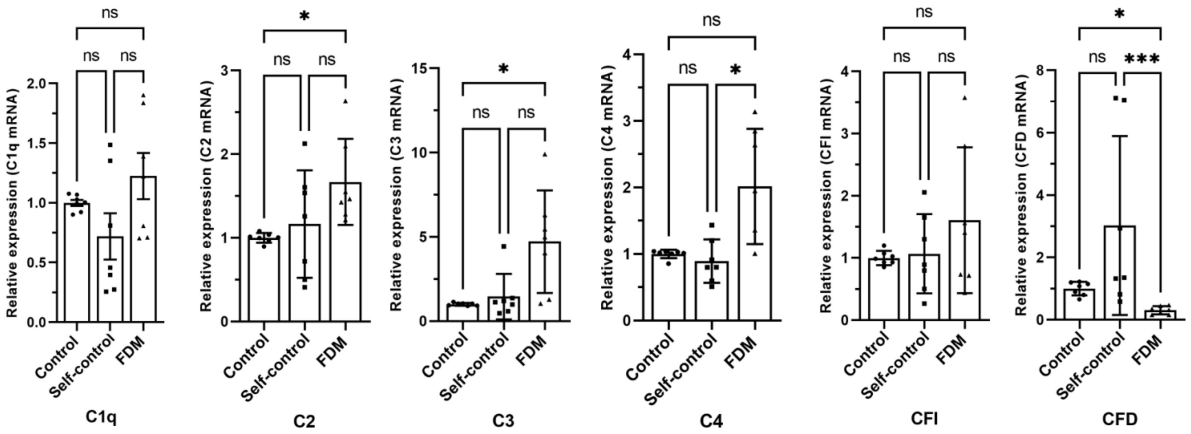

FIGURE 1
The relative gene expression of complement factors/components in different groups of guinea pig retina by qRT-PCR. Data presented as fold change of gene expression compared to control groups. Mean ± SEM, n = 7/group. ns, no significant difference, *$p < 0.05$. ***$p < 0.001$. One-way ANOVA followed by Dunn's Multiple comparison test. FDM, form-deprivation induced myopia.

to that in self-controls or in eyes from control guinea pigs. Interestingly, the expression of *CFD* was reduced in FDM eyes compared to the controls (**Figure 1**). No significant difference was observed in *C1q* and *CFI* genes (**Figure 1**).

5. Discussion

In this study, we detected significantly higher intraocular levels of complement proteins involved in the classic pathway (C1q, C2, C4 and C4b) and alternative pathway (CFB, CFI, C3b/iC3b) in human eyes with high-myopia or with pathological myopia. We further found that higher intraocular levels of C4 and C3b/iC3b were negatively correlated with the deep layer retinal thickness and microvascular density in the macula, as well as with the optic nerve head vascular density. Higher levels of retinal complement expression were also detected in a guinea pig model of myopia-induced retinal degeneration (Zeng et al., 2021). Complement fragments C4b, C3b/iC3b and C5a are evidence of complement activation. We detected C4b and C3b/iC3b but not C5a in the aqueous humor of myopic eyes, indicating partial activation of the intraocular complement system. Our results suggest that partial activation of the intraocular complement system is related to myopic retinopathy, particularly the degeneration of retinal neurons in the macula and microvascular degeneration in both the macula and optic disc.

Previous studies have reported the upregulation of the complement pathway, including C1q, C1qa, C2 and C1qb during the development stages of myopia in guinea pigs and chicks (Riddell and Crewther, 2017; Zeng et al., 2021). These animal models of myopia are valuable tools for understanding the mechanism of myopia onset and progression. All participants in our study are myopic, so the data are not suitable for evaluating the role of the complement system in myopia onset. However, by classifying the participants into low-myopia and high-myopia groups and into myopia with or without retinopathy, we could interrogate the involvement of intraocular complement system in myopia progression and the development of myopic retinopathy. The levels of C1q, C2, C4, C4b, CFB, CFI, C3, C3b/iC3b, and C5 in the aqueous humour were significantly higher in high-myopic eyes compared to those in low-myopic eyes. MBL was detected in all samples (albeit at low levels), but there was no difference between the two groups. Our results suggest that partial activation of the intraocular CP and AP of the complement system is involved in the progression from low-myopia to high-myopia.

Proteins in the intraocular fluids (aqueous humour and vitreous body) originate predominately from cells inside the eye when the blood retinal barrier is intact. In the context of complement proteins, retinal cells including neurons, glial cells and retinal pigment epithelial cells constitutively express complement and complement regulatory genes and their expression can be upregulated under oxidative stress and inflammatory conditions (Anderson et al., 2010; Luo et al., 2013; Xu and Chen, 2016; Liu et al., 2020). The alterations in the composition and quantity of intraocular proteins can truthfully reflect the health condition of intraocular tissues, particularly the retina. To understand the role of the complement system in pathological myopia, we classified the participants into three groups based on the degree of pathological myopia, SM (no pathological myopia), myopia-related PS (without pathological myopia-related retinopathy) and PS + CA (with myopic chorioretinal atrophy). This study design allowed us to investigate the link between myopia-mediated retinal neuronal and vascular changes and intraocular complement activation. Indeed, we found progressive thinning of the macular zone retinal neurons and the gradual loss of microvasculature in the macula (both superficial and deep layers) and the optic nerve head during the progression of pathological myopia. There was no significant difference in the vascular density inside the optic disc in different groups. Reduced retinal microvascular density has been observed in high-myopic eyes (Li et al., 2017; Ucak et al., 2020; Shi et al., 2021; Moon et al., 2023), but not in high-myopic anisometropia eyes (Wang et al., 2022), although the superficial and deep layer retinal neurons were thinner in high-myopic eyes including high-myopic anisometropia eyes compared to contralateral control eyes (Ucak et al., 2020; Shi et al., 2021; Wang et al., 2022). Our results were in line with previous reports.

We found that the levels of intraocular complement proteins, including C1q, C2, C4, C4b, CFB and C3b/iC3b progressively increase from SM to PS and PS + CA. More importantly, we observed negative correlations between intraocular complement levels and macular zone deep layer retinal thickness and microvascular density, particularly in the severe pathologcial myopia group (i.e., PS + CA). Among different complement proteins, the strongest correlation was observed in C4, followed by C3b/iC3b and CFB, suggesting that the CP complement system (along with AP) may be critically involved in retinal neuronal and vascular degeneration, particularly in the outer retinal layer, in pathological myopia-related retinopathy.

It is important to note that, although a significant amount of C3 (range: 48.80∼290.04 ng/ml) and its fragment C3b/iC3b (range: 12.17∼455.43 ng/ml) in this clinical study was detected in all samples, the aqueous level of C5 was very low (range: 0∼16.97 ng/ml) and C5a was only detected in 4 out of 147 myopic eyes. The results indicate that the intraocular complement cascade is only activated to the C3 cleavage step in the myopic eyes. The C3-derived complement fragments C3a and C3b are known to be involved in various immune responses. C3a can induce chemotaxis, immune cell activation, angiogenesis, and macrophage-to-myofibroblast transition through its receptor C3aR (Sacks, 2010; Wang et al., 2022); whereas C3b can opsonize pathogens and apoptotic cells for phagocytosis, as well as form the C3 convertase with CFB (C3bBb) (Xu and Chen, 2016). In our study, the level of intraocular C3b/iC3b increased progressively from simple myopia (SM: 75.67 ± 44.19 ng/ml) to myopia with posterior staphyloma (PS: 89.62 ± 51.88 ng/ml), and to myopia with posterior staphyloma and chorioretinal atrophy (PS + CA: 154.77 ± 114.20 ng/ml) (**Table 2**). The level of C3b/iC3b in the PS + CA myopic eye is at the same range as the level of C3 (141.75 ± 46.03 ng/ml, **Table 2**). This suggests that the level of intraocular complement activation (although partially) is in line with the severity of myopic retinopathy. The intraocular complement system may participate in myopic retinal degeneration by modulating retinal immune response through the release of C3a and C3b although further functional studies will be needed to confirm this.

This study has several limitations. Firstly, we do not have an emmetropic control group due to the unavailability of aqueous humour samples. Secondly, clinical evaluation and aqueous humour samples collection were conducted at the same time, and we did not follow up the participants during disease progression, therefore, it is difficult to establish the causal link between intraocular complement activation and myopic retinal degeneration. Myopia-induced retinal neuronal and vascular degeneration is a slow process. If intraocular complement activation is one of the key drivers, complement activation would exist many years prior to retinal degeneration. Third, we did not measure the circulating levels of complement protein and complement activity. We do not know if higher intraocular complement levels are due to systemic complement activation in the participants. Fourth, among different degrees of pathological myopia, only PS and PS + CA were included in the study. Further studies will be needed to understand the role of complement activation in other types of myopic retinopathy including the high prevalence peripheral retinal degeneration (Lam et al., 2005) and the more severe myopic maculopathy such as myopic choroidal neovascularization and macular hemorrhage. Finally, we were not able to conduct functional study to test the role of the complement system in the animal model of myopia-induced retinal degeneration due to the lack of guinea pig-specific complement inhibitors.

6. Conclusion

In this study, we uncovered progressive partial intraocular complement activation during the progression of low-myopic to high-myopia. Importantly, we found that the intraocular classical pathway and alternative pathway of the complement system are involved in the development and progression of pathological myopia, in particular, the outer retinal neuronal and vascular degeneration and optic head vascular degeneration.

Data availability statement

The raw data supporting the conclusions of this article will be made available by the authors, without undue reservation.

Ethics statement

All procedures concerning the collection of aqueous humour were performed following the principles of the Declaration of Helsinki. Informed consent was obtained from all participants and the Institutional Review Board (IRB) at the Aier Eye Hospital Group approved the study (IRB number: AIER 2019IRB03). The animal study protocols were approved by the Animal Care and Ethics Committee of the Central South University (Ref: 2021SYDW0026) and all procedures were performed according to the Association for Research in Vision and Ophthalmology (ARVO) statement for the Use of Animals in Ophthalmic and Vision Research.

Author contributions

LZ, HX, and ZY concepted and designed study, revised the manuscript. LZ, XL, YT, MW, JW, and LH collected experimental data. DL, WC, and RZ collected aqueous humour. LZ, WP, HX, and ZY analyzed data. LZ and HX drafted the manuscript. All authors contributed to the article and approved the submitted version.

Funding

This work was supported by National Science Natural Foundation of China (Grant No. 81770958), the Key Research and Development Programme of Hunan Province (2019SK2051), and the Research Fund Project of AIER Eye Hospital Group (AR2003D1 and AC2009D2). The sponsor or funding organization had no role in the design or conduct of this research.

Acknowledgments

The authors thank Hunan Province Optometry Engineering and Technology Research Center and Hunan Province International Cooperation Base for Optometry Science and Technology for supporting in this research.

Conflict of interest

The authors declare that the research was conducted in the absence of any commercial or financial relationships that could be construed as a potential conflict of interest.

Publisher's note

Supplementary material

The Supplementary Material for this article can be found online at: https://www.frontiersin.org/articles/10.3389/fncel.2023.1187400/full#supplementary-material

References

Akhtar-Schäfer, I., Wang, L., Krohne, T., Xu, H., and Langmann, T. (2018). Modulation of three key innate immune pathways for the most common retinal degenerative diseases. *EMBO Mol. Med.* 10:e8259. doi: 10.15252/emmm.201708259

Anderson, D. H., Radeke, M. J., Gallo, N. B., Chapin, E. A., Johnson, P. T., Curletti, C. R., et al. (2010). The pivotal role of the complement system in aging and age-related macular degeneration: hypothesis re-visited. *Progr. Retinal Eye Res.* 29, 95–112. doi: 10.1016/j.preteyeres.2009.11.003

Baudouin, C., Kolko, M., Melik-Parsadaniantz, S., and Messmer, E. M. (2021). Inflammation in glaucoma: from the back to the front of the eye, and beyond. *Progr. Retinal Eye Res.* 83:100916. doi: 10.1016/j.preteyeres.2020.100916

Gao, T. T., Long, Q., and Yang, X. (2015). Complement factors C1q, C3 and C5b-9 in the posterior sclera of guinea pigs with negative lens-defocused myopia. *Int. J. Ophthalmol.* 8:675. doi: 10.3980/j.issn.2222-3959.2015.04.06

García-Gen, E., Penadés, M., Mérida, S., Desco, C., Araujo-Miranda, R., Navea, A., et al. (2021). High Myopia and the complement system: factor H in myopic maculopathy. *J. Clin. Med.* 10:2600. doi: 10.3390/jcm10122600

Giummarra, L., Crewther, S. G., Riddell, N., Murphy, M. J., and Crewther, D. P. (2018). Pathway analysis identifies altered mitochondrial metabolism, neurotransmission, structural pathways and complement cascade in retina/RPE/choroid in chick model of form-deprivation myopia. *PeerJ.* 6:e5048. doi: 10.7717/peerj.5048

Gross, S. A., von Noorden, G. K., and Jones, D. B. (1993). Necrotizing scleritis and transient myopia following strabismus surgery. *Ophthal. Surg. Lasers Imaging Retina* 24, 839–841. doi: 10.3928/1542-8877-19931201-08

Heneka, M. T., Carson, M. J., El Khoury, J., Landreth, G. E., Brosseron, F., Feinstein, D. L., et al. (2015). Neuroinflammation in Alzheimer's disease. *Lancet Neurol.* 14, 388–405. doi: 10.1016/S1474-4422(15)70016-5

Herbort, C. P., Papadia, M., and Piergiorgio, N. (2011). Myopia and inflammation. *J. Ophthalmic Vis. Res.* 6, 270–283.

Holden, B. A., Fricke, T. R., Wilson, D. A., Jong, D., Naidoo, M., Sankaridurg, K. S., et al. (2016). Global prevalence of myopia and high myopia and temporal trends from 2000 through 2050. *Ophthalmology* 123, 1036–1042. doi: 10.1016/j.ophtha.2016.01.006

Jampol, L. M. (1996). Enlarged blind spots in chorioretinal inflammatory disorders-Discussion. *Ophthalmology* 103, 616–617. doi: 10.1016/s0161-6420(96)30645-3

Jonas, J. B., Ang, M., Cho, P., Guggenheim, J. A., He, M. G., Jong, M., et al. (2021). IMI prevention of Myopia and its progression. *Invest. Ophthalmol. Vis. Sci.* 62:6. doi: 10.1167/iovs.62.5.6

Kaarniranta, K., Xu, H., and Kauppinen, A. (2018). Mechanistical retinal drug targets and challenges. *Adv. Drug Deliv. Rev.* 126, 177–184. doi: 10.1016/j.addr.2018.04.016

Kauppinen, J. J., Paterno, J., Blasiak, J., Salminen, A., and Kaarniranta, K. (2016). Inflammation and its role in age-related macular degeneration. *Cell. Mol. Life Sci.* 73, 1765–1786. doi: 10.1007/s00018-016-2147-8

Lam, D., Fan, D., Chan, W., Tam, B., Kwok, A., Leung, A., et al. (2005). Prevalence and characteristics of peripheral retinal degeneration in Chinese adults with high myopia: a cross-sectional prevalence survey. *Optom. Vis. Sci.* 82, 235–238. doi: 10.1097/01.opx.0000159359.49457.b4

Li, M., Yang, Y., Jiang, H., Gregori, G., Roisman, L., Zheng, F., et al. (2017). Retinal microvascular network and microcirculation assessments in high myopia. *Am. J. Ophthalmol.* 174, 56–67. doi: 10.1016/j.ajo.2016.10.018

Li, S. M., Wei, S., Atchison, D. A., Kang, M. T., Liu, L., Li, H., et al. (2022). Annual incidences and progressions of myopia and high myopia in chinese schoolchildren based on a 5-year cohort study. *Invest. Ophthalmol. Vis. Sci.* 63:8. doi: 10.1167/iovs.63.1.8

Liu, J., Tang, M., Harkin, K., Du, X., Luo, C., Chen, M., et al. (2020). Single-cell RNA sequencing study of retinal immune regulators identified CD47 and CD59a expression in photoreceptors—Implications in subretinal immune regulation. *J. Neurosci. Res.* 98, 1498–1513. doi: 10.1002/jnr.24618

Livak, K. J., and Schmittgen, T. D. (2001). Analysis of relative gene expression data using real-time quantitative PCR and the 2(-Delta Delta C(T) Method. *Methods* 25, 402–408. doi: 10.1006/meth.2001.1262

Luo, C., Zhao, J., Madden, A., Chen, M., and Xu, H. (2013). Complement expression in retinal pigment epithelial cells is modulated by activated macrophages. *Exp. Eye Res.* 112, 93–101. doi: 10.1016/j.exer.2013.04.016

Moon, J. Y., Garg, I., Cui, Y., Katz, R., Zhu, Y., Le, R., et al. (2023). Wide-field swept-source optical coherence tomography angiography in the assessment of retinal microvasculature and choroidal thickness in patients with myopia. *Br. J. Ophthalmol.* 107, 102–108. doi: 10.1136/bjophthalmol-2021-319540

Neuringer, M., Anderson, G. J., and Connor, W. E. (1988). The essentiality of n-3 fatty acids for the development and function of the retina and brain. *Annu. Rev. Nutr.* 8, 517–541.

Nguyen, Q. D., and Foster, C. S. (1998). Saving the vision of children with juvenile rheumatoid arthritis–associated uveitis. *JAMA* 280, 1133–1134. doi: 10.1001/jama.280.13.1133

Ohno-Matsui, K., Kawasaki, R., Jonas, J. B., Cheung, C. M., Saw, S. M., Verhoeven, V. J., et al. (2015). International photographic classification and grading system for myopic maculopathy. *Am. J. Ophthalmol.* 159, 877–83.e7. doi: 10.1016/j.ajo.2015.01.022

Ohno-Matsui, K., Lai, T., Lai, C., and Cheung, C. (2016). Updates of pathologic myopia. *Progr. Retinal Eye Res.* 52, 156–187. doi: 10.1016/j.preteyeres.2015.12.001

Ohno-Matsui, K., Wu, P. C., Yamashiro, K., Vutipongsatorn, K., Fang, Y., Cheung, C. M., et al. (2021). IMI pathologic Myopia. *Investig. Ophthalmol. Vis. Sci.* 62:5. doi: 10.1167/iovs.62.5.5

Pascolini, D., and Mariotti, S. (2012). Global estimates of visual impairment: 2010. *Br. J. Ophthalmol.* 96, 614–618. doi: 10.1136/bjophthalmol-2011-300539

Pasqualetti, G., Brooks, D. J., and Edison, P. (2015). The role of neuroinflammation in dementias. *Curr. Neurol. Neurosci. Rep.* 15, 1–11.

Riddell, N., and Crewther, S. G. (2017). Novel evidence for complement system activation in chick myopia and hyperopia models: a meta-analysis of transcriptome datasets. *Sci. Rep.* 7:9719. doi: 10.1038/s41598-017-10277-2

Sacks, S. H. (2010). Complement fragments C3a and C5a: the salt and pepper of the immune response. *Eur. J. Immunol.* 40, 668–670. doi: 10.1002/eji.201040355

Shi, Y., Ye, L., Chen, Q., Hu, G., Yin, Y., Fan, Y., et al. (2021). Macular vessel density changes in young adults with high myopia: a longitudinal study. *Front. Med.* 8:648644. doi: 10.3389/fmed.2021.648644

Spaide, R. F. (2014). *"Staphyloma: part 1." Pathologic myopia*. New York, NY: Springer, 167–176.

Tang, J., and Kern, T. S. (2011). Inflammation in diabetic retinopathy. *Progr. Retinal Eye Res.* 30, 343–358. doi: 10.1016/j.preteyeres.2011.05.002

Tideman, J. W., Snabel, M. C., Tedja, M. S., Van Rijn, G. A., Wong, K. T., Kuijpers, R. W., et al. (2016). Association of axial length with risk of uncorrectable visual impairment for Europeans with Myopia. *JAMA Ophthalmol.* 134, 1355–1363. doi: 10.1001/jamaophthalmol.2016.4009

Tokoro, T. (1998). *Criteria for diagnosis of pathologic myopia*. Japan: Springer.

Ucak, T., Icel, E., Yilmaz, H., Karakurt, Y., Tasli, G., Ugurlu, A., et al. (2020). Alterations in optical coherence tomography angiography findings in patients with high myopia. *Eye* 34, 1129–1135. doi: 10.1038/s41433-020-0824-1

Wang, X., Chen, Y., Wang, Z., Li, H., He, Q., Rong, H., et al. (2022). Assessment of macular structures and vascular characteristics in highly myopic anisometropia using swept-source optical coherence tomography angiography. *Front. Physiol.* 13:918393. doi: 10.3389/fphys.2022.918393

Wei, C. C., Kung, Y. J., Chen, C. S., Chang, C. Y., Lin, C. J., Tien, P. T., et al. (2018). Allergic conjunctivitis-induced retinal inflammation promotes myopia progression. *Ebiomedicine* 28, 274–286. doi: 10.1016/j.ebiom.2018.01.024

Xu, H., and Chen, M. (2016). Targeting the complement system for the management of retinal inflammatory and degenerative diseases. *Eur. J. Pharmacol.* 787, 94–104. doi: 10.1016/j.ejphar.2016.03.001

Xu, H., and Chen, M. (2022). Immune response in retinal degenerative diseases–Time to rethink? *Progr. Neurobiol.* 219:102350. doi: 10.1016/j.pneurobio.2022.102350

Xue, M., Ke, Y., Ren, X., Zhou, L., Liu, J., Zhang, X., et al. (2021). Proteomic analysis of aqueous humor in patients with pathologic myopia. *J. Proteom.* 234:104088. doi: 10.1016/j.jprot.2020.104088

Yuan, S., Wu, S., Wang, Y., Pan, S., Wang, P., and Cheng, L. (2019). Inflammatory cytokines in highly myopic eyes. *Sci. Rep.* 9:3517. doi: 10.1038/s41598-019-39652-x

Zeng, L., Li, X., Liu, J., Liu, H., Xu, H., and Yang, Z. (2021). RNA-Seq analysis reveals an essential role of the tyrosine metabolic pathway and inflammation in myopia-induced retinal degeneration in guinea pigs. *Int. J. Mol. Sci.* 22:12598. doi: 10.3390/ijms222212598

frontiers | Frontiers in Cellular Neuroscience

TYPE Original Research
PUBLISHED 29 June 2023
DOI 10.3389/fncel.2023.1205261

OPEN ACCESS

EDITED BY
Aurel Popa-Wagner,
University of Medicine and Pharmacy of Craiova, Romania

REVIEWED BY
Vasileia Ismini Alexaki,
University Hospital Carl Gustav Carus, Germany
Medardo Hernández,
Complutense University of Madrid, Spain

*CORRESPONDENCE
Martine C. Morrison
✉ martine.morrison@tno.nl

†These authors have contributed equally to this work and share last authorship

RECEIVED 13 April 2023
ACCEPTED 12 June 2023
PUBLISHED 29 June 2023

CITATION
Seidel F, Fluiter K, Kleemann R, Worms N, van Nieuwkoop A, Caspers MPM, Grigoriadis N, Kiliaan AJ, Baas F, Michailidou I and Morrison MC (2023) Ldlr-/-.Leiden mice develop neurodegeneration, age-dependent astrogliosis and obesity-induced changes in microglia immunophenotype which are partly reversed by complement component 5 neutralizing antibody.
Front. Cell. Neurosci. 17:1205261.
doi: 10.3389/fncel.2023.1205261

Ldlr-/-.Leiden mice develop neurodegeneration, age-dependent astrogliosis and obesity-induced changes in microglia immunophenotype which are partly reversed by complement component 5 neutralizing antibody

Florine Seidel[1,2], Kees Fluiter[3], Robert Kleemann[1], Nicole Worms[1], Anita van Nieuwkoop[1], Martien P. M. Caspers[4], Nikolaos Grigoriadis[5], Amanda J. Kiliaan[2], Frank Baas[3], Iliana Michailidou[5†] and Martine C. Morrison[1*†]

[1]Department of Metabolic Health Research, Netherlands Organisation for Applied Scientific Research (TNO), Leiden, Netherlands, [2]Department of Medical Imaging, Anatomy, Preclinical Imaging Center (PRIME), Radboud Alzheimer Center, Donders Institute for Brain, Cognition, and Behavior, Radboud University Medical Center, Nijmegen, Netherlands, [3]Department of Clinical Genetics, Leiden University Medical Center, Leiden, Netherlands, [4]Department of Microbiology and Systems Biology, Netherlands Organisation for Applied Scientific Research (TNO), Leiden, Netherlands, [5]Laboratory of Experimental Neurology and Neuroimmunology and the Multiple Sclerosis Center, 2nd Department of Neurology, AHEPA University Hospital, Aristotle University of Thessaloniki, Thessaloniki, Greece

Introduction: Obesity has been linked to vascular dysfunction, cognitive impairment and neurodegenerative diseases. However, experimental models that recapitulate brain pathology in relation to obesity and vascular dysfunction are still lacking.

Methods: In this study we performed the histological and histochemical characterization of brains from Ldlr-/-.Leiden mice, an established model for obesity and associated vascular disease. First, HFD-fed 18 week-old and 50 week-old Ldlr-/-.Leiden male mice were compared with age-matched C57BL/6J mice. We then assessed the effect of high-fat diet (HFD)-induced obesity on brain pathology in Ldlr-/-.Leiden mice and tested whether a treatment with an anti-complement component 5 antibody, a terminal complement pathway inhibitor recently shown to reduce vascular disease, can attenuate neurodegeneration and neuroinflammation. Histological analyses were complemented with Next Generation Sequencing (NGS) analyses of the hippocampus to unravel molecular pathways underlying brain histopathology.

Results: We show that chow-fed Ldlr-/-.Leiden mice have more severe neurodegeneration and show an age-dependent astrogliosis that is not observed in age-matched C57BL/6J controls. This was substantiated by pathway enrichment analysis using the NGS data which showed that oxidative phosphorylation, EIF2 signaling and mitochondrial dysfunction pathways, all associated with neurodegeneration, were significantly altered in the hippocampus of Ldlr-/-.Leiden mice compared with C57BL/6J controls. Obesity-inducing HFD-feeding did not aggravate neurodegeneration and

astrogliosis in Ldlr-/-.Leiden mice. However, brains from HFD-fed Ldlr-/-.Leiden mice showed reduced IBA-1 immunoreactivity and increased CD68 immunoreactivity compared with chow-fed Ldlr-/-.Leiden mice, indicating alteration of microglial immunophenotype by HFD feeding. The systemic administration of an anti-C5 treatment partially restored the HFD effect on microglial immunophenotype. In addition, NGS data of hippocampi from Ldlr-/-.Leiden mice showed that HFD feeding affected multiple molecular pathways relative to chow-fed controls: HFD notably inactivated synaptogenesis and activated neuroinflammation pathways. The anti-C5 treatment restored the HFD-induced effect on molecular pathways to a large extent.

Conclusion: This study shows that the Ldlr-/-.Leiden mouse model is suitable to study brain histopathology and associated biological processes in a context of obesity and provides evidence of the potential therapeutic value of anti-complement therapy against obesity-induced neuroinflammation.

KEYWORDS

obesity, aging, brain, neurodegeneration, astrogliosis, neuroinflammation, anti-complement component 5

1. Introduction

Obesity has become a major health burden with important social and economic impacts. It has been increasingly associated with various comorbidities including vascular dysfunction, cardiovascular abnormalities and atherosclerosis (Andolfi and Fisichella, 2018; Csige et al., 2018). Recently, obesity has been further linked to brain pathology and cognitive impairment (Tanaka et al., 2020). Several human studies showed that obesity is associated with brain abnormalities, including smaller total brain and grey matter volumes (Pannacciulli et al., 2006; Brooks et al., 2013) and a higher risk to develop dementia (Pedditizi et al., 2016). Excessive accumulation of fat in the context of obesity is known to trigger white adipose dysfunction and release of pro-inflammatory cytokines leading to chronic and systemic low-grade inflammation (Kiliaan et al., 2014). Systemic inflammation, in addition to obesity-related vascular dysfunction, can affect the integrity of the blood-brain barrier and promote neuroinflammation (García-García et al., 2022). However, the full mechanism underlying obesity-related brain impairment is still not fully understood. Research on biological processes involved in obesity-related brain impairment is notably limited by a lack of proper translational animal models for obesity. Up to date, most studies describing the effect of obesity on brain pathology involve animal models that either do not use diets comparable to those of humans (e.g., too high fat content), do not develop important phenotypical characteristics of human obesity such as insulin resistance and dyslipidemia, or lack extensive characterization (reviewed in Guillemot-Legris and Muccioli, 2017). Moreover, translational models reflecting a broader spectrum of obesity-associated comorbidities and neuropathology are still scarce.

The Ldlr-/-.Leiden mouse model is a preclinical model for obesity that recapitulates its associated comorbidities with established translational value (Morrison et al., 2018; van den Hoek et al., 2020). When fed an energy-dense high-fat diet (HFD; with a macronutrient composition that is comparable to that of human diets), Ldlr-/-.Leiden mice develop obesity, insulin resistance and dyslipidemia in addition to atherosclerosis, with the involvement of adipose tissue inflammation and increased gut permeability (Gart et al., 2021, 2022a; van den Hoek et al., 2021). Under HFD feeding, behavioural analyses and brain imaging have shown that Ldlr-.-/Leiden mice exhibit impaired spatial memory and reduced hippocampal volume (Arnoldussen et al., 2022). However, the underlying brain pathology on a histological and gene expression level in this mouse model is still not fully described.

On the cellular and molecular level, obesity has been shown to induce neurodegeneration, together with astrogliosis and neuroinflammation (Dorfman and Thaler, 2015). Astrocytes, the most abundant cells of the brain, are glial cells known to support neuronal function that also play essential roles in blood-brain barrier formation and maintenance, regulation of neuronal synaptogenesis and immune signaling (Giovannoni and Quintana, 2020). Following neuronal injury, astrocytes may become reactive, followed by proliferation and hypertrophy of their cell bodies and cytoplasmic processes (Eng and Ghirnikar, 1994). This process, known as astrogliosis, is characterized by an extensive synthesis of glial fibrillary acidic protein (GFAP) (Eng and Ghirnikar, 1994; Sofroniew, 2009). In both humans and rodents, obesity-induced astrogliosis was notably shown in the hypothalamus, as well as other parts of the brain such as the cortex and the hippocampus (Thaler et al., 2012; Guillemot-Legris and Muccioli, 2017), which is also accompanied by an increase in GFAP immunoreactivity (Guillemot-Legris and Muccioli, 2017; Bondan et al., 2019; Bandala et al., 2022). Obesity-related astrogliosis has been associated with neuroinflammation, which is characterized by microglia activation. As the immune cells of the brain, microglia can be activated upon stress stimuli and undergo phenotypical and morphological changes (Guillemot-Legris and Muccioli, 2017). Obesity has been shown to induce microglia activation in multiple areas of the brain, including the hypothalamus, cortex and hippocampus (Thaler et al., 2012; Dorfman and Thaler, 2015; Guillemot-Legris and Muccioli, 2017), which seems to be accompanied with changes in microglia

immunophenotype: obesity-inducing HFD feeding in rodents has been shown to enhance the expression of the microglia-specific marker ionized calcium binding adapter molecule 1 (IBA-1) protein (Ito et al., 1998; Wahid et al., 2021) and to increase the number of IBA-1-positive microglia in the hippocampus (Thaler et al., 2012; Koga et al., 2014; Ahmad Tarmizi et al., 2022). However in humans, no difference in terms of IBA-1 density was observed in obese cases (Lier et al., 2019). Lier et al. further described the existence of areas exhibiting a loss of IBA-1 immunoreactivity while remaining immunopositive for other microglial markers. Consistent with this, a study suggested that HFD feeding in mice rather increases CD68-positive activated microglia in the hippocampus (Tucsek et al., 2014).

In parallel, it has been recently demonstrated that obesity increases the activity of the complement system in the brain, a part of the innate immune system implicated in host defence and inflammation (Graham et al., 2020). The complement system is activated through three major pathways, the classical, lectin and alternative pathways, all converging to the activation and cleavage of the downstream complement component C5 (Sarma and Ward, 2011). The activation of this terminal complement pathway notably results in the formation of the immunostimulating chemoattractant C5a and the terminal membrane attack complex (MAC). Activation of the complement system has been linked to systemic inflammation and atherosclerosis, two key components of obesity-related pathology (Vlaicu et al., 2016; Shim et al., 2020). In the brain, regulated complement system activation is essential for development as it mediates synaptic pruning (Stevens et al., 2007). However, in pathological conditions, overactivation of the complement system can also trigger neuroinflammatory cascades in which astrocytes and microglia are activated leading to the development of neurodegenerative diseases (Dalakas et al., 2020). Several studies further showed in acute neuroinflammatory conditions that the induction of neuroinflammation can be abrogated by inhibition of terminal complement system activation (Fluiter et al., 2014; Michailidou et al., 2018). However, in chronic neuroinflammation in a context of obesity, the implication of complement system activation and the therapeutic value of its inhibition are still poorly known.

In the present study we characterized the development of brain pathology in the Ldlr-/-.Leiden mouse model for obesity using (immuno)histology. To first understand the role of the Ldlr-/-.Leiden genotype, the development of brain histopathology was compared between young and aged Ldlr-/-.Leiden and aged-matched wild-type (C57BL/6J) mice. In parallel, the development of obesity-induced neuropathology was analysed in the Ldlr-/-.Leiden mice fed an obesity-inducing HFD compared with mice fed a standardized chow diet. We present data supporting that the genetically-determined impaired cholesterol metabolism is associated with brain neuroinflammation in this mouse model and further show that application of a HFD worsens the underlying brain pathology. To unravel potential underlying biological processes in the brain, gene expression was analysed in the hippocampus, the most important brain region involved in memory and learning. Finally, we tested in HFD-fed Ldlr-/-.Leiden mice whether an anti-complement therapy inhibiting systemic complement C5 (BB5.1 antibody; Zelek et al., 2020), shown to improve vascular function in the same mouse model (Seidel et al., 2022), can limit neurodegeneration and neuroinflammation. This study provides evidence supporting the Ldlr-/-.Leiden mouse model as a suitable model to study obesity-associated brain impairment against which anti-complement therapies may be promising.

2. Materials and methods

2.1. Animals

2.1.1. Animals and housing

The studies were approved by an independent Animal Welfare Body (IVD TNO; approval numbers TNO-451 and TNO-499) under project licenses granted by the Netherlands Central Authority for Scientific Procedures on Animals (CCD; project license numbers AVD5010020172064 and AVD5010020172931). All animal experiments were performed in compliance with the European Union directive 2010/63/EU regarding the use of laboratory animals. Male C57BL/6J and Ldlr-/-.Leiden mice obtained from the breeding stock at TNO Metabolic Health Research (Leiden, the Netherlands) were group-housed (two to six animals per cage) in a conventional animal room (temperature ∼21°C, relative humidity 50–60%, light cycle 07:00 to 19:00) and received food and water *ad libitum*. Until the start of the studies, the animals were fed a standardized chow diet (Sniff R/M V1530, Uden, the Netherlands). Randomization, blinding methods and power calculations were used as previously described (Seidel et al., 2022).

2.1.2. Effect of genetic background

To investigate the effect of genetic background on the development of neuropathology in Ldlr-/-.Leiden mouse model, two groups of Ldlr-/-.Leiden mice were terminated at 18 or 50 weeks of age (**Figure 1A**). For comparison, two groups of C57BL/6J mice were terminated at the same age. All groups were kept on chow diet. The mice were terminated by isoflurane inhalation (4%) and heart puncture followed by perfusion with phosphate-buffered saline (PBS) for 10 min (1 ml/min).

2.1.3. Effect of HFD feeding and anti-complement C5 treatment

To investigate the effect of HFD feeding and treatment with an established antibody (BB5.1) targeting complement C5 on neuropathology in Ldlr-/-.Leiden mice, 17–18 week-old Ldlr-/-.Leiden mice were matched into two groups based on body weight, blood glucose, plasma cholesterol and plasma triglyceride levels (**Figure 1B**). These two groups were fed an energy-dense HFD [45 kcal% fat with 39 kcal% fat from lard and 6 kcal% fat from soybean oil, 20 kcal% protein and 35 kcal% carbohydrates, D12451, Research Diets, New Brunswick, NJ, USA, Gart et al., 2021] for 32 weeks. During the last 12 weeks of HFD feeding, one group of mice received intraperitoneal injections with an established anti-C5 antibody (BB5.1, 5 mg/mL in PBS, 1 mg/mouse; Zelek et al., 2020). The BB5.1 antibody was produced as reported (Seidel et al., 2022). A HFD-fed control group received intraperitoneal injections of PBS (as a vehicle control). The anti-C5 treatment or PBS was administered twice a week until the end of the study as we detailed previously (Seidel et al., 2022). Mice were euthanized at 50 weeks

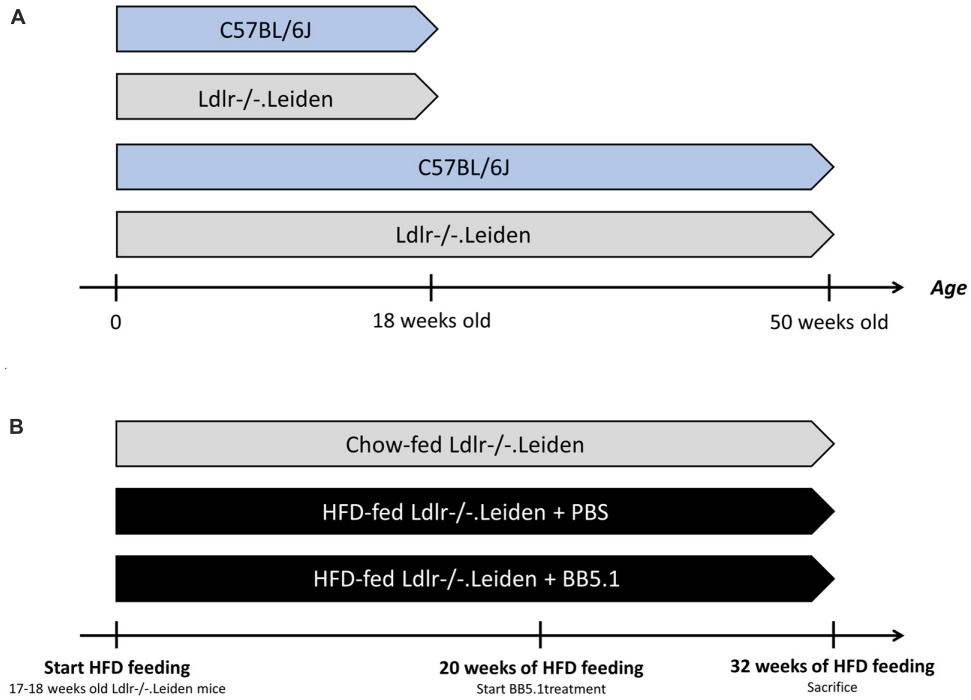

FIGURE 1
Experimental design. **(A)** To study the development of neuropathology over time, four groups of mice were fed a standardized chow diet: 18 week-old C57BL/6J mice (n = 8), 18 week-old Ldlr-/-.Leiden mice (n = 8), 50 week-old C57BL/6J mice (n = 8) and 50 week-old Ldlr-/-.Leiden mice (n = 8). **(B)** In a separate study, to investigate the effect of HFD feeding and an intervention on neuropathology development, two groups of Ldlr-/-.Leiden mice were fed an obesity-inducing HFD (n = 17 for the two groups). A separate group of chow-fed Ldlr-/-.Leiden mice served as a non-obese reference. During the last 20 weeks of HFD feeding, one group of HFD-fed groups received an BB5.1 antibody treatment while the other HFD-fed group and the chow-fed group received injections with PBS. The average age of the mice at the end the study was again 50 weeks.

old using the aforementioned method. A separate group of chow-fed Ldlr-/-.Leiden mice received similar injections with PBS and was sacrificed at 50 weeks of age as a non-obese reference.

2.2. Brain histology

Brains were collected at sacrifice and a mid-sagittal cut was performed. The right hemisphere was fixed in phosphate-buffered formalin (3.7%) for one week. The samples were dehydrated over 2.5 days (Automatic Tissue Processor ASP300S, Leica Biosystems, Amsterdam, the Netherlands) and then embedded in paraffin blocks. 6 μm-thick sagittal cross-sections were cut and stained for further analyses. Neurodegeneration was assessed on cross-sections stained with hematoxylin-eosin (HE). For this analysis four anatomic locations were examined: cortex, the hippocampus, the thalamus and the hypothalamus. The grade for degeneration was based on the following rubric: (1) one of a few foci of degeneration; (2) up to 5% (estimated) of the cells or structures degenerated; (3) 5–15% (estimated) of the cells or structures degenerated; (4) 15–40% (estimated) of the cells or structures degenerated; (5): greater than 40% (estimated) of the cells or structures degenerated.

2.2.1. Immunohistochemistry

Sagittal cross-sections were deparaffinized in xylene and rehydrated with alcohol gradients and demineralized water. The sections were stained for GFAP, IBA-1, CD68 and triggering receptor expressed on myeloid cells 2 (TREM2) as detailed in Table 1. Antigen retrieval was performed by heat in a water bath (96°C, 40 min) for GFAP and IBA-1 immunostaining or in citrate buffer (pH 6, 96°C, 20 min) using a Dako PT-link device (Dako, Glostrup, Denmark) for CD68 and TREM2 immunostaining.

2.2.2. Quantification of immunoreactivity

Quantification of immunoreactivity was performed on sections scanned with a Pathology Scanner Second Generation SG300 (Philips, Best, the Netherlands). For these analyses four anatomic locations were examined: the internal capsule, hippocampus, thalamus and hypothalamus. Non-overlapping images were acquired from the analysed groups from each of the aforementioned anatomic locations, at a 20× magnification for the CD68 and TREM2 immunostainings and at a 5 × magnification for the GFAP and IBA-1 immunostainings, using the Image Management System Viewer software (Philips). Quantitative analysis of immunostaining was performed using the 'measurement' function of the Image J software (Image Pro Plus 5.1, National Institutes of Health, Bethesda, USA). For each picture, the immunoreactive area was measured and divided by the total area of measurement. For measurement of the immunoreactive area a threshold was set and applied to all images (stained in a single batch). The percentage of immunoreactive area over the total area assessed was then calculated and plotted for each brain

TABLE 1 Immunohistochemical staining of brain cross-sections.

Antigen	Primary antibody	Secondary antibody
GFAP	Anti-GFAP, Z0334 (Dako), 1:500, 4°C, overnight	Biotinylated donkey anti-rabbit (Jackson Immunoresearch), 1:1,500, room temperature, 1 h
IBA-1	Anti-IBA-1, 019-19741 (Fujifilm), 1:1,000, 4°C, overnight	Biotinylated donkey anti-rabbit (Jackson Immunoresearch), 1:1,500, room temperature, 1 h
CD68	Anti-CD68, ab125212 (Abcam), 1:500, 4°C, overnight	Brightvision HRP (Immunologic), 1:1, room temperature, 1h
TREM2	Anti-TREM2, af1729 (R&D Systems), 1:400, 4°C, overnight	Biotinylated rabbit anti-sheep (Vector Laboratories), 1:500, room temperature, 1h

region. Average measurements per mouse were also calculated and plotted for each group.

2.3. Hippocampus gene expression and pathway analysis

The left hemispheres of the brains were snap frozen in liquid nitrogen. The hippocampi were isolated and used to prepare homogenates using glass beads and ribonucleic nucleic acid (RNA) was extracted as described (Salic et al., 2019). RNA integrity and concentration were examined for each sample using the RNA 6000 Nano LabChip kit and a bioanalyzer 2100 (both Agilent Technologies, Amstelveen, the Netherlands) and the samples were sequenced by GenomeScan BV (Leiden, the Netherlands). RNA sequencing and RNA counts processing were performed as reported previously (Gart et al., 2021; Seidel et al., 2022). Differentially expressed genes were determined using the Deseq2-pipeline (Love et al., 2014) with a statistical cut-off of p-value (p) < 0.05 and used for gene enrichment analysis across pathways and biological processes using the Ingenuity Pathway Analysis suite (IPA; www.ingenuity.com, accessed on 15 September 2022). The upstream regulator analysis tool of IPA was used to assess the activity of upstream regulators as detailed in Salic et al. (2019).

2.4. Analysis of chemokine and cytokine concentrations in brain homogenates

Homogenates of the cortex (~80 mg tissue) and thalamus (~25 mg tissue) were prepared in lysis buffer and subsequently analysed by multiplex analysis using a V-PLEX Custom Mouse Biomarkers set (Mesoscale discoveries [MSD], Maryland, USA) that includes 'Proinflammatory Panel 1' (IFN-γ, IL-1β, IL-2, IL-4, IL-6, KC/GRO (CXCL1), IL-10, TNF-α) and 'Cytokine Panel 1' (MCP-1, IL-33, IL-27-p28/IL-30, IL-17A/F and IP-10 for the cortex and MCP-1, IL-33, IL-17A/F, IP-10, IL-15, MIP-1α and MIP-2 for the thalamus) as described before (Gart et al., 2022b). Plates were read on a MESO QuickPlex SQ 120 reader (MSD). Protein concentrations were measured in the same homogenates using a BCA Protein Assay Kit (Thermo Fisher Scientific, Waltham, MA, USA) and cytokine levels were expressed per mg protein. IL-4 and INF-γ in the cortex and INF-γ, IL-2 and IL-4 in the thalamus were below the detection range and were not further considered in the results.

2.5. Statistical analyses

All statistics were performed with Prism (GraphPad software, v9, San Diego, CA, USA). The normality of the distributions were assessed using a Shapiro-Wilk test. Outliers were detected using the Grubbs test or the ROUT test (Q = 1%) and excluded from statistical analysis. When the distribution was normal, a one-way analysis of variance (ANOVA) was performed with a Bonferroni correction for multiple comparisons. When the data were not normally distributed, a non-parametric Mann-Whitney test or Kruskal-Wallis test were performed followed by a Dunn's multiple comparison test to assess intergroup differences. The results were considered significant when $p \leq 0.05$ (two-tailed) at a 95% confidence level. All data are expressed as mean ± standard deviation (SD).

3. Results

To investigate the development of neuropathology in Ldlr-/-.Leiden mouse model, brain histopathology and hippocampal gene expression were analysed in 18 and 50 week-old Ldlr-/-.Leiden mice fed a standardized chow diet. For comparison, age-matched C57BL/6J mice were included in these analyses.

3.1. Ldlr-/-.Leiden mice exhibit neurodegeneration and age-related astrogliosis

Severity of degeneration, as assessed by a semi-quantitative scoring of HE-stained brain sections, was higher in chow-fed 18 week-old Ldlr-/-.Leiden mice than in the age-matched C57BL/6J mice (p = 0.034, **Figure 2A**), indicating an effect of the genotype on neurodegeneration in this model. The difference between the genotypes was most pronounced in the thalamus (p = 0.019, **Figure 2B**). The severity of degeneration in the thalamus (p = 0.037) and the average degeneration scores of all brain areas assessed (trends for significance, p = 0.090) remained higher in Ldlr-/-.Leiden mice than in C57BL/6J mice at 50 weeks of age. Quantification of GFAP immunoreactivity (astrogliosis) on consecutive slides, showed that the 18 week-old Ldlr-/-.Leiden and C57BL/6J mice exhibited similar GFAP immunoreactivity, whereas 50 week-old Ldlr-/-.Leiden mice showed increased GFAP immunoreactivity compared with C57BL/6J mice (p = 0.040, **Figure 2C**), especially in the hypothalamus (p = 0.040, **Figure 2D**)

10.3389/fncel.2023.1205261

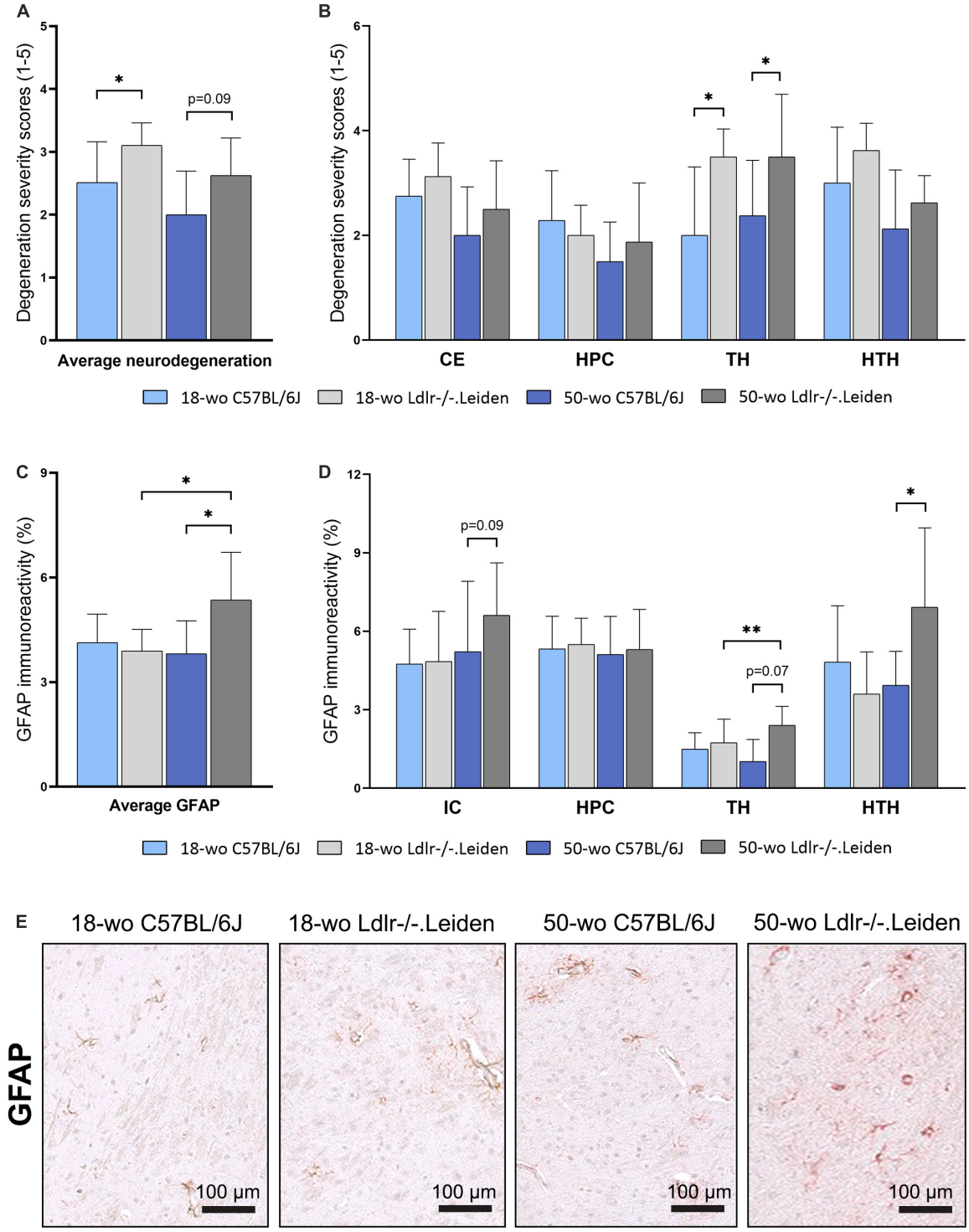

FIGURE 2
On chow diet, Ldlr-/-.Leiden mice developed neurodegeneration and age-dependent astrogliosis. **(A)** HE staining revealed that Ldlr-/-.Leiden mice developed more severe neurodegeneration than C57BL/6J mice and **(B)** the genotype effect was most pronounced in the thalamus. **(C)** Ldlr-/-.Leiden mice showed increased average GFAP immunoreactivity of all areas combined at 50 weeks of age, **(D)** which was mainly attributable to increases in the thalamus and hypothalamus. **(E)** Representative pictures of GFAP immunostaining in the brains of chow-fed C57BL/6J and Ldlr/-.Leiden mice of 18 weeks old and 50 weeks old respectively. $^{*}p \leq 0.05$, $^{**}p \leq 0.01$. GFAP, glial fibrillary acidic protein; CE, cortex; HPC, hippocampus; TH, thalamus; HTH, hypothalamus; IC, internal capsule. Data are shown as mean ± SD.

followed by the thalamus (trend for significance, $p = 0.072$) and internal capsule (trend for significance, $p = 0.094$). Representative pictures of GFAP immunostaining in chow-fed 18 and 50 week-old C57BL/6J and Ldlr-/-.Leiden respectively are provided in Figure 2E. In Ldlr-/-.Leiden mice, average GFAP immunoreactivity of all brain areas and GFAP immunoreactivity in the thalamus were

significantly increased between 18 and 50 weeks of age (p = 0.038 and p = 0.007 respectively), suggesting that Ldlr-/-.Leiden mice develop an age-dependent astrogliosis that is not observed in C57BL/6J mice.

3.2. On gene expression level, Ldlr-/-.Leiden mice show an increase in mitochondrial dysfunction and a decrease in eiF2 signaling in the hippocampus

We next used transcriptomics analyses to characterize the molecular processes affected in the hippocampus, the main brain region involved in memory. Transcriptomics (NGS) followed by pathway enrichment analysis were performed in hippocampus mRNA of 50 week-old C57BL/6J and Ldlr-/-.Leiden mice. In comparison with C57BL/6J mice, Ldlr-/.Leiden animals showed alterations of many pathways in the hippocampus (∼200, **Supplementary Table 1**). The most enriched canonical pathways are displayed in **Figure 3A**. The pathways 'Oxidative phosphorylation' and 'EIF2 signaling' were the most inactivated and 'Mitochondrial dysfunction' was significantly increased. The subsequent upstream regulator analysis revealed that Rapamycin-insensitive companion of mammalian target of rapamycin (RICTOR) protein was the upstream regulator most activated while MLX-interacting protein-like (MLXIPL) was the most inactivated (**Figure 3B**). In addition, the 'Synaptogenesis signaling pathway' was activated and upstream regulators involved in protein synthesis [e.g., Fragile X Messenger Ribonucleoprotein 1 (FMR1), La Ribonucleoprotein 1 (LARP1)] were activated.

3.3. HFD feeding and anti-complement C5 treatment did not further alter neurodegeneration and astrogliosis in Ldlr-/-.Leiden mice

Next, we investigated whether a subsequent addition of HFD feeding in Ldlr-/-.Leiden mice to induce obesity aggravates the metabolic disturbances in this model and potentially induces neuroinflammation. A separate group of Ldlr-/-.Leiden mice was fed an obesity-inducing HFD from 18 to 50 weeks of age and the aforementioned chow-fed group was used as a non-obese reference. We have previously shown that these HFD-fed Ldlr-/-.Leiden mice develop obesity and associated human-like dyslipidemia, NAFLD and atherosclerosis (Seidel et al., 2022). In the present study, HFD-fed 50 week-old Ldlr-/-.Leiden mice exhibited similar levels of neurodegeneration severity and similar amounts of GFAP immunoreactivity as the chow-fed animals in all anatomic areas examined (**Figures 4A–D**). To assess if an anti-complement therapy can rescue the brain health status, HFD-fed Ldlr-/-.Leiden mice were administered a systemic anti-complement C5 treatment (BB5.1 antibody) during the 12 last weeks of HFD feeding. BB5.1 treatment did not alter average neurodegeneration for all areas combined or neurodegeneration in the hippocampus, thalamus and hypothalamus. HFD-fed mice treated with BB5.1 treatment did however present with increased neurodegeneration in the cortex compared with HFD-fed control mice (p = 0.025). No effect of BB5.1 treatment was observed on GFAP immunoreactivity.

3.4. On HFD feeding, Ldlr-/-.Leiden mice exhibit changes in microglia immunophenotype, which were partially restored by an anti-complement C5 treatment

Although HFD feeding did not alter the development of neurodegeneration or astrogliosis, it did alter the microglia immunophenotype by decreasing the average IBA-1-positive immunoreactivity (p = 0.022, **Figure 5A**) while increasing the average of CD68-positive microglia (p = 0.010, **Figure 6A**). More specifically, analyses per anatomic region indicated that HFD-fed Ldlr-/-.Leiden mice showed lower IBA-1-positive immunoreactivity than chow-fed animals in the internal capsule (p = 0.013), hippocampus (p = 0.002) and thalamus (p = 0.006) but not in the hypothalamus (**Figure 5B**). BB5.1 treatment reversed the HFD-induced decrease in IBA-1 immunoreactivity: HFD-fed mice treated with BB5.1 exhibited increased average IBA-1 immunoreactivity relative to HFD-fed control mice (p = 0.008) which was notably attributable to increased IBA-1 immunoreactivity in the internal capsule (p = 0.015). BB5.1 treatment did not affect IBA-1 immunoreactivity in the hippocampus or thalamus. In the hypothalamus, HFD-fed mice treated with BB5.1 showed more IBA-1-positive microglia compared with HFD controls (p = 0.001) and chow-fed mice (p = 0.006). Representative pictures of IBA-1 immunostaining are displayed in **Figure 5C**.

To study whether the observed reduction in IBA-1 immunoreactivity induced by HFD feeding was due to microglial cell depletion or the result of a shift of the microglial cell immunophenotype, we examined the presence of CD68-positive and TREM2-positive microglial cells. HFD-fed Ldlr-/-.Leiden mice exhibited more CD68 immunoreactivity than chow-fed mice (p = 0.010, **Figure 6A**) which was attributable to a difference in the internal capsule specifically (p = 0.002, **Figure 6B**). No difference in CD68 immunoreactivity in the hippocampus, thalamus or hypothalamus was observed. BB5.1 treatment did not affect average CD68 immunoreactivity or CD68 immunoreactivity in the individual brain regions investigated. In addition, HFD-fed mice presented increased average TREM2-positive microglia compared to chow-fed mice (trend for significance, p = 0.069 **Figure 6C**) and HFD-fed mice treated with BB5.1 showed similar average TREM2 immunoreactivity as HFD controls. While no HFD feeding effect was observed in the individual brain regions, HFD-fed mice treated with BB5.1 showed higher average TREM2 immunoreactivity than chow-fed mice (p = 0.007) and higher TREM2 immunoreactivity in the internal capsule (trend for significance, p = 0.052), hippocampus and thalamus (p = 0.017 and p = 0.023 respectively, **Figure 6D**).

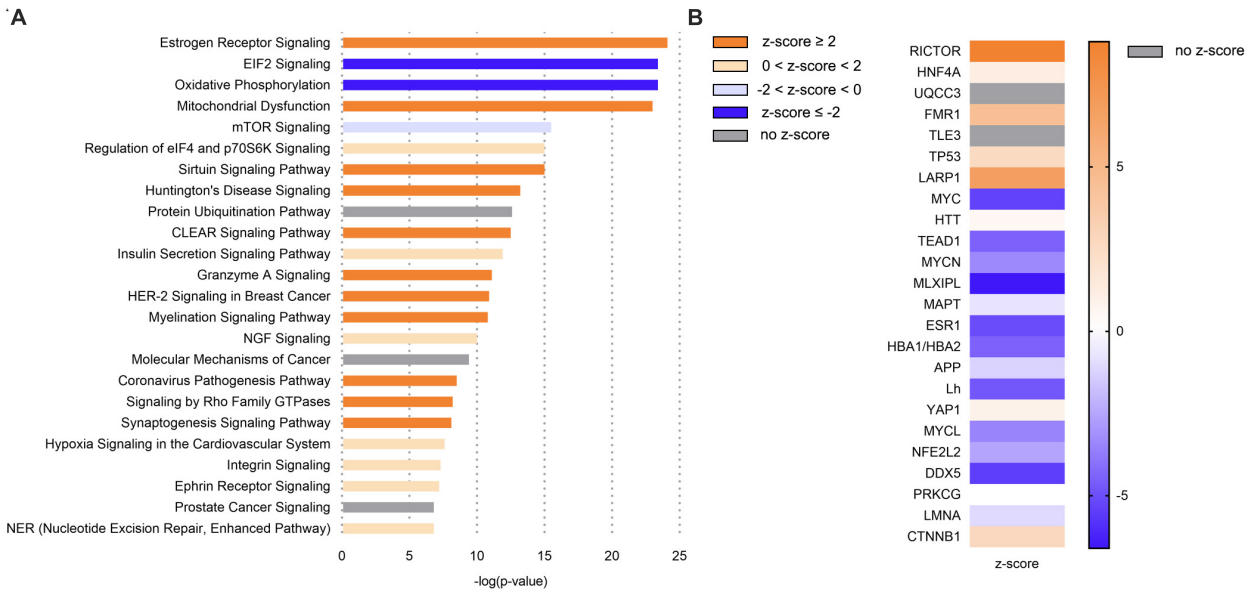

FIGURE 3
In comparison with C57BL/6J mice, Ldlr-/-.Leiden mice exhibited in the hippocampus a general overactivation of signaling pathways, including an increase in mitochondrial dysfunction, but also a downregulation of eiF2 signaling and oxidative phosphorylation. **(A)** Most significantly enriched canonical pathways based on hippocampal gene expression in chow-fed 50-wo Ldlr-/-.Leiden vs chow-fed 50-wo C57BL/6J mice. **(B)** Top 20 predicted upstream regulators (sorted by *p*-value) based on hippocampal gene expression in chow-fed 50-wo Ldlr-/-.Leiden vs chow-fed 50-wo C57BL/6J. The z-score indicates the predicted activation of a canonical pathway: z-score ≤ -2 indicates relevant inhibition of the pathway or regulator (indicated in dark blue); z-score ≥ 2 indicates relevant activation of the pathway or regulator (indicated in dark orange).

3.5. HFD feeding in Ldlr-/-.Leiden mice upregulates 'neuroinflammation signaling' and downregulates 'synaptogenesis signaling' pathways in the hippocampus while the anti-complement C5 treatment partially reverses hippocampal gene expression

Transcriptomics analyses in the hippocampus further revealed that HFD significantly inactivated the 'Synaptogenesis signaling' and 'SNARE signaling' pathways (Figure 7A). A full list of the canonical pathways significantly enriched by HFD feeding is provided in Supplementary Table 2. Consistently, the upstream regulator brain-derived neurotrophic factor (BDNF) was significantly inactivated by HFD feeding (Figure 7B). Compared with the chow-fed mice, HFD-fed mice also exhibited significant inhibition of signaling pathways involved in cholesterol biosynthesis (e.g., 'Superpathway of cholesterol biosynthesis', 'Cholesterol biosynthesis II' and 'Cholesterol biosynthesis III'). In addition, HFD feeding significantly activated the 'Neuroinflammation signaling' pathway, while enriching signalling downstream from interleukin 1β (IL1B, z-score 0.4) and tumour necrosis factor (TNF, z-score -1.3). BB5.1 treatment partially restored HFD-induced changes in hippocampal gene expression (Figure 7C): while HFD feeding inactivated 'Synaptogenesis signaling', BB5.1 reversely activated the pathway. Although BB5.1 treatment did not affect 'Neuroinflammation signaling', it tended to revert the HFD-induced inhibition of 'Chemokine signaling' and overactivation of 'triggering receptor expressed on myeloid cells 1 (TREM1) signaling'. The complete list of the canonical pathways that were significantly enriched by BB5.1 treatment is provided in Supplementary Table 3.

3.6. HFD feeding increases concentrations of IL-6 in the cortex and KC in the thalamus which are not altered by anti-complement C5 treatment

To further examine the effect of HFD feeding and BB5.1 treatment on neuroinflammation in Ldlr-/-.Leiden mice, cytokines and chemokines were measured in cortex and thalamus homogenates. In the cortex, HFD feeding specifically increased IL-6 concentrations ($p = 0.017$) and BB5.1 treatment did not alter this effect (Table 2). HFD-fed Ldlr-/-.Leiden mice treated with BB5.1 showed higher cortical concentrations of interleukin 33 (IL-33, $p = 0.013$), interleukin 1β (IL-1β, $p = 0.030$), tumor necrosis factor (TNF-α, $p = 0.008$) and interleukin 10 (IL-10, trend for significance, $p = 0.052$) compared to chow-fed animals. However, no difference in these concentrations were observed between HFD-fed and chow-fed mice or between HFD-fed animals treated with BB5.1 and HFD-fed controls. In the thalamus, HFD feeding increased the concentration of KC, the mouse homologue of the human growth-regulated oncogene (GRO) chemokine (trend for significance, $p = 0.057$, Table 3). BB5.1 treatment did not alter KC concentrations but HFD-fed mice treated with BB5.1 exhibited higher IL-33 concentrations compared with chow-fed mice ($p = 0.012$) and HFD-fed controls ($p = 0.031$).

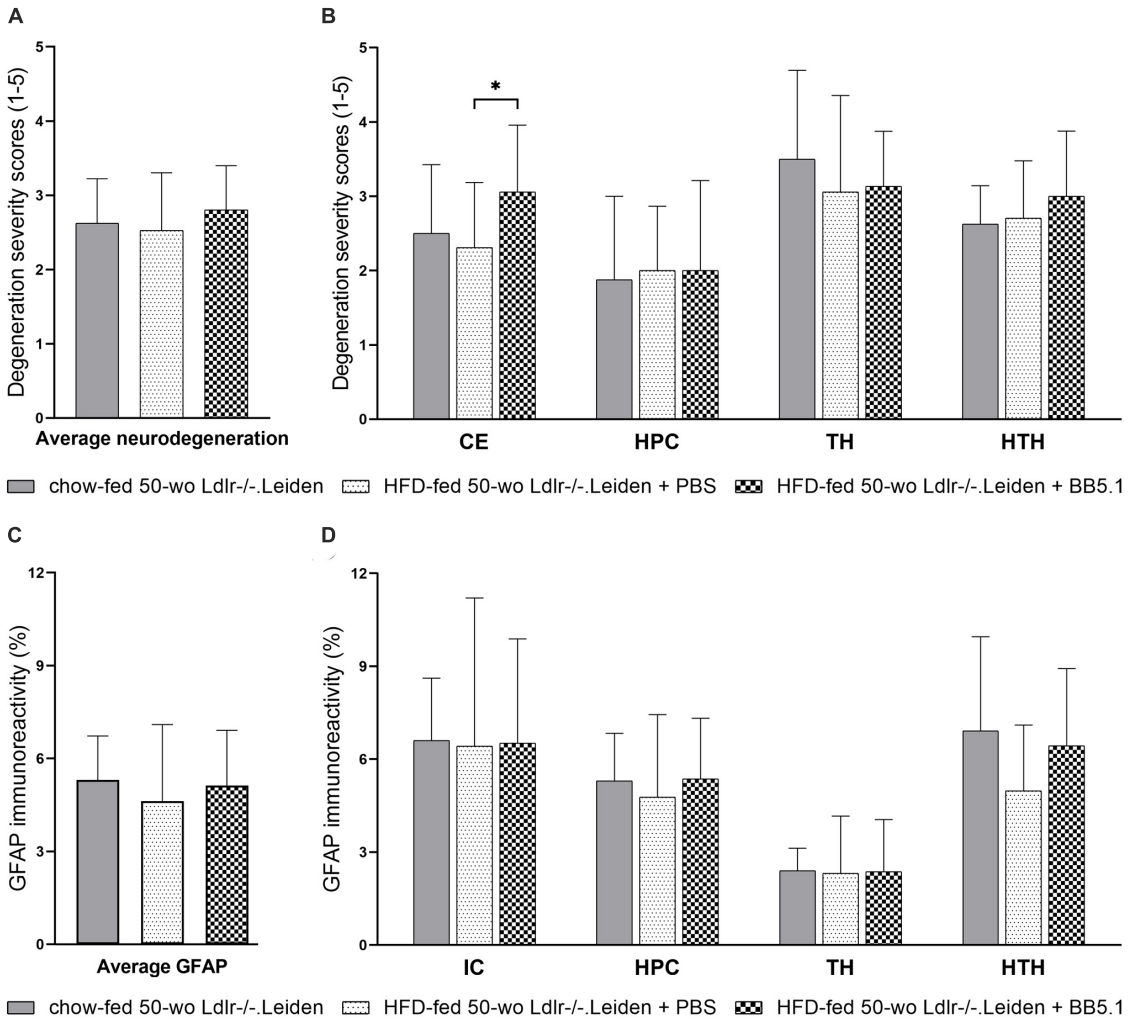

FIGURE 4
HFD feeding did not further aggravate neurodegeneration and gliosis in Ldlr-/-.Leiden mice. **(A)** HFD feeding did not affect average neurodegeneration of all areas combined or **(B)** neurodegeneration in individual brain regions. BB5.1 treatment had no effect except an increase in degeneration in the cortex. **(C,D)** HFD feeding and BB5.1 treatment did not alter GFAP immunoreactivity. *$p \leq 0.05$. GFAP, glial fibrillary acidic protein; CE, cortex; HPC, hippocampus, TH, thalamus; HTH, hypothalamus; IC, internal capsule. Data are shown as mean ± SD.

4. Discussion

Using (immuno)histological and hippocampal gene expression analyses, we showed that the Ldlr-/-.Leiden mouse model, an established translational model for obesity and related comorbidities, presents key signs of neurodegeneration and neuroinflammation, the severity of which is aggravated by aging and HFD feeding. In comparison with C57BL/6J mice, Ldlr-/-.Leiden mice exhibited more severe neurodegeneration and an age-dependent astrogliosis, especially in the thalamus. Transcriptomics analyses of RNA obtained from the hippocampus, the most important region of the brain involved in memory and cognition, further showed that Ldlr-/-.Leiden mice exhibited impaired oxidative phosphorylation and protein synthesis and repair (eiF2 signaling), in combination with increased mitochondrial dysfunction already on a chow diet. Application of obesity-inducing HFD feeding in Ldlr-/-.Leiden mice further triggered changes in microglia immunophenotype: HFD feeding reduced the reactivity of the IBA-1 marker for microglial cells and increased the CD68 immunoreactivity and TREM2 immunoreactivity (trend). HFD-induced neuroinflammation was accompanied by an increase in the protein concentration of IL-6 in the cortex and KC in the thalamus. On the gene expression level, HFD feeding increased neuroinflammation while inactivating the synaptogenesis signaling pathway. We further showed that this neuroinflammation can be modulated therapeutically: HFD-fed Ldlr-/-.Leiden mice responded to a therapeutic antibody intervention targeting complement C5 (BB5.1 antibody) which was previously shown to decrease neuroinflammation in acute models of neurodegenerative disease (Fluiter et al., 2014; Michailidou et al., 2018) and atherosclerosis in this mouse model (Seidel et al., 2022). The antibody treatment partially reverted the HFD-induced changes in microglial immunophenotype by increasing IBA-1 immunoreactivity without affecting CD68 and TREM2 immunoreactivities or cytokine levels in the brain. Hippocampal gene expression was also mostly reverted by the antibody

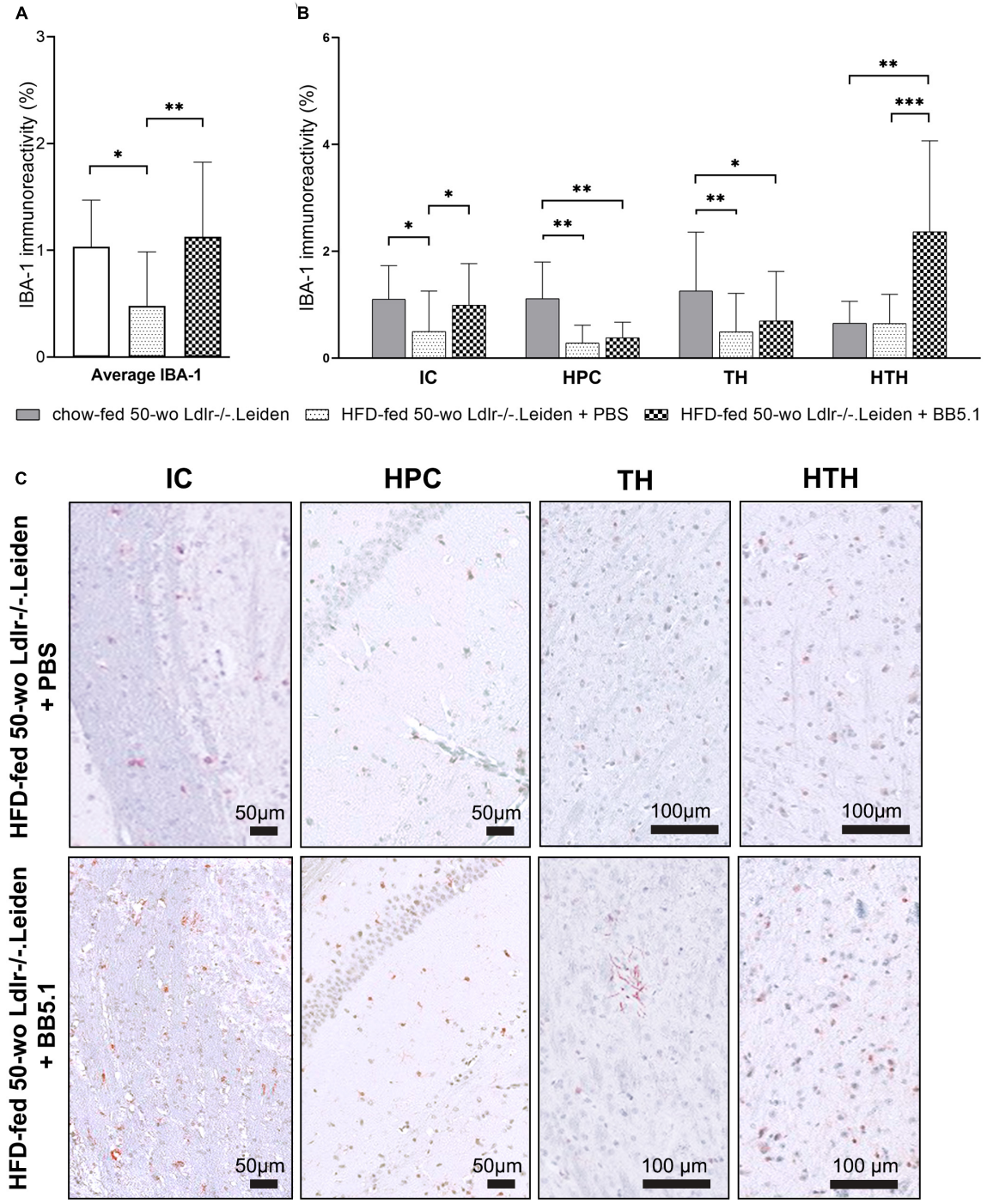

FIGURE 5
HFD feeding decreased IBA-1-positive microglia. **(A)** Average IBA-1 immunoreactivity was decreased by HFD feeding but restored with BB5.1 treatment, and **(B)** a pronounced reversal effect was observed in the internal capsule. **(C)** Representative pictures of IBA-1 immunostaining in individual brain regions of HFD-fed 50-wo Ldlr-/-.Leiden + PBS and HFD-fed 50-wo Ldlr-/-.Leiden + BB5.1 mice respectively. $^{*}p \leq 0.05$, $^{**}p \leq 0.01$, $^{***}p \leq 0.001$. IBA-1, Ionized calcium-binding adaptor molecule 1; IC, internal capsule; HPC, hippocampus; TH, thalamus; HTH, hypothalamus. Data are shown as mean ± SD.

treatment: the anti-C5 treatment notably reverted the HFD-induced inactivation of the synaptogenesis pathway; however, without affecting the neuroinflammation pathway.

Histopathological analyses of brain cross-sections showed that, already on a chow diet, Ldlr-/-.Leiden mice show signs of neurodegeneration as well as an aging-dependent astrogliosis that is not observed in C57BL6/J mice. When Ldlr-/-.Leiden mice were fed an obesity-inducing HFD, these pathological features remained. Neurodegeneration and astrogliosis are key features of obesity-related brain histopathology as described in both humans and mice (Thaler et al., 2012; Guillemot-Legris and Muccioli, 2017; Bondan et al., 2019; Bandala et al., 2022). In this study,

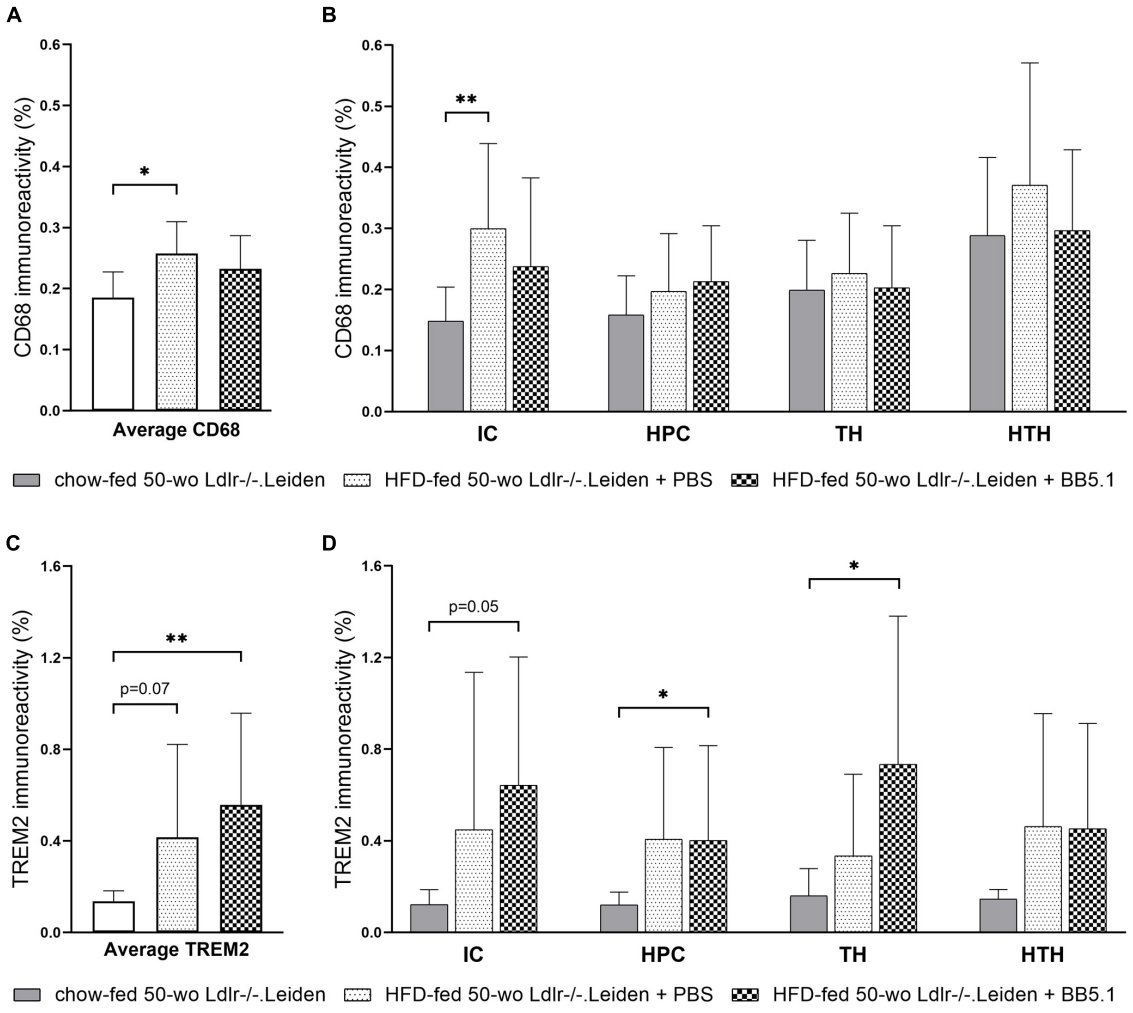

FIGURE 6
HFD feeding increased CD68-positive microglia and TREM2-positive microglia. **(A)** Average CD68 immunoreactivity was increased by HFD feeding but not altered by BB5.1 treatment. **(B)** HFD feeding specifically increased CD68 immunoreactivity in the internal capsule. **(C)** HFD feeding increased average TREM2 immunoreactivity (trend for significance) and BB5.1 treatment further increased TREM2 reactivity in comparison with chow-fed mice. **(D)** TREM2 immunoreactivity in individual brain regions was not altered by HFD feeding but was increased by BB5.1 treatment in comparison with chow-fed mice in the internal capsule, hippocampus and thalamus. $^{*}p \leq 0.05$, $^{**}p \leq 0.01$. IC, internal capsule; HPC, hippocampus; TH, thalamus; HTH, hypothalamus. Data are shown as mean ± SD.

neurodegeneration was prominently observed in the thalamus. Although neurodegeneration in the thalamus is poorly described in other rodent models, several human studies showed a reduction in grey matter volume in the thalamus in obese subjects compared to lean subjects (reviewed in Gómez-Apo et al., 2021), suggesting the development of an obesity-associated degeneration of the thalamus. In addition, the thalamus has been described to be sensitive to the development of lacunes related to cerebral small vessel disease that correlate with subsequent cognitive impairment (Benisty et al., 2009). At older age (50 weeks old), Ldlr-/-.Leiden mice also exhibited increased astrogliosis in the hypothalamus compared to C57BL6/J mice, which is consistent with the obesity-induced hypothalamic injury extensively described in literature (Thaler et al., 2012; Guillemot-Legris and Muccioli, 2017).

Neurodegeneration and astrogliosis in the context of obesity have been tightly linked to neuroinflammation (Dorfman and Thaler, 2015). In this study, HFD feeding induced changes in marker expression on microglial cells. We especially observed a reduction of IBA-1-positive microglia which was most pronounced in the internal capsule, hippocampus and thalamus. In animal models obesity-induced neuroinflammation has been mostly associated with an increase in IBA-1 immunoreactivity (Thaler et al., 2012; Koga et al., 2014; Ahmad Tarmizi et al., 2022). Depending on the age and duration of HFD feeding a similar increase in IBA-1 immunoreactivity has also been observed previously in Ldlr-/-.Leiden mice (Arnoldussen et al., 2017, 2022). In humans however, a recent study showed no differences in IBA-1 density between lean and obese subjects (Lier et al., 2019). The latter study also showed the existence of areas exhibiting a loss of IBA-1 immunoreactivity in the brain, areas that seemed related to the hepatic dysfunction of the patients (which is a comorbidity of obesity) rather than obesity itself. In line with this, Ldlr-/-.Leiden mice fed a HFD have been shown to develop hepatic dysfunction (van den Hoek et al., 2020; Gart et al., 2023) and the

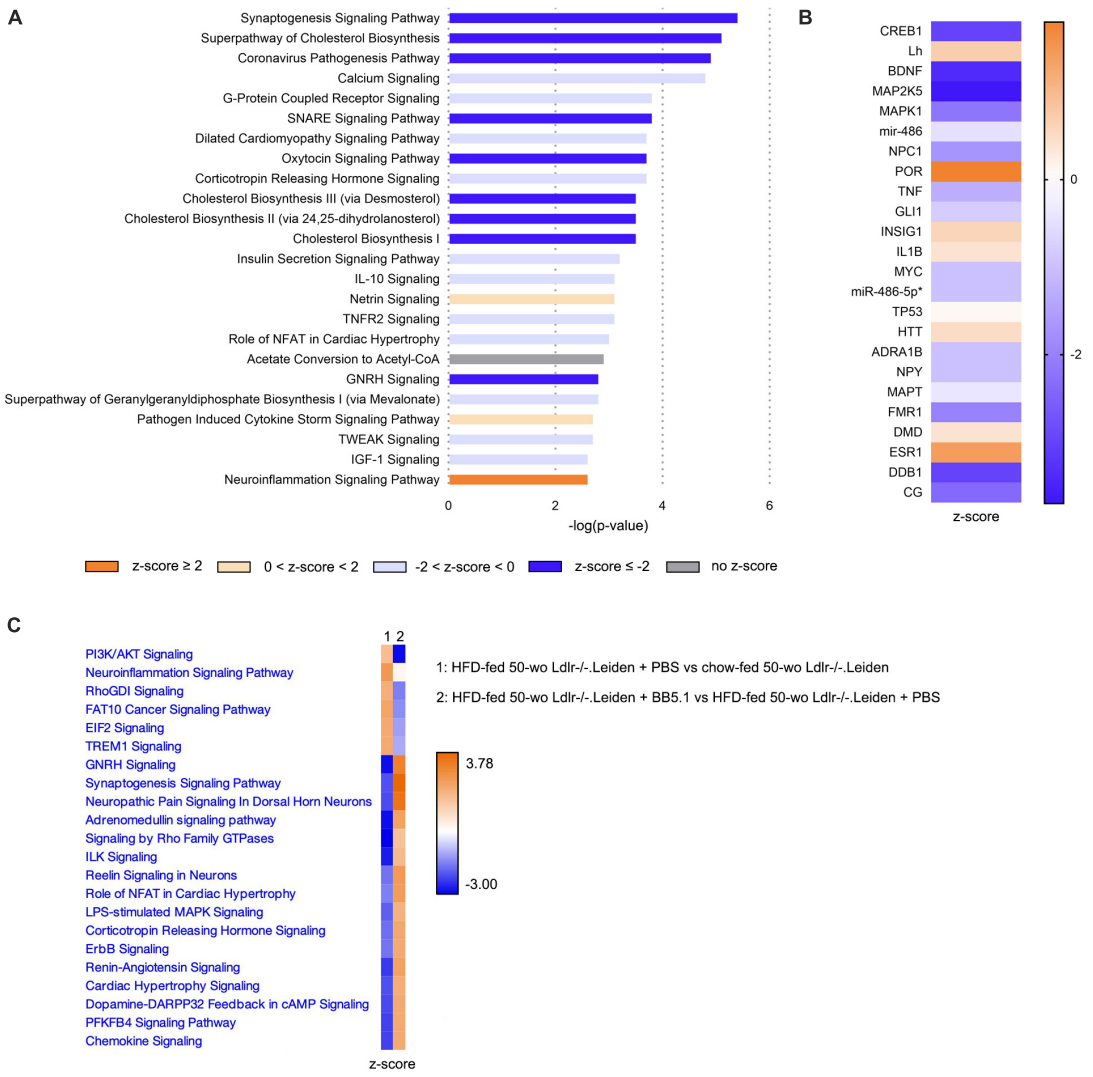

FIGURE 7
In Ldlr-/-.Leiden mice hippocampus, HFD feeding overall downregulated signaling pathways and increased neuroinflammation, while BB5.1 partly restored hippocampal gene expression. **(A)** Most significantly enriched canonical pathways based on hippocampal gene expression in HFD-fed 50-wo Ldlr-/-.Leiden + PBS vs chow-fed 50-wo Ldlr-/-.Leiden mice. **(B)** Top 20 predicted upstream regulators (sorted by *p*-value) based on hippocampal gene expression in HFD-fed 50-wo Ldlr-/-.Leiden vs chow-fed 50-wo Ldlr-/-.Leiden mice. **(C)** Comparison between canonical pathways significantly enriched in HFD-fed 50-wo Ldlr-/-.Leiden vs chow-fed 50-wo Ldlr-/-.Leiden mice and canonical pathways significantly enriched in HFD-fed 50-wo Ldlr-/-.Leiden + BB5.1 vs HFD-fed 50-wo Ldlr-/-.Leiden + PBS mice. The z-score indicates the predicted activation of a canonical pathway: z-score ≤ -2 indicates relevant inhibition of the pathway or regulator (indicated in dark blue); z-score ≥ 2 indicates relevant activation of the pathway or regulator (indicated in dark orange).

findings presented herein indicate that obese Ldlr-/-.Leiden mice also resemble human obesity-related brain pathology.

While HFD feeding decreased IBA-1 immunoreactivity, it increased CD68 immunoreactivity, especially in the white matter areas. Consistent with this, a previous study on C57BL/6 mice showed an increase in phagocytic CD68-positive microglia upon HFD feeding (Tucsek et al., 2014). A post-mortem study on elderly people further described the existence of microglia that are positive for CD68 but negative for IBA-1, which were found to be increased in deep subcortical white matter lesions (areas of abnormal myelination) (Waller et al., 2019). Interestingly, post-mortem analyses of the middle temporal gyrus in Alzheimer's disease demonstrated that the state of dementia was positively associated with CD68 microglia marker expression while negatively correlating with IBA-1 (Minett et al., 2016). Inversely, the same study showed that in people without dementia, cognitive function was positively correlated with IBA-1 but negatively with CD68. The increase in CD68-positive microglia suggests that HFD-induced obesity promotes microglia phagocytic activity (Lier et al., 2021). In addition, in this study we observed a tendency towards an increase in TREM2 immunoreactivity after HFD feeding which further supports that HFD feeding drives phagocytic activity (Neumann and Takahashi, 2007) in the microglial cells in the Ldlr-/-.Leiden model. TREM2, one of the most highly expressed receptors on microglia, is regarded as an important player in the transition of microglia from homeostatic to pathological state in the development of Alzheimer's disease (Qin et al., 2021). Altogether, this data suggests that HFD feeding induces a shift in microglia

TABLE 2 Effect of HFD feeding and BB5.1 treatment on chemokines and cytokines concentrations in cortex homogenates of 50 week-old Ldlr-/-Leiden mice.

Cytokines	Chow		HFD + PBS		HFD + BB5.1	
	Mean	SD	Mean	SD	Mean	SD
IL-17A/F	0.13	0.05	0.14	0.06	0.15	0.05
IL-27p28/IL-30	0.28	0.15	0.26	0.12	0.28	0.10
IL-33	**38.82**[a]	**31.75**	**78.50** [a.b]	**56.42**	**96.85**[b]	**45.84**
IP-10	0.79	0.11	0.89	0.31	0.86	0.22
MCP-1	1.94	0.58	1.89	0.35	2.16	0.49
IL-10	0.09[a]	0.05	0.14[a.b]	0.05	0.15[b]	0.04
IL-1β	**0.09**[a]	**0.06**	**0.13**[a.b]	**0.07**	**0.16**[b]	**0.07**
IL-2	0.03	0.01	0.03	0.01	0.03	0.01
IL-6	**0.29**[a]	**0.16**	**0.41**[b]	**0.07**	**0.44**[b]	**0.06**
KC/GRO	0.96	0.30	0.86	0.13	0.99	0.14
TNF-α	**0.02**[a]	**0.01**	**0.03**[a.b]	**0.01**	**0.04**[b]	**0.01**

Concentrations are expressed a pg/mg protein. Cytokines that differed between groups are marked in bold ($p \leq 0.05$) or underlined (trend for significance, $p \leq 0.1$). For these cytokines, groups with corresponding superscript letters are statistically comparable ($p > 0.05$).

TABLE 3 Effect of HFD feeding and BB5.1 treatment on chemokines and cytokines concentrations in thalamus homogenates.

Cytokines	Chow		HFD + PBS		HFD + BB5.1	
	Mean	SD	Mean	SD	Mean	SD
IL-15	6.08	4.07	6.53	4.87	7.09	4.21
IL-17A/F	0.52	0.40	0.36	0.26	0.53	0.30
IL-33	**295.96**[a]	**209.64**	**375.97**[a]	**224.7**	**568.55**[b]	**190.01**
IP-10	3.48	1.21	3.81	1.51	3.25	0.99
MCP-1	2.07	0.59	2.40	0.57	2.40	0.45
MIP-1α	1.96	0.76	2.19	1.02	2.76	1.23
MIP-2	0.35	0.11	0.31	0.06	0.41	0.11
IL-10	0.36	0.20	0.35	0.32	0.36	0.21
IL-1β	0.04	0.02	0.06	0.05	0.06	0.04
IL-6	0.90	0.60	0.79	0.46	0.84	0.35
KC/GRO	1.52[a]	0.31	1.90[b]	0.45	1.92[b]	0.26
TNF-α	0.03	0.02	0.04	0.03	0.04	0.02

Concentrations are expressed a pg/mg protein. Cytokines that differed between groups are marked in bold ($p \leq 0.05$) or underlined (trend for significance, $p \leq 0.1$). For these cytokines, groups with corresponding superscript letters are statistically comparable ($p > 0.05$).

immunophenotype. A more extensive characterization of the expression of markers on microglial cells may further substantiate the microglia phagocytic activity and provide information on the microglia activation state.

To study potential molecular mechanisms underlying brain pathology in Ldlr-/-.Leiden mice, gene expression data were analyzed in the hippocampus, the brain structure involved in memory and learning. Compared with 50 week-old C57BL/6J mice, Ldlr-/-.Leiden of the same age showed a inactivation of oxidative phosphorylation and an increase in mitochondrial dysfunction, in conjunction with a strong downregulation of the elongation factor eIF2 signaling pathway. The eiF2 signaling pathway is critical for mRNA translation in protein synthesis and has been shown to be important for cellular repair and replacement of dysfunctional cells or organelles, and for long-term synaptic plasticity and memory (Sutton and Schuman, 2006; Rios-Fuller et al., 2020). These features were already observed in Ldlr-/-.Leiden mice on a chow diet indicating that the Ldlr-/-.Leiden model as such (i.e., without HFD feeding) replicates human hallmarks of brain pathophysiology that cannot be studied in aged wildtype C57BL/6J mice, namely impaired mitochondrial function and protein synthesis (Cui et al., 2012; Anisimova et al., 2018). Mitochondrial dysfunction is one of the central mechanisms that can lead to an energy crisis in brain cells and has been proposed as a determinant feature in neurodegeneration and the development of neurodegenerative diseases (Mattson et al., 2008; Belenguer et al., 2019). For instance, pharmacological inhibition of mitochondrial function in the brain has been shown to increase the permeability of the blood-brain barrier *in vivo* and *in vitro* (Doll et al., 2015), and mitochondrial dysfunction in astrocytes

has been suggested to impact energy supply of neurons (Cunnane et al., 2021). Furthermore, while physiological concentrations of reactive oxygen species fulfil a signalling role, their overproduction is detrimental and is associated with lipid peroxidation and DNA damage (Wang et al., 2020; Angelova et al., 2021; Wareham et al., 2022), to which mitochondrial DNA is particularly vulnerable. The fact that Ldlr-/-.Leiden mice but not C57BL/6J mice develop mitochondrial dysfunction during aging on a chow diet advocates additional examination of the Ldlr-/-.Leiden mice as an aging model, the more so because these animals develop moderate visceral obesity and atherosclerosis on the long run, even on a normal chow diet (Verschuren et al., 2009; Gart et al., 2023). Impairment of mitochondrial function is also a key feature of the HFD-fed obese Ldlr-/-.Leiden mouse: while in the livers of the same mice as those described herein, oxidative phosphorylation and mitochondria dysfunction pathways were significantly altered by HFD feeding (Seidel et al., 2022), these pathways in the brain were not further impacted by HFD feeding. This suggests that differences seem to exist between the brain and peripheral organs such as the liver regarding the effect of additional metabolic stress from HFD feeding. It is unclear why HFD feeding does not further augment mitochondrial dysfunction in the brain. Possible explanations could be that the dysfunctionality is already maximal on chow diet and/or that the metabolic homeostasis is more tightly controlled in the brain.

In addition, we showed that HFD feeding increased neuroinflammation signaling pathway, which was in line with the changes in microglia immunophenotype that were observed in the histopathological analysis. HFD also decreased synaptogenesis signaling and SNARE signaling, which are essential pathways for synaptic vesicle exocytosis and neurotransmitter release. In addition to the impairment of synaptogenesis, diet-induced obesity has also previously been found to be associated with synaptic dysfunction and synapse loss (Bocarsly et al., 2015; Hao et al., 2016) which may be the result of synapse elimination by activated microglia (Hao et al., 2016). Interestingly, in an animal model for Alzheimer's disease, eliminated synapses were shown to exhibit mitochondrial dysfunction (Györffy et al., 2020), a pathway that is enriched in the hippocampus of the Ldlr-/-.Leiden mouse model as described earlier.

In this study, HFD-induced neuroinflammation was accompanied by an increase in the concentration of the pro-inflammatory cytokine IL-6 in the cortex. Consistent with this, others have shown that obesity-related systemic inflammation is associated with increased systemic as well as cerebral IL-6 levels, either by local production in the brain and/or by crossing of the blood-brain barrier from the periphery (reviewed in Arnoldussen et al., 2014). The latter review suggests that increased IL-6 in the brain, especially in the hippocampus, is associated with learning and memory dysfunction through the inhibition of neurogenesis and decreased synaptic plasticity. IL-6 levels were also shown to be increased in the cortex of aged mice and were associated with diverse detrimental effects in the brain (Godbout and Johnson, 2004). Furthermore, we found a tendency towards an increase in KC concentrations in the thalamus after HFD feeding, a pro-inflammatory cytokine also known as CXCL1/2. Local production of CXCL-1 in the brain upon chronic stress stimuli has been previously described (Song et al., 2020). Although the role of CXCL1 in the brain is little known, genetic knock-out of its receptor CXCR2 has been shown to reduce neutrophil recruitment and blood-brain barrier permeability which suggest a potential role of KC in neuroinflammation (Michael et al., 2020). Altogether the HFD-induced increases in IL-6 and KC concentrations in the brain support that HFD feeding induces a pro-inflammatory milieu in line with the observed increase in neuroinflammation.

To finally test whether the aforementioned pathophysiological features can be modulated in a therapeutic setting, obese Ldlr-/-.Leiden mice were treated with an anti-C5 antibody (BB5.1), which inhibits the terminal complement pathway. Increased activity of the complement system in the brain has been observed in obesity (Graham et al., 2020) and has been shown to trigger neuroinflammatory cascades with activation of astrocytes and microglia, which may cause neurodegenerative disease (Dalakas et al., 2020). Previous studies showed that this complement system-mediated neuroinflammation can be abrogated by inhibition of MAC, the terminal complex of the complement system cascade (Fluiter et al., 2014; Michailidou et al., 2018). We previously showed in Ldlr-/-.Leiden mice that blocking C5 in the circulation with BB5.1 antibody reduced the potential for complement activation, MAC deposition and plasma concentrations of macrophage migration inhibitory factor (Seidel et al., 2022). In the present study, we found that the anti-C5 treatment did not alter neurodegeneration or astrogliosis, but partially reversed the effect of HFD on microglial immunophenotype, notably by increasing IBA-1 immunoreactivity back to chow level. In addition, on the gene expression level, the anti-C5 treatment reversed the HFD-induced downregulation of multiple pathways, including synaptogenesis. In the present study, the observed effects of the systemic anti-C5 treatment on the brain are expected to be indirect as the BB5.1 antibody and complement proteins cannot pass through intact blood-brain barrier (Alexander, 2018; Zelek et al., 2020). The anti-C5 treatment may impact microglia via indirect effects involving at least partly the C5 activation by-product C5a and MAC which do not only have inflammatory functions but can also act as important modulators of vascular inflammation and permeability. C5a can notably affect vascular inflammation by inducing adhesion molecules and several selectins (Foreman et al., 1994; Albrecht et al., 2004) and has been shown to increase blood-brain barrier permeability (Jacob and Alexander, 2014). In addition, in sublytic concentrations MAC can activate endothelial cells by modulating the secretion of pro-inflammatory mediators and by upregulating adhesion molecules (Kilgore et al., 1997). In addition, it is possible that systemic inhibition of C5 may impact microglia indirectly through the alteration of activation state of circulating immune cells or changes in circulating cytokines. However, this effect appears to be only partial, since CD68 immunoreactivity and TREM2 immunoreactivity were not affected and the neuroinflammation signalling pathway in the hippocampus was unchanged by the anti-C5 treatment. This appears not to be fully in line with previous studies showing that terminal complement pathway inhibitors induce major reduction in neuroinflammation (Fluiter et al., 2014; Michailidou et al., 2018). However, these studies were performed in the context of acute disease (i.e., experimental autoimmune encephalomyelitis, traumatic brain injury) in which the blood-brain barrier is known to be more permeable. In our study, in a context of obesity (i.e., chronic low-grade inflammation), the blood-brain barrier is likely

to be less permeable and the systemic anti-C5 treatment may not have entered the brain to target local production of complement factors. In neurodegenerative diseases, reactive astrocytes have been proposed to induce the production of complement factors by reactive microglia and neurons (Stephan et al., 2012). These locally-produced complement factors are believed to subsequently label the synapses for elimination by microglia. As the systemic anti-complement C5 treatment in our study may not target this local production of complement factors, a complement-mediated elimination of synapses by microglia may explain the remaining phagocytic profile of microglia in anti C5-treated mice.

Additionally, we showed that the anti-C5 treatment did not reverse the HFD-induced increase in IL-6 or KC concentrations but increased IL-33 in the thalamus in comparison with both HFD-fed controls and chow-fed mice. Since IL-33 has been shown to have both pro- and anti-inflammatory effects in the brain (Rao et al., 2022), it is not clear whether the observed increase in IL-33 in the thalamus in this study is beneficial or deleterious. Given that the activation state of microglial cells is highly influenced by the cytokine environment (Hanisch, 2002), anti-C5 treatment-mediated changes in IL-33 may be linked to the partial reversal effect of the treatment on the expression of microglia surface markers.

5. Conclusion

In this study we show that Ldlr-/-.Leiden mice are more prone to develop neurodegeneration and age-related astrogliosis that is not observed in wildtype (C57BL6/J) mice. On the gene expression level, Ldlr-/-.Leiden mice exhibit pronounced mitochondrial dysfunction and impaired oxidative phosphorylation, and the pathway required for protein synthesis and repair (eIF2) is significantly inactivated in the hippocampus compared with wildtype mice. When fed an obesity-inducing HFD, Ldlr-/-.Leiden mice further exhibit microglia activation that is characterised by an immunotypic switch to a more phagocytic state, in line with what has also been reported in people with obesity or neurodegenerative disease such as Alzheimer's disease. On the gene expression level, HFD-fed obese Ldlr-/-.Leiden also exhibit increased neuroinflammation and decreased synaptogenesis in the hippocampus. This HFD-induced pathology in Ldlr-/-.Leiden mice can also be modulated by therapeutic treatment: the microglia immunotypic switch and hippocampal gene expression is partly reversed by a systemic therapeutic antibody intervention targeting complement C5. In sum, this study provides evidence supporting the Ldlr-/-.Leiden mouse model as an appropriate model to study the development of brain pathology in the context of aging and obesity.

Data availability statement

The transcriptomics data presented in the study are deposited in the Gene Expression Omnibus (GEO) repository (https://www.ncbi.nlm.nih.gov/gds), accession number GSE234425.

Ethics statement

The animal study was reviewed and approved by an independent Animal Welfare Body (IVD TNO; approval numbers TNO-451 and TNO-499) under project licenses granted by the Netherlands Central Authority for Scientific Procedures on Animals (CCD; project license numbers AVD5010020172064 and AVD5010020172931).

Author contributions

RK, KF, IM, and MM: conceptualization. FS, RK, KF, MM, and IM: methodology, writing—original draft preparation. FS, AN, NW, and IM: investigation. NG and AK: resources. FS, MC, and IM: data analysis. FS, RK, KF, NG, AK, FB, IM, and MM: data interpretation. MM and IM: supervision. MM: project administration. RK, FB, KF, and MM: funding acquisition. All authors: writing—review and editing.

Funding

This study was supported by the TNO Early Research Program 'Body Brain Interactions' and the TNO research program PMC9 and PMC13.

Acknowledgments

We would like to thank the biotechnicians from TNO Metabolic Health Research for taking excellent care of the mice used in this study. We also thank B. P. Morgan and T. Hughes for kindly providing the BB5.1 antibody.

Conflict of interest

The authors declare that the research was conducted in the absence of any commercial or financial relationships that could be construed as a potential conflict of interest.

Publisher's note

Supplementary material

The Supplementary Material for this article can be found online at: https://www.frontiersin.org/articles/10.3389/fncel.2023.1205261/full#supplementary-material

References

Ahmad Tarmizi, N. A. K., Kushairi, N., Phan, C. W., Sabaratnam, V., Naidu, M., and David, P. (2022). β-Glucan-rich extract of gray oyster mushroom, pleurotus pulmonarius, improves object recognition memory and hippocampus morphology in mice fed a high-fat diet. *J. Med. Food* 25, 230–238. doi: 10.1089/jmf.2021.K.0121

Albrecht, E. A., Chinnaiyan, A. M., Varambally, S., Kumar-Sinha, C., Barrette, T. R., Sarma, J. V., et al. (2004). C5a-induced gene expression in human umbilical vein endothelial cells. *Am. J. Pathol.* 164, 849–859. doi: 10.1016/S0002-9440(10)63173-2

Alexander, J. J. (2018). Blood-brain barrier (BBB) and the complement landscape. *Mol. Immunol.* 102, 26–31. doi: 10.1016/j.molimm.2018.06.267

Andolfi, C., and Fisichella, P. M. (2018). Epidemiology of obesity and associated comorbidities. *J. Laparoendosc. Adv. Surg. Tech.* 28, 919–924. doi: 10.1089/lap.2018.0380

Angelova, P. R., Esteras, N., and Abramov, A. Y. (2021). Mitochondria and lipid peroxidation in the mechanism of neurodegeneration: Finding ways for prevention. *Med. Res. Rev.* 41, 770–784. doi: 10.1002/med.21712

Anisimova, A. S., Alexandrov, A. I., Makarova, N. E., Gladyshev, V. N., and Dmitriev, S. E. (2018). Protein synthesis and quality control in aging. *Aging* 10, 4269–4288. doi: 10.18632/aging.101721

Arnoldussen, I. A. C., Kiliaan, A. J., and Gustafson, D. R. (2014). Obesity and dementia: Adipokines interact with the brain. *Eur. Neuropsychopharmacol.* 24, 1982–1999. doi: 10.1016/j.euroneuro.2014.03.002

Arnoldussen, I. A. C., Morrison, M. C., Wiesmann, M., van Diepen, J. A., Worms, N., Voskuilen, M., et al. (2022). Milk fat globule membrane attenuates high fat diet-induced neuropathological changes in obese Ldlr-/-.Leiden mice. *Int. J. Obes.* 46, 342–349. doi: 10.1038/s41366-021-00998-w

Arnoldussen, I. A. C., Wiesmann, M., Pelgrim, C. E., Wielemaker, E. M., Van Duyvenvoorde, W., Amaral-Santos, P. L., et al. (2017). Butyrate restores HFD-induced adaptations in brain function and metabolism in mid-adult obese mice. *Int. J. Obes.* 41, 935–944. doi: 10.1038/ijo.2017.52

Bandala, C., Cárdenas-Rodríguez, N., Reyes-Long, S., Cortes-Altamirano, J. L., Garciadiego-Cázares, D., Lara-Padilla, E., et al. (2022). Trends in gliosis in obesity, and the role of antioxidants as a therapeutic alternative. *Antioxidants* 11:1972. doi: 10.3390/antiox11101972

Belenguer, P., Duarte, J. M. N., Schuck, P. F., and Ferreira, G. C. (2019). Mitochondria and the brain: Bioenergetics and beyond. *Neurotox. Res.* 36, 219–238. doi: 10.1007/s12640-019-00061-7

Benisty, S., Gouw, A. A., Porcher, R., Madureira, S., Hernandez, K., Poggesi, A., et al. (2009). Location of lacunar infarcts correlates with cognition in a sample of non-disabled subjects with age-related white-matter changes: The LADIS study. *J. Neurol. Neurosurg. Psychiatry* 80, 478–483. doi: 10.1136/jnnp.2008.160440

Bocarsly, M. E., Fasolino, M., Kane, G. A., Lamarca, E. A., Kirschen, G. W., Karatsoreos, I. N., et al. (2015). Obesity diminishes synaptic markers, alters microglial morphology, and impairs cognitive function. *Proc. Natl. Acad. Sci. U.S.A.* 112, 15731–15736. doi: 10.1073/pnas.1511593112

Bondan, E. F., Cardoso, C. V., Martins, M. D. F. M., and Otton, R. (2019). Memory impairments and increased GFAP expression in hippocampal astrocytes following hypercaloric diet in rats. *Arq. Neuropsiquiatr.* 77, 601–608. doi: 10.1590/0004-282X20190091

Brooks, S. J., Benedict, C., Burgos, J., Kempton, M. J., Kullberg, J., Nordenskjöld, R., et al. (2013). Late-life obesity is associated with smaller global and regional gray matter volumes: A voxel-based morphometric study. *Int. J. Obes.* 37, 230–236. doi: 10.1038/ijo.2012.13

Csige, I., Ujvárosy, D., Szabó, Z., Lőrincz, I., Paragh, G., Harangi, M., et al. (2018). The impact of obesity on the cardiovascular system. *J. Diabetes Res.* 2018:3407306. doi: 10.1155/2018/3407306

Cui, H., Kong, Y., and Zhang, H. (2012). Oxidative stress, mitochondrial dysfunction, and aging. *J. Signal Transduct.* 2012:646354. doi: 10.1155/2012/646354

Cunnane, S. C., Trushina, E., Morland, C., Prigione, A., Casadesus, G., Andrews, Z. B., et al. (2021). Brain energy rescue: An emerging therapeutic concept for neurodegenerative disorders of ageing. *Nat. Rev. Drug Discov.* 19, 609–633. doi: 10.1038/s41573-020-0072-x

Dalakas, M. C., Alexopoulos, H., and Spaeth, P. J. (2020). Complement in neurological disorders and emerging complement-targeted therapeutics. *Nat. Rev. Neurol.* 16, 601–617. doi: 10.1038/s41582-020-0400-0

Doll, D. N., Hu, H., Sun, J., Lewis, S. E., Simpkins, J. W., and Ren, X. (2015). Mitochondrial crisis in cerebrovascular endothelial cells opens the blood-brain barrier. *Stroke* 46, 1681–1689. doi: 10.1161/STROKEAHA.115.009099

Dorfman, M. D., and Thaler, J. P. (2015). Hypothalamic inflammation and gliosis in obesity. *Curr. Opin. Endocrinol. Diabetes Obes.* 22, 325–330. doi: 10.1097/MED.0000000000000182

Eng, L. F., and Ghirnikar, R. S. (1994). GFAP and astrogliosis. *Brain Pathol.* 4, 229–237. doi: 10.1111/j.1750-3639.1994.tb00838.x

Fluiter, K., Opperhuizen, A. L., Morgan, B. P., Baas, F., and Ramaglia, V. (2014). Inhibition of the membrane attack complex of the complement system reduces secondary neuroaxonal loss and promotes neurologic recovery after traumatic brain injury in mice. *J. Immunol.* 192, 2339–2348. doi: 10.4049/jimmunol.1302793

Foreman, K. E., Vaporciyan, A. A., Bonish, B. K., Jones, M. L., Johnson, K. J., Glovsky, M. M., et al. (1994). C5a-induced expression of P-selectin in endothelial cells. *J. Clin. Invest.* 94, 1147–1155. doi: 10.1172/JCI117430

García-García, I., Michaud, A., Jurado, M. Á, Dagher, A., and Morys, F. (2022). Mechanisms linking obesity and its metabolic comorbidities with cerebral grey and white matter changes. *Rev. Endocr. Metab. Disord.* 23, 833–843. doi: 10.1007/s11154-021-09706-5

Gart, E., Salic, K., Morrison, M. C., Caspers, M., van Duyvenvoorde, W., Heijnk, M., et al. (2021). Krill oil treatment increases distinct pufas and oxylipins in adipose tissue and liver and attenuates obesity-associated inflammation via direct and indirect mechanisms. *Nutrients* 13:2836. doi: 10.3390/nu13082836

Gart, E., Salic, K., Morrison, M. C., Giera, M., Attema, J., de Ruiter, C., et al. (2022a). The human milk oligosaccharide 2'-fucosyllactose alleviates liver steatosis, ER stress and insulin resistance by reducing hepatic diacylglycerols and improved gut permeability in obese Ldlr-/-.Leiden mice. *Front. Nutr.* 9:904740. doi: 10.3389/fnut.2022.904740

Gart, E., van Duyvenvoorde, W., Caspers, M. P. M., van Trigt, N., Snabel, J., Menke, A., et al. (2022b). Intervention with isoleucine or valine corrects hyperinsulinemia and reduces intrahepatic diacylglycerols, liver steatosis, and inflammation in Ldlr-/-.Leiden mice with manifest obesity-associated NASH. *FASEB J.* 36:e22435. doi: 10.1096/fj.202200111R

Gart, E., van Duyvenvoorde, W., Snabel, J. M., de Ruiter, C., Attema, J., Caspers, M. P. M., et al. (2023). Translational characterization of the temporal dynamics of metabolic dysfunctions in liver, adipose tissue and the gut during diet-induced NASH development in Ldlr-/-.Leiden mice. *Heliyon* 9:e13985. doi: 10.1016/j.heliyon.2023.e13985

Giovannoni, F., and Quintana, F. J. (2020). The role of astrocytes in CNS inflammation. *Trends Immunol.* 41, 805–819. doi: 10.1016/j.it.2020.07.007

Godbout, J. P., and Johnson, R. W. (2004). Interleukin-6 in the aging brain. *J. Neuroimmunol.* 147, 141–144. doi: 10.1016/j.jneuroim.2003.10.031

Gómez-Apo, E., Mondragón-Maya, A., Ferrari-Díaz, M., and Silva-Pereyra, J. (2021). Structural brain changes associated with overweight and obesity. *J. Obes.* 2021:6613385. doi: 10.1155/2021/6613385

Graham, L. C., Kocalis, H. E., Soto, I., and Howell, G. R. (2020). Deficiency of complement component C1Q prevents cerebrovascular damage and white matter loss in a mouse model of chronic obesity. *eNeuro* 7:ENEURO.0057-20.2020. doi: 10.1523/ENEURO.0057-20.2020

Guillemot-Legris, O., and Muccioli, G. G. (2017). Obesity-induced neuroinflammation: Beyond the hypothalamus. *Trends Neurosci.* 40, 237–253. doi: 10.1016/j.tins.2017.02.005

Györffy, B. A., Tóth, V., Török, G., Gulyássy, P., Kovács, R., Vadászi, H., et al. (2020). Synaptic mitochondrial dysfunction and septin accumulation are linked to complement-mediated synapse loss in an Alzheimer's disease animal model. *Cell. Mol. Life Sci.* 77, 5243–5258. doi: 10.1007/s00018-020-03468-0

Hanisch, U. K. (2002). Microglia as a source and target of cytokines. *Glia* 40, 140–155. doi: 10.1002/glia.10161

Hao, S., Dey, A., Yu, X., and Stranahan, A. M. (2016). Dietary obesity reversibly induces synaptic stripping by microglia and impairs hippocampal plasticity. *Brain Behav. Immun.* 51, 230–239. doi: 10.1016/j.bbi.2015.08.023

Ito, D., Imai, Y., Ohsawa, K., Nakajima, K., Fukuuchi, Y., and Kohsaka, S. (1998). Microglia-specific localisation of a novel calcium binding protein, Iba1. *Mol. Brain Res.* 57, 1–9. doi: 10.1016/S0169-328X(98)00040-0

Jacob, A., and Alexander, J. J. (2014). Complement and blood-brain barrier integrity. *Mol. Immunol.* 61, 149–152. doi: 10.1016/j.molimm.2014.06.039

Kilgore, K. S., Schmid, E., Shanley, T. P., Flory, C. M., Maheswari, V., Tramontini, N. L., et al. (1997). Sublytic concentrations of the membrane attack complex of complement induce endothelial interleukin-8 and monocyte chemoattractant protein-1 through nuclear factor-kb activation. *Am. J. Pathol.* 150, 2019–2031.

Kiliaan, A. J., Arnoldussen, I. A. C., and Gustafson, D. R. (2014). Adipokines: A link between obesity and dementia? *Lancet Neurol.* 13, 913–923. doi: 10.1016/S1474-4422(14)70085-7

Koga, S., Kojima, A., Kuwabara, S., and Yoshiyama, Y. (2014). Immunohistochemical analysis of tau phosphorylation and astroglial activation with enhanced leptin receptor expression in diet-induced obesity mouse hippocampus. *Neurosci. Lett.* 571, 11–16. doi: 10.1016/j.neulet.2014.04.028

Lier, J., Streit, W. J., and Bechmann, I. (2021). Beyond activation: Characterizing microglial functional phenotypes. *Cells* 10:2236. doi: 10.3390/cells10092236

Lier, J., Winter, K., Bleher, J., Grammig, J., Müller, W., Streit, W., et al. (2019). Loss of IBA1-expression in brains from individuals with obesity and hepatic dysfunction. *Brain Res.* 1710, 220–229. doi: 10.1016/j.brainres.2019.01.006

Love, M. I., Huber, W., and Anders, S. (2014). Moderated estimation of fold change and dispersion for RNA-seq data with DESeq2. *Genome Biol.* 15:550. doi: 10.1186/s13059-014-0550-8

Mattson, M. P., Gleichmann, M., and Cheng, A. (2008). Mitochondria in neuroplasticity and neurological disorders. *Neuron* 60, 748–766. doi: 10.1016/j.neuron.2008.10.010

Michael, B. D., Bricio-Moreno, L., Sorensen, E. W., Miyabe, Y., Lian, J., Solomon, T., et al. (2020). Astrocyte- and neuron-derived CXCL1 drives neutrophil transmigration and blood-brain barrier permeability in viral encephalitis. *Cell Rep.* 32:108150. doi: 10.1016/j.celrep.2020.108150

Michailidou, I., Jongejan, A., Vreijling, J. P., Georgakopoulou, T., de Wissel, M. B., Wolterman, R. A., et al. (2018). Systemic inhibition of the membrane attack complex impedes neuroinflammation in chronic relapsing experimental autoimmune encephalomyelitis. *Acta Neuropathol. Commun.* 6:36. doi: 10.1186/s40478-018-0536-y

Minett, T., Classey, J., Matthews, F. E., Fahrenhold, M., Taga, M., Brayne, C., et al. (2016). Microglial immunophenotype in dementia with Alzheimer's pathology. *J. Neuroinflammation* 13:135. doi: 10.1186/s12974-016-0601-z

Morrison, M. C., Kleemann, R., van Koppen, A., Hanemaaijer, R., and Verschuren, L. (2018). Key inflammatory processes in human NASH are reflected in Ldlr-/-.Leiden mice: A translational gene profiling study. *Front. Physiol.* 9:132. doi: 10.3389/fphys.2018.00132

Neumann, H., and Takahashi, K. (2007). Essential role of the microglial triggering receptor expressed on myeloid cells-2 (TREM2) for central nervous tissue immune homeostasis. *J. Neuroimmunol.* 184, 92–99. doi: 10.1016/j.jneuroim.2006.11.032

Pannacciulli, N., Del Parigi, A., Chen, K., Le, D. S. N. T., Reiman, E. M., and Tataranni, P. A. (2006). Brain abnormalities in human obesity: A voxel-based morphometric study. *Neuroimage* 31, 1419–1425. doi: 10.1016/j.neuroimage.2006.01.047

Pedditizi, E., Peters, R., and Beckett, N. (2016). The risk of overweight/obesity in mid-life and late life for the development of dementia: A systematic review and meta-analysis of longitudinal studies. *Age Ageing* 45, 14–21. doi: 10.1093/ageing/afv151

Qin, Q., Teng, Z., Liu, C., Li, Q., Yin, Y., and Tang, Y. (2021). TREM2, microglia, and Alzheimer's disease. *Mech. Ageing Dev.* 195:111438. doi: 10.1016/j.mad.2021.111438

Rao, X., Hua, F., Zhang, L., Lin, Y., Fang, P., Chen, S., et al. (2022). Dual roles of interleukin-33 in cognitive function by regulating central nervous system inflammation. *J. Transl. Med.* 20:369. doi: 10.1186/s12967-022-03570-w

Rios-Fuller, T. J., Mahe, M., Walters, B., Abbadi, D., Pérez-Baos, S., Gadi, A., et al. (2020). Translation regulation by eIF2α phosphorylation and mTORC1 signaling pathways in non-communicable diseases (n.d.). *Int. J. Mol. Sci.* 21:5301. doi: 10.3390/ijms21155301

Salic, K., Gart, E., Seidel, F., Verschuren, L., Caspers, M., van Duyvenvoorde, W., et al. (2019). Combined treatment with L-carnitine and nicotinamide riboside improves hepatic metabolism and attenuates obesity and liver steatosis. *Int. J. Mol. Sci.* 20:4359. doi: 10.3390/ijms20184359

Sarma, J. V., and Ward, P. A. (2011). The complement system. *Cell Tissue Res.* 343, 227–235. doi: 10.1007/s00441-010-1034-0

Seidel, F., Kleemann, R., van Duyvenvoorde, W., van Trigt, N., Keijzer, N., van der Kooij, S., et al. (2022). Therapeutic intervention with anti-complement component 5 antibody does not reduce NASH but does attenuate atherosclerosis and MIF concentrations in Ldlr-/-.Leiden mice. *Int. J. Mol. Sci.* 23:10736. doi: 10.3390/ijms231810736

Shim, K., Begum, R., Yang, C., and Wang, H. (2020). Complement activation in obesity, insulin resistance, and type 2 diabetes mellitus. *World J. Diabetes* 11, 1–12. doi: 10.4239/wjd.v11.i1.1

Sofroniew, M. V. (2009). Molecular dissection of reactive astrogliosis and glial scar formation. *Trends Neurosci.* 32, 638–647. doi: 10.1016/j.tins.2009.08.002

Song, A. Q., Gao, B., Fan, J. J., Zhu, Y. J., Zhou, J., Wang, Y. L., et al. (2020). NLRP1 inflammasome contributes to chronic stress-induced depressive-like behaviors in mice. *J. Neuroinflammation* 17:178. doi: 10.1186/s12974-020-01848-8

Stephan, A. H., Barres, B. A., and Stevens, B. (2012). The complement system: An unexpected role in synaptic pruning during development and disease. *Annu. Rev. Neurosci.* 35, 369–389. doi: 10.1146/annurev-neuro-061010-113810

Stevens, B., Allen, N. J., Vazquez, L. E., Howell, G. R., Christopherson, K. S., Nouri, N., et al. (2007). The classical complement cascade mediates CNS synapse elimination. *Cell* 131, 1164–1178. doi: 10.1016/j.cell.2007.10.036

Sutton, M. A., and Schuman, E. M. (2006). Dendritic protein synthesis, synaptic plasticity, and memory. *Cell* 127, 49–58. doi: 10.1016/j.cell.2006.09.014

Tanaka, H., Gourley, D. D., Dekhtyar, M., and Haley, A. P. (2020). Cognition, brain structure, and brain function in individuals with obesity and related disorders. *Curr. Obes. Rep.* 9, 544–549. doi: 10.1007/s13679-020-00412-y

Thaler, J. P., Yi, C.-X., Schur, E. A., Guyenet, S. J., Hwang, B. H., Dietrich, M. O., et al. (2012). Obesity is associated with hypothalamic injury in rodents and humans. *J. Clin. Invest.* 122, 153–162. doi: 10.1172/JCI59660

Tucsek, Z., Toth, P., Sosnowska, D., Gautam, T., Mitschelen, M., Koller, A., et al. (2014). Obesity in aging exacerbates blood-brain barrier disruption, neuroinflammation, and oxidative stress in the mouse hippocampus: Effects on expression of genes involved in beta-amyloid generation and Alzheimer's disease. *J. Gerontol. A Biol. Sci. Med. Sci.* 69, 1212–1226. doi: 10.1093/gerona/glt177

van den Hoek, A. M., de Jong, J. C. B. C., Worms, N., van Nieuwkoop, A., Voskuilen, M., Menke, A. L., et al. (2021). Diet and exercise reduce pre-existing NASH and fibrosis and have additional beneficial effects on the vasculature, adipose tissue and skeletal muscle via organ-crosstalk. *Metabolism* 124:154873. doi: 10.1016/j.metabol.2021.154873

van den Hoek, A. M., Verschuren, L., Worms, N., van Nieuwkoop, A., de Ruiter, C., Attema, J., et al. (2020). A translational mouse model for NASH with advanced fibrosis and atherosclerosis expressing key pathways of human pathology. *Cells* 9:2014. doi: 10.3390/cells9092014

Verschuren, L., Kooistra, T., Bernhagen, J., Voshol, P. J., Ouwens, D. M., van Erk, M., et al. (2009). MIF deficiency reduces chronic inflammation in white adipose tissue and impairs the development of insulin resistance, glucose intolerance, and associated atherosclerotic disease. *Circ. Res.* 105, 99–107. doi: 10.1161/CIRCRESAHA.109.199166

Vlaicu, S. I., Tatomir, A., Rus, V., Mekala, A. P., Mircea, P. A., Niculescu, F., et al. (2016). The role of complement activation in atherogenesis: The first 40 years. *Immunol. Res.* 64, 1–13. doi: 10.1007/s12026-015-8669-6

Wahid, R. M., Samy, W., and El-sayed, S. F. (2021). Cognitive impairment in obese rat model: Role of glial cells. *Int. J. Obes.* 45, 2191–2196. doi: 10.1038/s41366-021-00880-9

Waller, R., Baxter, L., Fillingham, D. J., Coelho, S., Pozo, J. M., Mozumder, M., et al. (2019). Iba-1-/CD68+ microglia are a prominent feature of age-associated deep subcortical white matter lesions. *PLoS One* 14:e0210888. doi: 10.1371/journal.pone.0210888

Wang, W., Zhao, F., Ma, X., Perry, G., and Zhu, X. (2020). Mitochondria dysfunction in the pathogenesis of Alzheimer's disease: Recent advances. *Mol. Neurodegener.* 15:30. doi: 10.1186/s13024-020-00376-6

Wareham, L. K., Liddelow, S. A., Temple, S., Benowitz, L. I., Di Polo, A., Wellington, C., et al. (2022). Solving neurodegeneration: Common mechanisms and strategies for new treatments. *Mol. Neurodegener.* 17:23. doi: 10.1186/s13024-022-00524-0

Zelek, W. M., Menzies, G. E., Brancale, A., Stockinger, B., and Morgan, B. P. (2020). Characterizing the original anti-C5 function-blocking antibody, BB5.1, for species specificity, mode of action and interactions with C5. *Immunology* 161, 103–113. doi: 10.1111/imm.13228

Frontiers in
Cellular Neuroscience

Leading research in cellular mechanisms underlying brain function and development

Part of the world's most cited neuroscience journal series that advances our understanding of the cellular mechanisms underlying cell function in the nervous system across all species.

Discover the latest Research Topics

See more →

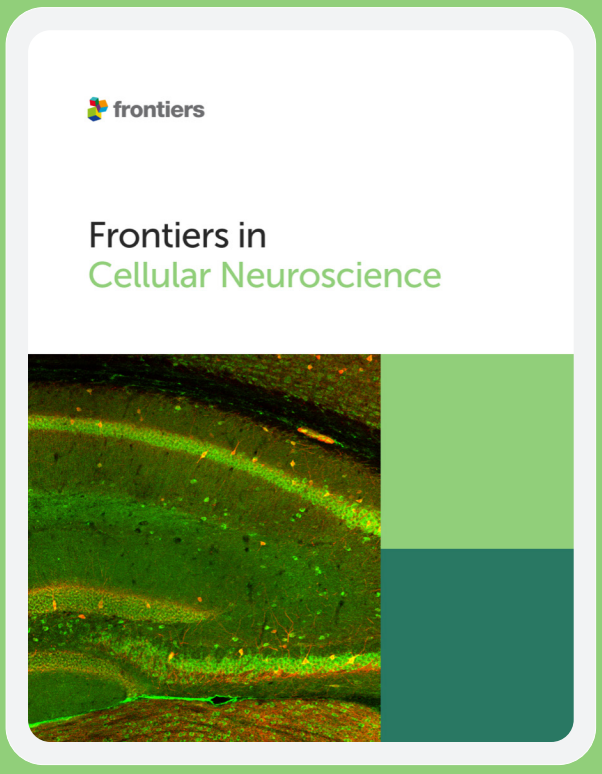

Frontiers

Avenue du Tribunal-Fédéral 34
1005 Lausanne, Switzerland
frontiersin.org

Contact us

+41 (0)21 510 17 00
frontiersin.org/about/contact